5

SQUIDs and Detectors

Editor: A. I. Braginski

Forschungszentrum Jülich GmbH, Jülich, Germany

5.1 Introduction

John Clarke, Arnold Silver and A. I. Braginski

The Superconducting QUantum Interference Device (SQUID) combines the phenomena of flux quantization and Josephson tunneling. First predicted by F. London[1], flux quantization was observed experimentally by Deaver and Fairbank[2] and Doll and Näbauer[3] in 1961. They showed that the flux contained in a closed superconducting loop is quantized in units of the flux quantum $\Phi_0 \equiv h/2e \approx 2.07 \times 10^{-15}$ Wb, where, $h \equiv 2\pi\hbar$ is Planck's constant, and $2e$ is the charge on the Cooper pair—the cornerstone of the Bardeen-Cooper-Schrieffer (BCS) theory of superconductivity[4]. Flux quantization originates in the fact that the macroscopic wave function $\Psi(\vec{r},t) = \Psi_0(\vec{r},t)exp[i\phi(\vec{r},t)]$ must be single-valued in going once around a superconducting loop. In the absence of applied fields

[1] F. London *Superfluids*, Wiley, New York (1950)
[2] B.S. Deaver and W.M. Fairbank, *Phys. Rev. Lett.* 7 (1961) 43
[3] R.Doll and M. Näbauer, *Phys. Rev. Lett.* 7 (1961) 51
[4] J. Bardeen et al., *Phys. Rev.* 108 (1957) 1175

or currents, the phase $\phi(\vec{r},t)$ takes the same value throughout the superconductor for all Cooper pairs. In the case of a loop threaded by a magnetic flux, however, the phase around the loop changes by $2\pi \cdot n$, where n is the number of enclosed flux quanta. In the year preceding the observation of flux quantization, Giaever[5] demonstrated the tunneling of single electrons between a superconductor (S) and a normal metal (N) separated by a thin insulating (I) layer. Subsequently, he observed the tunneling of single electrons through SIS junctions[6]. Single particle tunneling between superconductors was explained in terms of a tunneling Hamiltonian by Cohen, Falicov and Phillips[7].

In 1962, Brian Josephson (Figure 5.1) carried through this Hamiltonian to higher order to predict the tunneling of Cooper pairs through a barrier separating two superconductors[8]. He showed that the supercurrent I flowing through a junction is given by $I = I_0 sin\delta$ where $\delta \equiv \phi_1 - \phi_2$ is the difference between the phases ϕ_1 and ϕ_2 of the condensates in the two superconducting electrodes and I_0 is the critical current. Furthermore, in the presence of a voltage V between the electrodes, δ evolves with time t according to $d\delta/dt = 2eV/\hbar = 2\pi V/\Phi_0$. These equations predict that, as the current through a junction is increased from zero, the voltage across the junction remains zero until the current exceeds the critical current, at which point a voltage appears.

Just one year later, Anderson and Rowell[9] made the first observation of the dc Josephson effect, using a thin-film, Sn-SnOx-Pb junction cooled to 1.5 K in liquid helium. The observations of flux quantization and Josephson tunneling set the scene for the invention of the SQUID.

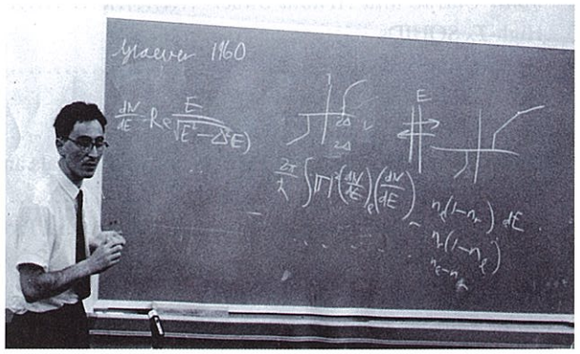

FIGURE 5.1: Brian Josephson discussing Giaever's work on single electron tunneling; circa 1965 (Courtesy Brian Josephson).

SQUIDs are a class of superconductor electronics devices consisting of one or more Josephson junctions that are shunted by small superconducting inductors to form a multiply connected circuit. There are three classes of SQUIDs:

- dc SQUIDs contain two junctions and have a dc current-voltage characteristic,
- rf SQUIDs contain a single junction and have only rf response, and
- R-SQUIDs are rf SQUIDs with a small resistor in series with the inductance and junction, also called relaxation oscillator SQUIDs.

All types were invented nearly 50 years ago and have remained at the core of active electronic devices, circuits and systems based on superconductivity since shortly after their discovery. In Section 5.2, Arnold Silver and John Clarke, respectively, describe the early discoveries and developments at The Ford Motor Company in the U.S. and at Cambridge University in the U.K., which culminated in today's SQUID devices deployed in applications ranging from fundamental physics to a variety of sensors, amplifiers and devices for signal processing, digital computing and, recently, for quantum computation and communication.

[5] I. Giaever, *Phys. Rev. Lett.* 5 (1960) 147
[6] I. Giaever, *Phys. Rev. Lett.* 5 (1960) 464
[7] M.H. Cohen et al., *Phys. Rev. Lett.* 8 (1962) 316
[8] B.D. Josephson, *Phys. Lett.* 1 (1962) 251
[9] P.W. Anderson and J.M. Rowell, *Phys. Rev. Lett.* 10 (1963) 230

With the advent of high-T_c cuprates, high-T_c Josephson junctions and SQUIDs were also developed, and eventually found applications. In Section 5.3, Alex Braginski outlines milestones in their developments and characterizes their current status. Developments leading to the successful use of SQUIDs as sensors for geophysical exploration of minerals are described in Section 5.4 by Cathy Foley, while in Section 5.5 Alex Braginski discusses attempts to use SQUID sensors for nondestructive evaluation of materials and structures. Section 5.6 of this chapter is written by Ron Sager. He presents the saga of the development of the world's most successful industrial SQUID instruments, now widely used in laboratory characterization of materials. Finally, in Section 5.7, John Clarke, Kent Irwin and Peter Michelson address the research leading to SQUID amplifiers and transition edge detectors of radiation and particles. These now find rapidly growing applications in various areas of science, such as astronomy and cosmology, as well as in analysis of materials. Concluding remarks are offered in Section 5.8.

Many other applications of SQUIDs as sensors are not included here, but are covered by or mentioned in other chapters. For example, Chapter 6 describes ongoing research in quantum computing with SQUIDs as qubits (quantum bits), while Chapter 10 includes the use of SQUID sensors in medical research and diagnostics. SQUIDs are widely used for the sensing and imaging of biological magnetic fields, such as those emitted by the brain and heart of humans and animals.

Overall, our chapter does not strive for comprehensive coverage of SQUIDs and their various uses. Rather, the co-authors present their personal perspectives on representative examples of SQUID research and development leading to selected practical applications. "Further Reading" offers a short list of textbooks devoted to a more systematic presentation of the subject and provides references to recently published conference proceedings presenting the current status of SQUIDs, detectors, and their applications.

5.2 History and Device Fundamentals

John Clarke and Arnold Silver

5.2.1 Initial Discovery

Arnold Silver

The first observations of macroscopic quantum interference in superconductors occurred at the Ford Motor Company Scientific Laboratory during 1963. Subsequent conceptual understanding, experimental verification, and expansion of those observations and concepts would eventually produce SQUIDs.

Based on prior developments and ongoing research in other institutions, SQUIDs would have been invented and developed somewhere, although under another name. However, the series of discoveries and inventions at the Ford labs occurred by an unusual sequence of events. It combined the collaborative efforts of Robert Jaklevic, John Lambe, James Mercereau, James Zimmerman, and myself (Figure 5.2), five physicists with differing technical backgrounds and interests. Here, I summarize those events and results. Since, after nearly 50 years, few records aside from publications are available, I rely on my memory to fill in the narrative.

The Ford work started in 1963, as the first publication date in February 1964 indicates. John Lambe and his collaborators first observed an anomalous periodic microwave response during electron-spin paramagnetic resonance (EPR) studies of doped Si at liquid helium (LHe) temper-

atures. These experiments were carried out at X-band (~ 10 GHz) in a high field electromagnet, an unlikely environment for SQUID research. That the measuring equipment was a very low-power super-heterodyne X-band receiver was essential to observing the very low-power signals. His observations could be characterized as follows: signals were periodic in magnetic field and microwave amplitude; they appeared as the temperature was lowered below the boiling point of LHe (4.2 K); they disappeared eventually as the temperature was lowered further; they disappeared as the magnetic field was increased significantly; and the signal was identified as arising from the Si samples.

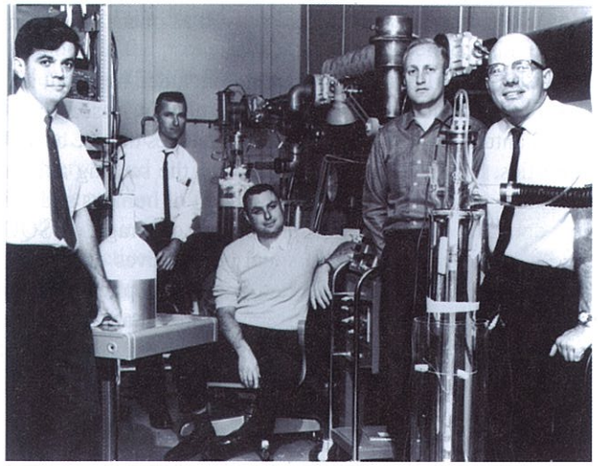

FIGURE 5.2: Photograph of the research team at Ford in 1964. Standing, left to right, J. Lambe, J. Zimmerman, R. Jaklevic, J. Mercereau. Seated, A. Silver. Courtesy of Ford Research Labs (Previously printed in *Physics Today*).

At the time, I was doing nuclear magnetic resonance (NMR) research in the same laboratory and was exposed to and intrigued by Lambe's unexplained discovery. Although the exact sequence of the events is uncertain, I joined him to help resolve the dilemma.

Critical to our success was that the Ford Motor Company Scientific Laboratory afforded most staff members the freedom to conduct self-motivated research. At one point, our new department manager asked if we knew what we were doing. We said probably not, but were determined to find out. That was that and we continued on.

Although we had only a general knowledge of superconductivity, we were inclined to attribute the effects to superconductivity of In contacts on the Si samples. The signals appeared at about the critical temperature of In (3.4 K) as we pumped on LHe. I should note here that the In contacts had been scratched in the process of characterizing the Si. Since direct observation of flux quantization in superconductors had recently been reported, we thought this was also relevant. We set out to understand the relevant literature, particularly F. London's theory of flux quantization[1].

The next task was to design experiments to replicate the microwave effects. Jaklevic, who had thin-film vacuum-deposition equipment, was engaged to deposit thin film superconductors such as In, Sn, and Pb on microscope slides. Small samples that fitted into the microwave cavity were cut; no signals were observed. However, when we damaged the films, either by scratching or, in the case of Pb, heating in air to corrode the Pb, we began to get familiar signals.

Jim Mercereau had joined the Laboratory from the California Institute of Technology, and was

interested in flux quantization in superconductors. He informed us of Josephson's recent publication[8], P.W. Anderson's interpretation[10] , and the Anderson and Rowell experiment[9]. These papers were certainly intriguing but not fully understood at that time. We were particularly interested in Anderson's physical description in terms of a macroscopic quantum wavefunction representing the Cooper pairs and its associated phase as being responsible for the behavior of the Josephson current in an applied magnetic field. Relating the magnetic field periodicity to the flux quantum by "carving" multiply connected thin films with microbridges was not very successful because of strong demagnetizing effects. Since there was no way we could relate the physics of thin film microbridges to Josephson tunnel junctions, we did not publish the microwave experiments until later[11].

5.2.2 Thin-Film Josephson Tunnel-Junction Quantum Interferometer

Arnold Silver

At that time, Jaklevic, Lambe, Mercereau, and I decided to try to produce the analog of a two-slit optical interferometer by using two Josephson tunnel junctions (JJ). The motivation was to demonstrate phase control of the superconducting current. Bob Jaklevic had the lead role here, first producing Josephson junctions, and then the two-junction thin-film interferometer shown in Figure 5.3. Since the magnetic field was in the plane of the films, we would be able to make quantitative measurements. Jaklevic's fabrication was successful and in late 1963 we began testing the two-junction device. Jaklevic called after lunch to say that he had a device cooled and was looking at the characteristic static current-voltage ($I-V$) curve of the JJ on an oscilloscope as it varied rapidly under a changing magnetic field. We assembled quickly and discussed what the next step should be. Mercereau suggested we take data and we began recording the critical current (I_c), read from the oscilloscope trace, as a function of the magnet current. The device was situated in a completely unshielded double glass cryostat in common use at that time, with liquid nitrogen (LN2) in the outer dewar and LHe in the inner dewar. Anything that moved in the lab or the adjacent hallway caused the critical current to change. The magnetic field period was so small that it soon became clear that the noise in the local magnetic field would render data, taken at the speed of manual reading and recording, almost meaningless. We needed to record the data on a time scale short compared with the changes in the ambient magnetic field. We had no equipment that could record the critical current directly.

At this point, I thought that I could assemble an automated recording system in short order. Jaklevic's junctions were of sufficiently high quality that when we displayed the voltage vs time, we observed a nearly square waveform switching between $V = V_g$ (the energy gap voltage) and $V = 0$. The fraction of the period where $V = V_g$ depended linearly on the critical current. From my NMR experience, I knew we could record this signal vs magnetic field using a synchronous detector, essentially one part of a lock-in amplifier. I collected a synchronous detector and X-Y recorder from my lab and found the dynamic range insufficient to record large and small I_c on the same trace. I remedied this by operating the synchronous detector out-of-phase with the current waveform. After reconvening, we made X-Y recordings of I_c vs magnetic field for two devices that Jaklevic had available. Figure 5.4 shows the two-junction interference patterns superimposed on the Fraunhofer-like dependence of the junction I_c. By then, the afternoon had passed and we went out to celebrate with pizza and wine!

The next task was to publish the work as soon as possible. We were concerned that Anderson and Rowell at Bell Labs were trying the same experiment with substantial lead time. Fortunately, this was not the case. We prepared the manuscript and submitted it to the *Physical Review Letters* as

[10] P.W Anderson, *Lectures on the Many-Body Problem*, Vol.II, edited by E.R. Caianiello (Academic Press, New York, 1964)
[11] J. Lambe et al., *Phys. Lett.* 11 (1964) 16

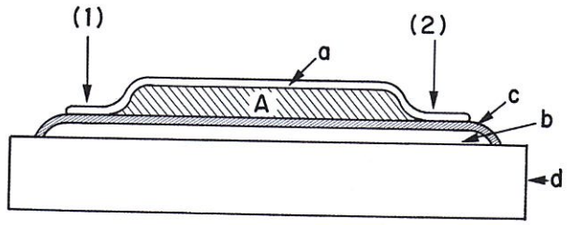

FIGURE 5.3: Cross-section of the first two-junction, thin-film, interferometer. (1) and (2) are Josephson junctions. The superconducting films are labeled a and b; c is the oxide barrier, d - the quartz substrate. Cross-section of the deposited insulating film is labeled A - it defines the loop area. Reprinted by permission from ref.12 (©1964 American Physical Society).

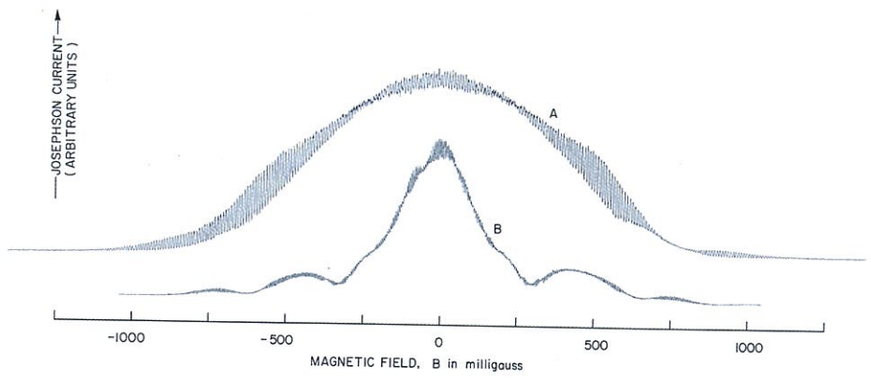

FIGURE 5.4: The first interference patterns illustrating both the single junction and two-junction interference in devices A and B. Reprinted by permission from ref.13 (©1964 American Physical Society).

rapidly as possible[12]. While we recognized the magnetic sensitivity of the technology, our focus was on the physics of long-range phase coherence. Meanwhile we planned and successfully performed two new experiments[13] with thin film JJs: First, the observation of quantum interference due to the magnetic vector potential in a magnetic field-free region, the Aharonov-Bohm (A-B) effect. Although we used the same measurement techniques as for the first interferometer experiments, the results were noisier. The A-B experiment presented a challenge to fabricate and insert a small solenoid into the thin film interferometer (see Figure 6 in Jaklevic et al.[13]). The solenoid current leads acted as an antenna for rf noise. In addition, the A-B experiment does not show the Fraunhofer suppression of I_c because there is no magnetic field at the junctions, although there is a vector potential.

Second, we measured the de Broglie wavelength of the supercurrent. This involved injecting a current into the superconducting film between the two JJs and measuring the phase shift as a function of the supercurrent.

[12] R.C. Jaklevic et al., *Phys. Rev. Lett.* 12 (1964) 159
[13] R.C. Jaklevic et al., *Phys .Rev.* 140 (1965) A1628

5.2.3 Point Contact Devices — dc SQUID

Arnold Silver

As our experiments were proceeding, Jim Zimmerman joined the activity. This marked the beginning of what would become SQUIDs. Fabricating tunnel junction devices was a slow, low-yield process. Zimmerman tried some other approaches to producing the "junctions" needed for future experiments and devices. He crossed two Nb ribbons and applied pressure from a hanging weight (Figure 5.5). A dab of epoxy permanently fastened the two ribbons together. This produced two weak-links with a small opening between them, matching the topology of the two-junction interferometers. These weak-links exhibited single-valued $I-V$ characteristics, which modulated as a magnetic field was applied to the aperture. From this we observed the periodic interference behavior determined by the size of the small aperture between the ribbons. There was no single-contact Fraunhofer effect. The single-valued $I-V$ curves permitted direct measurements with a low-noise amplifier without the need for a synchronous detector[14]. Since all our previous experiments were with type I superconductors, a new feature was the observation of macroscopic quantum interference in type II superconductors.

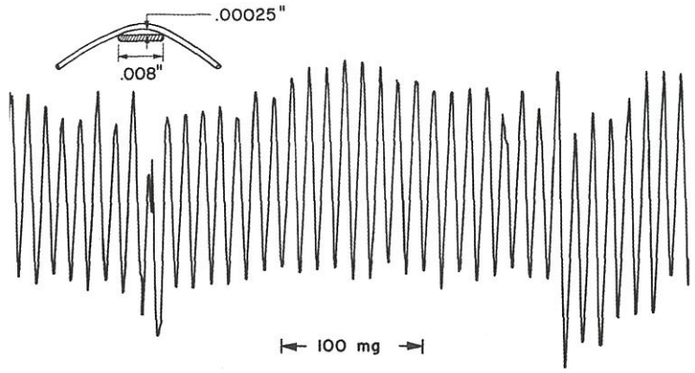

FIGURE 5.5: Cross-section of crossed Nb ribbons (upper left) and the recorded quantum interference pattern[14]. Reprinted by permission of Elsevier.

Eventually the team dissolved. Lambe and Jaklevic turned to other activities and Mercereau established an effort at Ford in California to pursue applications of quantum interferometers. Zimmerman and I continued to seek better methods of adjusting the critical current of the contacts. Devices made with a sharp point raised on a flat Nb surface and pressed against a second flat Nb surface were successful and provided impetus for an adjustable point-contact device. Jim fashioned a 000-120 (0.66 mm) Nb screw and tapped a corresponding hole in a Nb block. This block was pressed against a second Nb block and the screw adjusted to make contact with the second block. In this way, we had a mechanically adjustable contact. By using two screws with a hole drilled between them, we fashioned what became for a considerable time the dc-SQUID prototype (Figure 5.6). The adjustable-screw point-contact was our device of choice during the remainder of the 1960s. While others adopted this approach using 0-80 (1.19 mm) screws, we used 000-120 screws because Jim

[14] J.E. Zimmerman and A.H. Silver, *Phys. Lett.* 10 (1964) 47

had Nb wire whose diameter was very nearly that size. Therefore, we did not have to machine the screw, only run the wire through the die. At one point, our machine shop fabricated a device that did not work; we found they did not make it of Nb because Nb is difficult to machine; eventually our machine shop refused to do it. Consequently, we acquired a small milling machine and fabricated Nb devices in our lab.

Continuously repeating "superconducting quantum interference device" became tiresome and Zimmerman suggested we shorten the name to SQUID, which was not used outside Ford for some time. Consequently, when Jim and I authored a chapter in Academic Press' *Applied Superconductivity* in 1969-70, we avoided the name. By the time the book was published in 1975, the name SQUID had been widely adopted.

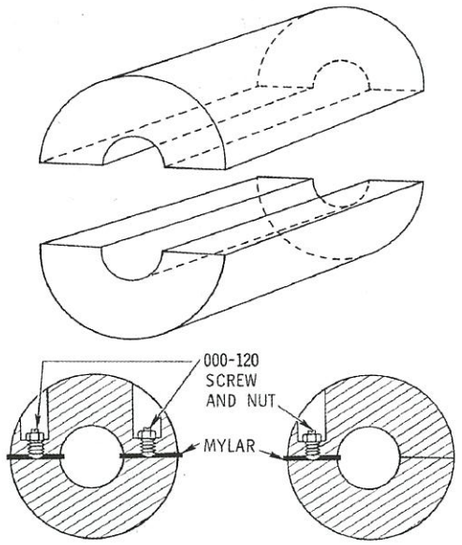

FIGURE 5.6: Drawing of typical point-contact SQUIDs machined from bulk Nb.

As the development of the SQUID structure was proceeding, we continued both to improve the measurement techniques and to develop a satisfactory model to understand and design SQUIDs. Our thinking shifted from an interferometer controlling a quantum wave to the device measuring the magnetic flux in units of the flux quantum, Φ_0.

Two concerns occupied a great deal of our time: what was the current-phase relation for the point contacts and how could we express the circulating currents and magnetic flux in terms of the independent magnetic field or external current? There was no a priori reason to accept the Josephson current-phase relation for point contacts. We tried to use a linear (London-like) relation with strong depairing. This did not yield the continuous mathematical solution that we desired; the Josephson relations certainly did. We adopted the Josephson model and developed equations describing the magnetic flux and the circulating supercurrent, I_J, in the SQUID ring as a function of applied currents and magnetic fields.

At first, we adjusted I_c at room temperature and then cooled and tested the devices. Jim devised wrenches with long handles that enabled us to adjust the contacts in situ at LHe temperatures. Using a point-contact SQUID, we measured the magnetic field (London moment) produced by a rotating superconductor. This SQUID had a hole about 10 mm in diameter, and was rotated at a fixed frequency in LHe as we measured the shift of the interference pattern due to the induced magnetic field[15]. To do this experiment we moved our setup to a remote nonmagnetic building on the Oakland County campus of the University of Michigan. We could correlate occasional shifts in the interference pattern with the motion of vehicles that were visible several hundred yards away, illustrating the extreme sensitivity of SQUIDs.

5.2.4 The rf SQUID

Arnold Silver

The RF SQUID was invented in another case of serendipity. In addition to improving the device

[15] J.E. Zimmerman and J.E. Mercereau, *Phys. Rev. Lett.* 14 (1965) 887

structure, we sought continuously to improve the measurements. Measurements of point contact devices were initially performed with low frequency transformers and dc amplifiers connected to an oscilloscope or X-Y recorder. These transformers and amplifiers did not have very wide bandwidths and the amplifiers were noisy. I thought that we could improve both by using rf instrumentation that was available from my NMR research. We used an rf source to supply the current and a low noise rf amplifier as the detector. A simple LC-resonant circuit connecting the SQUID to the amplifier achieved large voltage gain, large signal bandwidth, and limited the noise bandwidth. An integrated diode functioned as a homodyne detector to produce a base-band signal.

This approach worked well and was adopted. We occasionally observed that the rf signature changed and became independent of one of the contacts; this was the single-junction ring that became the rf SQUID[16]. This produced new results that we would not have discovered had we continued with traditional dc electronics. In addition to the $V(I_c)$ *vs* magnetic field response, there is also an rf-current-dependent response, which we called the rf $V-I$ curve. This is illustrated in Figure 5.7. We developed a simplified magnetic state equation for the rf SQUID (Φ *vs* Φ_x): $\Phi + LI_c \sin\delta = \Phi_x + n\Phi_0$. Here, Φ and Φ_x are the enclosed and external fluxes, δ is the phase difference across the junction and n is an integer. We derived the magnetic states of the rf SQUID in terms of one universal parameter that characterizes the SQUID, $\beta_{rf} \equiv 2\pi LI_c/\Phi_0$. Inserting β_{rf} into the expression above yields a frequently used equation in terms of the junction phase, $\delta + \beta_{rf}\sin\delta = \delta_x$.

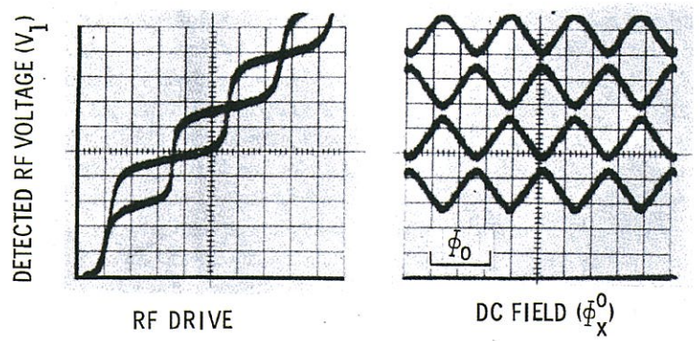

FIGURE 5.7: Typical response of an rf-SQUID. At left, "rf $V-I$ curve" at zero and half-flux quantum applied magnetic flux. At right, magnetic field dependence of rf voltage for fixed values of rf drive. Reprinted by permission from Silver and Zimmerman *Applied Superconductivity* vol. 1, New York: Academic Press 1975.

For $\beta_{rf} < 1$, the magnetic states are single valued, the SQUID can proceed continuously from one state to the next, and can be set stably at $\Phi = \Phi_x = \Phi_0/2$ and $I_J = 0$. This condition cannot exist for dc SQUIDs no matter the value of LI_c/Φ_0. This appeared to be an unusual situation and we spent considerable time trying to understand its significance, without success. It is now important for qubit research. Further, we reduced the wiring between room temperature and the SQUID at LHe to one rf cable that carried the rf drive, reflected signal and the flux generating static and low frequency current. We frequently injected the flux-generating current into the SQUID inductance instead of using a second coil.

[16] A.H. Silver and J.E. Zimmerman, Phys.Rev.Lett. 15 (1965) 888

5.2.5 Linear SQUID Response and Single Flux Quantum Transitions

Arnold Silver

While the SQUID was demonstrably a very sensitive detector, its response was nonlinear and periodic. We conceived and developed a "flux-locked loop" that linearized the response without sacrificing sensitivity, but reduced signal bandwidth. Again, this was a result of prior experience using modulation techniques to stabilize magnetic fields, and the availability of suitable equipment. Once we had a linear magnetometer, we used one SQUID to observe the magnetic states and single flux quantum transitions of a second SQUID[17]. We confirmed the behavior of $\beta_{rf} > 1$ (hysteretic in flux) and $\beta_{rf} < 1$ (nonhysteretic in flux) SQUIDS, and attempted to measure the current-phase relation of the point contacts.

5.2.6 R-SQUID, Oscillators and Detectors

Arnold Silver

Once we settled on the rf SQUID as the preferred device, we eliminated the second point contact and tried several other methods to close the ring. We found that a SQUID with a small resistance r in the loop (R-SQUID) behaved dynamically in much the same way as the rf SQUID. The rf $V-I$ curves were similar except for the absence of flux modulation at low frequencies. While the SQUID has perfect long-term memory, the R-SQUID has an L/r decay time. A second difference is that the junction in the R-SQUID can have a static voltage V_0 developed by a static current through r. Then the junction oscillates at the Josephson frequency given by the relation $V_0/f = \Phi_0 \approx 2.07\ \mu V/GHz$.

The physics is that the junction pulses single flux quanta into the SQUID L, and the flux escapes with a time constant L/r. The pulses are non-sinusoidal and have high harmonic content until the frequency approaches the plasma frequency. We used r between 10 and 50 $\mu\Omega$. These oscillations could be absorbed to excite resonant rf and microwave structures that were closely coupled to the SQUID loop. Embedding an R-SQUID in an X-band cavity in the cryogenic probe, we directly observed the cavity resonances[18]. We measured the standing wave resonance of the coaxial cable connecting the SQUID to the rf electronics. This experiment exhibited additional nonlinear properties of the SQUID. We observed the zero-field nuclear magnetic resonance of Co^{60} by placing finely powdered cobalt in the SQUID inductance and scanning the Josephson frequency across the Co^{60} resonance frequency. The latter two experiments were performed in the usual rf SQUID mode using our 27 MHz measuring system. The resonances were observed in a Josephson frequency scan with additional responses at $f_{res} \pm 27$ MHz, representing parametric idlers. In effect, the SQUID was operating as a parametric amplifier. Decades later, such parametric interactions were used to produce very low-noise microwave amplifiers[19].

Most experiments were performed with the SQUID devices sealed in a cylindrical stainless-steel tube. The stainless-steel tube was evacuated and refilled with a small amount of He heat-exchange gas. Thus, the devices were slightly isolated from the boiling LHe. We noticed, in the absence of any static current, a very-low-frequency oscillation whose linewidth was linearly dependent on the temperature. We attributed the voltage to a thermal emf from a temperature gradient across the metal resistor in the R-SQUID and the linewidth to Nyquist noise at LHe temperatures. This work continued jointly with R. Kamper at NBS in Boulder in an investigation of a primary temperature

[17] A.H. Silver and J.E. Zimmerman, *Phys. Rev.* 157 (1967) 317
[18] J.E. Zimmerman, et al., *Appl. Phys. Lett.* 9 (1966) 353
[19] A. Smith, et al., *IEEE Trans. Magn.* 21 (1985) 1022

standard[20].

In 1968, Jim left the Scientific Lab and joined Ford's Aeronutronics subsidiary in California to work on applications of SQUIDs. From there he moved to the National Bureau of Standards in Boulder, CO in 1970. I left Ford in 1969 to join The Aerospace Corporation in California.

5.2.7 SLUGs at Cambridge

John Clarke

I became a research student in the Royal Society Mond Laboratory, then part of the Cavendish Laboratory at the University of Cambridge, in October 1964. The Mond was presided over—with great kindness—by David Shoenberg. My thesis supervisor was Brian Pippard (Figure 5.8). He gave me a project to investigate the electrical resistance of the superconductor-normal metal (SN) interface, a topic that later became of considerable interest. Brian suggested I measure the resistance of SNS sandwiches in which the normal metal was too thick to sustain a supercurrent. Since the voltages would be tiny ($\sim$ 1 pV), Brian asked me to look into improving the cryogenic galvanometer he and George Pullan[21] had previously developed. This device involved a mirror and magnet suspended by a quartz fiber inside a vacuum can, surrounded by liquid helium, at the center of a Helmholtz coil through which one passed the current to be measured.

FIGURE 5.8: Brian Pippard (ca 1973; courtesy Cavendish Laboratory).

My thinking about ways to upgrade the galvanometer was brought to an abrupt end, however, by a Mond seminar given by Brian Josephson. He described the experiments demonstrating flux quantization, his own theory of pair tunneling, and the observation of quantum interference at Ford earlier that year[13]. To me, as a new research student, it was utterly fascinating, and I remember thinking how I would like to work on these new ideas. My opportunity came much sooner than I could possibly have expected! The very next day, Brian Pippard bounced into my laboratory with a big smile on his face. "John, how would you like a voltmeter with a resolution of $2 \cdot 10^{-15}$ V in 1 second?" he asked. I somewhat cautiously admitted that this did seem like an interesting possibility. Brian excitedly explained that he had dreamed up his new concept of a voltmeter the previous evening after hearing Brian Josephson's seminar. He sketched on the blackboard a voltage source V in series with a resistance R and an inductance L that was perfectly coupled to a SQUID, also with inductance L. The current through the resistor and inductor required to generate the flux quantum in the SQUID was simply Φ_0/L, and the corresponding static voltage V was thus $(\Phi_0/L)R$. Setting the time constant $\tau = L/R = 1$ s, Brian pointed out that the resolution was $2 \cdot 10^{-15}$V. His initial idea was to make a digital voltmeter, each digit being a flux quantum.

Needless to say, I was thrilled—not least because my enthusiasm for dangling a tiny magnet and mirror from a quartz fiber inside a vacuum can had already begun to wane. I talked to John Adkins, who had already made thin-film Josephson junctions in the Mond. He was not encouraging about the longevity of such devices, and I looked around for better alternatives. I came across an article

[20] A.H. Silver, et al., *Appl. Phys. Lett.* 11 (1967) 209
[21] A.B. Pippard and G.T. Pullan, *Proc. Camb. Phil. Soc.* 48 (1952) 188

by Zimmerman-Silver[14], which seemed like a good place to start. I made a similar device with the additional twist that I could adjust the vertical force on the bent wire (top of Figure 5.5) from the top of the cryostat. I remember rolling out a piece of niobium wire to make the narrow piece of sheet. In those days, one took one's glass cryostat to the helium liquefier for Paul Booth to fill it. After returning my dewar safely to my lab, I connected the simple current-voltage measurement system I had built—and my SQUID worked! I spent much of that day adjusting the force on the wire, and discovered that I could vary the critical current quite readily. Sometimes I observed oscillations in critical current when I varied the applied fields and sometimes I did not. I made several variants of this design, and they all more or less worked, but I was not entirely convinced that the device was sufficiently stable to use routinely as a voltmeter.

An important part of one's life in the Cavendish was—and still is—coffee at 11 a.m. and tea at 4 p.m. The Mond students and staff always sat at the same table. One tea-time, I discussed how I was looking for a Josephson junction technology that did not require thin films yet was mechanically stable. Paul Wraight—with whom I shared my lab—suddenly looked at me and said something like "How about a blob of solder on a piece of niobium wire? Solder is a superconductor and you keep telling me that niobium has a surface oxide layer." We rushed back to our lab, where fortunately I still had some liquid helium left in my dewar from the experiment I had been running earlier in the day. I made two devices consisting of a blob of lead-tin solder melted onto a short length of niobium wire, attached some leads and lowered the devices into the helium bath. They both worked! The critical currents were roughly 1 mA. Paul and I were thrilled. The next morning, Brian Pippard wandered into our lab to see how things were going, and Paul and I proudly showed him one of our new gadgets. Brian contemplated it thoughtfully for a while, and then—with a smile—said, "It looks as though a slug crawled through the window overnight and expired on your desk!"

I tried hard to make a SQUID by freezing a solder blob on a piece of niobium wire doubled back on itself so that there were two junctions. I applied a magnetic field to the loop of wire sticking out of the solder blob. This never worked, in retrospect because the inductance of the loop was too high. One day, I decided instead to pass a current along the wire, and immediately saw oscillations in the critical current when I changed the current. It did not take me very long to discover that the loop was irrelevant—I needed to pass the wire through the solder only once, and apply a current to the wire [Figure 5.9(a)]. How did it work? Apparently, there were typically just two or three dominant junctions between the wire and the solder. The current in the wire generated a magnetic field in the penetration depths of the wire and solder, so that the area of the "SQUID" was given by the sum of the penetration depths times the separation of the junctions[22]. The periodicity in current ranged randomly from about 0.2 to 1 mA. However unlikely, the majority of these devices showed interference between two or three junctions, and they generally survived at least scores of thermal cyclings. It is interesting to note that, as I increased the current through the niobium wire, I could generally observe thousands of oscillations in critical current with no evident diminution in amplitude. This lack of a discernible Fraunhofer pattern [Figure 5.9(b)] suggested that the junctions were essentially points.

The name for this new device had already been unwittingly provided by Brian Pippard, and we simply had to work out what it stood for. And so the "Superconducting Low-inductance Undulatory Galvanometer" (SLUG) was born.

Brian Pippard's original concept was a digital voltmeter, but I soon realized that one could readily measure changes in flux that were much less than one flux quantum. I applied a static current and a sinusoidal current through the SLUG [leads "I" in Figure 5.9(a)] so that voltage pulses appeared across the voltage leads (leads "V"). The area under these pulses depended on the critical current of the SLUG, enabling me to determine the critical current, and hence the current in the niobium wire [leads "I_B" in Figure 5.9(a)] to about ± 1 μA, using simple electronics. Once I had this worked

[22] John Clarke, *Phil. Mag.* 13 (1966) 115

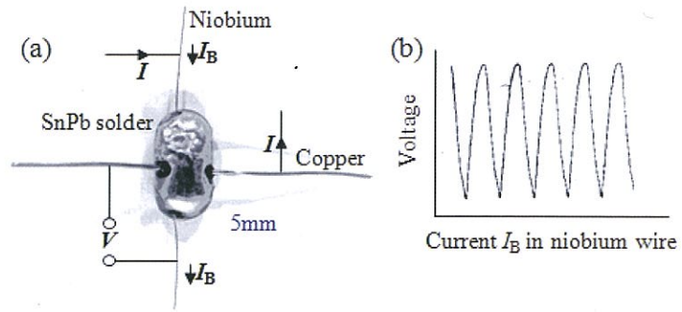

FIGURE 5.9: The SLUG. (a) Photograph showing attachment of current (I), voltage (V) and flux bias (I_B) leads. (b) V *vs* I_B.

out, I immediately put the SLUG to use as a voltmeter. A postdoctoral fellow in the Mond, Steve Lipson, was interested in measuring the resistance of a single crystal of copper (to be used for measurements of magnetoresistance) that he estimated to be about $10^{-8}\Omega$. We made a voltmeter by connecting the Cu block in series with a manganin wire, with a measured resistance of about $10^{-5}\Omega$, and the niobium wire through the SLUG. The idea was to make a potentiometer, adjusting the currents in the two resistors to produce zero current in the SLUG. After Steve and I cooled down our potentiometer, I was chastened to observe that the output from the SLUG was horribly noisy. Further inspection showed that the "noise" was in fact due to currents induced in the loop by 50-Hz magnetic fields. For the next run, Steve soldered a lead-foil box that enclosed the circuit, and our pickup problem was solved. This was an invaluable lesson for me: if you have a sensitive magnetometer or voltmeter, you have to protect it from the real world, which is a very noisy place.

I used the SLUG as a voltmeter for the rest of my graduate career (Figure 5.10), mostly to investigate SNS Josephson junctions. With a typical circuit resistance of 10^{-8} Ω, I could measure a voltage of about 10^{-14} V in a second. I built a feedback circuit incorporating an amplifier and an integrator that fed current back into the manganin resistor to maintain zero current in the Nb wire of the SLUG. Other members of the Mond subsequently used the SLUG, notably Eric Rumbo for measuring thermoelectric voltages and Pippard, Shepherd and Tindall for measuring the resistance of the SN interface—my original thesis topic.

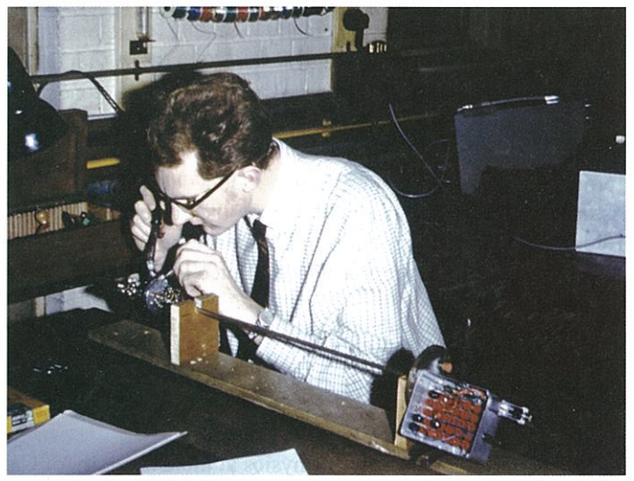

FIGURE 5.10: John Clarke makes a SLUG circa 1966. In those days, research students wore ties! (Courtesy Gordon Donaldson)

In addition to making a femtovoltmeter, I played with various other ideas with SLUGs. One

was a magnetometer, based on the idea of a superconducting flux transformer[23] (Figure 5.11). I inserted the two ends of the niobium wire of the SLUG into a blob of molten solder to make a superconducting contact, forming a superconducting loop, typically 50 mm in diameter. When I applied a magnetic field to the loop, the induced current was detected by the SLUG, which thus became a magnetometer. I made this null-balancing by connecting the output from my feedback loop to a 1000-turn, copper-wire coil that was tightly coupled to the niobium loop. I remember showing the magnetometer to Brian Pippard who stared at it thoughtfully for a while, and then said something like, "You know, John, if you were to put a twist in the loop, you would have a gradiometer." As usual, Brian was ahead of his time, but I did not need a gradiometer at that point in my life and did not then pursue the idea. In an attempt to improve the current-sensitivity of the SLUG, I coupled a 10-turn, niobium wire coil to the niobium-wire loop[23]. The voltage signal was connected to the ends of the 10-turn coil, in series with a resistor. Because of the relatively poor coupling between the 10-turn coil and the SLUG loop, as I recall, this arrangement improved the current sensitivity by a factor of only 2 or 3, but at least it worked.

As an extension of these ideas, I connected the voltmeter with the 1000-turn input coil to the output of a second SLUG, biased into the voltage state (Figure 5.11). Because setting up the bias current of the input SQUID produced a substantial flux in the superconducting loop of the magnetometer, I devised a thermal switch—a length of bifilar-wound manganin wire wrapped around a region of the niobium loop—and surrounded it with a blob of epoxy to provide thermal insulation from the helium bath. By passing a current through the heater, I could drive the niobium wire into the normal state, releasing the flux trapped in the loop. After juggling the four bias currents for a while, I actually made these cascaded SLUGs work[23].

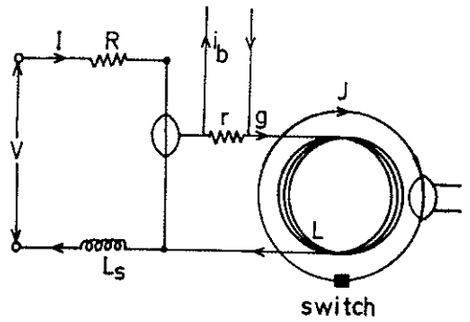

FIGURE 5.11: Two-SLUG amplifier. The niobium wire of the right-hand SLUG is connected into a superconducting loop, forming a magnetometer. A change in the current I in the left-hand SLUG induces a current into the 1000-turn coil, thus generating a current J in the magnetometer loop and finally an output voltage from the right-hand SLUG.

Another idea was an inductor-resistor relaxation oscillator[23]. SLUGs with higher values of critical current usually had hysteretic current-voltage characteristics. I connected a resistor in series with an inductor across the current-voltage leads of a SLUG, and applied a bias current to produce square wave oscillations. I had visions of using this SLUG oscillator to read out a second SLUG, but never actually attempted to do this.

5.2.8 SQUIDs at Berkeley

John Clarke

I moved to the Department of Physics at the University of California, Berkeley in January 1968. During the early 1970s, there was a general shift towards using the rf SQUID, including devices made of thin films deposited on cylindrical substrates. In 1973, a new postdoctoral scholar, Wolf Goubau, and a new graduate student, Mark Ketchen, and I decided to make dc SQUIDs borrow-

[23] John Clarke, in *Proc. Symposium on the Physics of Superconducting Devices*, University of Virginia, Charlottesville, April 28-29, 1967, Bascom S. Deaver, Jr. and William S. Goree, eds., page D1.

ing three ideas from the rf SQUID: a cylindrical geometry (which gives a large area for a low inductance), a tank circuit readout and thin films. At about the same time, Paul Hansma's group, at the University of California, Santa Barbara, had achieved good reproducibility and longevity with Nb-NbOx-Pb tunnel junctions[24], and we decided to adopt his technique. Figure 5.12 shows the geometry of our SQUID, grown on a 3-mm-diameter quartz tube[25]. We used shadow masks to pattern the films, which had a minimum linewidth of 75 μm. The slit in the PbIn cylinder was scribed with a razor blade. Subsequently, we submerged the SQUID in a solution of Duco cement (our favorite insulator!) dissolved in acetone and deposited a PbIn film over the slit and the various metal strips to reduce their inductances. This process sounds extraordinarily primitive by today's standards, but we could cool these devices to liquid helium temperature many times with no degradation.

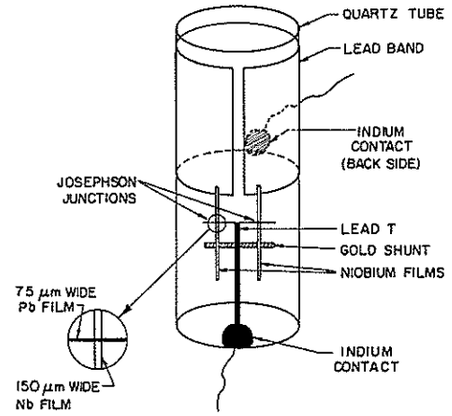

FIGURE 5.12: Configuration of cylindrical dc SQUID.

We tested our SQUIDs using 100-kHz flux modulation and a homemade flux-locked loop. We boosted the 100-kHz voltage across the SQUID with a cold resonant circuit, giving a substantially enhanced signal into the preamplifier, and a correspondingly reduced flux noise. The white noise in one device, $3.5 \cdot 10^{-5}\ \Phi_0\ \mathrm{Hz}^{-1/2}$, was a record at the time, and yielded a magnetic field noise of about 10 $\mathrm{fTHz}^{-1/2}$. We used our cylindrical SQUIDs in a variety of experiments. For example, Wolf, Tom Gamble and I used them for magnetotellurics, a geophysical surveying technique[26].

During the time we were working on our experiments, Claudia Tesche and I developed the theory for the dc SQUID[27]. Claudia spent roughly a year carrying out the computer simulations including the effects of white noise, which arises from Nyquist noise generated in the resistive shunts required to eliminate hysteresis on the current-voltage characteristics of the tunnel junctions[28]. We worked out the parameters required to minimize the noise energy of the SQUID, $\epsilon(f) = S_\Phi(f)/2L$; here $S_\Phi(f)$ is the spectral density of the flux noise and L is the inductance of the SQUID loop. At 4.2 K and for the optimized parameters $\beta_{dc} \equiv 2LI_0/\Phi_0 \approx 1$ and $\beta_c \equiv 2\pi I_0 R^2 C/\Phi_0 \leq 1$, the essential results are $S_\Phi(f) \approx 16 k_B T L^2/R$ and $\epsilon(f) \approx 9 k_B T L/R \approx 16 k_B T (LC)^{1/2}$, where R and C are the shunt resistance and self capacitance of each junction. These results make it clear that "smaller is better" and that $S_\Phi(f)$ and $\epsilon(f)$ decrease linearly with temperature. This theory has proved to be a good predictor of experimental results over a wide range of SQUID parameters and temperature. For a typical SQUID at 4.2 K, one finds $S_\Phi^{1/2}(f) \approx 10^{-6}\ \Phi_0 \mathrm{Hz}^{-1/2}$ and $\epsilon(f) \approx 10^{-32}\ \mathrm{JHz}^{-1} \approx 100\hbar$. When the temperature of the SQUID is lowered to a few tens of millikelvin, the noise energy is typically on the order of $\hbar$ at frequencies f above the $1/f$ noise. Claudia and I also calculated the noise current circulating around the SQUID loop and its partial correlation with the voltage noise[29]. These terms turn out to be crucial to the optimal design of SQUID amplifiers (see Section 5.7).

[24] C.M. Falco et al., *Phys. Rev. B* 10 (1974) 1865

[25] John Clarke et al., *J. Low Temp. Phys.* 25 (1976) 99

[26] T.D. Gamble et al., *Geophys.* 44 (1979) 53

[27] C.D. Tesche and J. Clarke, *J. Low Temp. Phys.* 29 (1977) 301

[28] The theory for the non-hysteretic characteristics of resistively shunted junctions (RSJ) was independently developed in D. E. McCumber, J. Appl.Phys. 39 (1968) 3113 and W. C. Stewart, *Appl. Phys. Lett.* 12 (1968) 277.

[29] C.D. Tesche and J. Clarke, *J. Low Temp. Phys.* 37 (1979) 397

5.2.9 The Square Washer SQUID

John Clarke

I think the cylindrical SQUID played a role in turning the attention of the community back from the rf SQUID to the dc SQUID despite the fact that, to my knowledge, no other group adopted this design. One reason may have been the realization that higher performance required tunnel junctions with smaller areas. Nobody was excited about using photolithography—having just been imported from the semiconductor industry—on a cylindrical surface! After graduating from Berkeley, Mark Ketchen moved to IBM, Yorktown Heights, where he and Jeffrey Jaycox developed the square washer SQUID[30]. Mark described this device as "The result of putting your thumb on one end of the cylindrical SQUID and squashing it flat, transforming it into a washer with a spiral input coil". The SQUID itself is a thin-film square washer, typically 1 mm across, with a hole in the middle and a slit that runs to the outer edge where two tunnel junctions are grown (Figure 5.13). The junctions are completed with an upper film that connects them, thus closing the SQUID loop. An insulating layer is deposited over the square washer, followed by a thin-film, spiral coil. A current passed through the coil generates a magnetic flux that the washer focuses into the hole, giving efficient coupling between the coil and the washer. However, these SQUIDs had initially one drawback: they were made from a PbInAu alloy, and were not particularly robust. Fortunately, in 1980 John Rowell and coworkers[31] developed the niobium-based junction technology that is universally used today. One first deposits a Nb film on a silicon wafer, followed immediately by an Al film a few nanometers thick. The Al film is subsequently oxidized in a controlled oxygen pressure for a prescribed time. The gas is pumped out and the upper Nb electrode is deposited. Subsequently, the "trilayer" is patterned to form Josephson junctions. The technology for the Nb-based, square washer dc SQUID–the workhorse of today's SQUID applications–was essentially in place by the early 1980s.

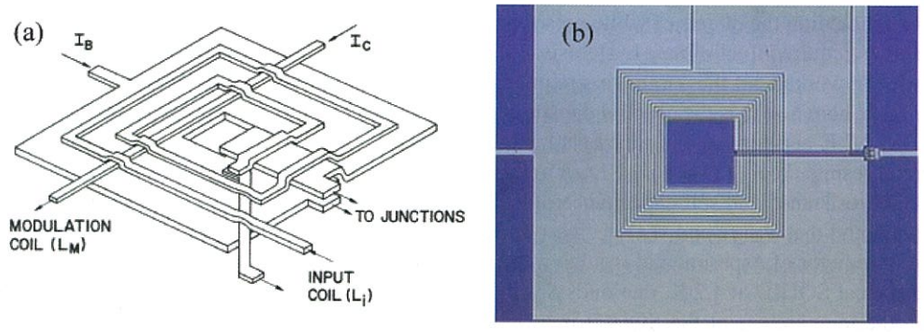

FIGURE 5.13: Square washer dc SQUID. (a) Schematic of original design. (Reproduced by permission from Reference 30.) (b) Today's typical practical device. The two resistively shunted Josephson tunnel junctions are at the right-hand edge, one on each side of the slit.

[30] M.B. Ketchen and J.M. Jaycox, *Appl. Phys. Lett.* 40 (1982) 736
[31] J.M. Rowell et al., *Phys. Rev. B* 24 (1981) 2278

5.2.10 The rf SQUID Revisited

John Clarke

The theory of the rf SQUID was worked out by Kurkijarvi[32]. In the hysteretic or dissipative mode ($\beta_{rf} > 1$), the applied rf flux causes the SQUID to make transitions between quantum states and to dissipate energy at a rate that is periodic in Φ_x. This periodic dissipation in turn modulates the tank circuit Q, so that when it is driven on resonance with a current of constant amplitude, the rf voltage is periodic in Φ_x (Figure 5.7). A detailed analysis shows that the SQUID is optimized when $k^2Q \approx 1$, where k is the coupling coefficient between the SQUID loop and the inductor of the resonant circuit. The intrinsic noise energy is $\epsilon(f) \approx LI_0^2(2\pi k_B T/I_0\Phi_0)^{4/3}/2\omega_{rf}$. Since the noise energy scales as $1/\omega_{rf}$, there is a strong motivation to use a microwave driving frequency. For rf SQUIDs at 4.2 K coupled to a room-temperature preamplifier, however, extrinsic noise contributions—notably preamplifier noise and loss in the line coupling the SQUID and preamplifier—may far exceed the intrinsic noise.

Subsequently, it was realized that the noise energy can be much lower in the nonhysteretic or nondissipative regime $\beta_{rf} < 1$ in which the SQUID remains in the zero voltage state[33]. The SQUID behaves as a flux-sensitive, nonlinear inductor since the inductance of a Josephson junction for $I < I_0$ is given by $\Phi_0/2\pi(I_0^2 - I^2)^{1/2}$. Thus, the circulating current produced by an applied flux induces a change in the SQUID inductance. When the tank circuit is driven off-resonance at constant amplitude and frequency, a flux change in the SQUID changes the resonant frequency, so that the rf voltage is periodic in the applied flux. In the limit $I_0\Phi_0/2\pi \gg k_B T$, the intrinsic noise energy is $\epsilon(f) \approx 3k_B T/\beta_{rf}^2\omega_c$ when the drive frequency is set equal to the SQUID cutoff frequency, ω_c[33]. In principle, at low temperatures the nondissipative SQUID can rival the noise energy of the dc SQUID, but in practice at the required high frequencies its noise is dominated by the post-amplifier.

5.2.11 Today's SQUIDs

John Clarke

For most practical applications at and below He^4 temperatures, the dc SQUID is dominant. The square washer dc SQUID, involving Nb trilayer tunnel junctions and typically made in batches of several hundred on silicon wafers that are diced to produce individual devices, is virtually indestructible. At 4.2 K, its white noise is typically $10^{-6}\Phi_0$ Hz$^{-1/2}$, with a $1/f$ knee of roughly 1 Hz. In most applications, the SQUID is inductively coupled to a superconducting flux transformer, to form a magnetometer—with a magnetic field noise of around 1 fTHz$^{-1/2}$—or a first- or second-order gradiometer. As the temperature of the dc SQUID is lowered, its performance can approach the quantum limit[34]. Its simplicity of use—requiring only low frequency readout techniques—is very appealing, especially in applications requiring large numbers of SQUIDs, for example magnetoencephalography (Chapter 10). There is, however, one situation in which rf SQUIDs have an advantage: high-T_c, nondissipative rf SQUIDs at 77 K can be operated with a higher loop inductance—and thus a larger area—than dc SQUIDs, giving them a lower magnetic field noise[35]. Finally, both rf[33] and dc SQUIDs can be used as parametric amplifiers, and can achieve the quantum limit at low temperatures[36].

[32] J. Kurkijarvi *J. Appl. Phys.* 44 (1973) 3729
[33] K.K. Likharev, *Dynamics of Josephson Junctions and Circuits* (Gordon Breach, New York, 1986)
[34] M. Mück et al., *Appl. Phys. Lett.* 78 (2001) 967
[35] Y. Zhang et al., *IEEE Trans. Appl. Supercond.* 3 (1993) 2465
[36] M. Hatridge et al., *Phys. Rev. B* 83 (2011) 134–501.)

5.3 High-T_c SQUIDs

A. I. Braginski

5.3.1 Past and Present

After the news of high-temperature superconductivity in lanthanum-barium cuprate spread across the superconductivity community worldwide, the early weeks and months in 1987 witnessed incredibly hectic activity by every group capable of synthesizing one of the new materials in polycrystalline bulk or thin film form (Chapter 4). The scouting went in all possible directions and high-T_c SQUIDs were naturally included. It was not immediately obvious to all of us that higher-angle cuprate grain boundaries (GBs) act as Josephson weak links, so the first bulk and thin-film SQUIDs[37] were fabricated from polycrystalline yttrium cuprate $YBa_2Cu_3O_{7-\delta}$ (YBCO). It exhibited an incredibly high $1/f$ noise due to the penetration and motion of vortices at grain boundaries. As I recall, it was the late Masaki Suenaga who first pointed to the weak link properties of GBs in his late night talk at the "Woodstock of Physics", at the American Physical Society March Meeting of 1987. From then onwards the more fruitful efforts were directed towards synthesizing epitaxial, nearly single-crystalline thin films of YBCO and other rare earth cuprates (REBCO), from which controlled weak links and SQUID structures could be patterned and fabricated.

Glossary of High-T_c Junction Terms

- A bicrystal epitaxial substrate consists of two crystals of the same material, but different crystalline orientation, that are fused together. The grain boundary between the two crystals is reproduced in the film growing epitaxially on the polished and undamaged substrate surface.
- A step-edge junction is formed when an epitaxial film grows over a sharp step etched by a photolithographic method in the undamaged single-crystalline surface of a substrate. A change in the crystalline orientation at any sharp edge nucleates a grain boundary there.
- An edge or ramp junction, either low- or high-T_c, involves a relatively shallow edge or wedge patterned in a superconducting thin film electrode using photolithographic techniques. A thin barrier layer and superconducting counter-electrode are deposited on top and patterned such that a layered narrow bridge structure exists over the inclined edge (ramp) area.

The research on epitaxial films and on Josephson properties of grain boundaries in epitaxial YBCO thin films on bicrystalline $SrTiO_3$ (STO) substrates was initiated at IBM Yorktown Heights under the leadership of the late Praveen Chaudhari[38,39]. This seminal work on the critical current I_c dependence upon the grain boundary angle (Chapter 3) laid the foundation of what is still today the most frequently used and reliable high-T_c Josephson junction technology for SQUIDs operating at

[37] R. H. Koch, et al., *Appl. Phys. Lett.* 51 (1987) 200
[38] P. Chaudhari et al., *Phys. Rev. Lett.* 58 (1987) 2684
[39] D. Dimos et al., *Phys. Rev. Lett.* 61 (1988) 219

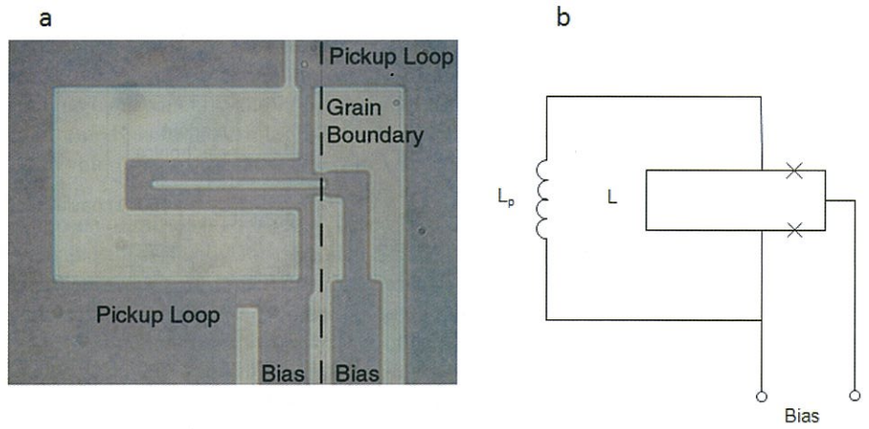

FIGURE 5.14: Directly-coupled high-T_c dc SQUID magnetometer: (a) photograph of layout on bicrystal substrate; (b) schematic diagram, where the two junctions are represented by crosses (reproduced from The SQUID Handbook, Figure 5.15, with permission).

or near the liquid nitrogen (LN2) temperature of 77 K. The dc SQUID loop is patterned such that two symmetric microbridges cross the GB. The typical range of angles is from 24° to 36° with a likely optimum around 30°. Many approaches to fabricating SQUIDs without using bicrystal substrates were demonstrated in the past, but only two withstood the test of time and are occasionally used in some applications: step-edge junctions, especially those on MgO crystal substrates which involve only one [100] tilt grain boundary[40] and edge or ramp junctions with PrBCO barriers[41]. All high-T_c junctions are internally shunted and their current-voltage characteristics roughly conform to the RSJ model. Therefore, high-T_c SQUIDs do not require shunting resistors (see the box "Glossary of High-T_c Junction Terms").

During the 1990s, epitaxial thin film and junction fabrication technologies reached a level of maturity sufficient to fabricate single-layer patterned structures, usually of YBCO, more or less reproducibly. On bicrystal substrates, the most typical and successful single-layer design of a magnetometer involves a small slit-like loop directly coupled to a much larger pickup coil, both shown in Figure 5.14[42]. This whole structure is patterned on a large, typically 10×10 mm^2 substrate. Of course, there is a large mismatch between the input coil and SQUID loop inductance, and the effective coupling coefficient is rather low. When a larger pickup coil is needed for magnetic field sensitivity, a single-layer flux transformer is patterned on a suitably large substrate with its input coil being a replica of the SQUID's pickup loop. For coupling, the two are brought into close contact by clamping them together in the so-called flip-chip configuration.

Multilayered flux transformers, analogous to low-T_c structures, which offer a much better coupling between the transformer input coil and the SQUID loop, are rarely used. It is still rather difficult to fabricate high-quality multilayers and multiturn coils; the yield is so low that the cost becomes too high. In special cases such transformers are made separately from the SQUID chip and used in the flip-chip configuration—allowing one to select and match the best performing SQUID and transformer chips. High-T_c SQUID magnetometers with planar single- and multilayer flux transformers are commercially available from several sources[43]. Flux transformers with pickup

[40] C.P. Foley et al., *IEEE Trans. Appl. Supercond.* 9 (1999) 4281
[41] Gao, J. et al., *Physica* C 171 (1990) 126
[42] An early design of this type: D. Koelle et al., *Appl. Phys Lett.* 63 (1993) 3630
[43] For example, STAR Cryoelectronics www.starcryo.com, SUPRACON http://www.supracon.com/, and MAGNICON http://www.magnicon.com/

coils wound of high-T_c wire do not exist because superconducting contacts between such wires and films cannot be made by known techniques.

As in early SQUID days, high-T_c rf SQUIDs were initially believed to be advantageous because only one junction had to be fabricated. However, the bicrystal GB topology favored the dc SQUID design with two symmetrical microbridges. Therefore, the majority of high-T_c devices in use today are dc SQUIDs. Early thin-film high-T_c rf SQUIDs usually employed step-edge junctions so that a single junction could be fabricated at the desired location on the substrate. For magnetometers, a large superconducting washer with a small hole has been used as a flux focuser to enhance the field sensitivity. This was the direction we pursued at FZJ[44], where the high-T_c SQUID development was led by my collaborator Yi Zhang. Today, the most successful rf SQUID design employs a single crystal, usually $SrTiO_3$, substrate as a dielectric microwave resonator instead of a patterned or wire-wound tank circuit[45]. The large flux-focusing washer covers the substrate and is flip-chip mated with the much smaller SQUID chip. Such SQUIDs are also commercially available[46]. Figure 5.15 shows schematically the components of the device.

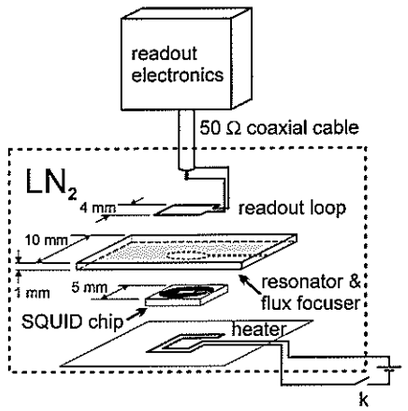

FIGURE 5.15: Schematic drawing of the substrate resonator SQUID. Dotted line surrounds the components immersed in liquid nitrogen. Adapted from Zhang et al.[45], with permission.

5.3.2 High-T_c SQUID Limits of Performance

The main advantage of the high-T_c SQUID is that it can operate at or near 77 K rather than at LHe temperatures, so cooling is much easier and less expensive. Furthermore, the liquid nitrogen cryostat walls are thinner than those of LHe cryostats allowing the SQUID pickup loop or coil to be positioned closer to the measured object thus partly compensating for the lower sensitivity due to higher noise. Indeed, the higher operation temperature sets the intrinsic limit of performance. As shown in Section 5.2.10, the thermal noise energy in the junction resistance scales with temperature over a wide range of frequencies. Furthermore, the $1/f$ flicker noise caused by critical current fluctuations, and by the motion of vortices in thin films and junctions, is dramatically higher than in low-T_c SQUIDs. The flux and energy resolution at a given loop inductance L of high-T_c SQUIDs are correspondingly limited. When L is on the order of 100 pH, a value typical for magnetometers with coupled input circuits, the lower limit imposed by thermal (white) noise is not much below 10 $\mu\Phi_0$ $Hz^{-1/2}$, an order of magnitude higher than that of low-T_c SQUIDs at 4.2 K. For single-layer magnetometers on a typical substrate (10×10 mm^2), the white magnetic field noise floor is at best $S_B^{1/2} = 40$ to 50 $fTHz^{-1/2}$ for both dc and rf SQUIDs. With flip-chip multilayer flux transformer, the best attained[47] is $S_B^{1/2} \leq 10$ $fTHz^{-1/2}$, while commercially available devices have $S_B^{1/2} \approx 15$ $fTHz^{-1/2}$.

At frequencies below 1 kHz the $1/f$ noise dominates and limits the device sensitivity. The component of that noise caused by critical current fluctuations can be removed by the use of ac bias (bias reversal), but the flux noise caused by vortex motion cannot. Vortices readily enter the less than perfect YBCO epitaxial films, even in very weak magnetic fields, B_0, like those generated by screening currents in the SQUID loop, and hop around due to the higher thermal energy and relatively weak flux pinning. Consequently, the $1/f$ noise measured with bias reversal strongly increases with B_0[48]. A partial remedy is to pattern high-T_c device structures with very narrow film lines of width w of only a few micrometers, because the vortex entry field is inversely proportional to the square of w: $B_{entry} \approx \Phi_0/w^2$.

The intrinsic limit of high-T_c SQUID performance in the presence of large thermal fluctuations was evaluated theoretically for dc and rf SQUIDs both analytically and by extensive simulations. The analytical work was done by Boris Chesca[49], the simulations by Reinhold Kleiner et al.[50]. For dc SQUIDs these simulations predicted thermal noise several times lower than experimentally measured. The consequence of lower flux and field sensitivity and dramatically higher low-frequency device noise is that after a decade of development the interest in high-T_c SQUIDs subsided and their use today is rather limited compared to that of low-T_c devices. Although the absence of LHe should facilitate portability and mobility, motion in external magnetic fields (i.e., the Earth's magnetic field) results in flux penetration and vortex motion, creating noise and hysteresis much higher than in mobile LHe-cooled devices. Although available commercially, at least in small quantities, high-T_c devices are also more expensive than their low-T_c counterparts due to low fabrication yield and limited reproducibility.

[44] FZJ is the German acronym for the Jülich Research Center (Forschungszentrum Jülich).

[45] Y. Zhang et al. (2002), *Physica* C 372-276, part I (2002) 282

[46] JSQuid, see www.jsquid.com

[47] E. Dantsker et al., *Appl. Phys. Lett.* 67 (1995) 725

[48] A.H. Miklich et al. (1994), *Appl. Phys. Lett.* 64 (1994) 3494.

[49] B. Chesca (1998), *J. Low Temp. Phys.* 112 (1998) 165-196, and J.LowTemp.Phys. 110 (1998) 963.

[50] R. Kleiner et al. (2007), *J. Low Temp. Phys.* 149 (2007) 230 and 261 (2 parts).

5.4 Geophysical Applications of SQUIDs

C. P. Foley

5.4.1 Introduction

Detection of variations or "anomalies" in the Earth's magnetic field was identified as an obvious application for SQUIDs soon after their invention. These anomalies could be due to the subsurface presence of bodies that are magnetic (such as iron ore, kimberlite pipes that contain diamonds, submarines or bomb casings), bodies that are electrically conducting (such as silver, gold or nickel sulphide), or bodies such as gas and oil that cause a local change in the Earth's magnetic field. Although initial trials were successful and early commercialization was attempted, by the late 1980s it became clear that SQUIDs would not be adopted for these applications, largely because of the need for LHe cryogenics, related cost and limited LHe availability in remote areas. However, the discovery of high critical temperature, T_c, superconductors in 1986 gave SQUIDs for geophysical prospection a second chance.

At this time, in 1988, I joined a team of researchers led by John Macfarlane at the Australian Commonwealth Scientific and Industrial Research Organization (CSIRO) to work on the emerging high-T_c material, YBCO. I had previously developed indium nitride thin films which I used for simple semiconducting photodiodes. Based on this background, I was charged with developing Josephson junctions and then SQUIDs from this new granular ceramic material.

From early 1967 on, CSIRO has made many successful contributions to superconducting electronic metrology and cryogenics and we were hopeful to build on these. Our HTS team, in collabora-

tion with Australian companies, BHP[51], Nucleus and AWA, had secured a $1M generic government-industry research and development grant to develop HTS SQUIDs, with the first application being nondestructive testing of steel. In 1990, we demonstrated the detection of a 1 mm wide slot in a piece of steel using our first YBCO thin film dc SQUID which had a poor flux noise level of $3.8 \cdot 10^{-4}$ $\Phi_0 \mathrm{Hz}^{-1/2}$ and was housed in a crude Styrofoam dewar. The device was powered by homemade SQUID drive electronics designed and fabricated by David Dart, the BHP company staff member who worked with us in our laboratory at Lindfield. After this first "success" in non-destructive evaluation, BHP management recommended that we turn our efforts to the development of SQUIDs for mineral exploration. This challenge required the detection of magnetic fields of an ore body with a magnetic field strength less than 2 pT in the presence of the Earth's magnetic field — seven orders of magnitude stronger. Detection was to occur in remote locations (where there is limited mains frequency noise), on the ground, in the air or under water when the system is either stationary or in motion. This ambitious goal ignited our enthusiasm for SQUIDs for geophysical applications, in spite of their lapse in this field during the early 1980s. I'll describe our successful work after introducing briefly the magnetic measurements used in geophysical prospecting, and equally briefly addressing the early geophysical measurements performed using low-T_c SQUIDs.

5.4.2 Magnetic Measurements Used in Geophysical Prospecting

Three types of magnetic measurements are made in geophysical prospecting: scalar measurements usually using vapor magnetometers (this provides the total magnetic field, B, intensity values — TMI), vector measurements which give the three axes of the magnetic field which can be directly measured by flux gates or SQUIDs, B_x, B_y and B_z, or their time differentials, $\partial B_i(t)/\partial t$, measured by induction coils with the vector components obtained by the integration of the measurements, and, thirdly, the gradient measurements, which measure the spatial variation of the magnetic field leading to the nine components of the Earth's magnetic field tensor.

Magnetotellurics (MT), a "passive" magnetic exploration method, determines the distribution of electrical conductivity in the Earth's subsurface by measuring the natural electromagnetic field variations (i.e., of both the electric and magnetic fields) caused by solar radiation/particles or atmospheric sources, such as lightning discharges that induce electric currents in the subsurface. By modeling and inversion (i.e., by solving the magnetic inverse problem[52]), an image of the distribution of electrical conductivity is obtained. Active variations of MT include Audio-MT and the underwater Controlled Source Electromagnetics (CSEM) where electromagnetic field variations are induced by audio or very-low-frequency electromagnetic waves from a transmitter.

Transient ElectroMagnetics (TEM) is an "active" exploration technique used to prospect for conducting ore bodies such as nickel, gold and silver and can be used with either an airborne or ground-based system. This technique evolved from the active MT methods. A transmitter coil is mounted either around the wing tips of an aircraft or placed on the Earth's surface. Such an antenna emits a short magnetic pulse which induces in the ground electrical eddy currents that decay over time. A sensitive magnetometer measures the associated decaying "secondary" magnetic field. Once the decay is completed, the process is repeated many times, so that the measured decay signal can be averaged to improve the signal-to-noise ratio (SNR) of the measurement. The measured decaying magnetic field data can be processed to derive the electrical conductivity of the ground as a function of depth. In this way, a TEM survey is used to generate three-dimensional (3-D) conductivity maps. Where conducting anomalies occur, the decay of the secondary magnetic field will be slower than in

[51] BHP Billiton is a global leader in the resources industry and was formed from a merger between BHP and Billiton in 2001.

[52] The magnetic inverse problem or "inversion" addresses the description of a magnetic source (such as the current distribution within a body) from measurements of its external magnetic field at various locations. The three-dimensional inverse problem is ill-posed, i.e., has no unique solution, and thus requires additional boundary conditions to be known.

the less-well conducting surroundings. This is manifest in the later stages of the decay curve where the SNR is poorest so high-sensitivity magnetometers are required.

Magnetic Tensor Gradiometry is a "passive" method that measures the magnetic field tensor. In orthogonal x, y, z coordinates, the tensor components characterize the magnetic field rate of change in one coordinate direction, say x, determined in the three different (x, y, z) directions. The combination of all of these components provides important information about the target characteristics and location that cannot be obtained from total or vector field measurements. Whereas a magnetic field vector has only three components, the gradient requires nine separate quantities. These nine elements form a square matrix representing the magnetic field in a so-called "tensor form". Of these, five are unique. Gradient measurements are relatively insensitive to sensor orientation. This is because gradients arise largely from anomalous (local) sources while the background gradient arising from the Earth's core is nearly negligible. This contrasts with the magnetic field vector, which is dominated by the background field. Gradient measurements are, therefore, most appropriate for airborne applications. Another advantage is they obviate the need for base stations and corrections for diurnal Earth's field variations. They also greatly reduce the need for regional corrections, which are required in TMI surveys because of deeper crustal fields that are not of exploration interest, or the normal (quasi-) latitudinal intensity variation of the global field.

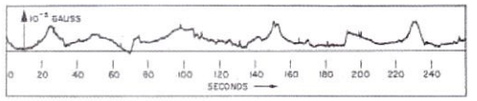

Fig. 11. Recording of fluctuations in vertical component of earth's field.

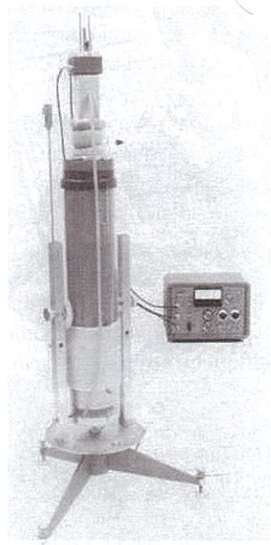

FIGURE 5.16: Earth's microfluctations (top graph) measured using a SQUID magnetometer setup shown; taken from the original publication[53], with permission.

5.4.3 Early SQUIDs in Geophysical Prospecting

Soon after the invention of the SQUID, in 1967, Forgacs and Warnick from the Ford Motor Company measured microfluctuations of the Earth's magnetic field[53] with the Silver-Zimmerman SQUID using the setup shown in Figure 5.16. This was the first-ever geomagnetic measurement using a SQUID. They used a single SQUID housed in a cryostat cooled by liquid helium contained within a nitrogen-cooled jacket; the cryogen hold-time was over 24 hours. The assembly could be rotated and tilted for the calibration required to determine the field components. During the survey, the probe assembly was protected from wind gusts by a tent to reduce vibrations—a method still commonly used. The magnetometer electronics and recorder were separated by approximately 32 m of cable from the probe to minimize noise from the drive electronics. This first survey was followed

[53] R.L. Forgacs and A. Warnick, *IEEE Trans. Instrum. Meas.* IM-15 (1966) 113

by the unsuccessful attempt by Jim Zimmerman to measure changes in the Earth's magnetic field due to perturbation of ionospheric current (equatorial electrojet) during a solar eclipse. His latter attempt (1978) to measure currents in the Alaskan oil pipeline induced by the polar electrojet was also unsuccessful.

FIGURE 5.17: John Clarke transfers liquid helium into a fiberglass cryostat containing three orthogonal cylindrical dc SQUIDs that form a three-axis LTS magnetometer. The cryostat is below ground to eliminate wind-induced motion. Circa 1982 (courtesy John Clarke).

The first commercial geophysical vector magnetometer for MT, with three SQUIDs measuring B_x, B_y, B_z, was a few years later introduced by the SHE Corporation (see Section 5.6). Of all the early geophysical uses of SQUIDs, the most enduring impact on geophysical prospecting was John Clarke's (Figure 5.17) research on MT conducted with Goubau and Gamble of the Earth Science Division, Lawrence Berkeley Laboratory, Berkeley. In 1975, their aim was to use a SQUID magnetometer with a sensitivity of 0.01 $pTHz^{-1/2}$ to reduce the bias errors that were plaguing MT measurements[54]. After several field experiments using the conventional single station scheme to measure the two orthogonal horizontal components of the electric and magnetic fields, they found that the significantly improved instrument noise did not improve the MT data quality. Rather, the noise was inherent in the measurement technique. Therefore, in 1979, Clarke, Gamble and Goubau introduced a second remote magnetometer to "lock-in detect" the naturally occurring plane wave magnetic and electric signals at the MT site. This remote reference technique substantially reduced the bias error of the MT measurements and provided reliable confidence limits on them. The technique makes surveying possible in regions of high cultural magnetic and electric noise. It is now standard practice in MT and magnetic gradiometry, and it is usually performed with nonsuperconducting systems such as flux gates and vapor magnetometers. It is an excellent example of Harold Weinstock's oft-repeated axiom: "Never use a SQUID when a similar, less expensive, technology will do the job. Use a SQUID only when nothing else (less expensive) will satisfy your need."

Momentum in the use of SQUIDs for a range of geophysical applications led Harold Weinstock and Bill Overton to organize a workshop "SQUID Applications to Geophysics" held at Los Alamos Scientific Laboratory, New Mexico in June 1980. Every paper presented at that workshop was a benchmark in innovative geophysical measurement. However, soon after, other measuring instruments, such as vapor magnetometers, dominated the field. This was because they were cheaper and did not require the management of cryogenics and LHe in remote areas.

Also, SQUID electronics at that time did not have sufficiently high slew rates necessary to track

[54] J. Clarke et al., *Geophys.Prospect.* 31 (1983) 149

the SQUID output in unshielded operation. SQUID use in geophysics was practically abandoned until the discovery of high-T_c materials and demonstration of practical high-T_c junctions and SQUIDs.

5.4.4 Transient ElectroMagnetics Using High-T_c SQUIDs

I now return to our work with high-T_c SQUIDs. By changing the research direction to mineral exploration, we could capitalize on the CSIRO's TEM system (see 5.4.2), SIROTEM, that had been developed by Ken McCracken in a sister division. This system used induction coils as the magnetic receiver. In the 1980s, the TEM method became popular and has been credited with the discovery and delineation of commercially viable ore bodies. Consequently, many TEM transceiver systems from a range of suppliers appeared on the market.

The TEM method has two major advantages: (1) excellent transmitter signal rejection, because the measurements start after the transmitter has pulsed, and (2) a broadband frequency/time spectrum due to the pulses having a spread Fourier transform. The latter provides depth discrimination because lower frequencies penetrate deeper into a conducting body than higher ones and therefore appear later in the decay of the secondary signal.

The disadvantages of TEM are that the measurement SNR decays rapidly in time with the signal (at a constant noise level), so the most interesting region from the point of view of resolving conductivity anomalies and looking deeper is compromised by poor SNR. Induction coil TEM receivers have additional limitations. First, the time derivative $\partial B(t)/\partial t$ decays faster than B, so the measurement may not detect the high quality ore bodies which have long decay times. Second, the SNR of an induction coil is proportional to frequency, so at low frequencies, i.e., at the longest decay times, the sensor performance is poor. Not only does the signal decay with time but the detector's sensitivity does as well, compounding the SNR problem. Another disadvantage of measuring $\partial B(t)/\partial t$ and integrating is that the initial integration point is unknown and different initial boundary conditions can lead to nonunique solutions to the location of the ore.

SQUIDs and fluxgate magnetometers offer a direct measurement of the magnetic field that removes all of these disadvantages. Optically pumped total field magnetometers are also sensitive enough, but their bandwidth is too narrow for active systems. For the deepest conductivity anomalies, SQUIDs are the only suitable sensors, although, in the early 2000s, there was a largely unsuccessful effort to promote fluxgates as the preferred receiver for TEM.

In 1991, our task became to develop a SQUID receiver that was inexpensive to fabricate, had low noise and could operate without a magnetic shield. Our original high-T_c SQUIDs fabricated in 1989 used Josephson junctions that were dependent on the natural formation of grain boundaries and constrictions in the SQUID loop. However, by that time epitaxial films on STO crystal substrates and controlled bicrystal grain-boundary junctions had been already reported (see Section 5.3). My colleague, Nick Savvides, soon developed epitaxial YBCO films on MgO substrates, chosen because they are significantly cheaper than STO, but still offer a reasonable lattice match. As bicrystal substrates were expensive and difficult to source, I was inspired by the original step-edge junction paper[55] to develop step-edge junctions on MgO substrates. I initially fabricated junctions which had multiple grain boundaries at the top and bottom of the step edge, which contributed to device noise. I wondered if it were possible to have a step with only one junction and a gentle return path allowing a single junction to be placed anywhere on the substrate. With the assistance of an undergraduate student, Simon Lam, I varied the angle of the ion beam to the substrate coated with a photoresist mask to align with the crystal lattice and successfully created a single grain boundary junction on MgO[40]. Our substrate selection was fortuitous as YBCO growth on MgO over a step-edge is different than that on other substrate materials often used (such as STO). We had better control of the junction formation leading to a single engineered grain boundary. Indeed, our resulting junctions did

[55] K. P. Daly et al., *Appl. Phys. Lett,* 64 (1990) 228

not contain any other grain boundaries cutting the device and their critical current was relatively stable in changing magnetic fields. Our best junctions, which operated unshielded in motion, required YBCO films to have a specific morphology to minimize flux movement, and a high film critical current to achieve this. These junctions are less than 2 μm wide. Over twenty years, our research group optimized our junction performance and increased both their yield and reproducibility.

The next step was to place our junction into a SQUID. We made a significant decision in 1991 to use rf SQUIDs for our TEM receiver. We thought that there were several advantages: a single junction (only one to get right), inductive coupling to the device and no need for wire bonding which can be fragile. Furthermore, the rf drive created automatic bias reversal which reduced the low-frequency device noise. It was necessary to fabricate a SQUID that could operate in varying magnetic field and remain in lock during the TEM pulse current time. We set a specification of 1 $pTHz^{-1/2}$ noise at 30 Hz and designed a 100×100 μm^2 hole, 2 mm square simple washer SQUID with a 125 pH inductance. In 1991, I also gave birth to my second child and fabricated devices late at night returning to the laboratory after the babies had been put to bed to make sure there were devices ready for testing the next day. As we used three SQUIDs to measure B_x, B_y and B_z, we needed three similar rf SQUIDs to assemble a sensor head capable of measuring the three orthogonal components of the magnetic field.

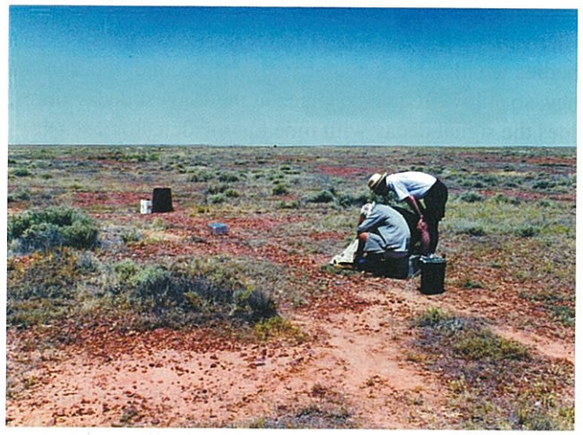

FIGURE 5.18: The first field trial in Cooper Pedy.

Rex Binks, our talented technical officer, recommended that we use glass cryostats to reduce the boil-off times. These cryostats were initially fabricated by the CSIRO in-house glass blower. The SQUIDs were inductively coupled to a small pancake coil of rf tuned circuit located adjacent to the washer and operated at about 180 MHz. Our mark one version used the traditional dip probe. We used Quantum Design VHF SQUID Amplifier Model 2000 and SQUID Control Unit Model 2010. David Dart developed the custom electronics to provide a synchronous reset unit allowing us to reset the Quantum Design amplifier synchronously with the pulsed output of the SIROTEM unit. Furthermore, Dart modified the electronics to achieve a higher linearity. We also introduced a novel feature of a separate large feedback coil to provide a uniform magnetic field environment for the SQUID to eliminate noise and nonlinearities arising from flux movement within the superconducting film. The system had a magnetic field sensitivity of 1-2 $pTHz^{-1/2}$ with a bandwidth of 100 kHz and slew rates of 300 mTs^{-1}. We undertook several experiments using a variety of rf shielding materials to arrive at a shield design which gave an acceptable self response[56] in the TEM survey.

We performed our first outdoor trial on the grounds of CSIRO in mid-1992. This was within sight of some TV broadcast towers, and proved to be an important test site as it set the standard for rf screening that was sufficient to keep out the rf while not creating self-field effects that reduced the

[56] Self response is the interference between SQUIDs and adjacent electronic components or metal shielding used to screen rf radiation. This response can be mitigated by appropriate design of shielding and increased distances between interacting components to provide satisfactory isolation. Whenever the rf screening is placed around a cryostat or located in the vicinity of SQUID sensors, it may increase noise due to eddy currents induced in the rf screen by the external changing fields.

system sensitivity. Over time, we optimized the rf shielding using homemade cables, shielded glass dewar and carefully anchored connectors. The first system affectionately called "The Rocket" was trialed at Cooper Pedy (a well-known opal mining town in South Australia) in December 1992. Figure 5.18 shows the historical photo taken during this trial. The trial led to three ground-based field trials at Murray Bridge, Cannington and Mt Isa, lasting until August 1995. Our most significant trial was that at Cannington where a large silver lode was known to be present. BHP was gearing up to undertake bore hole digging, the next stage for determination of the extent and quality of the ore deposit. This SQUID trial collected data that clearly indicated a double lode rather than a single one that had been suggested by the induction coil receiver measurements. Mike Asten, the geophysicist leading our trial for BHP, thus recommended a change in the location of the first bore hole. This advice led to the first core passing through the center of the $1B silver reserve. The BHP Chief Scientist at the time acknowledged informally that the Cannington Silver Mine came online 18 months earlier than initially planned because of our SQUID TEM survey.

After this success, BHP was keen to trial airborne SQUID magnetometers. When airborne, SQUIDs are under constant motion while data is recorded, unlike in the stationary ground-based system. The ground-based systems can be degaussed between stations to expel the trapped flux and reset the system. Moving an operating magnetometer in the Earth's field is the most challenging of tasks. It is also necessary to have a light and compact cryostat and electronics that is suitable to fit into a "bird" that is towed behind the aircraft. Rex Binks used a KMART 1 liter thermos flask, modified with rf screening and a metal cap. Rex invented also a housing that attached a module containing the three SQUIDs to the bottom of the dewar with twisted pair cables brought through the metal cap. Removing the dip probe increased the liquid nitrogen hold time to 13 hours and we achieved a very compact system. The liquid sloshing and the gas bubble noise were removed by filling the cryostat with cotton wool before charging with the cryogen. BHP developed a novel mechanical suspension system that successfully removed the motion noise above 20 Hz. Chris Lewis and Wayne Murray developed in-house rf electronics that operated at 300 MHz. The tank circuit had a low Q at the cost of sensitivity to provide a robust system that did not require retuning during the flight. Rex also developed a nonmetal, mechanical pressure valve to maintain the pressure above the liquid nitrogen at one atmosphere thus preventing changes in the nitrogen boiling point with the airborne altitude. The system operation was disrupted by flux jumps as at that stage we had not yet introduced a chip-based heater to allow resetting the SQUID when the flight reversed direction (this caused a field change of up to 100 μT). All these somewhat "small" innovations were essential to achieving a three-axis SQUID magnetometer that was effectively airborne. Figure 5.19 shows the "bird" (left photo) and the miniaturized cryostat with electronics (right photo). We undertook five airborne trials between September 1994 and November 1997. This work was confidential and we were unable to publish until 1999[57].

Over the next 14 years, we worked with several different mining and mineral exploration companies to further develop the CSIRO SQUID TEM receiver which we called LANDTEM®. After working with Falconbridge P/L, a Canadian mining company, on the recommendation of Ken Witherly, an ex-BHP Chief Geophysicist, we developed an auto-tuned robust LANDTEM system that is now licensed to a manufacturing company, Outer Rim Developments. Such systems have been since manufactured, are commercially available and extensively used in many countries. Their use assisted in the discovery and delineation of many billions of dollars worth of mines[58]. Figure 5.20 shows a photo of the commercial system at a test location. Over the years, and in addition to my colleagues mentioned above, leading technical contributions to this system were made by the late Graeme Sloggett, Jia Du and Emma Mitchell. Keith Leslie was instrumental in leading the system integration and commercial adoption.

[57] C.P. Foley et al., *IEEE Trans. Appl. Supercond.*, 9 (1999) 3786

[58] C.P. Foley, K.E. Leslie and R.A. Binks, *First Break*, 25 (2007) 73

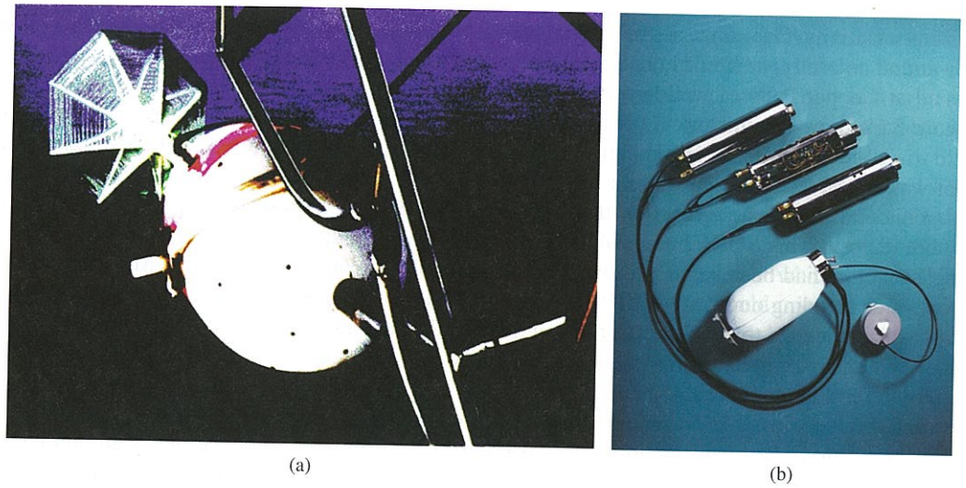

(a) (b)

FIGURE 5.19: The CSIRO high-T_c SQUID system in flight as it is released from a fixed wing aircraft on a tow rope (left photo). Right photo shows the light-weight, three axis, SQUID system with the miniature cryostat, electronics and pressure regulator.

The high-T_c SQUID TEM for ground-based applications has been so successful that there are currently Japanese, German, US and Australian systems on the market. Furthermore, the desire to improve sensitivity led to the development of two low-T_c systems exclusively used by two different major mining companies, Anglo American and BHP Billiton. It is now common for a mining company to send out a press release announcing a SQUID-based exploration survey with a view to increasing their share price. However the airborne TEM system has not been commercially successful so far, although there are renewed efforts underway with new systems being developed by CSIRO and IPHT (See the box "High Competition").

FIGURE 5.20: The CSIRO commercial LANDTEM system.

5.4.5 Tensor Gradiometry

It was a natural progression to develop a tensor gradiometer to survey localized disturbances in the dc Earth's magnetic field resulting from the presence of concentrations of ferromagnetic material. The main applications of magnetic tensor gradiometry include military sensing of submarines, unexploded ordnance, non-invasive archaeology and geomagnetic surveying.

However, I will consider only geophysical applications here. During the early stages of mineral exploration, it is mandatory to carry out passive magnetic surveys. The acquisition and processing of magnetic surveys using TMI data from airborne cesium vapor magnetometers have improved remarkably over the past two decades. It is now possible to create high quality magnetic images, similar to topographical maps, from survey data. Nevertheless, due to timeconstraints on surveys

High Competition

Competition was so "hot" for the use of HTS SQUIDs in airborne TEM that, in 1997, a major mining multinational secretly funded two competing research groups to develop an airborne SQUID magnetometer which was tested in Timmins in Canada over a two-week period. In order to prevent the two groups knowing about each other's involvement, the company did not have a researcher from either research group to assist with the trials. The trials were hampered by a pin-out problem, flux jumps and suspension system failures. However five days of flying were achieved and data were collected that showed a factor-of-two improvement in the late time channels in SNR compared to the coil systems flown at the same time. This trial was undertaken during a period of downturn in the minerals industry due to low commodities prices, and a ten-times improvement in SNR was required from this trial if further development were to continue. Thus the support for further development was not forthcoming. At that time, the exploration industry underwent a major restructuring and it became clear that the price point of $27 per kilometer of survey must be attained to be economically viable. More recently, the IPHT Jena group has developed an airborne AeroTEM III (low-T_c) which has been trialed slung under a helicopter in 2008 with effective surveying results still elusive.

and the lack of appropriate technologies, much magnetic information that could assist in mineral discovery remained inaccessible.

Our colleagues at the CSIRO Division of Exploration and Mining, Phil Schmidt and Dave Clark, published a paper that set the specification for gradiometry for mineral exploration and outlined the opportunities a magnetic tensor gradiometer survey would provide[59]. The sensitivity requirement of a tensor gradiometer is 0.01 nTm^{-1} gradient sensitivity for detection of a vertical contact between two paramagnetic rock units such as a mafic and a felsic gneiss, which contain no magnetite or pyrrhotite with a susceptibility contrast of about $6 \cdot 10^{-4}$ SI units at 100 meter range. The scale of the motion noise problem in this application can be comprehended when one considers that a SQUID magnetometer with 5.6 $fTHz^{-1/2}$ noise floor, edgeways on to a 56 μT Earth field needs only about a 10^{-10} degree rotation in one second before the motion is seen on the output. Luckily, a gradiometer with the same sensor noise floor (at the two points of measurement along the baseline) that is balanced to the 1 part in 10^6 level has a residual response of 5.6 $nTHz^{-1/2}$ and an allowable angular motion of about 10^{-4} degrees, still a formidable requirement.

For geophysical use, IPHT Jena has been most successful in airborne tensor gradiometry of minerals for Anglo American Company (see the box "Airborne Full Tensor Magnetic Gradiometry" below). The best results were obtained when using low-T_c gradiometer systems slung under a helicopter. Fixed-wing aircraft trials have also been performed[60]. The helicopter trials used a towed platform which carried the tensor gradiometer constructed of planar gradiometers that achieved a gradient resolution after software balancing of better than 10 $pTm^{-1}Hz^{-1}$ for frequencies above 0.1 Hz. The reports on the fixed-wing gradiometer trial have not been formally published but some conference presentations have revealed a full tensor gradient measurement with software compensation using tri-axial (triple) SQUID magnetometers providing data for the gradiometer compensation.

5.4.6 Laboratory Systems

The Superconducting Rock Magnetometer, a laboratory-based instrument for paleomagnetics, is a very successful product of long-term development of SQUIDs for geophysics. This specialized

[59] Schmit and Clark, *Preview,* April, 26, 2000

[60] H-G. Meyer, et al., *Phys. Stat. Sol.*, (c), 5 (2005) 1504

low-T_c instrument, manufactured by 2G Enterprises, has sold widely over the years. 2G Enterprises was founded in October 1981 as a result of a marketing agreement between the late Bill Goree of William S. Goree, Inc. and Bill Goodman of Applied Physics Systems, Inc. They focused on high performance superconducting systems for paleomagnetics. 2G received the first two contracts for such systems in 1981–1982. Figure 5.21 shows the two founders with their instrument. 2G has since installed and upgraded over 100 LHe-cooled systems and is currently offering their third generation "liquid helium-free" systems.

FIGURE 5.21: Bill Goree (left) and Bill Goodman (right) with a 2G Rock Magnetometer (courtesy of 2G Enterprises).

The magnetometer has a horizontal room-temperature access and is aimed specifically at determining the magnetic moment—along three axes—of rock core samples up to 0.12 m in diameter and 1.5 m in length. With the aid of cryo-cooled thermal radiation shields, the system can run for a remarkable 1000 days between liquid helium refills. Thus, the cryogenics is virtually invisible to the user. This instrument has become the standard rock magnetometer of the geophysics community. One significant application has been to measure the magnetic moment of sedimentary cores taken from the ocean basins to study the polarity reversal of the Earth's field over geologic time.

5.4.7 Final Comments

SQUID systems operating in real environments to measure the magnetic fields and their gradients originating from remote mineral sources remain technically challenging, particularly if the sensors are in motion. In applications where the SQUID environment can be controlled, such as rock magnetometers, SQUIDs are now well established at the high-sensitivity end of this fairly small market.

For field applications, where the sensor's magnetic environment cannot be controlled, industry acceptance has grown significantly since 2005 for SQUID ground-based TEM, as witnessed by a specialist workshop at the Society for Exploration Geophysics conference in New Orleans in 2006 and the fact that five companies are offering HTS SQUID TEM receivers for sale. Indeed, mining companies are announcing their plans for SQUID surveys with the intention to boost their share price. The growing acceptance has resulted from strong user requirements for higher sensitivity and better ore body discrimination than current conventional systems can offer.

Several SQUID research systems for geophysical survey applications other than TEM have been successfully tested in operation. Although these tests demonstrated that SQUIDs can be used in such applications, the only established first-choice technology is thus far the ground-based TEM. The success of this relatively small application, which has big indirect economic impact, has been significant and I am proud to have been involved.

The IPHT team with their LTS magnetic tensor gradiometer exclusively used by Anglo American has shown that even complex technology and cooling to liquid helium temperatures can be adopted by industry when the system clearly demonstrates economic and technical benefits. The market for geophysical SQUID systems can be expected to remain fairly limited; their economic impact is and will remain indirect—via the value of discovered ores. Market growth could occur if SQUID military

Airborne Full Tensor Magnetic Gradiometry (by Ronny Stolz, IPHT-Jena)

The development of our full tensor magnetic gradient systems (FTMG) started in 1997 with a request from the German Naval Research Center for a system to localize magnetic dipoles. Our team at the Institute for Physical High Technology (IPHT) in Jena, Germany included Slava Zakosarenko, Marco Schulz, Andreas Chwala, Hans-Georg Meyer and me. For sensors we used our planar-type, long-baseline first-order low-T_c gradiometers with noise as low as 15 $fTm^{-1}Hz^{-1/2}$. Because of their good intrinsic balance, i.e., the suppression of the homogeneous Earth's magnetic field by a factor higher than 10,000, they could be freely rotated in the Earth's magnetic field without compromising the dynamic range of the SQUID electronics. Patience was necessary in those early days because only one sensor could be patterned on a 3-inch-long substrate; it took more than five weeks to produce such a device.

FIGURE 5.22: Evolution of field tests of the IPHT-magnetic tensor gradiometer, 2001 to 2009. 2001 — Ronny carries the cryostat with sensors for an early ground-based test; 2002 — cryostat mounted on airplane stinger; 2006 — the system pod to be towed by helicopter; 2009 — the system "bird" towed by helicopter.

During his visit in 2001, Eddie Koestlin, chief geoscientist at Anglo American at that time, inspired us to develop a FTMG system with similar sensors for geophysical exploration of magnetic ore bodies like iron, kimberlites and so on. We demonstrated to Eddie the performance of our dual channel system against that of a total field gradiometer, which was already tested in 1999 in South Africa, and in motion.

We performed the first airborne tests (a tow bird below a helicopter and a stinger mounted on an aircraft) in 2002, together with Anglo American and Fugro Airborne systems. The big breakthrough occurred in the production-like tests during 2006, when the FTMG system was almost three months in operation and flew more than 22,000 line kilometers in different areas in Southern Africa without faults. Even a rough takeoff with a tumbling-down bird evaporating quite a bit of liquid helium, so precious in the southern hemisphere, couldn't do any harm to the system. Figure 5.22 shows pictorially the evolution of FTMG field tests.

The development is still ongoing. We aim for a noise floor an order of magnitude better than that of conventional airborne gradiometers—via better electronic components and software tools for post processing, as well as decreased motion. Nevertheless, our present system is already a very important tool for magnetic exploration as it measures a new physical quantity in the exploration process–the magnetic gradient tensor—allowing us to invert better the magnetic potential to reliably pinpoint magnetic sources which might become the mines for tomorrow. Many parts of our developed FTMG technology are used in other systems such as SQUID systems for ground-based TEM, the archaeological scanner, or the THz safety scanning camera.

applications, such as magnetic anomaly detection, for example of unexploded ordnance, would come into broad use. The system cost could then decrease through the economies of scale.

5.5 Application to Nondestructive Evaluation of Materials and Structures

A. I. Braginski

5.5.1 Past and Present

Nondestructive evaluation (NDE) of materials and structures or objects in industry, construction, transportation and other domains is a vast field of great economic and societal relevance. Public safety critically depends on it. The purpose is to detect cracks, material fatigue, impurity inclusions and other defects not accessible to visual inspection. Here, I address only the opportunities offered to NDE by SQUIDs used as sensitive magnetic flux and field detectors.

In the early 1980s, Harold Weinstock and Marty Nisenoff in the U.S., and independently Gordon Donaldson and collaborators in Scotland, U.K., were the first to demonstrate the usefulness of SQUIDs for NDE[61,62]. Harold's personal reminiscences are reproduced here (see box on p. 341). Obviously, they both used low-T_c SQUIDs then available.

Many NDE applications require portability, use in motion and/or in the presence of relatively strong magnetic fields. Furthermore, testing must be economical, i.e., inexpensive. All these requirements are significant handicaps for any SQUID sensor. Nevertheless, with the advent of high-T_c SQUIDs, many of us believed that once they reached a certain level of performance, reliability and cost they would become ideal detectors for difficult NDE tasks.

In early 1989, I joined the newly created Jülich group led by the late Christoph Heiden[63] and became responsible for all high-T_c R&D programs. Until 1991, the main part of our efforts was devoted to establishing a base for technology of low- and high-T_c materials and devices for superconducting electronics. The low-T_c SQUID work was pursued by a young and talented scientist, Michael Mück, who joined Christoph when he temporarily moved from Giessen to Jülich, while bulk and thin film high-T_c rf SQUIDs were worked on by a doctoral student from China, Yi Zhang. Yi soon graduated, but remained in the group and successfully continued his work. By early 1992, Yi had produced the (then) most sensitive epitaxial thin film rf SQUIDs in the world, based on step-edge junctions, and through Christoph's initiatives we became involved in evaluating their use for NDE. Our initial work was on highway bridge structures built from steel-reinforced concrete, and since 1993 we also worked on NDE of airplanes. Both initiatives were pursued in joint projects with, respectively, a bridge supervision authority, a major air carrier, a manufacturer of conventional eddy-current devices for airplane NDE and also a manufacturer of airplane turbine (jet) engines. After Christoph returned to Giessen in 1993, we continued to collaborate with his group there, especially in airplane testing.

Our projects were technically very successful; one was implemented (under our license) in aircraft engine manufacturing. Nevertheless, a decade later, it became clear that high-T_c SQUIDs had not been accepted in NDE of airplanes and bridges, mainly because of cost, necessity of cooling, reliability in the field and relatively complicated handling requirements. Also comprehensive studies by others on SQUID NDE in application to power plant component testing concluded that conventional sensors suffice[64]. Today, either high- or low-T_c devices are only occasionally used to solve

[61] H. Weinstock and M. Nisenoff, in *SQUID'85: Proc. 3rd Intl. Conf. on SQUIDs*, deGruyter, Berlin, (1985) 853

[62] R.J.P. Bain et al., ibid., (1985) 841

[63] In 1988, the late Prof. C. Heiden (1935-2000) from the University of Giessen, Germany, was invited by the Research Center Jülich, Germany, then known under the acronym KFA, to organize and head a new Institute devoted to superconductivity and its electronic applications

[64] Studies at Siemens and KWU, performed in collaboration with IPHT-Jena, Germany, 1997-2003. G. Daalmans — private communication (2010)

First NDE Ideas and Tests (by H. Weinstock, AFOSR, US)

As a faculty member at IIT in Chicago, I went on sabbatical in 1972–1973 to the Naval Research Lab (NRL) specifically to use a second-derivative SQUID gradiometer to detect magnetic signatures of cryocoolers being built under contract to the Office of Naval Research. When I discovered these cryocoolers were unlikely to arrive that year, 2 potential applications came to mind.

The first was to see if this sensitive gradiometer could be used to find holes in a buried pipeline by passing a current through a pipe and seeking magnetic field anomalies due to nonuniform current distribution. Since that was not something I could do directly, I thought it possible to simulate it. Marty Nisenoff, my host at NRL, produced a 5-cm diameter pipe about 70 cm long. With no elegance whatsoever, I drilled and sawed a couple of ragged holes several centimeters apart. When the pipe was found to be ferromagnetic, I decided to use a low frequency AC signal and an oscilloscope to monitor the height of the AC signal in the output of the SQUID's room-temperature electronics.

This arrangement allowed me to move the pipe beneath the SQUID dewar to simulate hunting for a leak and locating the pipe. It soon became clear that the SQUID gradiometer could detect the presence of the pipe when it was directly under the dewar, and when one of the holes was directly under it. It also was possible to rotate the pipe around its own axis to detect an anomalous signal when one of the holes was on the bottom while the SQUID dewar was above the pipe. It was possible to see this signal grow as the pipe was rotated about its own axis. Another remarkable thing about these crude measurements was that we obtained these definitive results despite the fact that the signal came from a distance several times greater than the baseline of the second derivative magnetic gradiometer.

The second attempt at nondestructive evaluation evolved from an idea I had that if we placed the tail of the dewar near a piece of steel clamped in a tensile testing machine, we might see changes in the ambient magnetic field near the center of the steel strip being tested. Despite some false starts, we did see a strong signal from the steel specimen, so strong that we had to switch to the lowest level of amplification. As stress increased, the magnetic field changed as well, with a linear relationship between the applied stress and the measured magnetic field. At a stress about 2/3 of the elastic limit, the magnetic field started to decrease. Beyond the elastic limit, the slope of the stress-strain curve flattened, indicative of plastic flow.

I learned later that at a stress about 2/3 of the elastic limit, one reaches the "endurance limit", indicative of microscopic particle movement that can be thought of as a precursor to the elastic limit. We also saw magnetic field oscillations as a function of stress in the plastic regime, and discovered these were analogous to stress-strain oscillations known as Lüders bands. Since the signals obtained were so large, these last observations were verified using a fluxgate magnetometer by others at NRL. Thus, while a SQUID gradiometer was not needed to see this effect, it might never have been discovered using conventional magnetometry.

especially tough NDE problems.

In the following I will reminisce about our past efforts and give examples of NDE applications which apparently survived the test of time, are currently in use or still hold promise for the future.

5.5.2 NDE Testing Methods Using SQUIDs

Testing using magnetic field sensors usually involves scanning the sensor over the tested object, at some distance from it, and is based on one or another of the following techniques:

- Detection of (weak) magnetic moments, e.g., of ferromagnetic impurities dispersed in a non-magnetic matrix, or of magnetization anomalies in nominally homogeneous ferromagnetic objects.
- Magnetic flux leakage technique (MFL), where the tested ferromagnetic object is magnetized, usually by a permanent magnet, and the induced stray field is then measured above the surface. This method was used in the pioneering work of Donaldson's group and later by us for testing of bridge structures.
- Eddy current technique of testing metallic nonmagnetic objects, semiconductors and laminated carbon-fiber-reinforced plastic (CFRP). Here, eddy currents are induced in the object below its surface and local anomalies in the distribution of the resulting magnetic field can be measured above the surface. Very low excitation frequency is required to avoid limitation by skin depth and to probe deep defects. Such excitation is practical when using SQUID detectors because the SQUID senses the magnetic field vector $\vec{B}$ rather than its time derivative $\partial\vec{B}/\partial t$ as is the case of induction (sensing) coils, making the SQUID's response frequency independent. The eddy-current technique with induction coil detectors is typically used for testing airplane parts and fuselage. Alternative magnetic response excitation methods by light, heat, etc., have been also used in other applications. Pulsed eddy current excitation permits conductivity tomography and flaw depth determination (in analogy to the TEM method of geomagnetic exploration).

In all such techniques the fault causes a local magnetic anomaly or deviation from the expected field distribution, which is detectable. Although theoretical calculations of such field distributions have been performed, practical testing usually involves empirical comparison with a fault-free reference sample. What SQUIDs bring to the game in comparison with conventional detectors (e.g., fluxgate or magnetoresistive magnetometers and induction coils) is the much higher sensitivity and signal-to-noise ratio when measuring field changes, the wider dynamic range and ability to operate in the presence of static fields. As noted above, in eddy-current testing much lower excitation frequency can be used, thus expanding the practical depth range. However, the penalty for SQUID use is the more sophisticated equipment, more difficult handling and maintenance, and, above all, the need for cryogenics. Consequently, the much higher investment and operational cost of the SQUID system can be justified only when no other sensor can do the job, as might be the case when searching for faults or impurities located very deep beneath the surface of the object to be tested.

5.5.3 Bridge Testing

In steel-reinforced concrete structures the pre-stressed steel tendons are located deep below the surface of a concrete bridge or roof. When water penetrates the tendon beam duct, tendon rupture due to corrosion cracks may have catastrophic consequences.

In May 1991, at Christoph Heiden's initiative, Yi Zhang's high-T_c rf SQUID, not yet at its ultimate sensitivity, was demonstrated at the German industrial fair "Sensor". At that show, a representative of an industrial construction company became interested in using our SQUID for locating

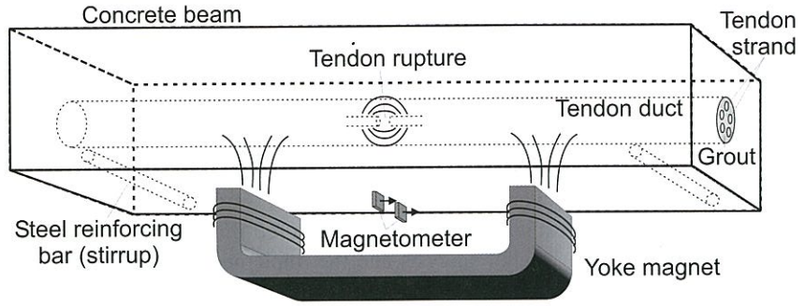

FIGURE 5.23: Principle of magnetic flux leakage detection of ruptures in tendon strands of pre-stressed concrete-reinforcing beams (from The SQUID Handbook, Figure 13.3, with permission).

reinforcing steel beams in thick concrete structures, which eventually resulted in our joint work with the bridge inspection authority of the German Land Baden-Württemberg (FMPA). Using the MFL method, a probe carriage containing a permanent yoke magnet and SQUID sensors was moved on rails over the surface to magnetize the local area and record the the magnetic stray field versus position. The principle of such detection is shown in Figure 5.23. In this application we eventually used an array of high-T_c dc SQUIDs with ramp junctions, which were much less sensitive to static magnetic fields than step-edge junctions in our rf SQUIDs[65].

FIGURE 5.24: Portable rail support frame with the magnetizing and sensing carriage during a bridge test (1999).

The bridge projects, started by Herbert Bousack and later led by H. Jochen Krause, were technically very successful and resulted also in significant progress in NDE signal analysis: new methods were developed for the separation of signals of the nonpre-stressed steel reinforcements from the signals of ruptures in pre-stressed steel tendons[66]. The culminating success consisted of finding dangerous flaws in two freeway bridges while automobile traffic continued (Figure 5.24).

The test results, confirmed by opening the bridge deck, resulted in decommissioning, demolition and replacement of these bridges. However, our success was somewhat self-defeating in the sense that the much improved signal analysis eliminated the absolute need for a sensor having a high signal-to-noise ratio in this application; SQUIDs were soon replaced by the conventional magnetometers used today. The sensitivity offered by SQUIDs would be necessary only if mandatory periodical bridge inspections were instituted to detect minute changes in the tendons' magnetic signature.

[65] These junctions and dc SQUIDs were developed by Ulrich Poppe and Michael Faley at another Jülich Institute, and are still available commercially.

[66] G. Sawade et al., in J.H. Edwards, B. Gasper, P. Flewitt, B. Tomkins, P. Stanley and A. McLarty (eds.) *Proc. 4th Conf. on Engineering Structural Integrity Assessment*, Cambridge, U.K., (1998) 353

5.5.4 Airplane Testing

In eddy-current testing, the very low excitation frequency can be an essential advantage when using a SQUID to test for flaws deep beneath the surface. This was the motivation for our involvement in eddy-current airplane testing also initiated by Christoph Heiden. The project included testing of both the fuselage and airplane wheels, which we were developing together with the Lufthansa air carrier and Rohmann GmbH, a German company manufacturing conventional eddy-current test devices ("Elotest"), which use induction coil sensors. Soon thereafter Heiden's group active at Giessen University joined the project. The work involved all aspects of testing with SQUIDs, starting with the development of appropriate excitation coils, which assured differential self-referencing excitation[67], and eventually including signal analysis and the implementation of a commercial Joule-Thomson cryocooler suitable for cooling the SQUID to ≈ 77 K. In all airplane tests we used our rf SQUIDs capable of operating in most unshielded environments due to the elaborate rf shielding perfected over the years (one can find more on rf shielding in Section 5.4).

After our Giessen colleagues first demonstrated the detection of deep-lying cracks in airplane wheels using Yi Zhang's SQUID[68], the joint work concentrated on developing an automated prototype system for testing such wheels in airport facilities with a high level of electromagnetic noise. System tests in the wheel testing facility at the Lufthansa base of the Frankfurt international airport were successfully performed: even the smallest specified flaws of 10% of the wheel rim's cross-section were detected among the much stronger signals of the wheel's keys, an achievement which was then impossible with sensing coils. Nevertheless, such systems were never implemented in practice, mainly because of concerns over high-T_c SQUID sensor's limited reliability and high cost.

The only airplane testing using our high-T_c SQUIDs that found its way into practice was the aircraft turbine engine blade inspection for ferrous inclusions[69]. A three-SQUID second-order gradiometer operating without magnetic shielding was used for that purpose. However, here also the SQUIDs were eventually replaced by conventional magnetometers, in spite of a sensitivity loss by a factor of 20. Overall, our technically successful projects contributed to the further development of NDE methods, but had otherwise no lasting impact on the NDE field. However, in the following I highlight a few successful examples of SQUID NDE that are currently used in practice or expected to be of great value soon.

5.5.5 Two Examples of SQUID NDE Now in the Field

A tough NDE problem, which is solved by the use of low-T_c SQUID, is the eddy-current testing of high-purity niobium sheets and aluminum wires at the manufacturer's facility. In the box "SQUID NDE at Heraeus," you will find a succinct reminiscence of Michael Mück (University of Giessen) on how this testing became a reality at a prominent specialty metals company, W.C. Heraeus.

To Mück's reminiscence I would like to add that quality control of superconducting striated high-T_c conductors for future electric ac power applications seems also to necessitate SQUID gradiometer sensor arrays to detect minute defects in striated conductor filaments[70].

Another example of NDE in the field that requires SQUID sensitivity is the detection of magnetic contaminants in commercial products, such as cheese. After the Product Liability Law was promulgated in Japan in 1995, the Japanese food industry started implementing new methods of quality control to avoid lawsuits. As a result of such a lawsuit, a major Japanese dairy company purchased and implemented in their production line a high-T_c SQUID system capable of detecting, by the MFL

[67] Self referencing compares signals from two spatially separated areas excited by a differential exciter, such as the double-D coil.

[68] M. von Kreutzbruck et al., *IEEE Trans. Appl. Supercond.* 7 (1997) 3279

[69] Y. Tavrin et al., *IEEE Trans. Appl. Supercond.* 9 (1999) 3809.

[70] T. Hato et al., *Physica C*, 469 (2009) 1630

SQUID NDE at Heraeus (by M. Mück)

At Giessen University, we were approached by David Lupton of W. C. Heraeus, Hanau, who was interested in testing Russian platinum coins for ferromagnetic inclusions. The amount of such inclusions could hint to the origin of the platinum metal of which the coins were made. As only a few of these coins survive today, a chemical analysis, which might have damaged the coin, was out of the question. Instead, a simple measurement of the static field produced by the coins using our SQUID microscope revealed abundant ferromagnetic inclusions in the coin, and from this their place of origin could be traced. That was back in 1999. Details about this work were published in the journal *Platinum Metals Review*. These measurements in turn raised the interest of Friedhold Schölz of Heraeus, and Waldemar Singer of DESY, Hamburg, who were working on superconducting cavities for particle accelerators. Such cavities are made from extremely pure niobium sheets; inclusions of foreign material in such sheets, even extremely small ones, will dramatically reduce the critical current density of the cavities and thus the obtainable acceleration voltage. As forming the cavities is quite expensive, Schölz and Singer were interested in a nondestructive testing method which could reliably find even the smallest inclusions in a rather short time. We quickly determined that when using eddy-current testing, the required field sensitivity of the SQUID should be better than 50 fTHz$^{-1/2}$, a sensitivity which can reliably be obtained only from a niobium (low-T_c) SQUID.

The potential customers quickly agreed that the additional few Euros per day for the liquid helium were not a major obstacle as the major cost of testing is in the labor. Subsequently, we developed two SQUID systems in Giessen, and made two more for Heraeus, two for WSK Meß-und Datentechnik, Hanau, and one for DESY, all designed for testing flat metal sheets. Subsequently, we tested several hundred sheets and compared the results to those obtained with a conventional eddy-current system; this proved the much higher detection sensitivity of the SQUID system. For the projected (and partly funded) tera-electron-volt accelerator TESLA, several hundred thousand niobium sheets will have to be tested[a]. The usefulness of the SQUID systems triggered their application to many other testing purposes at Heraeus. They are now regularly testing products, such as noble-metal sheets or sintered sputtering targets, with the SQUID system. Recently, we developed for them a new SQUID system which is used for testing 1-mm-dia. aluminum wires which they use to make 25-micron-diameter aluminum bond wires. When drawing the aluminum wire to smaller diameters, foreign inclusions (e.g., of aluminum oxide), which are larger than a few microns, will cause the wire to break. With a specially-designed helium cryostat that allows us to pull the wire at room temperature through superconducting pick-up loops connected to a SQUID, we have been able to detect minute inclusions of aluminum oxide or silicide, which were only a few microns in size. This eddy-current test allows now for discarding faulty wires even before drawing them to smaller diameters, and saves both labor and cost.

[a] That would require a higher number of test systems.

method, minute magnetic inclusions in cheese blocks at a depth up to 15 cm, which is impossible for conventional magnetometers. The system, developed by Saburo Tanaka and his group, contains three partly shielded dc SQUID magnetometers arranged along a line transverse to the direction of motion of the cheese-carrying conveyor such that the requisite detection sensitivity is assured at any point of that line above the tested object[71]. Cheese blocks pass first through a magnetization unit

[71] T. Nagaishi et al., *IEEE Trans. Appl. Supercond.* 17 (2007) 800

FIGURE 5.25: The cheese inspection system distributed in Japan by AFT (Advanced Food Technology Co., Ltd). Tested cheese blocks, placed on the conveyer belt on the left side, pass through the magnetizing unit and subsequently under the sensing SQUIDs. The operator's console is visible on the right side (Courtesy Saburo Tanaka).

and then move under the sensing magnetometers. The external view of this system is shown in Figure 5.25. Two such systems were installed in different plants and have been operating reliably (one has been continuously operated for five years). Another such unit is supposed to be installed soon. Occasional inspection of imported cheeses indicates that they often contain inadmissible amounts of magnetic contaminants. Unfortunately, high cost still hampers broader implementation of this method[72].

5.5.6 SQUID NDE Microscopy in Semiconductor Technology

An NDE application of high-T_c SQUIDs, which might still have a bright future, is the complex failure analysis of integrated circuits (ICs). This application was first proposed in the past decade. A Joule-Thompson cryocooled scanning SQUID microscope was then developed for magnetic analysis of current distribution in multichip packages[73] and put on the market under the name MAGMA^{TM}. This near-field flux imaging system permits one to image induced currents in interconnect wiring and is mainly useful for detection of shorts and high-resistance failures in IC packages held at room temperature. The close proximity of the SQUID to the tested IC, necessary for lateral resolution, is made possible by a very thin small-diameter sapphire window. Rather few such instruments have been sold for use by semiconductor industry, but they are still commercially available from Neocera, LLC., also with two complementary sensing heads–in addition to the SQUID a GMR (giant magnetoresistance) sensor provides enhanced spatial resolution[74].

The MAGMA system was perhaps developed ahead of its time because cheaper and simpler failure analysis tools were adequate in most cases. However, new opportunities might soon arise for

[72] A major Japanese effort in this area is planned to start in 2010–2011; it might eventually result in much broader implementation of SQUID NDE in Japanese food industry.

[73] E. F. Fleet et al., *Rev. Sci. Instr.* 72 (2001) 3281

[74] See http://www.neocera.com/semi_metrology.htm. The SQUID head lateral resolution is in the micrometer range, the GMR head resolves 250 nm. All unpublished information supplied by Antonio Orozco and Venky Venkatesan, Neocera, LLC.

the MAGMA because of the current trend towards more levels of interconnect in chips[75] and novel packaging technologies such as system-in-package, wafer-level-packaging and through-silicon-vias (TSV)[76]. These emerging multi-die 3D solutions may eventually replace today's multichip designs.

Stacking of multiple devices vertically in many opaque layers will make today's optical analysis tools useless. In contrast, magnetic field analysis appears as a natural option, provided it could localize defects both laterally and vertically with the required resolution, and identify not only shorts, but also open circuit failures. This is the performance actively pursued, but not yet fully attained, by the MAGMA development team.

A different approach to IC complex failure analysis using SQUID microscopy has been taken by Nikawa and coworkers at NEC, Japan[77]. They use laser beam excitation of photocurrents in p-n junctions, and in a two-step localization process can apparently identify and locate both shorts and open circuit failures. In the second localization step, the tested circuit is placed in the SQUID vacuum chamber to minimize the SQUID-to-circuit distance. By the time of this writing (2010), the method is apparently close to industrial implementation.

5.5.7 Concluding Remark

Of many SQUID applications, NDE is not one poised for rapid growth and major economic significance. However, in especially difficult cases, where nothing else can do, SQUID sensors are and will continue to be a valuable NDE tool.

5.6 SQUIDs — from Laboratory Devices to Commercial Products

Ronald E. Sager

5.6.1 Early SQUIDs as Laboratory Devices

I first encountered SQUIDs in 1974 when I joined Professor John Wheatley's group at the University of California San Diego as a graduate student, shortly after superfluidity in ^{3}He was discovered[78]. As part of the intense competition among research groups around the world to explore this new realm of quantum physics, John was using Zimmerman-style two-hole rf SQUIDs[79] to study ^{3}He's fascinating magnetic properties. At that time John was the unchallenged leader in using SQUIDs as tools for low-temperature research. Indeed, shortly after joining the group I was told that while most researchers were still struggling to make one SQUID work reliably, John had five SQUIDs in his cryostats and every one of them worked on every cool-down (see box). In 1971 John had published a comprehensive review article on the operation of rf SQUIDs, which became a sort of "SQUID Mechanic's Handbook" for the novice SQUID user.[80] This 78-page treatise discussed the theory of rf SQUIDs, the electronic circuits for driving them, their empirical characteristics and their operating parameters. It also included descriptions of various SQUID applications, such as

[75] The ITRS (International Technology Roadmap for Semiconductors) envisages, for example, 12 interconnect levels by 2014–2016, when the DRAM half-pitch (node) will decrease to 22 nm.

[76] ITRS 2009: see http://www.itrs.net/Links/2009ITRS/Home2009.htm

[77] K. Nikawa et al., *IEICE Trans. Electron.* E92-C (2009) 327

[78] D.D. Osheroff et al., *Phys. Rev. Lett.* 28 (1972) 885

[79] J.E. Zimmerman et al., *J. Appl. Phys.* 41 (1970) 1572

[80] R.P. Giffard et al., *J. Low Temp. Phys.* 6 (1971) 533

Adjusting the Critical Current in Early SQUIDs

Because the early two-hole rf SQUIDs typically used a pointed niobium screw contacting a hard flat niobium surface to create the point contact (see Section 5.2), the critical current of these devices would frequently shift rather dramatically from one cool-down to the next. Because the critical current of the SQUID needed to be within a fairly tight range for the SQUID to operate correctly, it was important to have a method for adjusting the critical current of the SQUID after the device was cold. Some researchers used a long screwdriver, extending from the top of the cryostat to the SQUID, to mechanically adjust the point contact while the SQUID was cold, but John's group developed a more innovative technique. Someone in the lab had discovered that, after the SQUID was cold, its critical current could be increased by discharging a capacitor through the rf coil—the bigger the capacitor, the more the critical current would increase. This naturally led to the practice of setting the point contacts at room temperature to have a rather low critical current and then adjusting the critical current in situ using a set of "calibrated capacitors", each of which was labeled with the expected increase in critical current.

pico-voltmeters and pico-ammeters, and it even described the use of SQUIDs to do thermometry at low temperatures.

5.6.2 First Commercialization of SQUIDs

In 1970 John and several of his colleagues in the low-temperature physics community invested their personal funds to found a new company in San Diego, CA, called SHE Corporation. "S", "H", and "E" were pronounced separately and represented SHE's three core competencies: superconductivity, helium and electronics. (Occasionally a reporter would telephone with a request to do an article on San Diego's "all-women company"!) SHE's business plan was to convert the dilution refrigerator and SQUID technology that already existed in John's laboratory into commercial products and sell them to the general low-temperature physics research community. The company succeeded in this endeavor from the very beginning.

Less than a year after being formed, SHE was shipping SQUIDs and dilution refrigerators on a commercial basis—the first company ever to offer a SQUID for commercial sale. These first products were essentially copies of equipment that was being used in John's lab. In particular, the first SHE rf SQUIDs used the Zimmerman two-hole design, and they were subject to the same instabilities in critical current that were inherent to this design. Consequently, each SHE SQUID was shipped with an adjustment tool so the customer could readjust the critical current of the device when it shifted.

By 1974 SHE had made two major advances which transformed the way SQUIDs were used. The first improvement was SHE's toroidal SQUID which they called the TSQ (see box). While the toroidal design itself offered some advantages, the most important improvement by far was the TSQ's permanently adjusted point contact. The new point contact design, developed by Michael Simmonds, used a small piece of electropolished niobium foil as the surface against which the pointed niobium screw was adjusted. The flexibility of the foil not only made it much easier initially to adjust the point contact, it also made the critical current very reproducible when the device was cooled down. In fact, the critical current of these devices was so stable that the TSQ was permanently sealed inside a hermetic package with just the screw terminals for the rf and input coils showing—and for the first time SHE offered a one-year warranty on their SQUIDs. This single innovation, by itself, transformed SQUIDs from temperamental devices that might fail on any cool-down into reliable tools for low-temperature research.

The Toroidal SQUID

The toroidal rf SQUID derives its name from the toroidal shape of the modulation and input coils as well as the toroidal nature of the SQUID body. The toroidal SQUID geometry has two major advantages: 1) both the coils and the point contact are shielded from external magnetic fields by the SQUID body and 2) the toroidal SQUID can be designed to have very low self-inductance which increases the SQUID's inherent sensitivity (see section 5.2.10). The toroidal geometry of the coils can be seen in Figure 5.26.

The second major innovation from SHE was a modern version of the SQUID control electronics which drove the SQUID. The new SQUID electronics, christened the Model 330 SQUID Controller, allowed the user to set up and adjust the RF drive, gain and other parameters without an oscilloscope, just by watching a meter on the front of the unit. The Model 330 was introduced about the same time as the TSQ SQUID, and together they revolutionized the use of SQUIDs by the research community.

SHE also introduced the next major improvement in commercial SQUIDs. When I joined SHE in December 1979, my first project was to assist Mike Simmonds in developing the SHE "Hybrid SQUID". This design employed true Josephson junctions formed on a silicon chip substrate using microcircuit fabrication techniques. The silicon chip, with its niobium films and Josephson junctions, was then mated to a bulk niobium SQUID body containing the toroidal modulation and input coils. The geometry of this design is shown in Figure 5.26. The design was originally developed as a dc SQUID, but since it was mechanically more stable under thermal cycling than the TSQ point contact design, we also developed an rf version of the Hybrid SQUID, which immediately replaced the TSQ. The dc Hybrid SQUID went on to become SHE's first dc SQUID, which offered a substantial improvement in sensitivity over SHE's rf SQUIDs and kept SHE at the forefront of commercial SQUID technology. However, this would be SHE's last significant contribution to that technology; the torch would soon pass to a new company about to be formed.

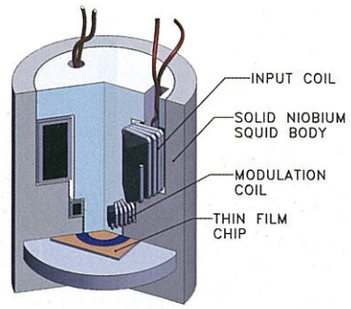

FIGURE 5.26: The SHE Hybrid SQUID showing the toroidal modulation and signal coils in a bulk niobium SQUID body. The Josephson junctions and niobium contact pads were fabricated on a thin-film chip, which was then mated to the niobium body forming superconducting contacts between it and the niobium pads on the chip.

5.6.3 SHE — Early SQUID Instrumentation

In addition to pioneering the commercialization of SQUID sensors, SHE also led the way in developing SQUID-based instruments for a variety of applications. Not surprisingly, SHE's initial

SQUID-based products were designed for applications similar to those found in John Wheatley's laboratory—a pico-ammeter, a pico-voltmeter and other equipment typically suitable for use only by highly skilled scientists. However, the company soon moved on to more user-friendly instruments. Their first major product of this type was a geophysical magnetometer system employing three SQUIDs with their respective detection loops configured as a 3-axis vector magnetometer. This instrument was constructed with the three detection loops wound around a quartz cube suspended from the end of a fiberglass cryogenic probe, with the SQUIDs mounted above in superconducting shields. The probe was then inserted into a fiberglass, nonmagnetic liquid helium cryostat. These instruments were primarily used in magnetotelluric research (see section 5.4.2).

The SHE SQUID Biomagnetometer employed a similar design with the cryogenic probe supporting the quartz substrate for the detection coil and SQUID, all within a small fiberglass cryostat. In this instrument, the cryostat had a special tail design that allowed the detection coil to be less than 1 cm from the outside surface of the cryostat tail while still being immersed in the liquid helium bath. The detection coil was wound in the form of a second-derivative gradiometer insensitive to magnetic fields which are uniform or have only a first-derivative spatial variation. Several researchers used these single channel biomagnetic gradiometer systems to perform some of the first experiments to detect the magnetic fields produced by electrical activity in biological neural systems—work which would eventually lead to their wider use in the field of biomagnetometry[81] presented in Chapter 10.

FIGURE 5.27: The SHE Variable Temperature Susceptometer (VTS). This instrument was the first commercial SQUID sample magnetometer that provided automatic control of the magnetic field, sample temperature and measurement process. SHE sold about 45 of these instruments before they were discontinued in mid-1986.

SHE also designed and manufactured the Variable Temperature Susceptometer (VTS), shown in Figure 5.27. (I will refer to SQUID-based sample measurement systems like the VTS as sample magnetometers to differentiate them from SQUID vector magnetometers such as those used in magnetotelluric measurements.) This instrument employed SQUID detection coils in a gradiometric arrangement positioned at the center of a superconducting solenoid which could generate a high magnetic field. A variable temperature sample chamber located in the center of the SQUID detection coils (but thermally isolated from them) allowed the sample temperature to be controlled independently. By moving the sample vertically through the SQUID detection coils the magnetic moment of the sample could be measured with high accuracy and tremendous sensitivity over a wide range of both magnetic field and temperature. The SHE VTS was the first commercial SQUID-based sample magnetometer, but it was extremely complicated and very difficult to build.

[81] D. Cohen, *Science* 175 (1972) 664

In spite of a strong technology lead in a variety of SQUID technologies, in about 1982 SHE made a corporate decision to pursue medical applications for SQUIDs, and they chose to focus on the field of magnetoencephalography (MEG). This would entail a massive development program, and in 1983 SHE accepted its first round of investment capital to pursue this potentially lucrative business. Soon after making their initial investment, the new investors renamed the company Biomagnetic Technologies, Inc. (BTi) and hired a new president whose primary duty was to raise money to fund the development effort—tens of millions of dollars would be needed to develop the 160-channel SQUID systems and data analysis software that would be required for this demanding application. With their total commitment to the medical business, BTi's interest in laboratory equipment began to decline.

5.6.4 Quantum Design — Advanced SQUID Instruments

Just before SHE decided to pursue the MEG business, Barry Lindgren, Mike Simmonds, David Cox and I left SHE to form Quantum Design, which was officially incorporated on April 12, 1982. Our first sales were externally funded research projects, but we also began to look for products that we might develop and manufacture, and our attention soon focused on the deficiencies of the SHE VTS. Believing that we could solve many of the VTS' problems with a different design approach, we undertook the development of the Quantum Design Magnetic Property Measurement System (MPMS). The first MPMS, with a conservative 2 T magnet, was shipped to Professor Robert Shelton at Iowa State University in July of 1984 and became an immediate success. It also brought us into direct competition with SHE's VTS, which forced us to immediately redesign the MPMS to accommodate a 5.5 T magnet; this field intensity was later increased to 7 T. The first of what would become the classic Quantum Design MPMS was shipped in December 1985.[82] One of these original MPMS systems is shown in Figure 5.28. Within a few months

FIGURE 5.28: The classic MPMS. This instrument, introduced in 1985, would become the first and only SQUID sample magnetometer to be widely sold in a commercial market. An enhanced version of this instrument, known as the MPMS-XL, is still being sold in 2010.

[82] To Prof. Allen Goldman, University of Minnesota.

the MPMS had captured the entire market for SQUID sample magnetometers and in mid-1986 BTi announced that they would no longer offer the VTS for sale.

In retrospect, it is clear that this was when the industrial leadership in SQUIDs and SQUID-based laboratory instruments shifted from BTi to Quantum Design. As a result of BTi's decision to pursue the MEG medical markets, Quantum Design now had the entire market for SQUID sample magnetometers all to itself—literally within a few weeks of the publication of the discovery of the high-T_c materials[83]. The initial publication of this ground-breaking discovery received remarkably little attention until other researchers confirmed the results in late 1986, culminating in the "Woodstock of Physics" at the March 1987 APS meeting in New York City. Prior to this meeting, sales of the MPMS had been slow but steady. This changed dramatically over the next few months, particularly in the Japanese market. At the time of the "Woodstock of Physics", we had shipped only 8 MPMS systems over the previous two years. Over the next 15 months we shipped nearly 40 instruments and by mid-1988 a veritable tidal wave of orders had driven our backlog to more than 50 instruments, pushing our quoted delivery times out to 15 months. With orders still pouring in, it took us two years to fully ramp up production to meet the demand. By the time the initial excitement of the HTS discovery had subsided, Quantum Design had sold nearly 200 MPMS instruments. SQUID sample magnetometers, which had previously been specialty instruments used by only a few select researchers, had become a laboratory necessity for anyone doing materials research.

The huge surge in sales of our MPMS system also drove the next significant development in commercial SQUID technology. In 1987 we were still purchasing all of our SQUID sensors from BTi at a cost of well over $300,000/year. When our request for a volume discount was declined, under the leadership of Mike Simmonds we constructed a clean room and developed our own all-thin-film SQUID sensor, in which the modulation and input coils are fabricated right on the SQUID chip. This work led to two more significant inventions by Mike: a double-balanced SQUID design (shown in Figure 5.29), which uses a symmetrical geometry to decouple the modulation and input coils, and a technique for creating superconducting bonds to the niobium input coils on the SQUID chip which allows input coil currents exceeding 20 mA. Within 18 months Quantum Design was producing its own SQUID sensors, thereby eliminating our dependence on BTi SQUIDs. Ironically, Quantum Design would eventually reverse its relationship with BTi by supplying several thousand dc SQUID sensors to BTi, complete with transformer and matching network, for use in their MEG instruments. In addition, we supplied an additional 10,000 bare chips to BTi to insure their supply of SQUIDs. Although BTi no longer exists (the company declared bankruptcy in February 2009), Quantum Design still supplies SQUID sensors to several other companies that build SQUID-based instruments for special applications.

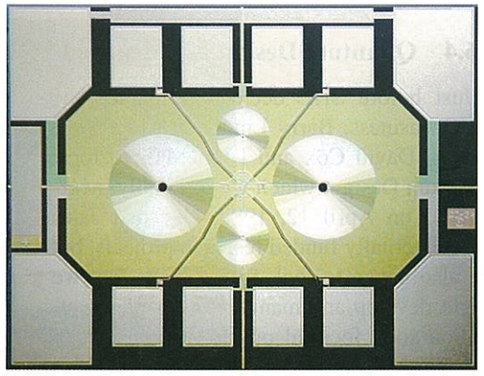

FIGURE 5.29: The Quantum Design double-balanced SQUID. The large and small circles are the input and modulation coils respectively. The SQUID itself is the octagonal structure under the coils, and the rectangular structures around the edges are the electrical contact pads. This chip is used in both rf and dc SQUIDs manufactured by Quantum Design.

The nature of the high-T_c materials, in particular their flux-pinning behavior at very low magnetic

[83] J.G. Bednorz and K.A. Mueller, *Z. Phys.* B64 (1986)189

fields, had a significant impact on the further development of the MPMS technology. The need to study these behaviors in detail led to the development of the MPMS Low-Field Option with its precision magnet control and the MPMS AC Magnetization Option. Other options provided researchers with the ability to measure samples at higher temperatures and with greater sensitivity in high magnetic fields. These options made the MPMS a powerful research tool with a temperature range of 2 K to 800 K, magnetic field range of 1 μT to 7 T and the ability to measure magnetization over a dynamic range spanning 11 orders of magnitude.

The automated temperature and magnetic field control of the MPMS led to Quantum Design's next major product. In response to repeated customer requests for an "MPMS without the SQUID", the company developed the Physical Property Measurement System (PPMS), which provided the requisite temperature and magnetic field control, but was designed to offer a much broader suite of non-SQUID measurements, including ac-dc magnetization, magnetic anisotropy, heat capacity, electro-transport and thermo-transport measurements. In addition, the PPMS operating temperature range was extended up to 1000 K and down to 50 mK. The Low-Field Option was also adapted to the PPMS, and the system can now accommodate magnetic fields up to 16 T. This suite of measurement capabilities has made the PPMS an extremely versatile, multipurpose instrument.

Another major advance in the technology of SQUID sample magnetometers occurred in the mid-1990s when cryocoolers employing regenerators based on magnetic materials such as erbium-nickel and holmium-copper became available. These coolers could reliably achieve temperatures below 3 K, and in 1998 Quantum Design began to use these coolers in the EverCool option for the MPMS. After an initial transfer to cool the system down from room temperature, the MPMS EverCool completely eliminated the need for additional liquid helium. The MPMS thus became the first SQUID magnetometer to eliminate the need for constant LHe replenishment. After its introduction, the EverCool became an immediate success, particularly in Japan where liquid helium has been approximately twice as expensive as in America. By 2000 this technology was also available on PPMS systems.

FIGURE 5.30: The Quantum Design SQUID-VSM. This instrument, which combines a vibrating sample drive with a SQUID-based detection system, provided substantial improvements over earlier SQUID sample magnetometers in sensitivity, temperature control and the speed of data collection.

During the 1990s the MPMS faced significant competition from several other manufacturers prompting us to upgrade the system in 1996 to provide faster measurements and enhanced temperature control. The upgraded instrument, designated the MPMS-XL, was still the world leader in SQUID Sample Magnetometers until it was finally eclipsed by the next major advance in SQUID instrumentation, the Quantum Design SQUID-VSM (Vibrating Sample Magnetometer) shown in Figure 5.30.

The slow measurement process of both the MPMS and its predecessor, the SHE VTS, was a significant weakness of both instruments. The Reciprocating Sample Option introduced on the MPMS-XL improved the measurement speed, but its relatively low oscillation frequency still limited its effectiveness. To further improve the speed of data collection, the SQUID-VSM works at frequen-

cies up to 40 Hz and employs the full power of phase-sensitive detection. When the SQUID-VSM was introduced in March 2006, its temperature control was also much faster than the MPMS-XL and a new patented superconducting magnet technology permitted high-sensitivity measurements to be made without de-energizing the magnet power supply. These features allow the SQUID-VSM to make measurements at least five times faster than the original MPMS. Furthermore, the higher operating frequency and more powerful phase detection scheme improved the sensitivity of the SQUID-VSM in high magnetic fields by nearly a factor of 100 over the original MPMS system.

5.6.5 The Market for SQUID-based Instruments Today

From the story above, it might appear that the history of commercial SQUID-based laboratory instrumentation is like a tale of two companies. There is reasonable justification for this. After developing the early commercial SQUID sensor and instrument technology, SHE Corporation chose to pursue medical applications, leaving Quantum Design as the dominant player in the SQUID instrumentation market. The extent to which this is true can be appreciated by reviewing the small group of companies that sell SQUIDs and SQUID-based instruments today. These are listed in Table 5.1, along with a brief note on the types of instruments they offer. This table is not necessarily comprehensive, and does not include most companies working in the fields of medicine, and applications discussed in other chapters of this book.

With the sole exception of Quantum Design, the companies listed in Table 5.1 have all failed to find significant commercial applications for SQUIDs; at best, some of them have found small niche markets for a particular product. For example, 2G Enterprises (presented in Section 5.4) has enjoyed a stable market for their rock magnetometers of about four systems per year for the past 25 years.

Tristan Technologies appears to offer the broadest range of products, including HTS and LTS SQUID microscopes, a rock magnetometer, a Biomagnetic Liver Susceptometer and various other SQUID-based specialty instruments. However, these instruments were all designed as specialty products for a specific customer with the hope that they will eventually find a broader market.

Other than Quantum Design, Cryogenics Ltd. (CL) is the only company in Table 5.1 that has achieved significant size or that offers a SQUID sample magnetometer. The CL Model S700X SQUID Susceptometer does compete with Quantum Design's MPMS products, but CL sells very few of these instruments, and their business is based primarily on their superconducting magnet technology. All the other companies listed in Table 5.1 offer only niche products in markets smaller than \$1-\$2 million dollars/year and have only a few employees. Hence, it is probably fair to say that Quantum Design is the only company in the world that has achieved significant commercial success with SQUID-based laboratory instruments.

5.6.6 Future Directions for SQUIDs in Laboratory Instrumentation

While MEG is the largest application for SQUIDs in terms of device numbers, with astronomy rapidly catching up (see Section 5.7), SQUID-based laboratory instruments will continue to be an important market. SQUID sample magnetometers have become an essential tool in materials research and this market remains robust. It is not clear, however, where SQUID enthusiasts will find other significant commercial markets. Since SHE first brought SQUIDs into the commercial market in 1971, many companies have tried to apply the devices to a variety of different problems, and most of those companies have either failed completely or remained very small.

In general, there are always two major obstacles to using SQUIDs: (1) they require a cryogenic environment to operate, and (2) their exquisite sensitivity to magnetic fields, which is their most important strength, is also their most important weakness. The first problem, the need for a cryogenic environment, is not necessarily prohibitive for many applications, but it does increase the cost and complexity of SQUID-based instruments. The second problem is equally vexing. The SQUID's incredible sensitivity to magnetic fields gives it a unique capability, but the SQUID is equally sensitive

TABLE 5.1: Companies Manufacturing SQUIDs and SQUID Instrumentation

Company	Products
2G Enterprises (USA)	LTS Rock Magnetometers
Aivon Oy (Finland)	LTS SQUIDs: SQUID Sensors & Electronics
Cryogenics Ltd (UK)	LTS Sample Magnetometer System
Cryoton (Russia)	LTS and HTS SQUIDs: 3-Axis Vector Magnetometers, MCG Systems[a]
EZ SQUID (Germany)	LTS dc/rf SQUIDS, NDE Measurement Systems
Juelicher SQUID GmbH (Germany)	HTS SQUIDs: Resonators/Phase-Locked Oscillators
Magnesensors (USA)	HTS SQUIDs: Externally Funded Research
Magnicon GmbH (Germany)	LTS and HTS SQUIDs: Vector Magnetometers/Gradiometers & Fast Electronics
Quantum Design (Worldwide)	LTS SQUIDs: SQUID Sensors & Sample Magnetometers
Star Cryoelectronics (USA)	LTS and HTS SQUIDs: SQUID Sensors & Electronics
Supracon AG (Germany)	LTS SQUIDs: MCG, JJ Standard[b], Geomagnetic Systems
Tristan Technologies (USA)	LTS/HTS Specialty SQUID Systems

[a] MCG refers to magnetocardiography, measurement of magnetic fields originating from the heart.
[b] JJ Standard refers to Josephson Junction Voltage Standard.

to background magnetic fields—and the world is full of them. There are several ways to address this problem such as counter-wound detection coils (gradiometers of various orders), magnetic shielding and the use of ancillary sensors to numerically analyze and remove the interfering signals, but these measures all increase the cost and complexity of SQUID-based instruments and, to some extent, reduce their utility. In some cases, even though the SQUID instrument is more sensitive or more capable than a competing room temperature instrument, the additional cost and complexity of the SQUID instrument makes it financially uncompetitive against its more conventional and cheaper competitors. So it seems likely that the same factors that have limited the use of SQUIDs in the past will continue to haunt them in the future.

Nonetheless, SQUIDs are a powerful tool for certain uses, and when applications are found where SQUIDs provide a unique solution to an important problem, they will be accepted in spite of their expense and complexity. In the meantime we can be sure that a small but dedicated group of researchers and companies will continue to search for promising new commercial applications for these amazing and unique sensors—and occasionally one of them may be successful.

5.7 Electromagnetic and Particle Detection and Readout

John Clarke, Kent Irwin and Peter Michelson

5.7.1 DC SQUID Amplifiers

John Clarke

The notion of using a dc SQUID as an amplifier goes back to my Cavendish days, when I coupled together two SLUGs[23]. It was not until 1979, however, after Claudia Tesche and I had worked out the noise theory of the SQUID,[27,29] that we developed the theory for the SQUID amplifier that subsequently led to the development of radiofrequency amplifiers with high gain and low noise temperature. We calculated the flux-to-voltage transfer coefficient, V_Φ, the spectral densities of the voltage noise across the SQUID, $S_V(f)$, and current noise around the loop, $S_J(f)$, and the voltage-current cross spectrum, $S_{VJ}(f)$. This partial cross correlation arises from the additional voltage noise induced across the SQUID by the circulating current noise provided $V_\Phi \neq 0$. The essential concept for a tuned amplifier is shown in Figure 5.31. An rf signal $V_i(f)$ with source impedance R_i coupled to the tuned input circuit induces a current that in turn generates a flux in the SQUID and hence a voltage $V_o(t)$ at the output. Together with the late Robin Giffard[84], we realized that the SQUID amplifier is in a sense the dual of a semiconductor amplifier, for example, a field effect transistor (FET). In our picture, the voltage noise across the SQUID is represented as a "virtual" current noise in the input circuit, while the current noise in the SQUID loop injects an "actual" voltage noise into the same circuit. In the case of the FET, the current noise at the input is "actual" whereas the voltage noise is "virtual". Either way, by tracing the effects of the two noise sources to the output, one can calculate the amplifier noise temperature[85], T_N, which can be minimized by varying the parameters of the system. In the case of the SQUID tuned amplifier, under certain approximations, the minimum noise temperature is $T_N = (\pi f/k_B V_\Phi)(S_V S_J - S_{VJ}^2)^{1/2}$ at a frequency below that of maximum gain. The cross-term S_{VJ} reduces T_N significantly, by roughly a factor of 3, compared with its value on resonance, where S_{VJ} drops out. At the same time, off-resonance operation results in a modest reduction in gain.

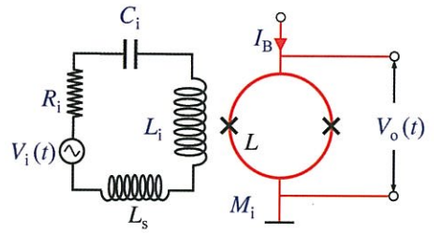

FIGURE 5.31: Configuration of SQUID tuned amplifier. V_i is the input signal with source impedance R_i, L_s is stray inductance, C_i is the tuning capacitor, L_i and M_i are the input inductance and its mutual inductance to the SQUID, which has loop inductance L and bias current I_B.

Subsequently, Claude Hilbert, John Martinis and I explored SQUID tuned and untuned amplifiers in considerable detail[86,87,88]. In the tuned case, Claude achieved a gain of about 19 dB and a noise temperature of 1.7 K in an amplifier at 4.2 K, on resonance at 93 MHz[88]. These results were in good agreement with the theoretical model. Later, Claude, Erwin Hahn, Tycho Sleator and I used a SQUID-tuned amplifier to detect nuclear quadrupole resonance in ^{35}Cl at 30.6856 MHz. In particular, we were able to observe "spin noise"[89]. The $KClO_3$ sample was placed in a superconducting coil, replacing the resistor and voltage source of Figure 5.31. We equalized the populations of the two (doubly degenerate) nuclear spin levels by means of an rf signal at the NQR frequency, and then turned off this signal. We observed the spontaneous emission of photons emitted into the tuned circuit as the excess spin population of the upper level relaxed towards its equilibrium value. The spontaneous emission rate, given by Einstein's A coefficient, corresponds to roughly one spin flip every one million centuries! Nonetheless, there was an observable signal from the 2×10^{21} spins.

An intriguing aspect of the dc SQUID amplifier is that it can, in principle, approach the quantum limit. In 1982, the late Roger Koch, Dale van Harlingen and I revisited Claudia's SQUID equations, replacing the classical Nyquist current noise spectral density in the resistive shunts, $4k_BT/R$, with the quantum expression $(2hf/R)\coth(hf/2k_BT)$. In the limit of zero temperature, this expression reduces to $2hfR$. Roger ran the equations in the $T = 0$ limit[90], and found $T_N = hf/k_B$ for a SQUID tuned amplifier—the quantum limited value for a linear, phase-preserving amplifier. In this case, on average, one-half photon exists in the tuned circuit (the zero-point energy of a quantum harmonic oscillator) and the other one-half photon is contributed by the amplifier. The cross-spectral density makes a significant reduction in the noise when the parameters are optimized; the amplifier cannot be quantum limited on resonance.

Attaining a quantum-limited noise temperature implies a signal frequency $f > k_BT/h$; for $f =$ 1 GHz, $T \approx 50$ mK. In the 1980s, we were interested in frequencies below—often far below—100 MHz, and quantum-limited noise temperatures were not something we thought about. All this changed, however, when Leslie Rosenberg and Karl van Bibber visited me in 1994. They had recently commissioned a novel experiment at Lawrence Livermore National Laboratory to search for the putative axion (see below), and were keenly interested in an amplifier operating in the 1 GHz frequency range with a noise temperature substantially lower than that of a cold HEMT (high electron mobility transistor), typically 2 – 5 K.

How does one do this with a SQUID? The essential problem with operating a square-washer SQUID (Figure 5.13) at 1 GHz is the parasitic capacitance between the coil and the washer that rolls off the gain at frequencies above typically 100 MHz. To tackle this problem, Marc Olivier André and I at Berkeley joined forces with Michael Mück, Jost Gail and the late Christoph Heiden at the University of Giessen in Germany. Michael made the crucial breakthrough. Instead of applying the signal between the two ends of the input coil, as in the conventional SQUID, he moved one wire and applied the signal between one end of the coil and the SQUID washer. The washer now serves as a groundplane for the coil, forming a transmission line or microstrip, thus making a virtue of the coil-washer capacitance[91] [Figure 5.32 (a)] . When the length of the microstrip corresponds to a half-wavelength of the signal, the resonance produces a substantial level of gain—typically 20 dB — as shown in Figure 5.32(b). As one progressively shortens the coil, the resonance moves to higher frequency. The actual dependence of the frequency on the coil length is somewhat complicated because the inductance of the microstrip is dominated by the inductance coupled in from the SQUID loop. Suffice it to say, the microstrip SQUID amplifier (MSA) attains useful levels of gain from 0.2 to 2 GHz.

[84] J. Clarke et al., *J. Low Temp. Phys.* 37 (1979) 405

[85] The noise temperature T_N is defined as follows. In the classical limit, a resistor R_i at the input terminals of the amplifier produces a Nyquist noise power k_BTR_iG at the output, where G is the power gain. The total noise power at the output is $k_BR(T_i + T_N)G$. Thus, T_N is a simple way of representing the noise of any amplifier.

[86] J. Martinis et al., *J. Low Temp. Phys.* 61 (1985) 227

[87] C. Hilbert and J. Clarke, *J. Low Temp. Phys.* 61 (1985) 237

[88] C. Hilbert and J. Clarke, *J. Low Temp. Phys.* 61 (1985) 263

[89] T. Sleator et al., *Phys. Rev. Lett.* 55 (1985) 1742

[90] R.H. Koch et al., *Appl. Phys. Lett.* 38 (1981) 380

[91] M. Mück et al., *Appl. Phys. Lett.* 72 (1998) 2885

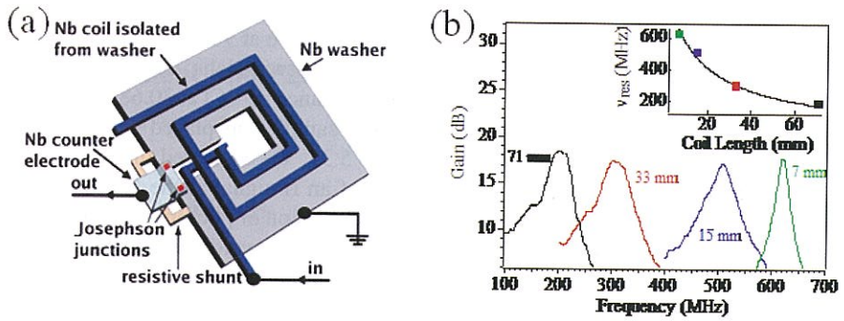

FIGURE 5.32: Microstrip SQUID amplifier. (a) Configuration. (b) Gain versus frequency for four coil lengths.

Michael, Jan Kycia and I measured the noise temperature of an MSA cooled in a dilution refrigerator. To overcome the noise of the cooled HEMT postamplifier, we used a second MSA as a postamplifier. As we cooled the experiment, we found that T_N indeed scaled with T as expected from the expression for the noise energy. Below roughly 100 mK, however, T_N flattened out. Separate experiments showed that the flattening was due to hot electrons generated in the resistive shunts by the bias current, an effect studied years earlier by Fred Wellstood, Christian Urbina and myself[92]. Nonetheless, the MSA attained a noise temperature on resonance of 47 ± 10 mK at 519 MHz, a factor of about two higher than the quantum limit[93].

Subsequently, Darin Kinion and I repeated the experiment, redesigning the MSA slightly to increase the gain so that we did not require a second MSA[94]. In addition, we added cooling fins to the shunts to lower the electron temperature. Figure 5.33 shows the gain and noise temperature versus frequency for our best device, cooled to 45 mK. The maximum gain, 20.4 dB, occurred at 620 MHz, at which frequency $T_N = 66 \pm 5$ mK. The lowest noise temperature, however, 48 ± 5 mK, occurred at 612 MHz, slightly below the resonance frequency, in qualitative agreement with our prediction 30 years earlier. The lowest achieved noise temperature was a factor of 1.6 above the quantum-limited value of 29.4 mK at 612 MHz. This value of T_N is about 30 times lower than that of the best cooled HEMT amplifiers.

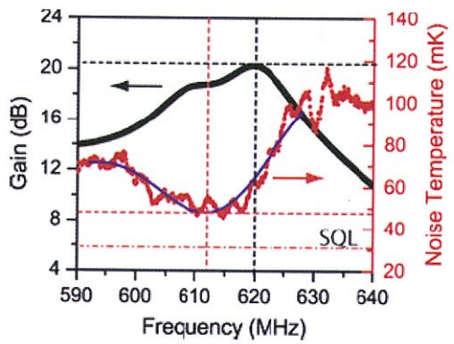

FIGURE 5.33: Performance of microstrip SQUID amplifier at 45 mK. Gain and noise versus frequency[94].

[92] F.C. Wellstood et al., *Phys. Rev. B* 49 (1994) 5942
[93] M. Mück et al., *Appl. Phys. Lett.* 78 (2001) 967
[94] D. Kinion and John Clarke, *Appl. Phys. Lett.* 98 (2011) 202503.

5.7.2 Transition Edge Sensors

Kent Irwin

The SQUID is an important detector of electromagnetic signals in its own right, but it also plays a critical role as a follow-on amplifier for other types of superconducting detectors. One of the most important of these is the superconducting transition-edge sensor (TES), which consists of a superconducting film biased in the narrow transition region between the normal and superconducting states. In this temperature region, the resistance of the film is a sensitive thermometer that can be used to detect an extraordinary range of photons and other particles. Often, measurements with a TES are more sensitive than any other technique. Arrays of SQUID-coupled TES detectors are presently deployed as detectors of photons from millimeter-wave to gamma rays, in applications ranging from astrophysics to nuclear materials analysis.

The SQUID amplifier is the natural amplifier for TES detector arrays since it can be readily noise-matched to low impedance and is obviously compatible with low-temperature operation. The implementation of SQUID amplifiers to read out the current from voltage-biased TES detectors makes it possible to implement large arrays of TESs. However, the TES was developed well before the SQUID.

The TES was invented by Donald Hatch Andrews, a professor of chemistry in Johns Hopkins University's Cryogeny Laboratory, while he relaxed on a beach in Nassau in 1938. Professor Andrews [Figure 5.34(a)] realized that, on its transition, a superconducting film had a much larger temperature coefficient of resistance than conventional resistive thermometers, and that it could be used to create a more sensitive detector. He published[95] the idea in 1938, and demonstrated[96] an infrared detector based on a TES bolometer in 1942. He even developed a real-time infrared imaging system in 1946 based on a NbN TES that used scanning optics to display live images on the screen of an oscilloscope. An infrared image of Professor Andrews is shown in Figure 5.34(b).

The low resistance of the TES made it difficult to noise-match it to a semiconductor amplifier. In recent years, this problem has been largely eliminated by the use of SQUID current amplifiers, which are readily noise-matched to low-resistance TES detectors[97]. The final barrier to the large-scale practical use of TES detectors was the difficulty of operating them within the extremely narrow superconducting transition region. When it is current-biased, Joule heating of the TES can lead to thermal runaway, and small fluctuations in bath temperature significantly degrade performance. Furthermore, variations in the transition temperature between multiple devices in an array of TES detectors can make it impossible to bias them all at the same bath temperature.

The solution to these problems was worked out[98] when I was a graduate student in Blas Cabrera's laboratory at Stanford University, developing TES detectors to search for Weakly Interacting Massive Particles (WIMPs). We realized that when TES detectors are voltage biased, they self-regulate their temperature within the transition, operate without thermal runaway, and have much less sensitivity to fluctuations in the bath temperature. Equally importantly, large arrays of TES detectors with slightly different transition temperatures can be sensitively operated at a common bath temperature when they are voltage biased. Since that time, TES detector arrays have been widely used.

The general noise theory for resistive bolometric detectors such as the TES was worked out in John Mather's classic papers[99]. However, superconducting transition-edge sensors often exhibit excess noise well beyond that predicted by Mather's theory. In 2005, I revisited Mather's calculations, and realized that the conventional noise theory of bolometers is rigorous in equilibrium systems, but

[95] D.H. Andrews, *American Philosophical Society Yearbook* (1938) 132
[96] D.H. Andrews et al., *Rev. Sci. Instrum.* 13 (1942) 281
[97] W. Seidel et al., *Phys. Lett. B* 236 (1990) 483
[98] K. D. Irwin, *Appl. Phys. Lett.* 66 (1995) 1998
[99] J. Mather, *Appl. Optics* 21 (1982) 1125

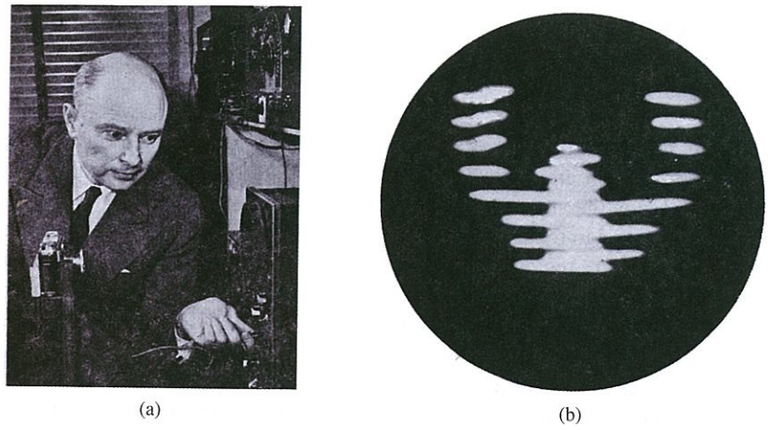

(a) (b)

FIGURE 5.34: (a) Donald Hatch Andrews, the inventor of the superconducting transition-edge sensor. Shown in 1946 with a TES infrared imager (Photograph credit: "An Eye For Heat," *Popular Science*, July 1946, p.126.) (b) An infrared image of Donald H. Andrews with his hands raised. The image was acquired with a NbN TES in 1946 in complete darkness, and displayed in real time on an oscilloscope synchronized to the scanning optics. (Photograph credit: "An Eye For Heat," *Popular Science*, July 1946, p.126.)

not when the bolometer temperature is different from the bath temperature. Using a simple model of the electrical and thermal system of the bolometer, and applying the nonequilibrium fluctuation-dissipation relations developed by Stratonovich, I was able to derive rigorously the correlations in a nonlinear bolometer operated with a first-order deviation from equilibrium[100]. One of the predictions of this theory is that the power spectral density of the random fluctuations in the voltage across the resistive bolometer is $S_V = 4k_B TR(1+2\beta)$, rather than the Nyquist value $S_V = 4k_B TR$ assumed by Mather. Here $\beta \equiv [\partial log(R)/\partial log(I)]_T$, where I is the bias current. This theoretical prediction has since been strongly supported by experimental results, making it clear that many TES detectors operate with no measurable deviation from fundamental thermodynamic noise limits. The development of TES detectors with well-understood noise performance has opened up a wealth of applications in photon detection from millimeter wave through gamma rays.

5.7.3 Photon Energy Resolving Detectors

Kent Irwin

When a photon of energy E_γ is absorbed in a material with heat capacity C, the resulting temperature rise is $\Delta T = E_\gamma/C$. A microcalorimeter determines the energy of a single photon by using a sensitive thermometer to measure[101] ΔT. A TES can be used to make an excellent microcalorimeter if the heat capacity is chosen so that ΔT is a significant fraction of the superconducting transition width. The full-width-at-half-maximum (FWHM) energy resolution of this measurement of E_γ is limited by thermodynamics to $\Delta E_{FWHM} = 2.35\xi[k_B T E_\gamma(1+2\beta)^{1/2}]^{1/2}$, where $\xi \approx 3$ is a dimensionless parameter whose value is determined by the details of the thermal link to the heat bath, k_B is the Boltzmann constant, and T is the temperature of the TES. The $1+2\beta$ term is the correction

[100] K.D. Irwin, *Nucl. Instr. Meth.* A559 (2006) 718
[101] S. Moseley, et al., *J. Appl. Phys.* 56 (1984)1257

from non-equilibrium thermodynamics discussed earlier. As an example, putting in realistic values of $\beta = 1$ and $T = 100$ mK, we find that TES calorimeters are capable of measuring the energy of a 6 keV x-ray photon to about 1 part in 3,000. In contrast, the best commercial semiconductor detector is limited by Fano statistics of the electron-hole pair generation to an energy resolution of 1 part in 50. The startling improvement of almost two orders of magnitude available with microcalorimeters enables new applications, including x-ray astronomy and nuclear materials analysis with gamma rays.

5.7.4 X-Ray Astronomy and Materials Analysis

Kent Irwin

X-rays provide a sensitive probe of nearly all classes of astrophysical objects by either emission or absorption. Energetic sources of x-rays include plasmas in stellar winds, supernova remnants, accretion features in active galactic nuclei and intracluster gas. However, x-ray detectors that have been flown in satellite-based x-ray observatories had either extremely limited collection area (making it possible to study only the brightest sources) or relatively poor energy resolution. The TES x-ray calorimeter is an excellent candidate instrument for a satellite observatory that will provide both high collection area and excellent energy resolution.

X-ray spectral measurements are also a critical tool in materials analysis and nuclear safeguards. The excellent energy resolution provided by TES x-ray detectors can enable more precise measurement of the elemental composition of matter on a nanometer scale in a scanning electron microscope. TES x-ray calorimeters can be used to measure gamma-rays and excited x-rays from a sample of nuclear material to provide important information for nuclear safeguards and treaty verification[102].

In 1995 I joined John Martinis' group at NIST as a postdoc. John had recently developed high-bandwidth amplifiers based on series arrays of SQUIDs. We realized that the combination of these SQUID amplifiers with the voltage-biased TESs could be used to create extremely sensitive x-ray microcalorimeters. John, Gene Hilton, and I developed transition-edge sensors based on bilayers of a normal metal and a superconductor with a proximitized superconducting transition temperature of about 100 mK. Within a year, these TES calorimeters were outperforming all other superconducting x-ray detectors. Modern TES calorimeters have the highest energy resolution of all energy-dispersive detectors[103]. The first spaceborne TES x-ray calorimeters will be flown in 2012 in the Micro-X sounding rocket experiment, and TES x-ray calorimeters are now the baseline technology for the International X-Ray Observatory (IXO).

To obtain an image of an extended astrophysical object such as a supernova remnant, one requires hundreds or preferably thousands of such sensors mounted at the focal plane of an x-ray telescope. Needless to say, this is a challenging prospect. Although it is perfectly feasible to fabricate hundreds or thousands of SQUIDs, a serious concern is the thermal heat load generated by the leads when each TES requires its own readout SQUID with its own dedicated set of readout wires. In 1996, Erich Grossman at NIST suggested that we read out an array of TESs by wiring their output SQUIDs in series, and turning them on one at a time. Under appropriate conditions, the signal from each TES can be faithfully reconstructed[104]. The eventual outcome was the 32-channel time-division SQUID multiplexer (MUX) chip. In this circuit, all of the SQUIDs in a "column" are wired in series on one chip, and read out with one output wire (Figure 5.35). One SQUID is turned on at a time on each chip, using a single "row" wire going between multiple MUX chips. One feedback

[102] D.T. Chow et al., *Nucl. Instr. Meth.* A444 (2000) 196
[103] A.S. Hoover et al., *J. Radioanal. Nucl. Chem.* 282 (2009) 227
[104] J.A. Chervenak et al., *Appl. Phys. Lett.* 74 (1999) 4043

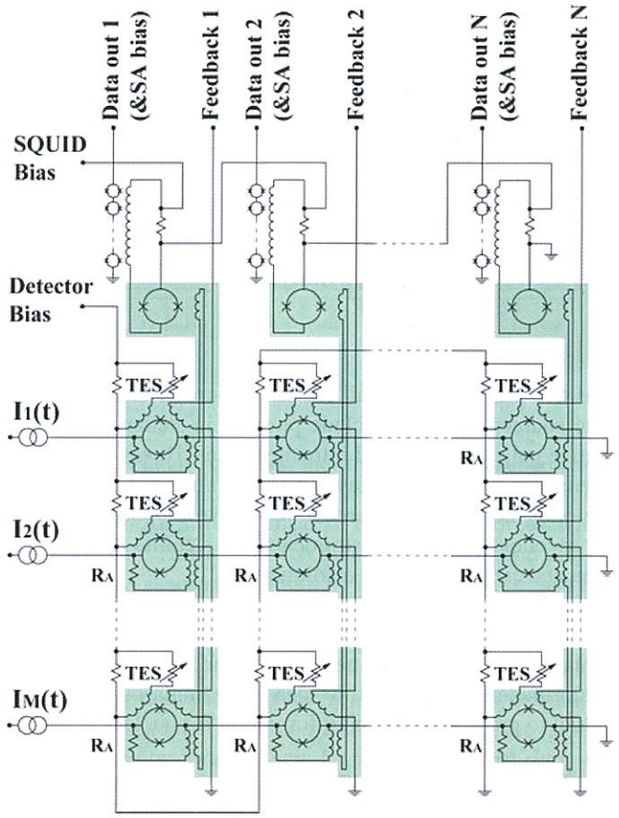

FIGURE 5.35: Circuit for a TES time-division multiplexer. Each TES (shown as a variable resistor) is coupled to a dedicated first-stage SQUID switch (on a green background). The first-stage switch SQUIDs are switched on one row at a time with common address leads $I(t)$. Each column has a readout SQUID that consists of 100 SQUIDs in series.

wire is also required for each MUX chip to linearize the SQUID response, and the value of the feedback is switched to linearize the response of whichever SQUID is on at the time. This basic chip architecture is now being used for the Micro-X TES arrays, and is baselined for IXO. A 256-channel TES calorimeter instrument using 8 SQUID MUX chips, shown in Figure 5.36(a), was co-developed by Joel Ullom at NIST and Michael Rabin at the Los Alamos National Laboratory (LANL). This instrument is now at LANL, where it is used to analyze the gamma- and x-ray spectra of complex nuclear materials for nuclear safeguards applications [Figure 5.36(b)][103].

5.7.5 Dark Energy and Cold Dark Matter

John Clarke

Measurements of the cosmic microwave background[105] (CMB) have taught us much about the origin of the universe. The CMB, which has a Planck distribution with a characteristic temperature of 2.726 K, originated 377,000 ± 3,000 years after the Big Bang and has been traveling for 13.7

[105] P. James et al., *Finding the Big Bang* (Cambridge University Press, Cambridge, England, 2009)

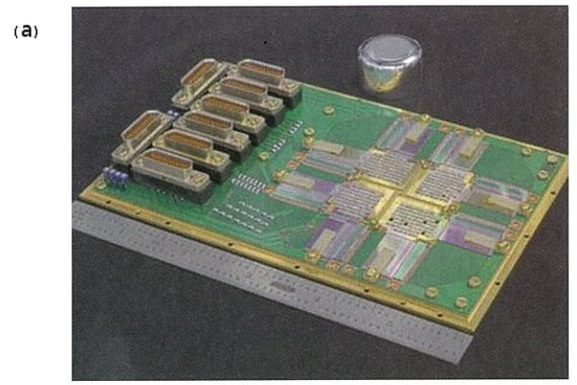

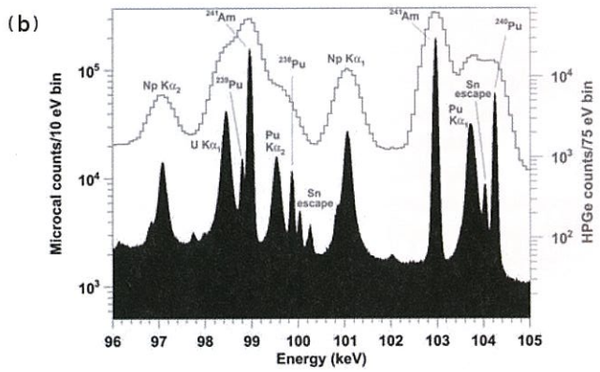

FIGURE 5.36: (a) A 256-channel TES x-ray / γ-ray detector array and a measured spectrum. A photograph of the detector array. (Photo credit: Dan Schmidt, NIST.) (b) Analysis of an isotopic mixture of plutonium and uranium. The spectrum is shown both for a state-of-the-art high-purity germanium (HPGe) detector (top line and axis on right), and for the TES calorimeter array (solid bars and axis on the left). (Figure credit: A. Hoover, LANL.)

billion years since then. We now know that the Universe consists of 0.6% neutrinos, 4.6% baryons, 73% dark energy (DE) and 22% cold dark matter (CDM). SQUID amplifiers are being used to investigate all four of these components. SQUIDs are used in direct detection experiments to search for axions and weakly interacting massive particles (WIMPs), two candidates for the cold-dark matter. Cosmic microwave background measurements using SQUID-coupled TESs are being used to constrain the properties of DE and the sum of the neutrino masses. SQUID-coupled TESs will also be used for x-ray measurements to search for the "missing" half of the baryons in the Warm-Hot Intergalactic Medium (WHIM).

5.7.6 Dark Energy: Searching for Galaxy Clusters

John Clarke

Galaxy clusters contain typically several hundred galaxies and, with a mass of 10^{14} to 10^{15} solar masses, are the largest gravitationally bound objects in the universe. Measuring the density of galaxy clusters as a function of red shift enables one to determine the parameters of the equation of state for DE. Optical surveys are being conducted to map galaxy clusters, but they are inherently biased. More distant clusters at higher red shift have weaker signals, so fewer of them will be found, leading to systematic errors in the determination of cosmological parameters.

A newly implemented search technique based on the Sunyaev-Zel'dovich Effect (SZE)[106] is now being used to survey galaxy clusters without this bias. This technique is based on the fact that the space between galaxies in a cluster contains a hot electron gas. When a microwave background photon passes through this gas, it has a small (1-2%) chance of being scattered to a higher energy, so that a fraction of the CMB spectrum is shifted to slightly higher frequencies. Thus, as the telescope scans across the sky, one expects to find regions in which there is a shifted Planck spectrum superimposed on the unshifted spectrum—the signature of a galaxy cluster. SZE surveys are based on the distortion of a signal coming from behind the cluster, and the ratio of the SZE effect to the CMB is independent of red shift. Hundreds to thousands of SZE clusters are expected to be found using this unbiased technique.

Since the CMB spectrum peaks at a frequency of about 150 GHz, one needs ultrasensitive detectors in the far infrared. The detector of choice for these measurements is the TES bolometer, which is very similar to a TES calorimeter. However, in a bolometer, the power in a photon signal, P_γ, is measured instead of the energy of a single photon. When a photon signal is absorbed in the optical element, the thermal energy is transferred to the TES, initially raising its temperature and increasing its resistance. As the resistance begins to increase, however, the dissipation generated by the voltage bias drops, so that the power dissipation in the TES remains constant. The change in the current flowing through the SQUID input coil is related to the absorbed energy. This electrothermal feedback results in a fast, linear response. Furthermore, the power dissipation is low, typically a few picowatts. The noise in an optimized sensor is limited by fluctuations in the arrival rate of photons rather than by noise in the TES bolometer itself.

To obtain an image of a galaxy cluster, one requires hundreds or preferably thousands of such sensors mounted at the focal plane of a telescope. The time-division SQUID multiplexer described earlier is used for just such measurements in the Atacama Cosmology Telescope. However, an alternative approach to multiplexing the signals from the TES arrays was developed at Berkeley for SZE measurements. In the spring of 1999, Paul Richards walked into my office to discuss the feasibility of using a single SQUID to read out an array of TESs simultaneously with a frequency-division multiplexer. I found this a very interesting problem, and the eventual outcome was the 8-channel multiplexer[107] shown in Figure 5.37. Each TES is connected in series with a capacitor and an inductor to form a resonant circuit, each with a different frequency. An oscillator provides a comb of voltages $V_i(f_i)$ at frequencies f_i corresponding to the resonant frequencies of the tuned circuit. The currents from the eight tuned circuits are summed at one end of the input coil of a SQUID (actually a 100-SQUID series array); the other end is grounded. The oscillator applies a nulling comb of voltages $-V_i(f_i)$ to the same summing point so that, in the absence of any photon flux, the total current injected into the input coil is zero. When a photon is absorbed by one of the sensors, the resulting change in current is injected into the input coil of the SQUID, which is operated in a flux-locked loop. Since the 8 frequencies are distinct, all 8 sensors can be read out simultaneously with the aid

[106] R.A. Sunyaev and Y.B. Zel'Dovich, *Comments Astrophys.* 4 (1972) 173

[107] T.M. Lanting et al., *Appl. Phys. Lett.* 86 (2005) 112511

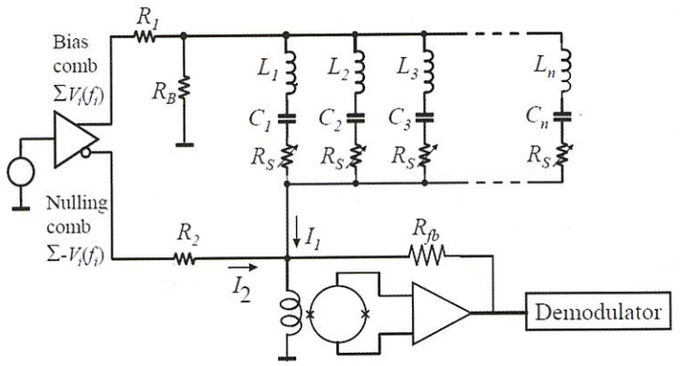

FIGURE 5.37: Circuit for a TES frequency-domain multiplexer. The readout SQUID consists of 100 SQUIDs in series. Reproduced from ref. 107, with permission.

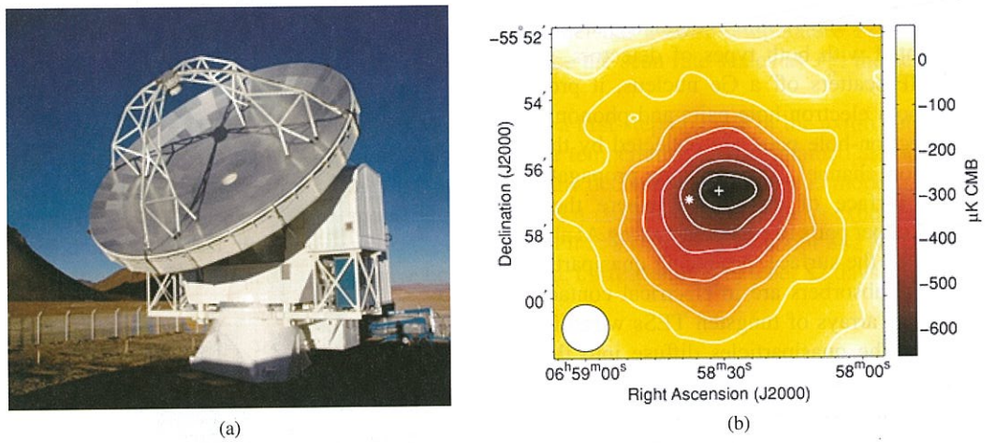

(a) (b)

FIGURE 5.38: APEX telescope and first results. (a) Telescope at Atacama. (b) SZE image of the "Bullet Custer"; the contour interval is 100 mK_{CMB}. Disk at lower left represents the full width at half-maximum (FWHM) resolution. (Reproduced from Reference 108, with permission.)

of a demodulator.

The Berkeley group, in collaboration with several other groups, first implemented this scheme on APEX (Atacama Pathfinder EXperiment), a 12-m telescope at about 5100 m on the Atacama plateau in Northern Chile [Figure 5.38(a)]. The receiver contains about 280 working channels with multiplexed readout. As a first demonstration of the system operation, Figure 5.38(b) shows an SZE image of the "Bullet Cluster"—actually two merging clusters[108]. The signal-to-noise ratio is 20 in the central 1 minute of arc beam. Subsequently, the Berkeley group and others began a cluster search with SPT (South Pole Telescope), a 10-m telescope at Antarctica at about 2900 m; there are about 660 TESs with multiplexed readout. In the next two years, SPT will survey 4000 square degrees of sky.

[108] N.W. Halverson et al., *Astrophys. J.* 701 (2009) 42

5.7.7 Cold Dark Matter: WIMPs and Axions

John Clarke

Since we do not know what CDM is, we have to postulate some kind of particle and then search for it. One of the leading candidates is the WIMP (Weakly Interacting Massive Particle)[109]. However, since WIMPs do not interact with electromagnetic forces, their direct detection is challenging. Their scattering rate in a Ge crystal is expected to be less than 0.1 per day per kilogram! A detector technology is needed that can detect the energy deposited when a WIMP scatters off a nucleus, and discriminate these events from the much more common electron-scattering events from the radioactive background.

The Cryogenic Dark Matter Search (CDMS) originated out of a marriage of the ionization detectors developed by Bernard Sadoulet's group at Berkeley and the TES detectors developed by Blas Cabrera's group at Stanford. In CDMS, large germanium crystals (10 mm thick and 76 mm in diameter) are instrumented with both types of detectors. If a WIMP scatters off a Ge nucleus, it produces both electron-hole pairs and phonons. The electron-hole pairs are collected by the ionization channel. The phonons propagate to the surface of the crystal where they break Cooper pairs in superconducting Al absorbers on the surface, producing quasiparticles. The absorbers are in electrical contact with large arrays of tungsten TESs wired in parallel. The quasiparticles diffuse into the TESs, where they are trapped, raising the temperature. Each parallel TES array is biased with a constant voltage, and its current is read out with a series array of 100 SQUIDs. Nuclear scattering events, including WIMP recoils, generate a larger fraction of phonons than electron-scattering events, so CDMS can veto the electron-scattering background. CDMS has now set the most stringent limits on WIMPs of any direct-detection experiment[110], and larger scale experiments are in development to push the limits still further.

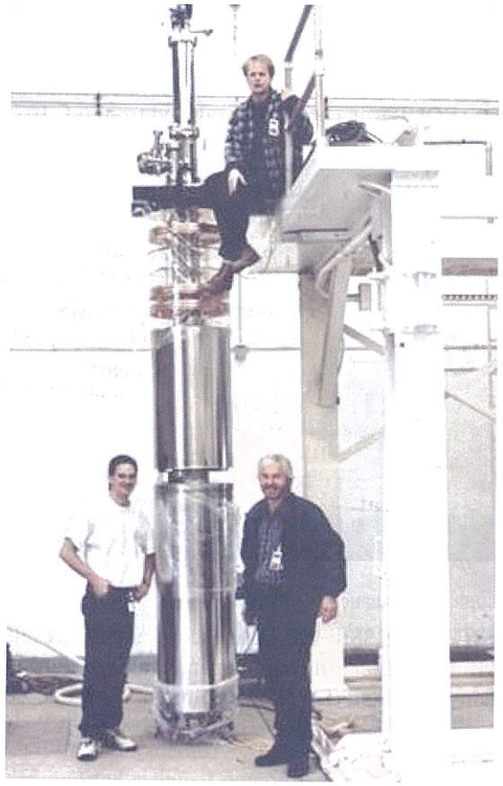

FIGURE 5.39: Axion detector installed at Lawrence Livermore National Laboratory.

Another candidate for CDM is the axion, first proposed in 1978 to explain the absence of a measurable electric dipole moment on the neutron. The axion mass m_a is predicted to be 1 μeVc^{-2} to 1 $meVc^{-2}$ (corresponding to 0.24 to 240 GHz). Since the measured CMB density ρ_a is 0.45 $GeVcm^{-3}$, a mass of 1 μeV corresponds to an axion density of 4.5 x 10^{14} cm^{-3}. How does one

[109] G. Steigman and M.S. Turner, *Nucl. Phys.* B 253 (1985) 375
[110] Z. Ahmed et al., *Science* 327 (2010) 1619

search for this light, spinless, chargeless particle? In 1983, Pierre Sikivie[111] suggested that it could be found via Primakoff conversion: in the presence of a large magnetic field B, the axion converts to a photon (together with a virtual photon) with energy $m_a c^2$. The conversion takes place in a cooled cavity of volume V with a tunable resonance frequency. An antenna couples the signal in the cavity to a cooled, low-noise amplifier. When the cavity frequency corresponds to the frequency of photons from the putative axions, the amplifier is expected to detect a peak; off-resonance, it detects only blackbody noise. Clearly, one has to scan the cavity frequency to search for the axion. The axion-to-photon conversion power is given by $P_a \propto B^2 V g_\gamma^2 m_a \rho_a$, where g_γ is a coupling coefficient; its lowest predicted value is $|g_\gamma| = 0.36$.

The axion detector (Figure 5.39) at LLNL, known as ADMX (Axion Dark Matter eXperiment), began operation in 1996. The cavity and the surrounding 7-T persistent-current magnet were cooled to 1.5 K The cooled HEMT amplifier had a noise temperature $T_N = 1.7$ K, giving a system noise temperature $T_S = T + T_N = 3.2$ K. For the parameters of the experiment and assuming $|g_\gamma| = 0.36$, the time to scan from $f_1 = 0.24$ GHz to $f_2 = 0.48$ GHz is $\tau(f_1, f_2) \approx 4x10^{17}(T_S/1K)^2(1/f_1 - 1/f_2)$ sec ≈ 270 years. Evidently, this experiment was not likely to find an axion very quickly!

The dilemma was solved by replacing the HEMT with a MSA. The potential impact on the scan rate of the axion detector is dramatic. As a scenario, suppose that the cavity is cooled to $T = 50$ mK with a dilution refrigerator, and that the readout amplifier has a noise temperature $T_N = 50$ mK. Thus, the system noise temperature $T_S = 100$ mK. Since the scan rate scales as T_S^2, the scan time becomes $270(0.1/3.2)^2$ years ≈ 100 days!

The very low noise temperature of the MSA spurred a first-step upgrade of the axion detector in which the HEMT was replaced with an MSA while the temperature was maintained at about 2 K. Since blackbody noise from the cavity is not reduced, the decrease in scan time is modest. Rather, the object of the upgrade was to demonstrate that the MSA could indeed operate as expected on the axion detector. In fact, the system worked extremely well at a frequency of about 842 MHz. As of this writing, 88,732, 80-sec data sets have been acquired, corresponding to a net 82 days of data[112].

5.7.8 Gravitational Radiation Detectors

Peter F. Michelson

The early ideas about cryogenic resonant-mass detectors of gravitational radiation began with discussions at Stanford University between William Fairbank and William Hamilton in the mid-1960s concerning experiments to measure gravitational effects with high precision (see Hamilton's essay[113] for more details.). Hamilton was a graduate student at the time, working with George Pake and Arthur Schawlow. Eventually Hamilton worked as a postdoc with Fairbank. In 1967 Fairbank and Hamilton visited Joseph Weber at the University of Maryland and saw what he was doing with large, resonant-mass gravity wave (GW) detectors operated at room temperature.

A resonant-mass GW detector couples to the time-dependent "tidal" force of a gravitational wave. The tidal force is transverse to the direction of propagation. A pulse of such radiation, produced by a cataclysmic cosmic event such as the coalescence of a binary neutron star system or a supernova core collapse, will excite mechanical modes of the antenna (a large, solid cylindrical bar), particularly the fundamental mode. One of the limiting sensitivity factors for such an antenna is the Brownian motion noise that is proportional to $k_B T/Q$, where T is the temperature of the antenna and Q is the mechanical quality factor of the mode[114].

[111] P. Sikivie, *Phys. Rev. Lett.* 51 (1983) 1415
[112] S.J. Asztalos et al., *Phys. Rev. Lett.* 104 (2010) 041301
[113] J.D. Fairbank et al., *Near Zero: New Frontiers of Physics* (W.H. Freeman and Company, New York, 1988)
[114] P.F. Michelson et al., *Science* 237 (1987) 150

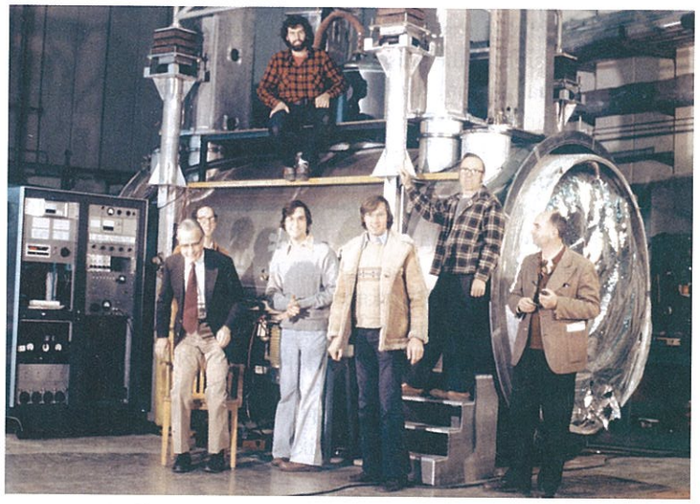

FIGURE 5.40: The Stanford 4,800 kg low-temperature gravitational radiation detector, circa 1980. Team members shown are (left-to-right) Bill Fairbank, Mike McAshan, Steve Boughn (above), Jim Hollenhorst, Robin Giffard, and Brad Reese. Vladimir Braginsky on the far right was visiting. (Courtesy Jack Gilderoy).

It was immediately clear to Fairbank and Hamilton that an enormous gain in sensitivity could be made by designing a detector to operate at low temperature. Fairbank's initial idea was to operate a five-ton resonant-mass aluminum cylinder at 3 mK! This would reduce the thermal noise by at least a factor of 10^5. There were other benefits of low-temperature operation. In particular, the mechanical Q of the antenna material improves significantly as the temperature is reduced, thus further reducing the mechanical noise contribution. So, with much promise of major improvements in sensitivity, the group at Stanford first designed and constructed a 680 kg detector operated at 4 K, followed by a 4,800 kg detector, initially operated at 4 K. The photograph in Figure 5.40 shows some of the members of the Stanford team, circa 1980.

Aside from the cryogenic design, two of the key challenges in the design of the detector were (i) vibration isolation and (ii) the readout system for detecting the vibrations of the fundamental mode of the antenna. The readout system developed for the Stanford detector is an example of "applied superconductivity". Both Robin Giffard and Ho Jung Paik played key roles in the development of the superconducting transducer readout of the antenna, shown schematically in Figure 5.41. Oscillations of the antenna are coupled to the fundamental eigenmode of a superconducting diaphragm, which modulates the inductance of current-carrying superconducting pickup coils, causing an oscillating voltage proportional to the velocity of the diaphragm to appear at the output terminals. The output signal from the transducer is fed to the input coil of a SQUID.

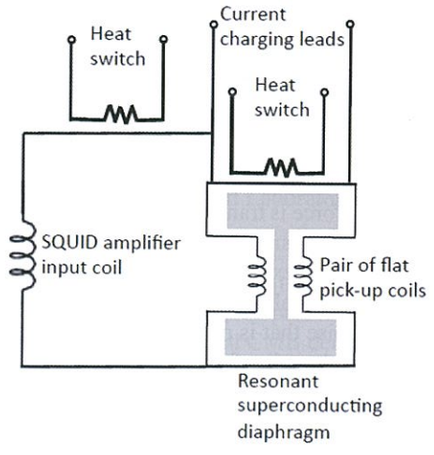

FIGURE 5.41: Superconducting motion transducer.

Giffard showed[115] that the ultimate sensitivity of a gravitational radiation detector of this type (i.e., a detector that uses a linear motion detector) is determined by the quantum-mechanical limit of linear amplifier performance, namely, the noise temperature of the system T_N obeys the limit $T_N \geq \hbar\omega/k_B$. This limit is equal to 40 nK at 850 Hz, the frequency of the Stanford detector. In operation at 4 K, this detector achieved a noise temperature of 10 mK, corresponding to a dimensionless strain sensitivity $\Delta l/l \approx 3 \cdot 10^{-18}$. The strain sensitivity of a quantum-limited detector is $\Delta l/l \approx 6 \cdot 10^{-21}$.

In recent years, long-baseline (4 km) laser interferometer detectors such as LIGO have surpassed the sensitivity of resonant-mass detectors, primarily because the baselines of interferometers are much longer (that is, 4 km versus 4 m).

5.7.9 Future Directions

John Clarke, Kent Irwin

In the spring of 2010, the axion detector (ADMX) was moved from LLNL to the University of Washington in Seattle, Washington. Over the course of the next several years a second-step upgrade will include the incorporation of a dilution refrigerator to cool the cavity and the MSA to 100 mK or lower. The combination of the cavity and the MSA cooled to this temperature will turn the axion search into an extremely viable project. As part of the upgrade, new cavities and MSAs will be designed and fabricated to extend the operating frequency to substantially higher values to increase the axion-mass range of the search. Furthermore, it has become apparent that ADMX can be used to search for other kinds of exotic particles, such as chameleons[116] and hidden sector photons[117].

Other applications of the MSA are also being pursued, notably as a near-quantum limited readout amplifier for superconducting qubits (Chapter 6).

As larger arrays of superconducting transition-edge sensors are developed, it will be necessary to increase the number of pixels that can be multiplexed in each output channel. A promising approach is to couple each TES pixel to an rf SQUID that is part of a high-Q, lithographically-patterned superconducting microwave resonator. Many thousands of these rf SQUID resonators can then be read out with a single HEMT amplifier, making it possible to develop arrays of hundreds of thousands of TES detectors.

5.8 Concluding Remarks

A. I. Braginski, John Clarke and Ronald E. Sager

This Chapter presents largely personal reminiscences on how SQUIDs and also superconducting radiation and particle detectors were conceived, understood and developed. Today, the fundamental principles of SQUIDs are well understood and the technology of low-T_c devices is relatively mature. While high quality low-T_c SQUIDs are readily available, there is an ongoing need for improved, high-yield and low-cost fabrication processes for the large SQUID arrays and related readout circuits that are now coming into use. The technology of high-T_c SQUIDs is not yet mature.

Low-T_c SQUIDs are solidly anchored in a growing number of applications at the frontiers of science—as extremely sensitive sensors of magnetic field or flux, as amplifiers, and as a variety

[115] R.P. Giffard, *Phys. Rev. D* 14 (1976) 2478
[116] G. Rybka et al., *Phys. Rev. Lett.* 105 (2010) 051801
[117] A. Wagner et al., *Phys. Rev. Lett.* 105 (2010) 171801

of readout devices. As examples, we have seen the remarkable improvements in the detection of far infrared and X-ray radiation, in the search for exotic particles, in the quest for understanding dark energy and in the detection of nuclear materials for security purposes. Some of these systems involve thousands of sensors; none of them would be remotely possible without the extremely low noise energy of the SQUID that permits one to benefit from the extraordinary sensitivity of TES detectors. Quantum Design's measurement systems using low-T_c SQUIDs have become indispensable scientific laboratory tools and a remarkable industrial and market success. Other applications do not necessarily take advantage of the ultimate noise energy of the SQUID, and are implemented because SQUIDs offer significant advantages over other techniques. An excellent example is geophysics, where the growing use of low- and high-T_c SQUIDs in geophysical mineral exploration has led to the discovery of large ore deposits. In nondestructive evaluation (NDE), low- and high-T_c SQUIDs are used to solve especially difficult problems. An example is the major success in locating impurities in niobium sheets destined for superconducting cavities for particle accelerators. In both geophysics and NDE, the use of SQUIDs resulted in a significant improvement of the methodology using conventional sensors.

Over the last decade, the supremacy of SQUIDs as the lowest noise magnetometers has been challenged by the development of optically pumped atomic (absolute) magnetometers. These operate at and above room temperature with a noise floor of the same order of magnitude as SQUIDs[118]. However, the vector nature of the SQUID response, its inherently wide bandwidth, and the fact that it is sensitive to magnetic flux (field) change rather than to its absolute value have made it hard or impossible to replace in most current applications. Nevertheless, as they are shrunk, SQUIDs achieve lower flux noise, but higher field noise. Should one need the lowest magnetic field noise in a device with extremely small area, the atomic magnetometer may be the device of choice in some future applications. The issue of SQUID cooling and the importance in many applications of replacing liquid cryogens with low-noise (and minimal maintenance) mechanical cryocoolers were emphasized in the context of laboratory devices. While in advanced and especially long-term space applications this mode of cooling might be the only possibility, the availability of suitable cryocoolers could also lower the acceptance threshold of SQUIDs in some other fields of application, especially industrial and clinical. The development of sufficiently "quiet" cryocoolers, "invisible" to the user, highly reliable, nearly maintenance-free and relatively inexpensive remains a highly desirable goal for the future of SQUID applications.

Acknowledgments

In co-authoring this chapter, John Clarke was supported by the Director, Office of Science, Office of Basic Energy Sciences, Materials Sciences and Engineering Division, of the U.S. Department of Energy under Contract No. DE-AC02-05CH11231.

[118] I.K. Kominis, et al., *Nature* 422 (2003) 596

5.9 Further Reading

SQUIDS and SQUID Applications

1. *The SQUID Handbook*. vol. I: *Fundamentals and Technology of SQUIDs and SQUID Systems*, eds. J. Clarke and A. I. Braginski, Wiley-VCH GmbH & Co., Weinheim, 2004.

2. *The SQUID Handbook*. vol. II: *Applications of SQUIDs and SQUID Systems*, eds. J. Clarke and A. I. Braginski, Wiley-VCH GmbH & Co., Weinheim, 2004.

3. *SQUID Sensors: Fundamentals, Fabrication and Applications*, ed. H. Weinstock, Kluwer Academic Publishers, Dordrecht, 1996.

4. Trends in SQUIDs and their applications are well covered by bi-annual proceedings of the Applied Superconductivity Conference (ASC), which appear in *IEEE Transactions on Applied Superconductivity* (TAS). The most recent are *Proceedings of ASC 2008*: TAS vol. 19, No. 3 (2009).

5. Another bi-annual conference covering progress in SQUIDs is the European Conference on Applied Superconductivity (EUCAS). Its proceedings appear in the *Journal of Physics: Conference Series* (JCPS). Invited papers are usually published in *Superconductor Science and Technology* (SuST). Both are Institute of Physics (IOP, UK) publications. The most recent are *Proceedings of EUCAS 2009: JCPS* vol. 234 (2010) and *SuST* vol. 23, No.3 (2010).

Superconducting Radiation and Particle Detectors

1. An excellent book reference for TES detectors is a textbook chapter: K.D. Irwin and G.C. Hilton, Transition-Edge Sensors, Ch. 3 in *Cryogenic Particle Detection*, Christian Enss, ed., *Topics Appl. Phys.* 99, 63–149 (2005), Springer-Verlag, Berlin Heidelberg 2005.

2. A representative and recent collection of articles can be found in: *AIP Conference Proceedings* Vol.1185, 13th International Workshop on Low Temperature Detectors, LTD-13. Stanford, CA, 20–24 July 2009.

6

Qubits

Editor: J. E. Mooij

6.1 Qubits

J. E. Mooij

6.1.1 Introduction

Quantum mechanics and superconductivity are intimately connected on many levels. Quantum mechanics is needed to understand why a metal is a metal. The BCS condensate of Cooper pairs would not exist without quantum mechanics, nor could Cooper pairs tunnel through the barriers of Josephson junctions. The name SQUID is the abbreviation of superconducting quantum interference device. Yet another level of quantumness has been added in the last two decades. It turns out to be possible to design and fabricate superconducting objects that have macroscopic dimensions and properties, but behave as if they are single quantum particles. Amplitude and phase of the superconducting wavefunction act as conjugate quantum variables. Practical devices and circuits make use of Josephson junctions to reach the parameter values that are needed, but there is a clear distinction from the Josephson electronics circuits in the other chapters of this book. The latter may, in this context, well be referred to as being classical.

Quantum bits, or qubits, are two-level systems that can be brought into a controlled quantum superposition of their two states. Quantum entanglement of two qubits can be realized by specific gate operations on interacting qubits. Single qubits and entangling two-qubit gates are in first theory sufficient to build a universal quantum computer, which can use quantum algorithms to perform certain tasks exponentially faster than a conventional computer. However, for an algorithm-processing type of quantum computer to become relevant in a practical sense, one needs qubit numbers of more than 1 million and unrealistically high operation and measurement fidelities. No technology can provide such numbers in the foreseeable future. Quantum information processing, a completely new concept with deep fundamental roots and implications, is nevertheless likely to lead to essentially new applications that are not envisioned at this time. Superconducting circuits are attractive candidates for quantum bits and quantum circuits because of their intrinsic coherence. This coherence is lower than for the more traditional quantum particles such as atoms and photons, but the possibility to design and fabricate quantum circuits on a chip has proven to be very attractive.

Quantum computation became seriously established around 1995 when qubit manipulation was

demonstrated using magnetic resonance on nuclear spins in liquids and when single trapped ions and atoms could be controlled. No superconducting quantum bits had been made at that time, but in preceding years several experiments had demonstrated remarkable quantum properties. Although no theory could guarantee that quantum mechanics would work at the level of individual control of macroscopic objects, several groups moved towards the development of intentional quantum circuits. After a number of years, breakthrough experimental results established the new area of superconducting quantum information processing. This chapter will describe some of the early experiments that preceded quantum bits, it will describe various qubit types, and it will show some of the latest developments at the time of writing. The chapter is meant to give an impression of this new aspect of superconductivity, rather than a review of the field. Several reviews of the field have been published.[1,2,3]

6.1.2 Early Experiments

Macroscopic Quantum Coherence

The potential energy of a Josephson junction that is biased with a current I is equal to $V = E_j(\cos\varphi - \varphi I/I_o)$, where φ is the phase difference, E_J the Josephson energy and I_o the critical current. This is the so-called washboard potential which has many local minima as long as $I < I_o$. Around 1985, the escape from a local well, for currents near the critical value, was addressed experimentally and theoretically. The junction has capacitance, which leads to a capacitive energy $T = CV^2/2 = C(\phi_o d\varphi/dt)^2/8\pi^2$ and a natural frequency for small oscillations in the bottom of the well, called the plasma frequency. The escape rate by thermal activation could be calculated, but at very low temperatures a higher rate was measured. This might be associated with quantum processes, but obviously a small level of spurious noise could have the same effect. The decisive experiment by the Clarke group in Berkeley showed that the escape rate could be enhanced by resonant microwave excitation of the plasma oscillations. With increasing DC current the well becomes shallower and the plasma frequency decreases. This was exactly what was observed, providing the first spectroscopic evidence for quantum behavior of the macroscopic SQUID.

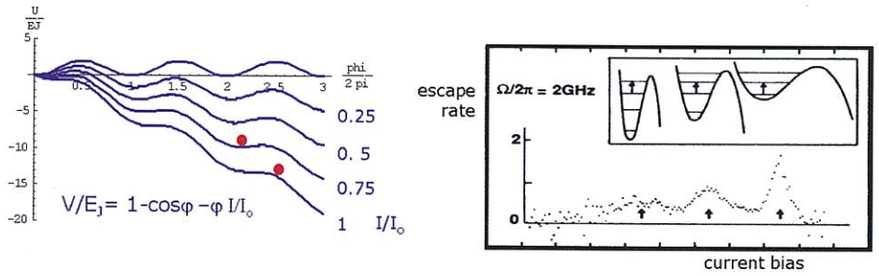

FIGURE 6.1: Current-biased Josephson junction. Left: the washboard potential is tilted more and more with increasing current. At the critical current no metastable well remains. The oscillation frequency in the well decreases for higher current. Right: evidence for quantized oscillations, the escape rate exhibits resonances when an external RF signal is resonant with different transitions in the anharmonic well.[4]

[1] M.H. Devoret, A. Walraff and J.M. Martinis, arXiv:cond-mat/0411174 (2004 and updates)
[2] G. Wendin and V.S. Shumeiko, *Low Temp. Phys.* 33 (2007) 724
[3] J. Clarke and F.K. Wilhelm, *Nature* 453 (2008) 1031

The theory for this effect was worked out by Leggett and collaborators. The equation of motion is identical to that of a particle with mass $C(\phi_0^2/4\pi^2)$ in one-dimensional space with coordinate φ. Leggett boldly quantized the equation of motion of the "particle" by replacing the "momentum" $C(\phi_0^2/4\pi^2)d\varphi/dt$ with an operator $-i\hbar\partial/\partial\varphi$. This approach gave excellent agreement with the experimental results. Caldeira and Leggett for the first time introduced damping in this quantum problem by coupling to large sets of harmonic oscillators. This method was subsequently used in many areas of physics. A good overview of experiment and theory has been presented by Clarke and collaborators[4].

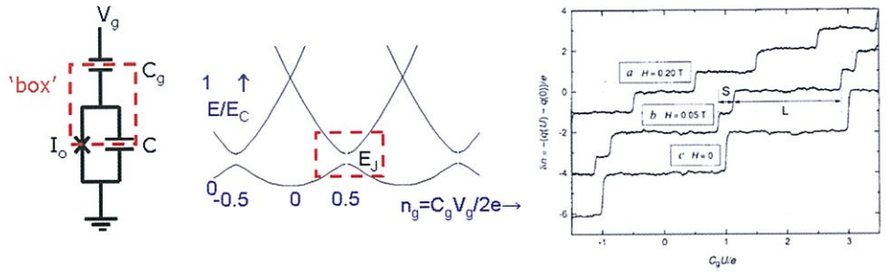

FIGURE 6.2: Cooper pair box. Left: circuit, the "box" is indicated. Middle: Energy values around a charge e on the gate capacitor. The Josephson coupling induces a superposition of the pure charge states with 0 and 1 Cooper pair on the island. Right: Measured electrical potential of the box[5]. In zero magnetic field the charge increases in units of $2e$.

Cooper Pair Box

Around 1990, several groups started to investigate the quantization of charge in a superconducting volume with small electrical capacitance. The behavior of normal metal tunnel junction circuits in the Coulomb blockade regime was by that time well understood, but it was certainly not clear what would happen in a superconducting circuit. Would the Cooper pairs be the only mobile particles, or would there always be at least a few quasiparticles? Cooper pairs are built up from many electron states in a dynamic fashion, and the range of electron states around the Fermi sphere that are involved is very vaguely defined. Could the difference between N (of order 10^7 or more) and $N+1$ Cooper pairs have any real measurable significance? Such questions were conclusively answered in experiments on the so-called Cooper pair box. This superconducting version of the single-electron box is depicted in Figure 6.2. A superconducting "island" is a metallic volume that is separated from other metallic regions by tunnel barrier and dielectrics. There is one tunnel junction that allows transfer of particles. The charge $q = n2e$ on the box is quantized, starting from $n = 0$ where electronic charges are compensated by the positive ionic background. The charging energy is defined as $E_c = 4e^2/2C_\Sigma$, where C_Σ is the sum of all capacitance values (usually the junction capacitance C dominates). The Josephson junction creates a coupling between charge states which differ by one Cooper pair (in Figure 6.2 these are states with $n = 0$ and $n = 1$). The Hamiltonian is $H = E_c(n - n_g)^2 - E_J\cos\varphi$, where $n_g = C_gV_g/2e$. The quantum nature is introduced with the commutation relation $[\hat{n},\hat{\varphi}] = i$, and the Hamiltonian operator $\hat{H} = E_c(\hat{n} - n_g)^2 - E_J\cos\hat{\varphi}$. This leads to

[4] J. Clarke, A.N. Cleland, M.H. Devoret, D. Esteve and J.M. Martinis, *Science* 239 (1988) 992

avoided crossings in the energy spectrum at those values of the gate voltage where charging energies for states n and $n+1$ are the same. Figure 6.2 shows the experimental evidence for clear pairing behavior of the Coulomb energy[5]. It took some years to develop the experimental conditions where the last quasiparticles could be banned, by careful filtering of leads and sometimes the addition of low-gap regions to trap the remaining single charges. Also, clear evidence for superpositions of Cooper pair states was later obtained.

Heisenberg Transistor

A peculiar experiment that nicely demonstrated the quantum nature of Josephson circuits[6] is illustrated in Figure 6.3. The experiment directly demonstrated the connection between fluctuations of the dual variables phase and charge. It is explained in the caption of Figure 6.3; squeezing of phase fluctuations leads to enhancement of charge fluctuations, visible in the transport current. The examples shown here and other experiments clearly demonstrated that Josephson circuits could be brought into the quantum regime. Almost surprisingly, the naive straightforward quantization of the macroscopic systems worked fine in explaining the new experimental findings. Now, fifteen years later, the validity of this approach is taken for granted.

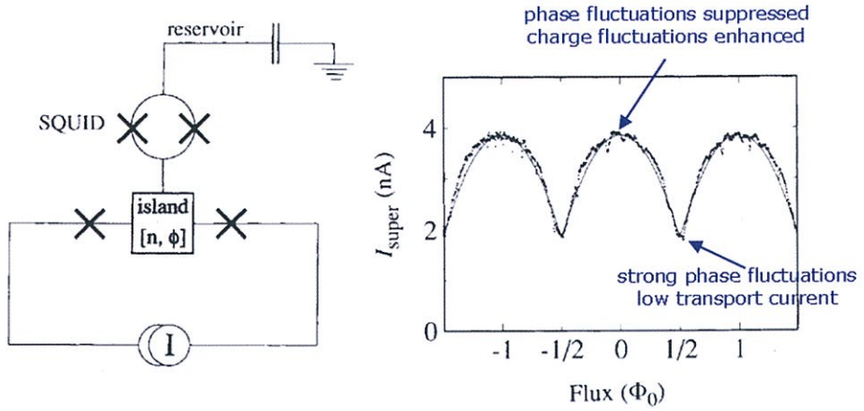

FIGURE 6.3: Heisenberg transistor[6]. On the left is the circuit with a current source connected to a Coulomb transistor without gate. The maximum supercurrent is measured. The system is in the Coulomb regime with $E_C > E_J$ and transport is possible only through fluctuations of the charge on the central island. That island is connected to a large superconducting reservoir by means of a SQUID. When the flux in the SQUID is varied, the charging energies are completely unaffected, but the supercurrent changes considerably. This is fully in agreement with quantum calculations. Strong coupling to the reservoir suppresses phase fluctuations, which in turn enhances the charge or number fluctuations. A higher supercurrent is found for zero flux in the SQUID.

[5] P. Lafarge, P. Joyez, D. Estéve, C. Urbina and M.H. Devoret, *Nature* 365 (1993) 422

[6] W.J. Elion, M. Matters, U Geigenmüller and J.E. Mooij, *Nature* 371 (1994) 594

6.1.3 Qubit Types

Common Features

There are many ways in which two-level states can be created in superconducting circuits. Always, number/charge and phase/current/flux act as conjugate quantum variables. Superconducting qubits make use of relatively small Josephson junctions where the ratio E_J/E_C is not too far from 1 so that quantum transitions are possible. The circuits are almost without exception made with aluminum-aluminum oxide-aluminum junctions. A high quality of the junctions is more important than a high critical temperature. Energy splittings are typically in the 5-20 GHz range; to prevent thermal occupation of levels, the experiments are performed in a dilution refrigerator at temperatures below 50 mK. Excitation and manipulation of qubit circuits is performed with resonant microwave pulses, similar to operations in magnetic resonance.

Charge Qubits

When Josephson junctions are used with charging energy E_C larger than E_J, the two levels are primarily associated with numbers of Cooper pairs on an island. The Cooper pair box, as described in the previous section, is the prototype of a charge qubit. It is used at or around a gate bias where the charge on the gate capacitor is e, half the Cooper pair charge. The first coherent manipulation of quantum states in a superconducting circuit was performed in a breakthrough experiment by Nakamura, Pashkin and Tsai[7] in 1999. In their experiment, they started by biasing the Cooper pair box at a position away from the symmetry point (Figure 6.4) where the charge is zero. Then, using

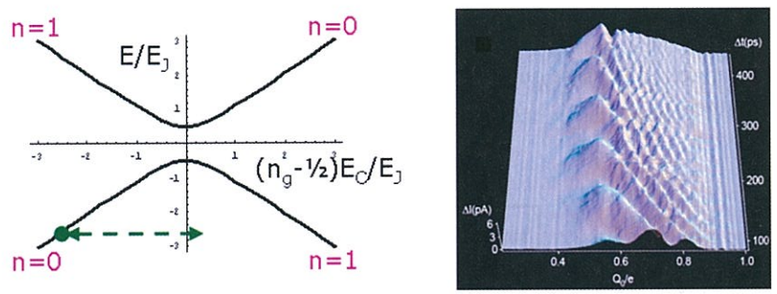

FIGURE 6.4: Left: Cooper pair box energy spectrum. The avoided crossing is shown where the Coulomb energies for zero and for one Cooper pair cross. The energies are normalized to the Josephson energy. E_j determines the splitting in the symmetry point $n_g = 1/2$. Right: Result of experiment by Nakamura et al.[7] that first demonstrated coherent dynamics of a superconducting circuit. The procedure is explained in the text. In this 3D plot x is the gate voltage normalized to e (on the scale as shown 1.0 corresponds to $n_g = 1/2$), y is the time spent in the symmetry point, z is the measurement result.

a very fast pulse generator, the bias was changed to a position close to $n_g = 1/2$ (x- axis in Figure 6.4 right) and kept there for a certain time (y-axis). The ground state is a superposition state at that bias and coming from $n = 0$ the system starts to oscillate between $n = 0$ and $n = 1$ with a frequency equal to the energy splitting. The switch back to low bias projects the system into one of the charge

[7] Y. Nakamura, Y.A. Pashkin and J.S. Tsai, *Nature* 398 (1999) 786

states. In their experiment Nakamura et al. detected the occupation of the $n = 1$ state with a special quasiparticle current detector (z-axis). A very clear oscillation pattern is visible which corresponds to the theoretical expectation. Later these experiments were expanded to direct qubit manipulation near the symmetry point and, again using ultrafast shifting techniques, to a two qubit system.

The very serious disadvantage of charge qubits is the strong noise due to variation of background charge configurations that is observed in practice. Not only the metallic gate couples to the box, but also a multitude of charged defect states. The occupation of such states varies in time with a $1/f$ spectrum that extends to high frequencies. The resulting coherence times are typically below 10 ns. So far it is impossible to fabricate circuits by means of thin film deposition and lithographic patterning without a high level of background charge noise. Using superconducting quantum bits with a ratio $E_C/E_J >> 1$ is asking for serious trouble. Therefore the group of Devoret and Estéve in Saclay developed a hybrid charge-phase qubit called the quantronium[8] that couples the charge states to a circulating current in a junction loop. The ratio E_C/E_J is about 10 for this system; the coherence time is typically 100 ns. The emergence of a new device based on the Cooper pair box, called the transmon, with an E_C/E_J ratio significantly below 1, has now taken all priority. As the charge signal cannot be detected directly for this device, the transmon is always used in combination with a microwave resonator. The transmon will be described in Section 6.3.4 together with the resonator.

Phase Qubits

In section 6.2.1 the quantum effects in a current-biased Josephson junction were described, including the quantized states of the nonlinear resonator which is formed by the Josephson junction acting as a nonlinear inductance and the capacitance of the tunnel junction structure. The two lowest of these quantized states can be used[9] to define a quantum bit that is known as the phase qubit. This nomenclature is a bit arbitrary, as all superconducting qubits make use of phase and charge and for all of them E_J/E_C cannot be very much higher or very much lower than 1 on the penalty of losing the quantum character. The phase qubit does have the highest E_J/E_C ratio, originally around 50 but more recently about 5.

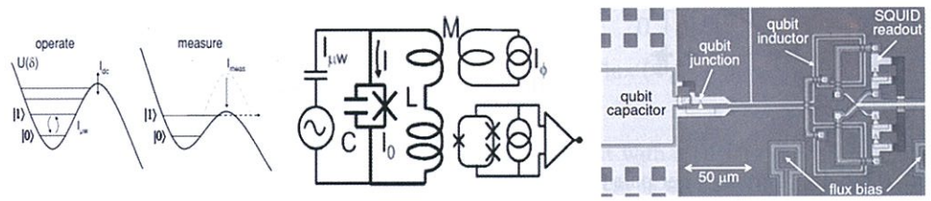

FIGURE 6.5: Phase qubit[9]. On the left the principle of operation is indicated. The bottom two levels in a metastable trap of the "washboard potential" are used as the two states of the qubit. After operations, readout is performed by increasing the bias current just enough that escape is possible from the excited but not from the ground state. The circuit is shown in the middle; a very stable current bias is created by placing the junction in a loop with large inductance. Microwaves can be applied as well as fast current shifts. If escape from the excited level has taken place, the junction phase has shifted by 2π and a fluxoid has escaped from the loop. This can be measured afterwards with the asymmetric SQUID that is at bottom right. The right picture shows the actual circuit.

[8] D. Vion, A. Aassime, A. Cottet, P. Joyez, H. Pothier, C. Urbina, D, Esteve and M.H. Devoret, *Science* 296 (2002)

[9] J.M. Martinis, S, Nam, J. Aumentado and C. Urbina, *Phys. Rev. Lett.* 89 (2002) 117901

The circuit for the phase qubit is shown in Figure 6.5. The energy splitting is tuned by the value of the bias current. For higher current the potential well becomes shallower and the oscillation frequency goes down. It is extremely important that the potential well itself is not parabolic. A harmonic oscillator would have identical distances between levels, so that selective operations on levels 0 and 1 are not possible. Here, due to the nonlinear junction inductance, the distances are different but still relatively close. Strong excitation of the qubit must be avoided to prevent leakage to the higher levels.

The phase qubit has been systematically improved, in particular by John Martinis and his group. Coherence was originally severely limited by the presence of spurious two-level defect states with energy splittings in the range of qubit energies. By reducing the junction area and by improving the materials properties, a strong reduction of their number was obtained. Coherence times are now around 500 ns. Readout is possible with a fidelity of more than 95%.

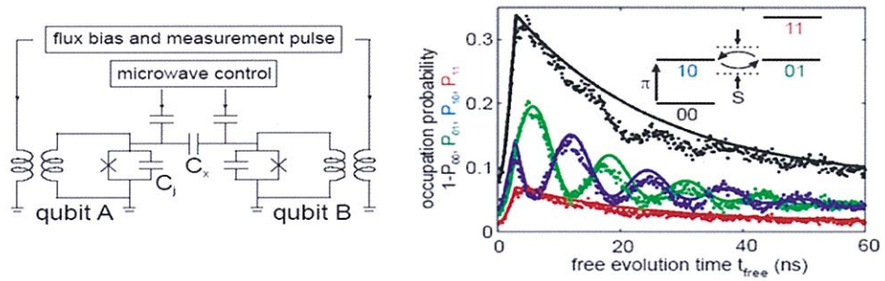

FIGURE 6.6: Swap gate for two phase qubits[10]. Left: schematic diagram showing capacitive coupling. Right: measured evolution of qubit states. The blue and the green curves indicate the states of qubits 1 and 2 respectively. They exchange their occupation periodically, for the swap gate the operation is stopped at the highest amplitude.

The Martinis group has created multi-qubit circuits by capacitive coupling of two or more qubits. Each qubit retains its own well-defined environment, driving and readout circuit. The qubits can be far apart so that cross-talk is small and qubit coherence is not reduced. Figure 6.6 shows the first SWAP gate produced in this manner[10]. Later coupling was also achieved by means of a microwave stripline, providing increased separation.

Flux Qubits

Flux qubits consist of a closed superconducting ring that is biased with a magnetic flux of about half a flux quantum.[11] Here, two degenerate or almost degenerate states are present that differ by the phase winding in the loop. The persistent currents have opposite sign. Inclusion of a small Josephson junction in the loop allows quantum tunneling of a fluxoid, at exactly half a flux quantum creating a symmetric (ground state) and an antisymmetric (excited state) of the persistent current states. The persistent currents generate a magnetic flux of about 1 $m\Phi_0$, which is measured with a SQUID. Two or more slightly bigger junctions are included to provide enough inductance for the two (meta) stable states. The tunnel coupling has a strength Δ that depends exponentially on the

[10] R. McDermott, R. Simmonds, M. Steffen, K.B. Cooper, K. Cicak, K.D. Osborn, S. Oh, D.P. Pappas, J.M. Martinis, *Science* 307 (2005) 1299

[11] I. Chiorescu, Y. Nakamura, C.J.P.M. Harmans and J.E. Mooij, *Science* 299 (2003) 1869

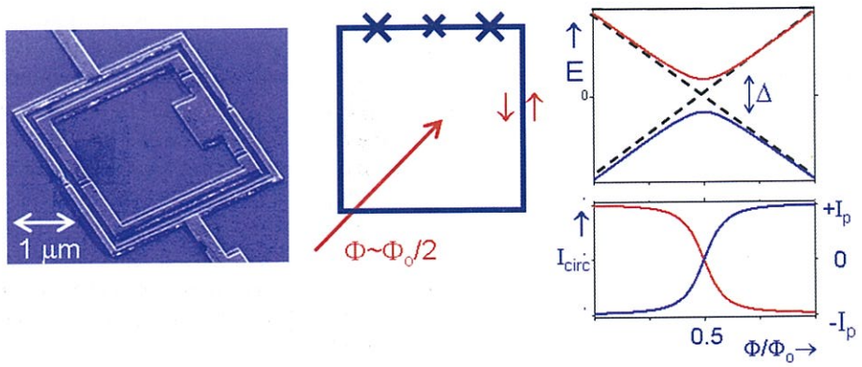

FIGURE 6.7: Flux qubit. A superconducting loop contains three or more small Josephson junctions. The flux through the loop is about $\Phi_0/2$. The classical states with lowest energy have persistent currents with opposite sign. With small Josephson junctions in the loop, quantum superpositions of these persistent current states are created as shown on the right. The ground state is blue, the excited state red. In the symmetry point 0.5, the level separation is given by the tunnel coupling Δ. The circulating currents are shown below. Qubit readout is by means of a SQUID, here shown around the qubit loop (left).

junction parameters. The flux qubit is the quantum dual to the Cooper pair box. As nature does not provide magnetic monopoles, flux noise in superconducting loops is much smaller than charge noise in capacitors. Under proper conditions the coherence time is around 1 μs at the symmetry point, where flux noise does not lead to dephasing to first order. However, at this bias point no readout signal is available as in both states the current is zero. A fast shift away from symmetry before measurement is needed. The circulating currents in the flux qubit can be used for relatively strong coupling, either to a detector, other qubits[12] or a resonator circuit. The required bias of half a flux quantum can also be provided by using a strong loop without junctions to trap one fluxoid, and attaching the qubit junction symmetrically across the middle (Figure 6.8)[13].

Coupling to Resonator, Transmon

The transmon[14] is a Cooper pair box with an E_J/E_C ratio of about 12, coupled to a resonator (figure 6.9). The energy of the charge states depends extremely weakly on the gate voltage, thereby strongly reducing the effects of charge noise. The charge states can be measured only by their dispersive effects on the resonator. The absence of other electrical circuitry helps the coherence. The system of two-level qubit plus resonator is described by means of the Jaynes-Cummings Hamiltonian

$$H_{JC} = H_r + H_a + \hbar g(a^\dagger \sigma^- + a\sigma^+) \tag{6.1}$$

which is well known in quantum optics. Here g is the coupling energy, σ indicates the qubit states and $a^\dagger$, a are the usual creation and annihilation operators for a photon. At resonance the eigenstates of the coupled system of resonator with one photon and the qubit are symmetric and antisymmetric

[12] J.H. Plantenberg, P.C. de Groot, C.J.P.M. Harmans and J.E. Mooij, *Nature* 447 (2007) 836

[13] A. Fedorov, A.K. Feofanov, P. Macha, P. Forn-Diaz, C.J.P.M. Harmans and J.E. Mooij, *Phys. Rev. Lett.* 105 (2010) 060503

[14] A. Walraff, D.I. Schuster, A. Blais. L. Frunzio, R.-S. Huang, J. Majer, S.M. Girvin and R.J. Schoelkopf, *Nature* 431 (2004) 162

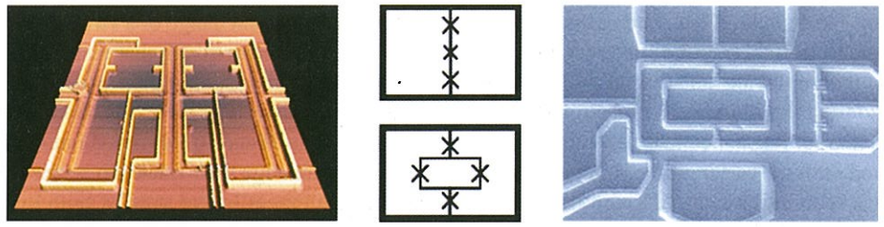

FIGURE 6.8: Flux qubits with trap loop. Left: Controlled-NOT gate[12] with two flux qubits, coupled by mutual inductance. On top are the two SQUID detectors and control lines for shifting the flux. Middle: schematic for flux qubit with trap loop. Top picture shows qubit line across the loop in which a 2π phase difference is trapped. The bias is the difference in fluxes left and right. Bottom picture shows version with tunable weakest junction. Right: flux qubit with tunable gap13. The layout is symmetric to provide decoupling of flux bias and gap tuning. SQUID is on the right.

superpositions of both elements, with energy splitting $2g$. When the frequencies differ by more than g, the apparent frequency of the resonator is shifted from its intrinsic value by $\pm g^2/\Delta$, depending on the state of the qubit. As a consequence, measuring the transmission or reflectance of the resonator gives information about the qubit state. The qubit itself can be addressed with microwave pulses that are resonant with its level splitting in the usual way. In this dispersive regime the qubit experiences shifts from two terms in the Hamiltonian. One, called the Lamb shift, is equal to the shift experienced by the resonator. The other term, called the AC Stark shift, is proportional to the number of photons in the resonator.

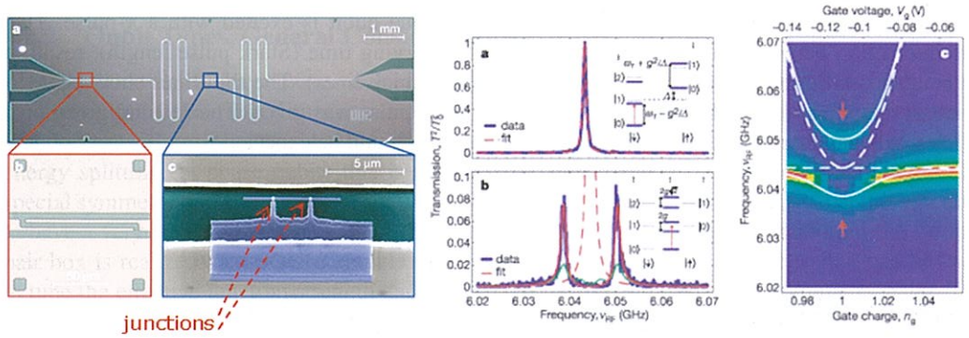

FIGURE 6.9: Transmon and resonator[14]. Left: layout of sample. The resonator is a microstripline, consisting of a center line between two ground planes. At the ends the center line is interrupted with a capacitor (bottom left) that provides partial transmission but mostly reflection. The qubit is a Cooper pair box that is capacitively coupled to the middle of the center line. The Josephson coupling strength is tuned by the magnetic flux in the junction loop. The transmission and reflection of the resonator are measured. Middle: a. transmission spectrum of resonator. At the top the qubit frequency is far away; in b. the qubit frequency is equal to the resonator frequency. Right: spectroscopy when the qubit splitting at the symmetry point is equal to the resonator frequency.

When two qubits are coupled to the same resonator and they are tuned to have the same energy

splitting, they can "see" each other via the resonator, by means of the exchange of a virtual photon[15]. Figure 6.10 (left) shows the spectroscopic observation of the avoided crossing that results. For that picture the qubits are tuned with the flux through the SQUID in the Cooper pair box. The qubits can also be shifted by means of a strong microwave pulse to the cavity that increases the Stark shift. Out of mutual resonance the two qubits do not see each other. In Figure 6.10 (right) interaction is switched on for a varying time. In resonance, the two qubits exchange their quantum states (SWAP gate), as seen in the red and green traces. Independent measurement of the state of both qubits is possible through the dispersion of the cavity.

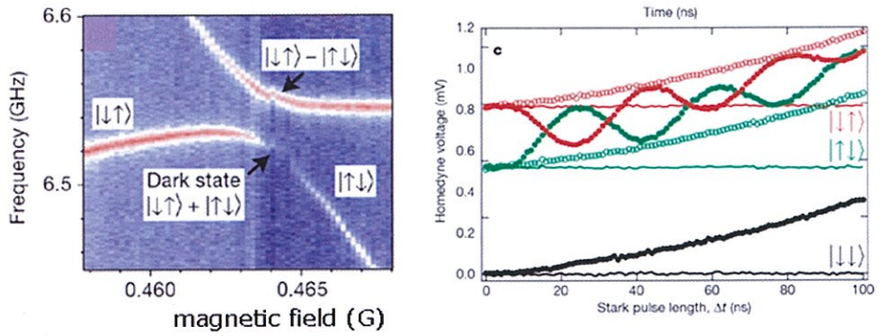

FIGURE 6.10: Coupling of two qubits via the resonator[15]. Two transmon qubits are attached to the same cavity at two different positions 4 mm apart. Left: spectroscopy on the system as a function of the magnetic field that is applied to both Cooper pair boxes, modifying the qubit frequencies. The two qubits exhibit an avoided crossing as shown. Near the crossing one qubit is not visible over a certain range, in accordance with theory. Right: First one qubit is excited with a π-pulse. Then the interaction between the qubits is switched on for varying time (Stark pulse length), resulting in counter-oscillating qubit occupations (red and green thick lines). The thin lines show behavior without coupling, the black line is the result when no π-pulse was given. The red and green open circles indicate the maximum oscillation amplitudes that should be expected.

6.2 General Aspects

J. E. Mooij

6.2.1 (De)coherence

For all superconducting quantum circuits the time of coherence for the quantum states is a severe limitation. The qubits are easy to couple to, which is often an advantage, but uncontrolled variations in the environment can have a similarly strong effect. Two different processes are distinguished,

[15] J. Majer, J.M. Chow, J.M. Gambetta, J. Koch, B.R. Johnson, J.A. Schreier, L. Frunzio, D.I. Schuster, A.A. Houck, A. Walraff, A. Blais, M.H. Devoret, S.M. Girvin and R.J. Schoelkopf, *Nature* 449 (2007) 443

characterized by a T_1 time and a T_2 time, in analogy with practice in NMR. The T_1 time indicates the rate at which the qubit exchanges energy with the environment, leading to relaxation from the excited state to the ground state. The opposite process, excitation of the qubit by a high temperature environment, is not usually important. The two main sources of decoherence are the electromagnetic coupling to the circuitry that is used for biasing, driving and readout, and coupling to materials defects that change in time.

Decohering effects from the electromagnetic environment can be approached on an engineering basis. One can calculate the spectral density of noise coming from all connections, using the real and imaginary components of the impedance as seen from the qubits over the full frequency range. For relaxation, the real component at the frequency of the qubit energy splitting is the relevant figure, as it is connected with energy transfer. For dephasing T_2 processes, it is important how the qubit energy splitting changes in time at lower frequencies. Software tools cam be used to obtain the relevant numbers and to optimize the design.

Decoherence due to materials defects can be reduced with careful optimization of fabrication processes, by operating qubits at bias values where the influence is minimal (charge or flux qubit in symmetry point), or by changing the design so that particular defects have lower effect (shunt capacitor for phase qubits). For charge and flux noise it has become clear that the noise sources are of a highly local kind and cannot be circumvented by gradiometer-type arrangements. As stated before, charge noise is very strong in the usual circuits. It is associated with electrons that are trapped and detrapped in defects. Flux noise may be connected with similar electron trapping/detrapping processes, due to the associated electron spin orientation. The choice for materials with superconducting qubits is fully dominated by the need to reduce defect noise. Aluminum yields high quality tunnel junctions, but the films are granular and have top surfaces that oxidize when exposed to air. Epitaxial fabrication of films and tunnel barriers with suitable cap layers should yield solutions. However, the small junction size that is needed to obtain the desired E_J/E_C ratio provides a severe challenge in the combination with high quality film deposition.

6.2.2 Qubit Types, General Considerations

Particular atoms all have the same quantum states with the same energies, proscribed by quantum mechanical rules. Fabricated superconducting qubits have a variation of their parameters. Josephson junction critical currents vary by several percent. It is necessary to have the ability to adjust the energy splitting. In phase qubits this is achieved by adjustment of the bias current. There is no special symmetry point where the derivative of the energy versus current is zero, so that it is essential to have a very stable current bias. In charge qubits and in the transmon the junction of the Cooper pair box is realized as a SQUID double junction, so that the enclosed magnetic flux can be used to tune the effective junction strength and the associated level splitting in the symmetry point. The magnetic flux has no effects on the Coulomb energy, which is a strong advantage. In both phase qubits and charge qubits the energy splitting is directly proportional to the junction critical current. In contrast, in flux qubits the energy splitting in the symmetry point depends exponentially on the critical current of the weakest junction in the loop. As a result, wide variations are possible after fabrication. Tunability of the weakest "alpha" junction is strongly needed, but has only recently been realized[13]. Tuning is again performed by variation of the magnetic flux in a SQUID loop, but here cross-talk to the main qubit loop has to be avoided by symmetric design or compensated.

The so-called anharmonicity is another important factor. In a harmonic oscillator all levels have the same distance, and resonant activation of the 0-1 transition has the same impact on the transitions 1-2 and higher. The phase qubit is based on oscillatory states, but due to the junction nonlinearity the oscillator has an anharmonic character (distance between 1-2 levels is 10% smaller than distance 0-1). Because these distances are still relatively close, the qubit cannot be driven strongly for fear of "quantum leakage". The transmon effectively also has an oscillator-like character and must be handled with similar caution. Qubit and gate operations have to be extended over a certain length

of time. In contrast, for pure charge qubits and for flux qubits the third level is typically more than 40 GHz away and the term anharmonicity has no relevance. Qubits and gates can be driven much stronger without fear of quantum leakage.

6.2.3 Recent Results

General View

The field of superconducting qubits and quantum circuits is little more than ten years old. The first half of that time focus was on the development of qubits that were sufficiently coherent to perform the necessary single qubit operations. In the last few years emphasis has shifted to manipulation of circuits of multiple qubits, often in combination with one or more resonators. Circuit quantum electrodynamics is becoming an established field of research. Superconducting resonators in the microwave regime have a very high quality; strong coupling to the qubit two-level systems is possible. This allows experiments that are not easily paralleled in quantum electrodynamics with atoms in the optical regime. In addition, first results on mechanical oscillators that exhibit quantum behavior have been achieved. Quantum measurement, in the strongly projective as well as in the weak regime, is studied intensively.

Examples

A few examples of new developments will be given, but one should realize that even in a time as short as half a year there will be significant additional progress. Progress in the direction of performing quantum algorithms has been limited until now. The Schoelkopf group at Yale used their two-transmon system, as described in Section 6.3.5, to execute basic two-qubit algorithms[16]. In general for quantum computation one needs single-qubit gates and two-qubit gates that provide quantum entanglement. The generalized single qubit operations require accurate control of the phases of driving signals in order to reach all arbitrary superpositions of $|0>$ and $|1>$, i.e. $\sin\alpha|0> + \cos\alpha\exp(i\varphi)|1>$ with two parameters α and φ. The two-qubit gate used in their experiment is a conditional phase gate that induces phase shifts in the target qubit, depending on the state of the control qubit. After the operations, the state of the two qubits was determined by means of tomography, which consists of various combinations of single qubit phase pulses followed by readout of both qubits. The table in Figure 6.11 gives a comparison of ideal and measured values. The results are significantly better than the classical outcomes. The whole set of operations takes about 10% of the coherence time, consistent with the deviations.

Both the Yale group of Schoelkopf (transmons) and the Santa Barbara group of Martinis (phase qubits) have succeeded in creating and detecting three-qubit entanglement. Figure 6.12 illustrates the method of the latter group[17] to create two fundamentally different three-qubit entangled states, indicated as $|GHZ>$ and $|W>$. The results are not ideal, but prove genuine entanglement.

Spectacular progress has been made in circuit quantum electrodynamics with superconducting resonators coupled to qubits. Resonators can be used to manipulate and to couple qubits, as well as to read out. Conversely, qubits can be used to manipulate and couple resonator states, as well as detecting the photon states of the cavity. A beautiful example is the creation, by the Martinis group, of arbitrary Fock states of a resonator.[18] A Fock state has a distinct number of photons. With the aid of qubits it is possible not only to load photons one by one into the resonator, but also to create

[16] L. DiCarlo, J.M. Chow, J.M. Gambetta, L.S. Bishop, B.R. Johnson, D.I. Schuster, J. Majer, A. Blais, L. Frunzio, S.M. Girvin and R.J.Schoelkopf, *Nature* 460 (2009) 240

[17] M. Neeley, R.C. Bialczak, M. Lenander, E. Lucero, M. Mariantoni, A.D. O'Connell, D. Sank, H. Wang, M. Weides, J. Wenner, Y. Yin, T. Yamamoto, A.N. Cleland and J.M. Martinis, *Nature* 467 (2010) 570

[18] M. Hofheinz, H. Wang, M. Ansmann, R.C. Bialczak, E. Lucero, M. Neeley, A.D. O'Connell, D. Sank, J. Wenner, J.M. Martinis and A.N. Cleland, *Nature* 459 (2009) 546

Element		Grover search oracle*				Deutsch–Jozsa function†			
		f_{00}	f_{01}	f_{10}	f_{11}	f_0	f_1	f_2	f_3
$\langle 0,0\|\rho\|0,0\rangle$	Ideal	1	0	0	0	0	0	1	1
	Measured	0.81(1)	0.08(1)	0.076(2)	0.065(7)	0.010(3)	0.014(5)	0.909(6)	0.841(9)
$\langle 0,1\|\rho\|0,1\rangle$	Ideal	0	1	0	0	0	0	0	0
	Measured	0.066(7)	0.802(9)	0.05(1)	0.054(8)	0.012(4)	0.008(4)	0.031(8)	0.04(2)
$\langle 1,0\|\rho\|1,0\rangle$	Ideal	0	0	1	0	1	1	0	0
	Measured	0.08(1)	0.05(1)	0.82(2)	0.07(1)	0.93(1)	0.93(1)	0.05(1)	0.04(1)
$\langle 1,1\|\rho\|1,1\rangle$	Ideal	0	0	0	1	0	0	0	0
	Measured	0.05(2)	0.07(1)	0.06(1)	0.81(1)	0.05(1)	0.04(1)	0.012(9)	0.07(2)

Fidelity of the reconstructed output states of the Grover and Deutsch–Jozsa algorithms to their ideal outputs. These results suggest that, if combined with single-shot readout, the two algorithms executed with this processor would give the correct answer with probability far exceeding the 50% success probability of the best classical algorithms limited to single calls of the oracle' or function.

FIGURE 6.11: Quantum algorithms performed with two transmon qubits[16]. A comparison is shown between the ideal outcome values and the measured values for the Grover search and Deutsch-Jozsa algorithms for two qubits.

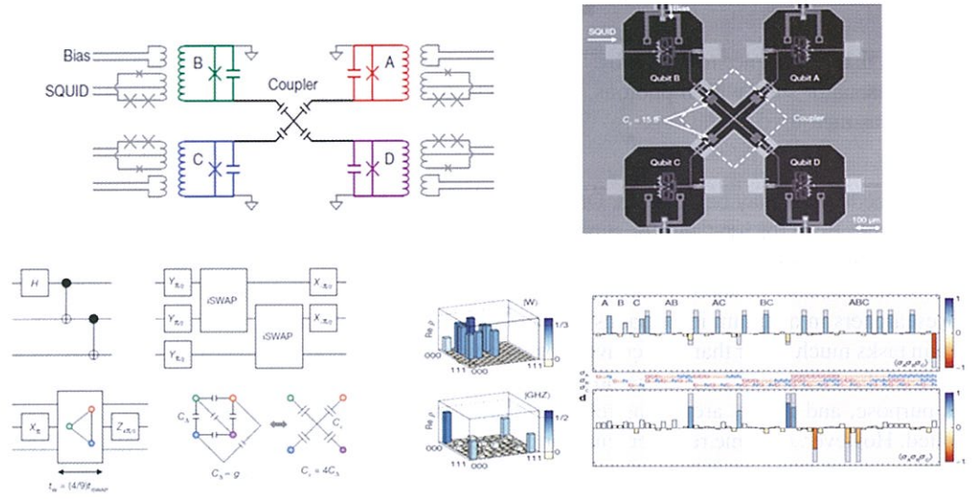

FIGURE 6.12: Experiment to create three-qubit entangled states with phase qubits[17]. Top: circuit employed, with four qubits which are capacitively coupled. Only three qubits are used in the experiment. Bottom left: protocols to create the entanglement. Bottom right: tomographic analysis of the outcome states with outcomes for the $|GHZ>$ state on top and for the $|W>$ state below. Ideal outcomes are indicated with grey, real outcomes are colored.

superpositions of these Fock states. Figure 6.13 demonstrates how close the actual result comes to the calculation.

6.2.4 Future

Can a useful quantum computer be built with superconducting qubits? Are superconducting qubits better than trapped ions when scaling up to large systems? Will spin-qubits in semiconductor quantum dots in the long run be more efficient? Such questions should be asked, but cannot be answered yet. At present, atoms and ions are still clearly ahead when it comes to the number of qubits, fidelity of operations and fidelity of readout. However, the fast rate of development for superconducting circuits will quickly reduce their advantage. Spins in quantum dots have not yet reached the coherence needed for scaling up to more than one or two qubits. Elimination of noise due to nuclear

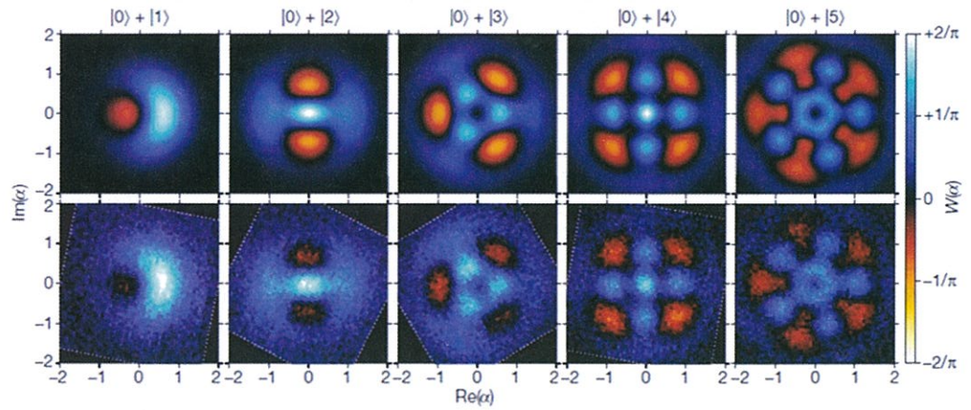

FIGURE 6.13: Wigner tomography[18] of superpositions of the resonator state with zero photons and the resonator state with n photons, n =1-5. The top shows the result as calculated, the bottom the result as measured.

spins is needed and may be possible. Other qubit types, such as hybrid optical-electronic elements, may emerge. Both for ions and for superconducting qubits there is as yet no clear path for scaling up to very large numbers. With superconducting qubits the general notion is to use a resonator as a "bus" to couple a set of about 10 qubits. Coupling between resonators is possible using qubits.

Researchers in quantum informatics are busily developing quantum algorithms that can perform certain tasks much faster than any conventional computation method. The flagship example is Shor's algorithm for factorization of large numbers. Quantum computers will be exponentially faster for this purpose, and if they are not as reliable as Intel processors, quantum error correction may be applied. However, extreme requirements for numbers and for fidelity will have to be satisfied. Technically no hard walls against further development are visible, but it seems very unlikely that the effort of many thousands of man-years needed to obtain the materials control and the reliable operation methods will be financed by any sponsor, with no intermediate valuable goals in sights.

It is almost certain that at the time of the second centennial anniversary of superconductivity there will be important applications of quantum circuits made with superconducting elements. So far, quantum mechanics was mainly used to understand the structure of nature around us. As we learn, as engineers, to build new objects that follow quantum mechanical rules, a new world is opening. At this time full simulation of a quantum system with only 25 independent variables is not possible on the largest conventional computer system. In a few years we will be able to fabricate systems of that size and we can investigate how they behave in our experiments. We should not primarily try to imitate known substances, but we should look for completely new phenomena. Superconducting qubits and circuits are naturally suited to explore this new realm. Applications are likely to be very different from what we can imagine now.

7

Digital Electronics

Editor: Shinya Hasuo

7.1 Introduction

Shinya Hasuo

Since the first electronic computer, ENIAC, was demonstrated in 1946, we human beings have been pursuing faster computers. Basic computer elements executing digital operation have been progressing continuously from the age of vacuum tubes. The basic elements have been changed to transistors, integrated circuits, and then large scale integrated circuits in this half century. During these periods, the operating speed of today's computers has increased more than one billion times that of ENIAC. Some applications, such as weather forecasting, protein design, and astronomical simulation will never be satisfied by the speed of today's computers. In the field of telecommunication, we also require very large scale routers with operation speed faster than 10 terra bits per second to deal with the huge amount of information on the Internet. Moreover, modern wireless communications requires wider and wider bandwidths in order to handle higher data rates and increase data capacity. This demands higher sample rate mixed signal circuits and higher clock rate digital signal processing circuits. In order to satisfy the need for higher speeds, researchers have been developing tiny transistors with shorter gate lengths; now they are developing transistors with twenty nanometer gate lengths. Many engineers fear, however, that the switching speed of transistors will saturate in

the near future. Thus, completely new switching elements, such as superconducting devices, single electron transistors, molecular devices, spin transistors, quantum devices and so forth, are now being investigated. Among them, superconducting devices have made remarkable progress.

The most important feature of the superconducting device to be applied to the digital circuits is high-speed switching and low power consumption. The aim of development of digital circuits with superconducting devices is not only for high speed computers but also for telecommunication systems such as high-speed router systems and wireless communication systems including satellite communications. Superconducting digital circuits can also be applied to high-speed measurement systems such as real-time oscilloscopes and digital processing circuits for multichannel sensor systems and q-bit systems. Superconducting digital circuits can be applied to a wide variety of fields that require extremely-high-speed operation with low power dissipation.

The commencement of digital application of superconducting devices is historically rather old. In 1956, a superconducting device named "Cryotron" was applied to make digital circuits. It utilized switching between the superconducting state and the normal-conducting state of a thin film. Since then, superconducting devices have progressed stepwise or discontinuously. In the end of the 1960s, the Josephson junction was applied as a switching element instead of the "Cryotron". It utilized the switching between the voltage state and the superconducting state of a Josephson junction, so-called "voltage-state" switching. It was much faster than the "Cryotron". Various high speed circuits were developed using the "voltage-state" switching. From the beginning of 1990s, the circuit operation speed was drastically improved by using a different switching mode of superconducting devices. It is called the "SFQ" mode switching, which utilizes the single flux quantum as an information carrier. The "SFQ" mode operating circuits are much faster than the "voltage-state" mode circuits. Thus almost all digital circuits are now constructed with the "SFQ" mode switching of superconducting devices. Although silicon transistors, of course, have progressed steadily in this half century, superconducting devices have progressed with much faster speed because of drastic changes of the switching mode. Superconducting devices have kept an advantage of higher speed operation than that of silicon transistors of the time. These histories are described in this Chapter and the predominance of the "SFQ" over any other high-speed devices is discussed.

This chapter describes, firstly, operating principles of digital electronics, and then its brief histories in the USA, Europe, and Japan. The recent fabrication process of digital circuits with mainly niobium material is introduced. High speed digital circuits and mixed signal processing are described with the latest data, which show the advantage over other high speed systems.

7.2 Operating Principles of Digital Circuits

Theodore Van Duzer

7.2.1 The Basic Switch

There are two different and important simple circuits with embedded Josephson junctions that will act as switchable devices. Their importance lies in the very high speed at which the switching occurs as well as the very low energy dissipated in the switching. A number of families of logic and memory have been based on them.

Shortly after the demonstration of the Josephson effect in 1963, it was realized that the Josephson junction could be used as the basis of digital circuits[1,2]. Figure 7.1 shows the type of circuit for which the "0" and "1" of binary logic are represented by zero voltage and a few millivolts, respectively. Numerous families of logic were based on this so-called "voltage-state" type of switch but they were limited in speed by the need to provide clocking that would reset the switches. After the early 1990s, new logic families were almost exclusively based on a single-flux-quantum (SFQ) switching concept to be discussed below. Still, there are situations where voltage-state switching is required. One such case is the interface of high-speed SFQ Josephson logic circuits having extremely small switching energies to higher energy level semiconductor devices.

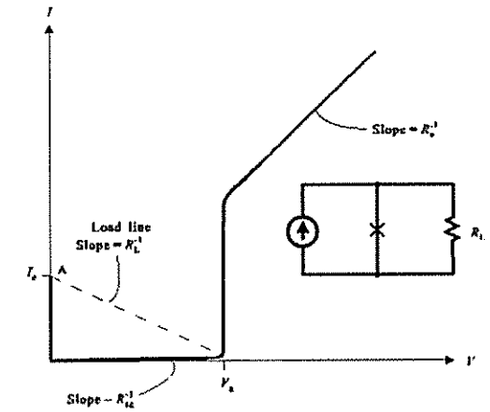

FIGURE 7.1: Basic Josephson hysteretic $I-V$ characteristic for voltage-state digital circuits and the embedding circuit (inset).

The voltage-state switch in Figure 7.1 has a resistive load, in this case matched to the normal-state resistance of the Josephson tunnel junction. Figure 7.2 shows a pattern of drive (inset) and switching response to the drive. As long as the supply current is below the "critical current" I_c, the voltage is zero. After switching, The resulting voltage across the junction builds up and contains oscillations at the Josephson frequency, $f = 2(e/h)V$, where V is the instantaneous voltage across the junction (with the oscillation amplitude determined by the circuit parameters), as long as the drive is applied. When the drive is removed, the junction resets to the zero-voltage state but with decaying oscillations.

Figure 7.3 shows the switching of a circuit representative of the switching that occurs in single-flux-quantum circuits. The input pulse causes a current to flow through the input junction that briefly exceeds its critical current. A transient voltage pulse, typically a fraction of a millivolt in amplitude and a few picoseconds in width, appears across the junction. The energy in such a pulse is typically on the order of 10^{-19} J, which is several orders of magnitude lower than the energy involved in a CMOS switching event. Some of the many logic circuits that have been based on this kind of switching will be discussed below.

[1] J. M. Rowell, Cryogenic Supercurrent Tunneling Devices, US Patent No. 3,281,609, October 25, 1966.

[2] J. Matisoo, *Appl. Phys. Lett.*, Vol. 9, pp. 167-168, 15 Aug.1966.

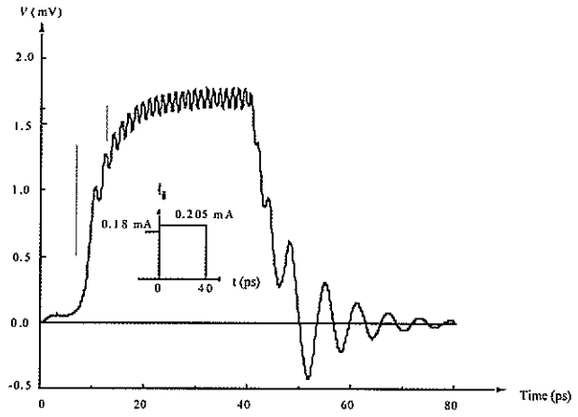

FIGURE 7.2: Typical switching event for an overdriven Josephson junction with a hysteretic $I-V$ characteristic as in Figure 7.1. The pattern of current drive is shown in the inset.

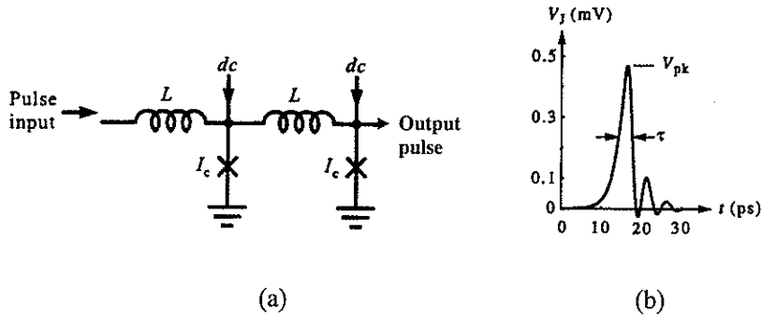

FIGURE 7.3: (a) A common circuit situation in Rapid Single Flux Quantum (RSFQ) logic for switching a Josephson junction with a nonhysteretic I-V characteristic. Part (b) shows the voltage across the input junction when the circuit is triggered by an input pulse.

7.2.2 Logic Circuits

In the 1970s and 1980s, a variety of families of voltage-state logic circuits were developed. The largest single project was at IBM, which started just before 1970 and continued until 1983 and reached about 150 researchers at its apex. A large multi-laboratory project in Japan during the 1980s developed several voltage-state logic families. A group at Moscow State University developed a family of logic circuits based on the movement of single magnetic flux quanta[3]. These so-called Rapid Single Flux Quantum (RSFQ) circuits have been the basis of almost all subsequent research in Josephson digital circuits worldwide since then. More detail on the history of Josephson digital circuits can be found in Van Duzer and Turner[4] and Duzer[5].

[3] K. K. Likharev, O. A. Mukhanov, and V. K. Semenov, in *SQUID'85*, Berlin, Germany: W. de Gruyter (1985) 1103

[4] T. Van Duzer and C. W, Turner, *Principles of Superconductive Devices and Circuits*, 2nd Ed., Ch. 5, Prentice-Hall, Upper Saddle River, NJ, USA, 1999

[5] T. Van Duzer, *IEICE Trans. Electron.* E91 (2008) 260

Voltage-state Circuits

Mainly in the 1970s and 1980s, there was extensive research on logic families using Josephson switches based on the principal in Figures 7.1 and 7.2. Although the logic subsequently studied in the 1990s and beyond employed single flux quantum circuits, there continues to be a need for some voltage-state circuits. An example is the interface between the SFQ logic and semiconductor devices. As mentioned above, the pulses in the single-flux-quantum circuits are of very low energy. While this is attractive for ultra-high-speed logic, it is a problem when interfacing these circuits to semiconductor circuits. Some voltage-state circuits find application in this niche. One simple compact circuit that can convert an SFQ pulse to a sustained voltage pulse with an amplitude of a few-millivolts is the 4JL gate shown in Figure 7.4 [6]. The junctions have the hysteretic I-V characteristic shown in Figure 7.1. The loop containing the junctions is small; its operation depends on the phase shifts in the junctions, not on inductance in the loop. The supplied clock sets the current through J_2 close to its critical current. An input current pulse causes J_2 to switch to the voltage state which, in turn, causes a transfer of the supply current to the right-hand branch. This switches the right branch to the voltage state thus leading to an output voltage sustained by the applied clock.

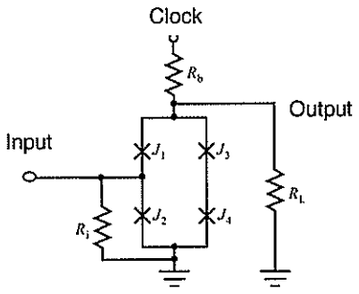

FIGURE 7.4: The basic 4JL voltage-state logic gate comprising Josephson junctions with hysteretic *I-V* characteristics.

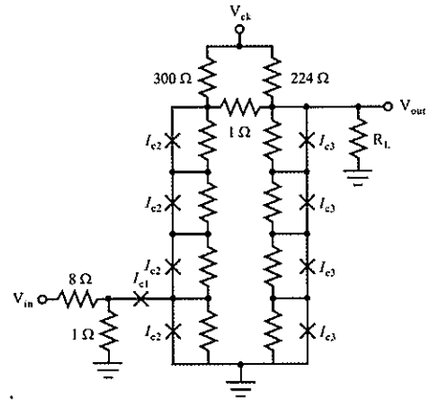

FIGURE 7.5: Suzuki stack. Operation is similar to that of the 4JL in Figure 7.4 but with higher voltage output.

Another circuit frequently employed for interfacing millivolt Josephson circuits to volt-level semiconductor circuits employs two parallel series arrays, each with a number of Josephson junctions as shown in Figure 7.5. It is frequently succinctly referred to as a "Suzuki stack" after one of its inventors[7]. The junctions are either unshunted or somewhat resistively shunted; the voltage output is the sum of the gap voltages in the series, or somewhat less if they are shunted. The resistive shunting is used to improve the high-frequency operating margins. The input causes the bottom junction in the left branch to switch into the voltage state. This diverts the current that was flowing in the left branch into the right branch, causing, in turn, the switching of the junctions in the right branch. The voltage thus developed diverts the supply current to the left branch and switches those junctions. At that final point, all of the junctions are in the voltage state. This process takes place in

[6] H. Nakagawa, E. Sogawa, S. Kosaka, S. Takada, and H. Hayakawa, *Jpn. J. Appl. Phys.* 21 (1982) L198

[7] H. Suzuki, A. Inoue, T. Imamura, and S. Hasuo, *Tech. Digest*, International Electron Device Meeting San Francisco, (1988) 290. A similar double stack was used at the same time independent work: S. R. Whiteley, E. R. Hansen, G. K. G. Hohenwarter, F. Kuo, and S. M. Faris, in *Interconnection of High Speed and High Frequency Devices and Systems*, SPIE 947 (1988) 138

a few tens of picoseconds, depending on the design.

Single-Flux-Quantum Logic Circuits

Early SFQ circuits demonstrated in the 1970s and early 1980s included shift registers[8] and counters[9]. The counters comprised a series of binary dividers and were used in analog-to-digital converters. We will concentrate here on RSFQ logic circuits, which mainly came later[10].

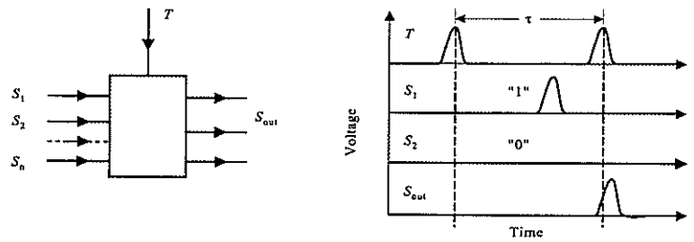

FIGURE 7.6: Method of identifying "1"s and "0"s in RSFQ logic gates shown here for an OR gate.

The basic idea of a logic block is shown in Figure 7.6 for an OR gate. The circuits are clocked by a continuous series of clock, or timing, pulses. If an input pulse arrives on one of the inputs during the interval between timing pulses, as for S_1 in the figure, it is considered to be a logical "1" input. If no pulse arrives on an input, as for S_2 in the figure, it is considered to be a logical "0". Since this example is an OR gate, an output pulse S_{out} results as shown. Other logic functions employ the same criteria for distinguishing "1"s and "0"s.

The RSFQ family contains two types of circuits, unclocked connection circuits and clocked latches. The unclocked connection circuits provide the functions of buffering the input from the output, combining inputs, and providing fan-out for latching gates. As an example of an unclocked interconnecting circuit, consider the pulse splitter shown in Figure 7.7, which is used to provide fan-out. The input at terminal A switches junction J_1, which is biased by the dc current I_{b1} close to its critical current. That switching produces a pulse that drives both output branches, causing switching of junctions J_2 and J_3 with consequent pulses at outputs B and C.

One of the common RSFQ latches is the RS flip-flop shown in Figure 7.8. In its initial state, the bias current I_b is divided between junctions J_3 and J_4 such that J_3 is biased close to its critical current and J_4 is biased at a lower level. When a pulse arrives at the input S, it drives J_3 above its critical current, which then switches briefly to the voltage state and causes a diversion of the bias current to J_4, raising its bias to a level close to its critical current. (The currents in J_3 and J_4 are equivalent to an equal current in the two junctions plus a clockwise circulating current in the J_3, L, J_4 loop corresponding to one magnetic flux quantum in the loop.) When a clock or timing pulse arrives at the reset R input, it drives J_4 beyond its critical current; a voltage pulse is generated that causes a resetting of the currents in J_3, L, and J_4 to their initial conditions and the production of an

[8] T. A. Fulton, R. C. Dynes, and P. W. Anderson, *IEEE* 61 (1973) 28

[9] J. P. Hurrell and A. H. Silver, SQUID digital electronics in *Future Trends in Superconductive Electronics*, B. S. Deaver, C. M. Falco, J. H. Harris, and S. A. Wolf (Eds.): New York, American Institute of Physics, (1978) 437 and C. A. Hamilton and F. L. Lloyd, *IEEE Electron Dev. Lett.* 3 (1982) 335

[10] K. K. Likharev and V. Semenov, *IEEE Trans. Appl. Superconduct.* 1 (1991) 3

output pulse at F. The RS flip-flop is but one of many latching logic gates that have been devised in the RSFQ family.

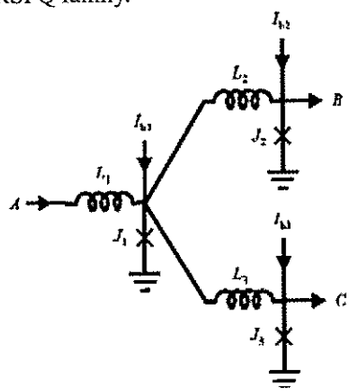

FIGURE 7.7: Splitter circuit, an unclocked connecting circuit in the RSFQ logic family, provides fan-out.

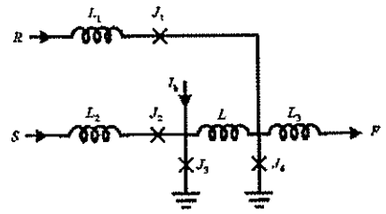

FIGURE 7.8: RS flip-flop, a latching gate in the RSFQ logic family.

7.2.3 Memory

Most of the effort to provide memory for superconducting digital systems has been directed toward random access memory (RAM), but some work has been done on first-in-first-out register-type memories[11]. Random access memories are the main interest and we focus on them here. It is well known that a circulating current in a superconducting loop will persist as long as the superconducting state is maintained. Most of the numerous concepts for random access memory cells have been based on persistent circulating currents. The earliest was reported in 1969 at IBM[12]. A later version of the IBM cell is shown in Figure 7.9. The devices shown as the write and sense gates are three-junction SQUIDs. The two states of the cell are zero circulating current to represent a logical "0" and a clockwise circulating current to represent a "1". By appropriate combinations of the currents on the I_x, I_y, and $I_{y'}$ lines, one can write either a "0" or a "1" in the cell. If a "1" is stored, the circulating current will cause the sense gate to switch when the I_{sense} is applied; the resulting voltage on the sense line signals that a "1" was stored in that cell. A complete 1 kbit memory with decoding and driving circuits was made. The difficulty of extending it to memories with larger capacity became clear and was an important part of the decision to terminate the entire IBM superconducting computer project in 1983.

Other circulating-current memory cells were developed subsequently in projects in Japan during the 1980s and complete memories were made. The project at NEC developed the vortex-transitional cell shown in Figure 7.10 and continued the development of a fully functional 4-kbit memory, which was reported in 1999 [13]. This is the largest successful memory based on circulating current memory cells that has been reported although some attempts at 16-kbit memories have been reported.

By its nature, memory employs a large number of junctions and long lines for accessing the cells. The addressing circuits are clocked at gigahertz frequencies and for practical reasons constitute an increasingly challenging design problem for memory with larger capacity. Component statistical spreads, including junction critical currents, inductances, and resistances become increasingly

[11] Q. P. Herr and P. Bunyk, *IEEE Trans. Appl. Superconduct.* 13 (2003) 563

[12] W. Anacker, *IEEE Trans. Magn.* MAG-5 (1969) 968

[13] S. Nasagawa, H. Numata, Y. Hashimoto, and S. Tahara, *IEEE Trans. Appl. Superconduct.* 9 (1999) 3708

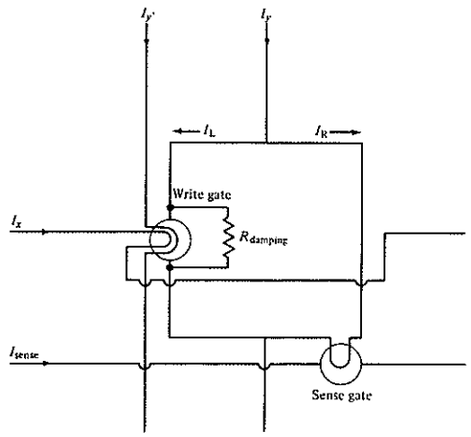

FIGURE 7.9: The IBM circulating-current memory cell.

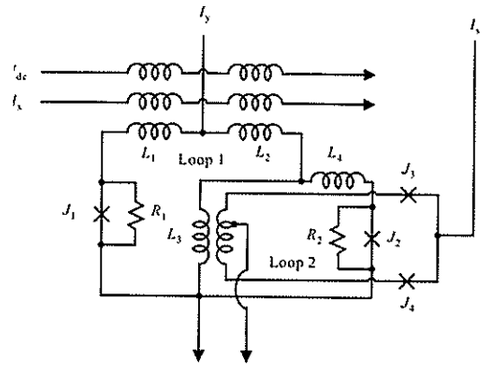

FIGURE 7.10: NEC vortex-transitional circulating-current memory cell.

limiting as the number of components increases. An added problem for circulating-current memory cells is ambient magnetic flux and flux due to large supply currents, both of which can cause malfunctions of memory cells that function by storing magnetic flux.

An alternative approach to providing memory uses a CMOS memory which operates at volt levels and must be interfaced to the millivolt-level signals of a superconducting processor. This has the advantage over superconducting circulating-current cells in that CMOS memory structures are very compact and are highly developed. Large memory can be made with high yield. CMOS works even better at 4 K, the usual operating temperature of niobium superconducting circuits, than at 300 K, so it can be in close physical proximity to the processors.

A project at the University of California, Berkeley is focused on a hybrid of Josephson interfacing circuits and a CMOS memory as shown in Figure 7.11. The amplification of millivolt signals to volt-level signals at the input is accomplished with the combination of a Suzuki stack and a hybrid amplifier comprising a MOS device with a large series array of Josephson junctions as its load. The output current from a memory bit line is detected by a Josephson device.

An access time of 600 ps was measured for a single cell in a 64-kbit memory array using a CMOS

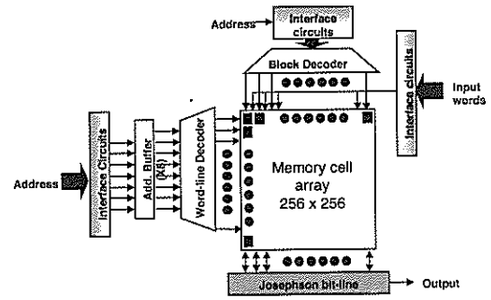

FIGURE 7.11: Architecture of a hybrid Josephson-CMOS 4 K memory.

chip made in a 180 nm process and a Josephson chip made with a 2.5 kA/cm^2 niobium process[14]. The chips were bump bonded together. Current work is directed toward writing and reading words and making improvements in access time. The use of more advanced CMOS and Josephson processes will reduce the access time considerably.

7.3 Digital Electronics in Japan

Shinya Hasuo

In this section, a brief history is described on the progress of superconducting digital electronics in Japan from the middle of 1970s to today. More than 30 years have passed since the research on digital electronics started in Japan. Many researchers have endeavored to develop advanced high speed systems during these years. But high speed conventional systems with silicon transistors have progressed steadily and continuously; the superconducting devices should have superior performance to silicon devices of the day. Thus, noteworthy changes have occurred in the history of superconducting devices for digital applications. One was the change of superconducting materials. A lead-alloy was initially used as the Josephson junction material, but it was changed to niobium (Nb) in the middle of the 1980s. In the end of the 1980s, high T_c superconductors (HTS) were introduced as junction materials, but it was difficult to make a high-quality, uniform, and reliable HTS junctions equivalent to the Nb junctions. Nb is the most reliable junction material for digital applications at present. The other change was the operating mode of the digital circuits. Until the early 1990s, "voltage-state" switches were used for the circuits, but a faster switching mode was proposed in those days. Thus, the operating mode was changed to the "SFQ" switch from the middle of the 1990s. Since then almost all digital circuits have been made with the "SFQ" mode switch, and they can be operated much faster than circuits with advanced silicon transistors. Researchers have continuously endeavored to develop superconducting high speed systems for a long time, thus a lot of remarkable and distinguished results were obtained. Typical activity and progress in these three decades are introduced here.

Many abbreviated words are used in this section for Japanese ministries and organizations, so the abbreviations used here are listed below.

[14] K. Fujiwara, Q. Liu, T. Van Duzer, X. Meng, and N. Yoshikawa, *IEEE Trans. Appl. Supercond.* 20 (2010) 14

AIST	National Institute of Advanced Industrial Science and Technology
CRL:	Central Research Laboratory, presently NICT
ETL:	Electrotechnical Laboratory, presently AIST
FED:	Research and Development Association for Future Electron Device
IEICE:	The Institute of Electronics, Information, and Communication Engineers
ISTEC:	International Superconductivity Technology Center
JSPS:	Japan Society for the Promotion of Science, which belongs to MESC (presently MEXT)
JST:	Japan Science and Technology Agency, which belongs to MEXT
METI:	Ministry of Economy Trade, and Industry
MESC:	Ministry of Education, Science and Culture, presently MEXT
MEXT:	Ministry of Education, Culture, Sports, Science and Technology
MITI:	Ministry of International Trade and Industry, presently METI
NICT:	National Institute of Information and Communication Technology
NTT:	Nippon Telegraph and Telephone Public Corporation of the day, presently Nippon Telegraph and Telephone Corporation
STA:	Science and Technology Agency, presently merged in MEXT

7.3.1 The Dawn of Research on Digital Applications

In around 1970, many Japanese computer companies suffered from the limitation of operating speed of bipolar transistors. With increasing integration density of the transistors, the huge power consumption caused a serious rise in temperature of integrated circuits, and it sometimes resulted in circuit breakdown. Thus, they were trying to find the next generation high speed electronic devices. They developed various kinds of high speed devices which could replace high speed bipolar transistors. Candidates were high-speed CMOS, GaAs FET (Field Effect Transistor), and many other functional devices.

It was in the middle of the 1970s that many Japanese companies and research institutes started the development of Josephson computers. IBM had been energetically developing the Josephson computer from the end of the 1960s, and IBM's results stimulated the Japanese companies. The Josephson junction device was selected as one of the candidates for the next generation high speed device. ETL, NTT and computer companies, such as Fujitsu, Hitachi, and NEC, and many other companies and universities started the research on the Josephson computer. This was the dawn of research on superconducting devices for digital application in Japan.

In these days, superconducting circuits were constructed with the "voltage-state" switching mode, which was described in Section 7.2. This mode was continually applied to digital circuits from the beginning of the research to around 1990. But thereafter a new mode of operation, the "SFQ" mode, which can construct much faster circuits than those with the "voltage-state" switching mode, was proposed by Likharev, Mukhanov and Semenov in 1985 [15]. Since then SFQ switching mode operation has become the main stream of digital circuits. But it must be noted that another operating mode, "phase mode" operation, similar to the SFQ mode operation, had been proposed by Nakajima et al. in Tohoku University in the middle of the 1970s [16].

Since Japanese researchers in companies and universities started research and development of digital applications of superconducting devices, the Japanese government strongly supported the activities. Companies increased the number of researchers for superconducting electronics, and ministries of the Japanese government, such as MITI and MESC, started national projects to support the companies and universities from the end of the 1970s. JSPS organized a specialist committee,

[15] K. K. Likharev, O. A. Mukhanov and V. K. Semenov, *Proc. SQUID'85*, Berlin (1985) 1103

[16] K. Nakajima, Y. Onodera, and Y. Ogawa, *J. Appl. Phys*. 47 (1976) 1620

called #146 Committee, for superconducting electronics in 1982, and it is still working. The Technical Group on Superconducting Electronics was also organized in 1982 in IEICE, and it is still active.

Since those days, almost three decades have passed. Many fruitful results have been obtained. Efforts in those days form the basis of today's research and development on digital applications.

7.3.2 Brief History of Japanese Projects on Superconducting Digital Electronics

The progress on superconducting digital electronics has been supported by the Japanese government. The progress in this field is based on the national projects. Japanese national projects in these 30 years are described here in chronological order.

Figure 7.12 shows Japanese projects on superconducting digital devices. The upper part shows the projects with LTS (low T_c superconductor) materials, and the lower shows those with HTS (high T_c superconductor) materials. The flow of research and development of Japanese superconducting digital electronics is mostly summarized in this figure, although many other small projects are omitted here. Years for the following descriptions are expressed in the Japanese fiscal year (FY), which starts on April 1 and ends on March 31.

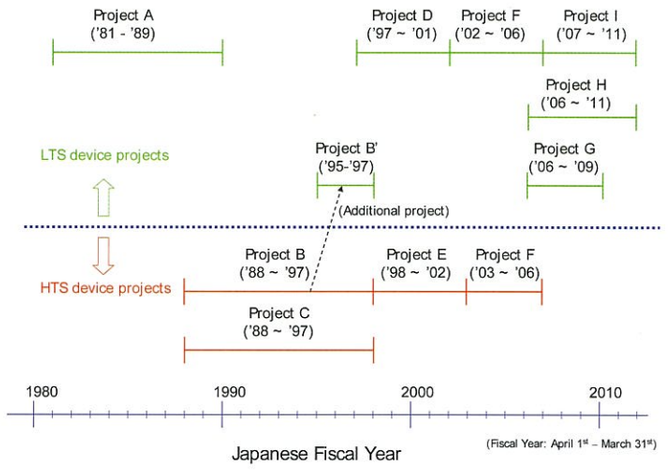

FIGURE 7.12: Japanese projects on digital electronics 1980–2010. The name of each project is, A: Scientific Computing System, B: Superconducting Electron Devices, B': Added project to B for LTS devices as Development of Josephson Device Hybrid System Technologies, C: Superconducting Electron Materials, D: Ultimate Information Processing Function Based on a Single Flux Quantum as an Information Carrier, E: R&D of Fundamental Superconducting Application Technologies, F: Low-power Superconducting Network Device, G: Single-flux-quantum Integrated Circuits Based on Localized Electromagnetic Waves, H: Low-power, High-performance, Reconfigurable Processor Using SFQ Circuits, and I: Development of Next Generation High-efficiency Network Device Technology.

Project A

In 1981, MITI started a national project Scientific Computing System, in which 10 GFLOPS HPC (high performance computer), so-called supercomputer system, was developed. The main system was constructed with multi-CPUs (central processing units) made of high-speed CMOS. Besides the main system, three kinds of high speed devices were developed as candidates for future HPCs. These devices were Josephson junction, GaAs FET, and HEMT (high electron mobility transistor). ETL and 6 companies, Fujitsu, Hitachi, Mitsubishi Electric, NEC, Oki Electric, and Toshiba were involved in this project and they shared the technologies to be developed for the supercomputer and high speed devices. As for Josephson junction devices, ETL, Fujitsu, Hitachi and NEC were responsible for the future high speed computers.

In the beginning of the project, a lead-alloy was used for the Josephson junction material. But the lead-alloy junction was very unstable and reliable circuits could not be fabricated. From the middle of 1980s, the junction material was changed from the lead-alloy to niobium (Nb). Since then many reliable digital circuits were demonstrated. Typical distinguished results are shown later.

Project B and C

In 1988 ISTEC was established in Japan as a collaborating laboratory of many companies for the development of superconductivity technology. Many researchers joined ISTEC from not only Japanese companies and universities but also from abroad. Many Japanese companies were executing their research on HTS technology in their own laboratories and also in ISTEC by temporarily transferred researchers.

In the same year, 1988, two projects with high-T_c superconductors started. One is Project B: Superconducting Electron Devices supported by MITI through NEDO and FED, and the other is Project C: Superconducting Electron Materials supported by MITI through NEDO. They continued until 1997. Project B was carried out by ETL and eight companies, Fujitsu, Hitachi, Mitsubishi Electric, NEC, Oki Electric, Sanyo, Sumitomo Electric, and Toshiba. Nine universities collaborated with them. Project C was mainly executed by ISTEC, and ten universities collaborated. In these projects, initially various kinds of three terminal devices and YBCO thin film technology were developed. But three terminal devices were revealed to be difficult to realize with enough power gain, so the direction of the projects was slightly changed to develop YBCO thin film Josephson junctions and apply them to simple digital circuits, sampler circuits and so forth.

Project B'

LTS devices were not supported after the end of Project A (Scientific Computing System) because endeavors were concentrated on the HTS devices. But it was found to be difficult to construct large circuits with HTS devices as was done with Nb junction devices in a short term, so LTS devices were also involved in Project B from 1995 as Development of Josephson Device Hybrid System Technologies. It continued until 1997, when Superconducting Electron Devices project ended. In 1997 the LTS and HTS device projects were inherited by new projects. The LTS device was supported by STA as Project D, and the HTS device was transferred to a new MITI project (Project E).

Project D

The STA project Ultimate Information Processing Function Based on a Single Flux Quantum as an Information Carrier started in 1997 and continued to 2001. AIST, ISTEC and three companies, Fujitsu, Hitachi, and NEC, were involved and five universities, Japan Women's University, Nagoya University, Tohoku University, University of Tokyo, and Yokohama National University collaborated with them. In this project, SFQ devices and circuits were mainly developed. Interface circuits between SFQ circuits and conventional silicon devices at room temperature were also investigated.

Project E

The MITI project was funded by NEDO as R&D of Fundamental Superconducting Application Technologies. The project was a big one which included a wide area of HTS applications. It included not only HTS devices but also bulk HTS, coated conductors, and materials. In HTS devices, fabrication processes of mainly Josephson junctions and high speed circuit design were executed. Development of HTS devices was mainly carried out by ISTEC, and many companies also joined in this project such as DuPont, Fujitsu, Hitachi, Mitsubishi Electric, NEC, and Toshiba.

Project F

The LTS STA project ended in 2001, and it was inherited by a new METI project, Project F: Low-power Superconducting Network Device. In the next year, 2002, Project E ended and the HTS device was merged into Project F. Thus the project including LTS and HTS devices started as a NEDO project and continued until 2006. This project was mainly carried out by ISTEC, Nagoya University, Yokohama National University for LTS devices, and by ISTEC, Hitachi, and Advantest for HTS devices. Many remarkable results were obtained in this project both in LTS and HTS devices. These results are introduced later.

Project G

In 2006, MEXT started a new project as Grants-in Aid for Scientific Research. Six universities, University of Electro-Communication, Nagoya University, Saitama University, Tohoku University, Tokyo University of Agriculture and Technology, and Yokohama National University, joined in this project to develop basic technology for digital circuits. The project was named Single-flux-quantum Integrated Circuits Based on Localized Electromagnetic Waves. It ended in 2009.

Project H

The JST project named Low-power, High-performance, Reconfigurable Processor Using SFQ Circuits started in 2006. Kyushu University, Nagoya University, Yokohama National University, and ISTEC joined this project. The aim of this project is to develop basic technologies for a 10-TFLOPS desk-side computer based on SFQ and reconfigurable data-path (RDP) architecture. It will continue to March 2012.

Project I

After the NEDO project (Project F) for LTS and HTS devices ended, the work was inherited by new NEDO projects. The LTS device was involved in a new NEDO project, Project I: Development of Next Generation High-efficiency Network Device Technology, which started in June 2007. This project is mainly for optical communication systems. It aims at establishing enabling technologies for the next generation high-efficiency networks. In this project, the main target is to develop highly efficient large-scale edge routers, ultra high-speed local area networks and related telecommunication systems. The main technologies are developed with CMOS high-speed devices and optical I/O devices. LTS devices are also included in this project. A real-time monitoring system for optical communication will be developed using LTS SFQ devices. AIST, six IT companies and ISTEC are included in this project. Among them, only ISTEC is developing superconducting devices. The present project will continue to 2011.

The HTS device integration technologies developed in the former project (Project F) have been inherited by a new NEDO project, Technological Development of Yttrium-based Superconducting Power Equipment, so-called M-PACC Project (Materials & Power Application of Coated Conductors Project). In this project, however, HTS device technology is not applied to digital systems but to SQUID systems, so this project is not shown in Figure 7.12. By using integration technology of HTS

devices, SQUID sensors are fabricated on the same chip with integrated pickup coils. The inspection system utilizing such an integrated SQUID is being used to find defects in coated conductors.

7.3.3 Progress in the 1980s

As shown in the previous section, the MITI project, Project A: Scientific Computing System, continued until 1989. ETL and three companies attained excellent results in this project. Typical achievements are summarized into two technologies. One is the fabrication technology of integrated circuits with Nb/AlOx/Nb junctions, and the other is the demonstration of high speed logic and memory circuits which are operated in the "voltage-state" mode. Fabrication technology is described in detail in Section 7.6 including recent data. High speed circuits developed in the 1980s are introduced here.

ETL demonstrated a 4-bit Josephson computer (ETL-JC1) which consisted of four chips: register and arithmetic logic unit, sequence control unit, instruction ROM (Read Only Memory) unit, and data RAM (Random Access Memory) unit[17]. The sizes of the ROM and RAM were both 1-kbit. Functional operation for 27 instructions was confirmed at low frequency. Total power consumption was 6.2 mW, and the number of Josephson junctions was 22,000. It was estimated by computer simulation that the single chip CPU including the whole circuits mentioned above could be operated at 1 GIPS (Giga-instruction per second).

Fujitsu developed two types of high-speed processors. One was a 4-bit microprocessor, and the other was an 8-bit DSP (Digital Signal Processor). The Josephson microprocessor was fabricated in 1988 for the first time[18]. It was installed in a cryostat which was connected to a refrigerator and operated in a closed cycle as shown in Figure 7.13. It functioned in the same way as the Am2901 microprocessor manufactured by Advanced Micro Devices, Inc. The Am2901 was considered the world's standard 4-bit microprocessor. A GaAs version of the Am2901 was also developed. The table in Figure 7.14 compares the performance of the Am2901 microprocessors for the three different materials. The Josephson microprocessor could be operated up to a clock frequency of 770 MHz and had a power consumption of 5 mW. Comparing these characteristics with those of the microprocessors constructed of other materials, it can be seen that the Josephson microprocessor operated at much faster speeds and with much less power than semiconductor circuits of the day.

The largest scale Josephson LSI chip of the day was an 8-bit DSP[19]. It included 23,000 Josephson junctions and it operated 100 times as fast as its CMOS logic counterpart. A photograph of the chip is shown in Figure 7.15.

The NEC group proposed a Josephson RAM with a memory cell named vortex transition memory cell. Firstly 1-kb memory circuit was published, and then it was advanced to 4-kb circuit with 21,000 Josephson junctions. Its access time was 380 ps and power dissipation was 9.5 mW [20]. This access time was the fastest of any memory chip of the day. Finally, 99.8% of the cell was confirmed to be correctly functional. A photograph of the chip is shown in Figure 7.16.

Besides the Scientific Computing System project, the Hitachi group proceeded with a new operating mode of superconducting devices, named QFP (Quantum Flux Parametron), which was originally proposed by Professor Goto of University of Tokyo. The QFP has an advantage of lower power consumption than SFQ mode operation. Hitachi demonstrated its basic function in collaboration with Professor Goto [21].

[17] H. Nakagawa, I. Kurosawa, M. Aoyagi, S. Kosaka, Y. Hamazaki, Y. Okada, and S. Takada, *IEEE Trans. Appl. Supercond.* 1 (1991) 37

[18] S.Kotani, N.Fujimaki, T.Imamura, and S.Hasuo, A Josephson 4b microprocessor, *Digest of Tech. Papers of 1988 International Solid-State Circuits Conf.* (ISSCC 1988), pp. 150

[19] S.Kotani, A.Inoue, T.Imamura, and S.Hasuo, *IEEE J. Solid-State Circuits* 25 (1990) 1518

[20] S. Nagasawa, Y. Hashimoto, H. Numata and S. Tahara, *IEEE Trans. Appl. Supercond.* 5 (1995) 2447

[21] Y. Harada, E. Goto, and N. Miyamoto, Quantum Flux Parametron, *Technical Digest International Electron Devices Meeting* (1987) 389

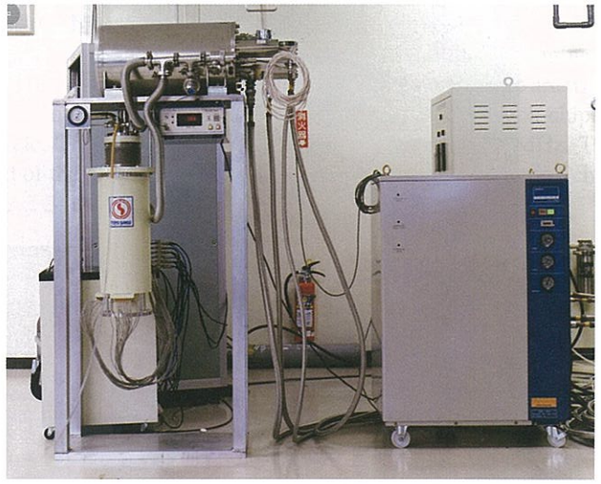

FIGURE 7.13: World's first Josephson microprocessor was installed in a cryostat, which was connected to a refrigerator and operated in a closed cycle.

Device	Si [1)]	GaAs [2)]	Josephson Junction
Maximum Clock Frequency (MHz)	30	72	770
Power Consumption (W)	1.4	2.2	0.005

1) AMD. 1985 Data Book
2) Vitesse. 1987 GaAs IC Symposium

FIGURE 7.14: Comparison of Am2901 type 4-bit microprocessor performance for Si, GaAs, and Josephson junction versions.

7.3.4 Progress in the 1990s

The 1990s were very busy years for researchers because HTS devices were expected to replace LTS devices. Thus projects were concentrated in the development of HTS devices. However, it was found to be difficult to make HTS Josephson junctions as reliable as the Nb/AlO_x/Nb devices. In the middle of 1990s, an LTS project was added as project B', as shown in Section 7.3.2. Consequently, both HTS and LTS devices progressed to a certain extent in those days. Topical results in the Project B and B' are shown here.

A basic fabrication process for HTS junctions, i.e., a ramp-edge junction with an interface-modified barrier, was developed in 1997 by the NEC group[22]. This technology was improved in the succeeding projects (Project E and Project F) by the ISTEC group, as shown in Section 7.3.5. The NEC group also developed a sampler circuit using the ramp-edge junction[23]. This technology

[22] T. Satoh, Mo. Hidaka, and S. Tahara, *IEEE Trans. Appl. Supercond.* 17 (1997) 3001

[23] M. Hidaka, S. Satoh, M. Kimishima, M. Takayama, and S. Tahara, *IEEE Trans. Appl. Supercond.* 11 (2001) 267

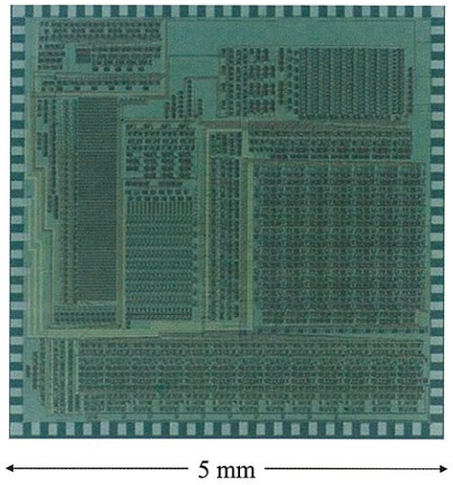

FIGURE 7.15: Chip photograph of the 8-bit DSP (©1990 IEEE).

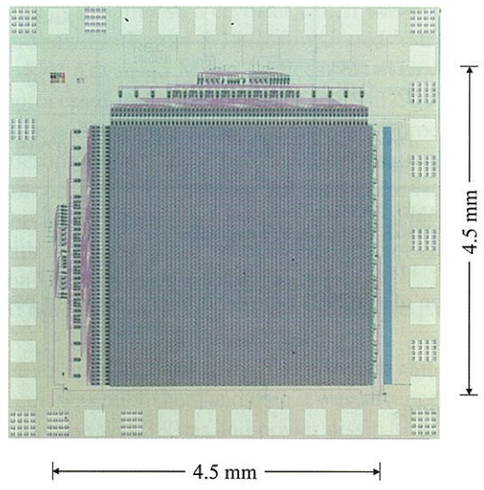

FIGURE 7.16: A 4-kb memory chip (©1995 IEEE).

was inherited by the ISTEC group in Project F, and a very compact sampling oscilloscope was demonstrated as shown in Section 7.3.5. The Hitachi group demonstrated a 2:1 multiplexing circuit using QFPs with HTS bicrystal junctions[24].

[24] H. Hasegawa, Y. Tarutani, U. Kabasawa, N. Sugii, T. Fukazawa, and K. Takagi, *IEEE Trans. Appl. Supercond.* 7 (1997) 3446

Using LTS devices, the NEC group demonstrated a superconducting ring network system as shown in Figure 7.17 [25]. Three PCs were connected with a superconducting network switch chip. The chip has a function like a traffic rotary, i.e., data coming from one node are transferred to another node so data exchange can be performed. It was confirmed that the switch chip could be operated up to 2 GHz clock cycle. The network system was operated up to 100 MHz. This frequency was restricted by the speed of the interface ICs, not by that of the superconducting chip.

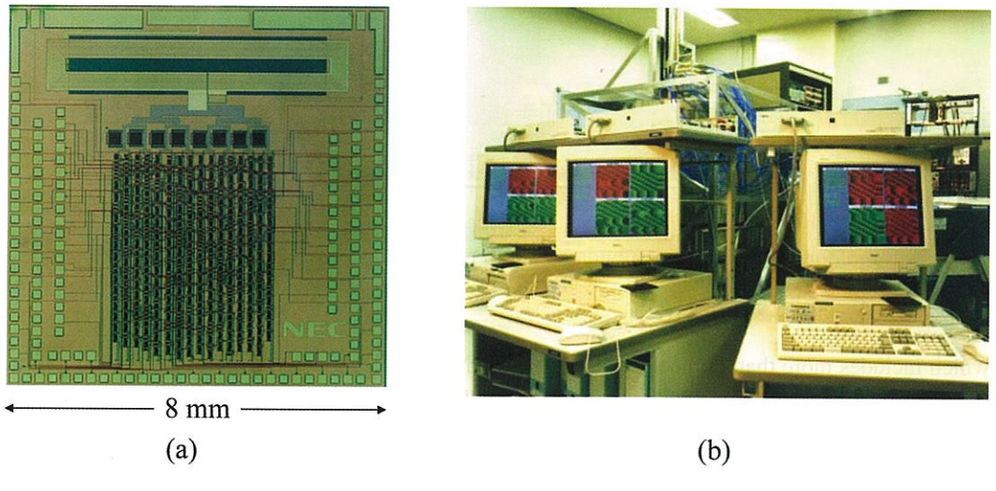

FIGURE 7.17: Demonstration of superconducting network system. (a) shows the network switch chip and (b) shows three PCs as processor elements and a cryostat in which the switch chip and interface chips are installed (©1999 IEEE).

The interface circuit between an SFQ circuit and a room temperature electronic circuit was developed by the Fujitsu group with LTS devices[26]. They stacked eight Josephson junctions in each branch of the "Suzuki stack". They demonstrated that SFQ pulses could be amplified to 10 mV at 3 GHz and to 7 mV at 10 GHz clock. These output signals can be amplified to the order of 1 V by using semiconductor circuits at room temperature.

7.3.5 Progress in the 2000s

The integration technologies of Josephson devices with LTS and HTS materials have been advanced in Project F: Low-power Superconducting Network Device. Typical results are shown below.

LTS SFQ circuits have progressed remarkably in this project. It has become possible to integrate more than 10,000 Josephson junctions on a chip with an excellent operating chip yield as high as 10%. Josephson junctions in these SFQ circuits have been made with two different current densities. One is the critical current density J_c of 2.5 kA/cm^2 and the other is 10 kA/cm^2. The minimum line width in circuits fabricated by this process is usually 1 μm. SFQ processors and a switch for a router system have been developed. These circuits are constructed with the CONNECT cell library,

[25] S. Yorozu, Y. Hashimoto, H. Numata, S. Nagasawa, and S. Tahara, *IEEE Trans. Appl. Supercond.* 9 (1999) 2975
[26] N. Harada, A. Yoshida, and N. Yokoyama, *Jpn. J. Appl. Phys.* 39 (2000) L1158

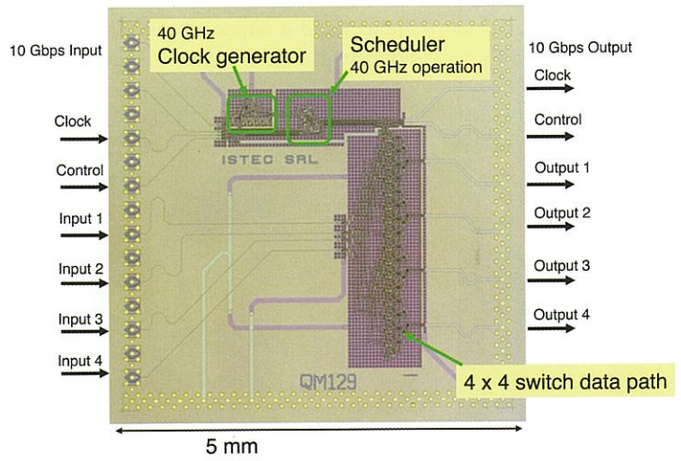

FIGURE 7.18: A 4×4 switch chip.

which includes more than 200 cells. The name "CONNECT" originally came from "Collaboration of Nagoya University, NEC, and CRL teams"[27]. But the current CONNECT group consists of ISTEC, Nagoya University, NICT, and Yokohama National University. The cell library is the basis of the integrated circuits. By using this library, SFQ microprocessors have been developed[28]. Details will be described in Section 7.7. Another example of the CONNECT cell application is a 4×4 network switch. Its photograph is shown in Figure 7.18. This chip was operated with a clock frequency of 40 GHz; thus an effective 160 Gbps throughput was attained[29]. Using the 4×4 switch chip with a high-speed interface of 10 Gbps installed in a cryocooler, a video data transfer among four PCs was also demonstrated, as shown in Figure 7.19.

Fabrication technology for HTS integrated circuits also progressed remarkably in Project F. Typical results for the HTS fabrication technology are introduced briefly here. Figure 7.20 shows a cross-sectional view of an HTS integrated circuit. (a) is a schematic illustration and (b) shows a cross-sectional TEM (transmission electron microscope) image. The main feature of this circuit is the multilayer structure including three HTS layers, SSO ($SrSnO_3$) insulation layers, and a ramp-edge type Josephson junction with a minimum junction width of 2 μm. By optimizing the fabrication process of each layer, functional HTS circuits have been reproducibly obtained. The standard deviation $1-\sigma$ of the critical current I_c is typically 6–10% and run to run spread of I_c is ±12% [30].

This process was used to fabricate a sampler circuit. A sampling oscilloscope system has been demonstrated as shown in Figure 7.21 [31]. The system consists of a cooling unit, a control unit, and a PC. The size of the cooling unit is 140 mm*times*150 mm*times*200 mm and its weight is less than 4 kg. It is a single-stage Stirling cooler with a cooling capacity of 1 W at 77 K. A typical 50 GHz waveform has been observed with this sampler system and it has been shown that it has a potential

[27] S. Yorozu, Y. Kameda, H. Terai, A. Fujimaki, T. Yamada, and S. Tahara, *Physica* C 378-381 (2002) 1471

[28] M. Tanaka, T. Kondo, N. Nakajima, T. Kawamoto, Y. Yamanashi, Y. Kamiya, A. Akimoto, A. Fujimaki, H. Hayakawa, N. Yoshikawa, H. Terai, Y. Hashimoto, and S. Yorozu, *IEEE Trans. Appl. Supercond.* 15 (2005) 400

[29] Y. Kameda, Y. Hashimoto, and S. Yorozu, *IEICE Trans. Electron*. E91-C (2008) 333

[30] H. Wakana, S. Adachi, A. Kamitani, K.Nakayama, Y. Ishimaru, Y. Oshikubo, Y. tarutani, and K. Tanabe, *IEEE Trans. Appl. Supercond*. 15 (2005) 153

[31] H. Suzuki, M. Maruyama, T. Hato, H. Wakana, S. Adachi, K. Tanabe, T. Konno, K. Uekusa, N. Sato, and M. Kawabata, Stand alone portable HTS sampler system, EXT Abs., 11th International Superconductive Electronics Conference (2007) O-R01

to observe signals at frequencies higher than 100 GHz.

The integrated circuit technology with HTS ramp-edge Josephson junctions is now applied to fabricate a SQUID chip. The SQUID sensor with a pickup coil can be integrated on the same chip. This SQUID sensor is robust against application of AC magnetic fields up to several mT, which is four orders of magnitude higher than that for conventional HTS SQUIDs made on bicrystal substrates. This is because ramp-edge junctions and pickup coils without parasitic weak links have less probability of flux trapping. Thus, this SQUID is very useful for NDE (non-destructive examination) under fairly large excitation magnetic fields[32].

7.4 Digital Electronics in the USA

Fernand (Doc) Bedard

There have been a number of efforts to develop superconductivity into a technology for use in high performance computing.

Cryotron

Project LIGHTNING: 1956 to 1963

Josephson Junctions

Josephson Signal Processor (JSP): 1971 to 1983

Superconductive Crossbar Switch: 1991 to present

Hybrid Technology Multi-Threaded Architecture (HTMT): 1997 to 2003

Superconducting Technology Assessment (STA): 2005 to present

[32] T. Hato, S. Adachi, Y. Sutoh, K. Hata, Y. Oshikubo, T. Machi, K. Tanabe, *Physica* C 469 (2009) 1630

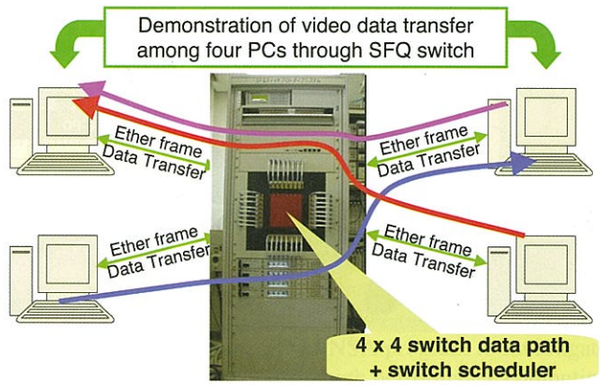

FIGURE 7.19: Video data transfer demonstration with 4×4 switch system installed in a cryocooler.

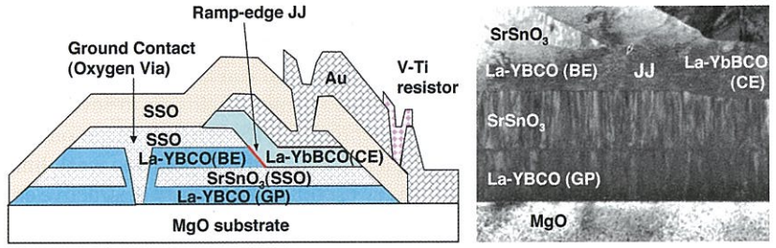

(a) (b)

FIGURE 7.20: Schematic cross-sectional view of an HTS integrated circuit.

7.4.1 Cryotrons

In 1954, Dudley Buck, a Department of Defense, National Security Agency (NSA) electronics engineer attending graduate school at MIT, proposed that one could make a switching device by using two features of superconductivity:

1. zero electrical resistance,
2. the suppression of superconductivity by applying a magnetic field to a superconductor.

In his doctoral thesis Buck says, The magnetic destruction of superconductivity is proposed as the basis for an electronic component having current gain and power gain. The component appears to be well adapted to a new kind of printed circuit technique wherein the entire circuit, including all active and passive elements, can be made in a single operation, such as vacuum evaporation. Circuits made in this way will make possible digital computers with greater computing capability than the present-day machines, and at the same time with smaller size, lower power dissipation, and a high

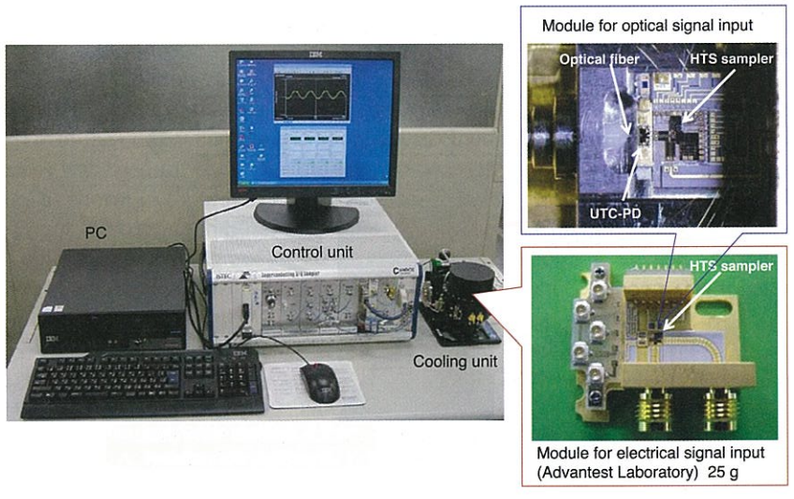

FIGURE 7.21: Photograph of the sampling oscilloscope system with HTS integrated circuit.

degree of reliability.[33]

Buck called this device a "Cryotron". His first device used a .003 inch Niobium wire coil wound around a .009 inch tantalum wire. Current applied to the Nb coil transitioned the Ta wire to the resistive state. This demonstrated that one could use a small current to control a large current.

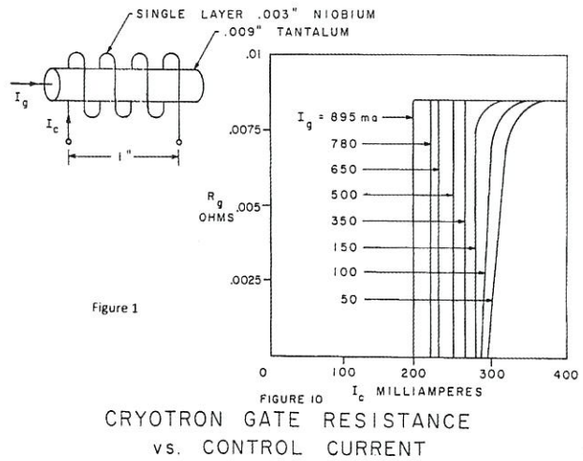

FIGURE 7.22: Cryotron gate resistance.

Buck used this "gain" to build a logic "flip-flop" which would switch the current to either of two paths. He further investigated the building of Cryotrons using crossed films which would produce smaller, faster and lower power devices in large numbers.

This prospect led to a Department of Defense (NSA) program called "LIGHTNING" with the IBM Corporation. The intent was to develop Cryotron devices for memory and logic in a high-end computing. The attraction was *very high speed at very low power*. A number of circuits were built including logic and memory, for example, a 1000 bit random access memory and some specialized logic "chips". Small systems were also fabricated. The technology was aimed toward high speed. Unfortunately, it was found that there is a fundamental limit to the time required for the Cryotron to switch states. This discovery took place at a time when semiconductor integrated circuits were also being developed and they operated at room temperature.

The program was terminated in 1963.

7.4.2 Josephson Signal Processor (JSP)

In 1971 a paper was presented by an IBM researcher, Dr. Juri Matisoo, concerning the creation of a small memory circuit using Josephson junction devices. Again, the attraction was very high speed at very low power. An NSA researcher contacted Dr. Matisoo and arranged for a meeting. The result of this exchange was the creation of a joint IBM I NSA program to investigate the applicability of this device technology, the Josephson junctions in high performance computing.

[33] Superconductive Electronic Components, Dudley A. Buck Dr. Science Thesis; Massachusetts Institute of Technology, June 1958

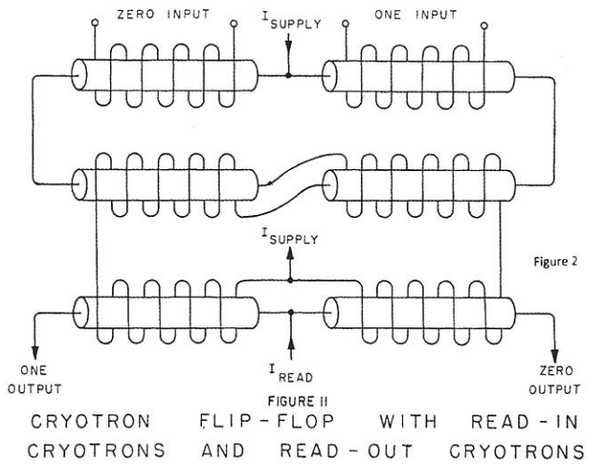

FIGURE 7.23: CRYOTRON Flip Flop

The program methodically went through demonstrations of logic, memory, packaging, powering and cooling.[34,35,36,37,38] The "demonstration vehicle" chosen was a digital signal processor, the Josephson Signal Processor (JSP).

Given success, it was deemed that this would be sufficient to prove the features necessary for general purpose computing use. Fabrication materials technology moved from using lead and tin to niobium. The basic logic gate selected was "latching logic" which was found to have a switching speed limitation. (This was sufficiently high to be acceptable at that time.)

The program stopped in 1983 when it was judged that adequate memory would not be demonstrated as soon as was desired. (Also, at that time new semiconductor technologies appeared promising.)

7.4.3 Superconductive Crossbar Switch

The Microelectronics and Computer Corporation (MCC) carried out studies to address the problem of a large number of processors (~ 1000) being called upon to access a large shared memory in future high end computer (HEC) systems. Their studies investigated a number of technologie:

1. a large number of entry ports, ~1000 or more,
2. a large number of exit ports, ~1000 or more,
3. very high speed channels, multi-GHz,
4. the ability to resolve contention among requesting processors, and

[34] IBM Journal of Research and Development 24 (1980)

[35] W.Anacker (IBM), Computing at 4 degrees Kelvin, *IEEE SPECTRUM* 16 (1969)

[36] Wilhelm Anacker, Potential of superconductive josephson tunneling technology for ultrahigh performance memories and processors, *IEEE Trans. Mag.* MAG 5 (1969)

[37] RSFQ logic/memory family: A new Josephson junction technology for sub-terahertz digital systems, K.K.Likharev and V.K.Semenov, *IEEE Trans. on Appl. Supercond.* 1 (1991)

[38] Development of superconductor electronics technology for high-end computing, A. Silver, A. Kleinsasser, G. Kerber, Q. Herr, M. Dorojevets, P. Bunyk and L. Abelson, *Superconducting Science and Technology* 16 (2003)

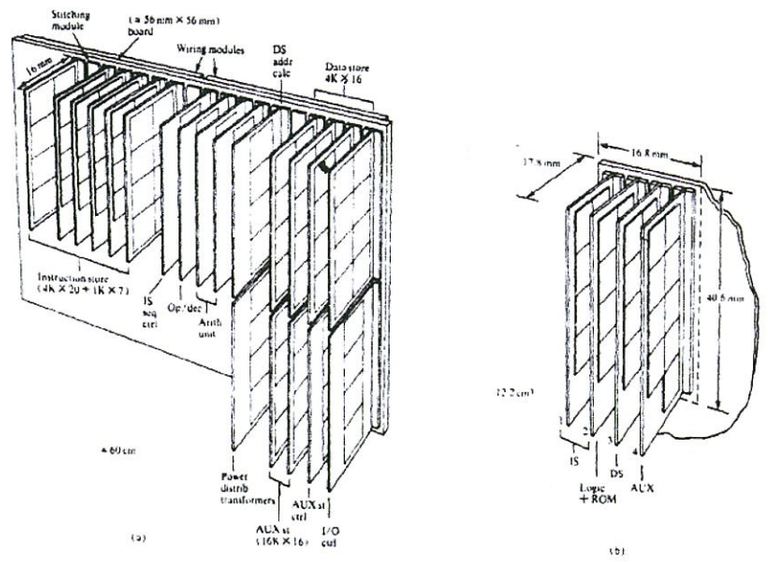

FIGURE 7.24: JSP package.

5. very high system throughput under heavy request loads.

A proposal was made by a DoD (NSA) member of MCC's Technical Advisory Board to use 11 devices in a unique architecture to solve the problem. A Crossbar switch was proposed using superconductive Josephson devices. Its architecture is based on a 32(input) × 32(output) "Switch" chip and an interface chip, "Glue", which directs and senses the data-and control-pulses coming from the room temperature processors and memory. The architecture allows expansion from the 32×32 basic switch to a $(N \times 32) \times (M \times 32)$ structure while maintaining the serial data rate per port and resolving contention. The basic 32×32 "Switch" chip contains ~ 5000 Josephson junctions.

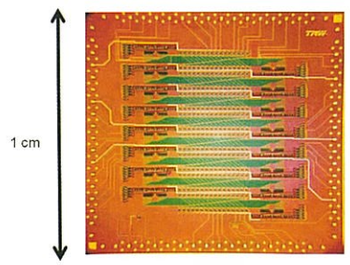

FIGURE 7.25: 2.5 Gb/s per channel, self-routing, 16×16 switch based on NSA design, demonstrated to 4 Gb/s in 1996.

A development program was undertaken to evaluate performance and feasibility.

- The ability to carry high speed signals to and from the 4 K environment using copper ribbon

cable was proven.

- MCC designed and built the multichip module (MCM) and the chip bonding tool.
- The Johns Hopkins University Applied Physics Laboratory carried out electromagnetic simulation and measurements of the behavior of the (MCM) and its input/output connections.
- Superconducting chips were fabricated by TRW (now Northrop Grumman), HYPRES and MIT Lincoln Laboratories.
- Semiconductor electronics, cryogenic cabling and 300 K to 4 K cabling were built by Tektronix, Inc.
- MCC performed computer simulations of the Crossbar system to evaluate its throughput and access time. These showed very high total throughput even with very high contention rates among processors.

Discrete event simulations (computer mimicking of the hardware system) were performed by David Bisant (NSA) and Marc Snir et al. (University of Illinois)[38] for a 1024×1024 Crossbar. They also showed high throughput data rates under very high processor request rates.

A 128×128 Superconductive Crossbar system was built and successfully tested by Tektronix at 2.5 Gbits per second per input port, and a 16×16 Crossbar was built and tested by TRW (now Northrop Grumman) at 10 Gb/s per input port.

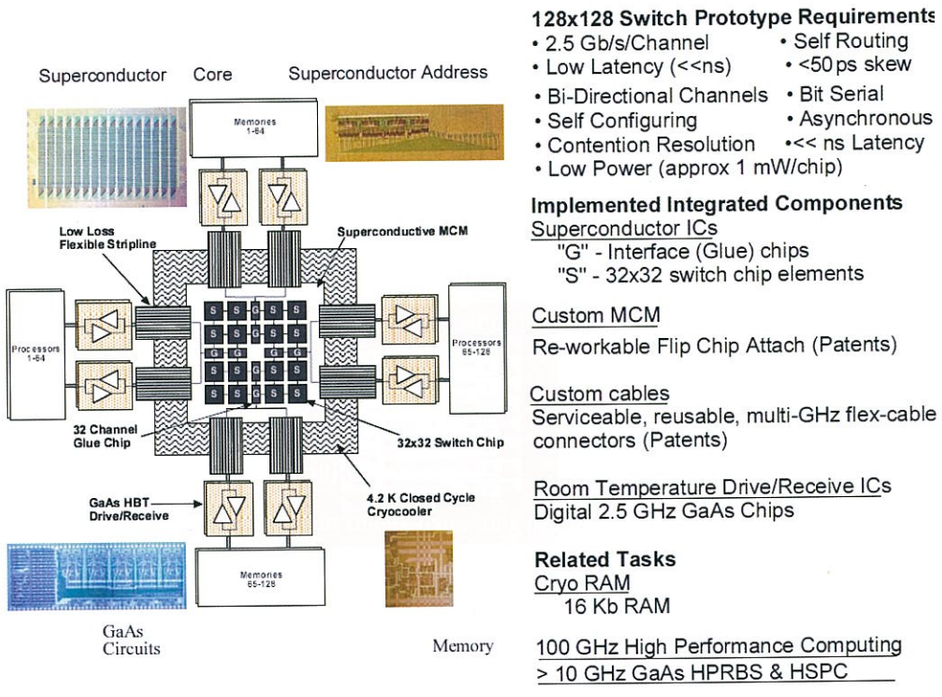

FIGURE 7.26: Superconducting crossbar switch for high performance computing: assembly and demonstration.

7.4.4 Hybrid Technology Multi-Threaded Architecture (HTMT)

A new way of using Josephson junction devices to achieve higher speed and lower power than latching logic had been developed. The concept relied on the use of single flux quanta as the individual "bits". By measuring the presence or absence of flux quanta in a time window one could carry out the required logic functions called for in a computer. The very small energy of a quantum of flux resulted in a very low power consumption even at clock speeds ~100GHz. This rapid single flux quantum (RSFQ) technology appeared to be a very promising candidate for use in very high performance computing systems.

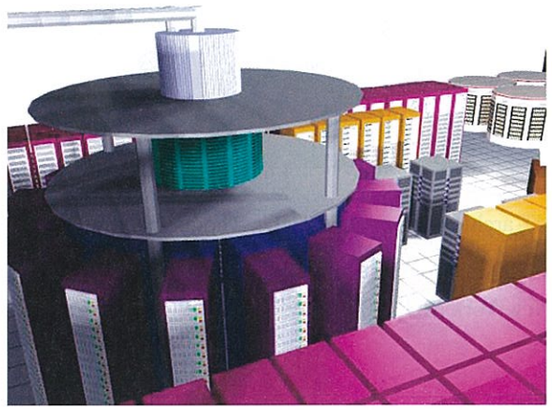

FIGURE 7.27: HTMT facility (conceptual drawing). Cryopackage concept: 1 m^3 package, 1 kW 4 K, built with achievable technology.

A number of studies evaluated the requirements and candidates for achieving "Petaflops" class of computing (10^{15} floating point operations per second). The studies covered computational problems, architecture, software, logic technology and memory technology. The conclusion was that the wide range of performance requirements dictated the use of a number of different technologies:

- superconductive devices,
- superconductive interconnects,
- semiconductor devices,
- metal conductors,
- magnetic media, and
- optical components.

The very high speed of Josephson junctions used in RSFQ (rapid single flux quantum) circuits and their very low power consumption would be the core of a very compact computing system having low power.

The architecture chosen was Multi-Threading. Since multiple technologies were employed in the system the effort was named HTMT hybrid technology multi threaded architecture. The program, supported by NSA and NASA (JPL/CalTech), had the goal of building a prototype petaflops system. The participants were

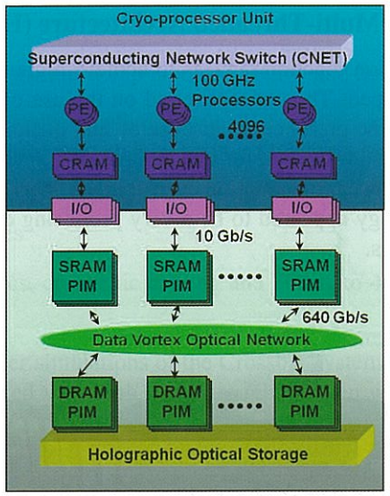

FIGURE 7.28: HTMT architecture created by Dr. Thomas Sterling (JPL).

State University of New York (SUNY)
at Stony Brook,
Columbia University,
University of Notre Dame,
University of Delaware,
TRW (now Northrop Grumman),
Argonne National Laboratory,
California Institute of Technology, and
Jet Propulsion Laboratory (JPL).

The petaflops processor used superconducting rapid single flux quantum RSFQ circuits. The machine was partitioned into 4096 processing elements operating at 4 K. These processors interface with processor in memory (PIM) random access memory. The memories are connected to a multi-ported optical switch (DATA VORTEX) whose output was fed to a bank of conventional dynamic random access memory (DRAM). The large data store was chosen to be an optical memory.

A demonstration superconductive chip, FLUX 1, was built. It was a 5000 gate, 8 bit microprocessor RSFQ chip and used 1.75 micron 4000 A/cm^2 current density Nb-NbAlO$_x$-Nb Josephson junctions. The chip was designed to dissipate ~ 9 mW at a 20 GHz clock rate. Chip to chip communications over a 2.5 cm path through solder bumps matched transmission lines and passive MCM was demonstrated at 60 G bits per second. Due to funding restrictions the program was not continued to completion but was terminated in 2003.

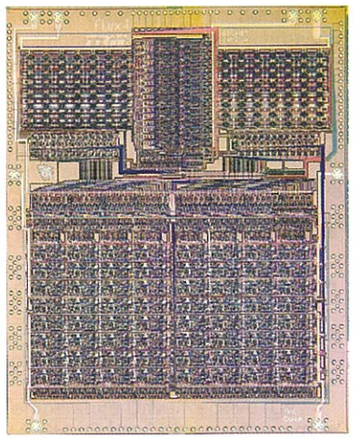

FIGURE 7.29: FLUX I.

7.4.5 Superconducting Technology Assessment (STA)

The U.S. Department of Defense (NSA) convened a team of experts to address the problem of high end computing. It was noted that:

1. "Recent industry trends clearly establish that design tradeoffs between power, clock and metrology have brought silicon to the limits of its scalability".

2. "The Semiconductor Industry Association (SIA) International Roadmap for Semiconductors (ITRS) has identified superconducting rapid single flux quantum (RSFQ) technology as the most promising technology in the continuing demand for faster processors and low power."

The panel report[39] stated: "This assessment is an in-depth examination of RSFQ technologies with the singular purpose of determining if a comprehensive roadmap for technology development is possible, aiming for industrial maturity in the 2010–2012 timeframe."

The team was composed of members from academia, industry and government. The conclusions reached were affirmative:

> "The STA concluded that there were no significant outstanding research issues for RSFQ technologies. Speed, power and Josephson junction density projections could be made reliably. Areas of risk have been identified and appropriately dealt with in the roadmap with cautionary comments on mitigation or alternatives."

The report, STA #1, was delivered in June 2005, not in time for DoD budget insertion. STA #1 was followed by a re-evaluation in 2007, STA #2, to update the original findings. STA #2 reaffirmed STA #1 and noted that, due to low funding, progress had been slow in the elapsed time.

7.5 Digital Electronics in Europe

Horst Rogalla

In this section I will give a personal view on the European situation of superconducting electronics in general and especially on digital superconducting electronics over the last 30 years. It will be neither complete nor well balanced—it just maps my personal experience in this area over the last 30+ years.

7.5.1 The Early Days

My experience with digital electronics starts about 47 years ago in the 1960s when I built a simple 2-bit arithmetic unit, as a high-school student, from old computer parts: at that time logic elements consisted of small circuit boards with individual transistors and many discrete elements soldered on top. It is no wonder, looking back, that cryrotrons[40] could have been a serious speed competitor in the early days of semiconductor logic circuits. Building the arithmetic unit was a great learning experience, but it was slow, just like the semiconductors at that time. It was also the time when the future of semiconducting computing was founded — the first circuits of the 7400-family, the *de facto* industrial standard for digital circuits for a long time appeared, integrating just four NAND-gates on one chip. And with the release of the PDP-7 (which had a clock rate of about 700 kHz) the minicomputer age started. The cryotron was quickly left behind with a fundamentally limited switching speed and low complexity. It did, however, pave the way for integration in superconducting thin-film techniques.

[39] See http://www.nitrd.gov/pubs/nsa/sta.pdf

[40] See e.g., D. A. Buck, Memorandum 6M-3843, MIT Lincoln Laboratory (1955)

In the early 1970s, I was a student at the University of Muenster in Germany and one rainy day in November (the saying is "it rains in Muenster or the church bells ring") I stayed quite long in the library. In a popular science magazine I found an article about Josephson tunnel junctions, about their natural 0 (superconducting) and 1 (gap-voltage) state, about their incredible switching speed and how they would revolutionize the computer world. I went home wondering how you can create logic circuits with 2-terminal elements without amplification, started drawing circuits similar to the old diode-logic, and found that by far I did not know enough about superconductivity: my interest and fascination in superconductivity had caught fire. At that time few groups worked on superconducting electronics in Europe, but the prediction of the Josephson effect and its experimental verification by John Rowell et al. (see Chapter 3 Section 1) changed the picture, groups started to work with rf-SQUIDs and dc-SQUIDs, and on simple digital circuits. The development culminated in the announcement that IBM was going to build a Josephson computer. This announcement caught not only the imagination of researchers, but it was also essential for the funding situation—only national funding was actually available since there were no European Framework programs at that time (the first one (FP1) started in 1984 with only a tiny amount of funding). This was an exciting time, many new superconducting digital circuits were developed, all based on "voltage state" switching, but they were more or less copies of semiconductor logic cells and designed for standard computer architectures. I remember talks about the IBM project and about the design and properties of the superconducting digital circuits at meetings of the Low-Temperature Community of the German Physical Society—at that time still taking place in Freudenstadt in the Black Forrest in a vibrant atmosphere with the feeling that something big was happening. But at that time, I also started to get doubts, at least about the material choice for the project–lead is not a very stable material, neither mechanically nor chemically. The reports about "hillocks" growing in the planar junction area after a few thermal cycles were disturbing. In my group in Giessen, Germany in the Institute of the late Christoph Heiden, we had made a number of such junctions; initially they worked with excellent *IV*-characteristics, but after a few thermal cycles they badly degraded and mostly resulted in high sub-gap currents or even shorts. Many attempts to prevent a deterioration of the material by alloying with gold, indium, antimony, etc. improved the situation and looked promising, but did not seem to be a real solution — still the Josephson junctions were not very reliable and were sensitive to thermal cycling and humidity. The difficulty in realizing memory circuits and its scalability may have been the main reason for IBM to stop the project, but the material difficulties also must have played an important role in this decision.

In 1983 I heard about Nb/Al/Al_2O_3/Nb-junctions[41], and on the way to a conference I visited Michael Gurvitch at Bell Labs to see how this process worked. I had some experience with dc- and rf-magnetron sputtering of Nb in an old semiconductor evaporation system, in which we prepared Nb/NbO_x/Nb-junctions with bad but stable *IV*-characteristics. It became immediately clear that this was a technology with which the advantages of Nb could be combined with the excellent barrier characteristics of Al_2O_3. This technique was quickly introduced in many laboratories in Europe and we were able to use this technique on a small scale to make SQUIDs, but any attempt to enter the research on digital circuits failed—the negative fallout of the end of the IBM project hit hard: funding agencies in Europe were very reluctant to invest in a technology that industry had "proven" to be a dead end. In Europe, only a few groups were able to continue this research, leading among them Jutzi's group in Karlsruhe, Germany. Jutzi had been with IBM Rüschlikon for many years, first developing semiconductor memory circuits[42] and later becoming involved in the IBM Josephson computer project[43]. After the end of the project, Jutzi and his group continued working on digital

[41] M. Gurvitch, M. A. Washington. and H. A. Huggins, *Appl. Phys. Lett.* 42 (1983) 472
[42] W. Jutzi, C. H. Schuenemann, *IBM J. Res. Devel.* 16 (1972)
[43] see e.g. W. Jutzi, *Cryogenics* 16 (1976) 81

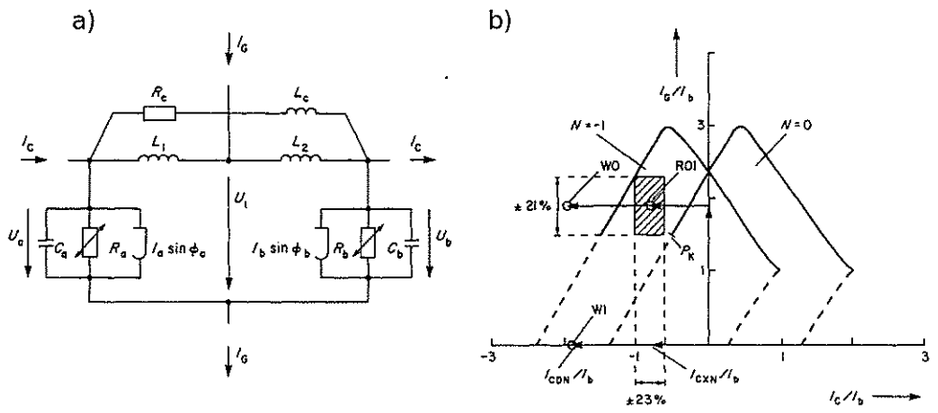

FIGURE 7.30: a) Equivalent circuit of the interferometer memory cell and b) its threshold curve. (With permission[44].)

Josephson circuits for many years, with special interest in memory cells[44]. Other important groups in Europe working on Josephson junctions and their applications were the group around Tord Claeson in Gothenburg, Sweden, in Copenhagen, Antonio Barone in Napels and Jüergen Niemeyer at the PTB in Braunschweih, Germany—each with some specialty, but no common program and no focus on digital applications. The work on Josephson voltage standards at the PTB in Braunschweig had the most advanced techniques for Josephson junction preparation, the standards required large numbers of junctions with small parameter spread and good microwave design (see Chapter 9 Section 5). The step towards complex digital circuits would have been small, but a national or a European program for a digital Josephson computer on the research laboratory or university level was in the best of circumstances "fiction".

In discussion with industry, often the argument came up that cooling Nb circuits, either with liquid helium or cryocoolers, was too painful and that one needed to use materials with an operation temperature of ~10 K—at least for small applications. This industry requirement was fulfilled when in 1985 Shoji et al. of the ETL in Japan reported the reproducible fabrication of high-quality NbN/MgO/NbN-junctions[45]. At that time Villégier at LETI in Grenoble was also working on NbN-films[46]. In the following years, he established a high-quality NbN junction fabrication in Grenoble, applying these junctions in all areas of superconducting electronics, including digital circuits. This effort still continues and this group is the most advanced in Europe in the use of NbN, either "stand-alone" or in conjunction with Nb-layers[47]. The importance of a NbN technique for industrial applications is the higher operation temperature. The A15 materials offered an even higher operation temperature and I concentrated with my group in Giessen on Nb_3Ge, which at the time had the highest T_c of up to 23 K. In this institute in Giessen, materials science work on the A15 materials had been going on for a long time: Braun had set up an ultrahigh vacuum system to co-sputter Nb_3Ge already in 1978 [48]. We used this system in 1984 and the following years to prepare Nb_3Ge-films for superconducting electronics applications. Together with Bernd David and Michael Mück we

[44] D. Drung, W. Jutzi, *Cryogenics* 24 (1984) 179
[45] A. Shoji, M. Aoyagi, S. Kosaka, F. Shinoki, H. Hayakawa, *Appl. Phys. Lett.* 46 (1985) 1098
[46] Akkermans, E., Laborde, O., Villégier, J.C., *Solid State Commun.* 56 (1985) 87
[47] E. Baggetta, M. Maignan, J.-C. Villégier, http://stinet.dtic.mil/dticrev/pdfs/ada445484.pdf (2005)
[48] H. F. Braun, E. J. Saur, *J. Low. Temp. Phys.* 33 (1978) 87

succeeded in structuring nano-bridges of less than 100 nm width and a T_c above 20 K. We also developed a multilayer technique to fabricate more complex circuits, a very challenging task because the Nb_3Ge deposition takes place at a temperature above 900 °C [49]. These circuits were tested and operated in liquid hydrogen: dc-SQUIDs and the first relaxation oscillation SQUIDs showed very nice properties. Michael Mück even successfully realized a planar Nb_3Ge Josephson junction, but the fabrication was very challenging and its properties were not great. At Stanford, the group of M. Beasley was working on a similar program with Nb_3Sn. Originally I planned to develop the Nb_3Ge technique towards more complex circuits, but neither the quality of the planar junctions was good enough for "voltage state" switching for digital circuits nor was the nano-bridge fabrication reproducible enough to apply it to the upcoming RSFQ technology. In short, interesting physics but a dead end for applications; superconducting electronics and digital applications were in general in a bad state in the mid-1980s in Europe and funding was scarce.

Then everything dramatically changed in 1986 within a very short time: the discovery of Ba-La-Cu-O by Bednorz and Müller at IBM Zürich (see Chapter 4, Section 2) and of the first material superconducting in liquid nitrogen by Paul Chu and his group in Houston (see Chapter 4, Section 4), $YBa_2Cu_3O_{7-\delta}$, started a "Cold Rush". Within a few months, groups became experts in the field that never before had been seen in superconductivity and they promised a "superconducting world" within a few years, from superconducting cables replacing the high-voltage power lines, magnetically floating cars and roller skates, to supercomputers operated in liquid nitrogen. It seemed that the more science fiction-like the proposal, the easier it got funded. Together with some colleagues from the pre-high-T_c time, we warned about overselling the high-T_c superconductivity—at that time, not even high-T_c Josephson junctions were available—but without success. Progress was made, more slowly than predicted, but steadily: the first grain boundary junctions and step-edge junctions appeared and epitaxial films were grown on single crystal substrates like $SrTiO_3$. Based on our experience with Nb_3Ge, we succeeded in setting up a multilayer technique based on $YBa_2Cu_3O_{7-\delta}$ and, using this technique, Hans Hilgenkamp prepared the first HTS dc-SQUID with an integrated multi-turn input coil.[50]

Gerrit Gerritsma and I were particularly interested in superconducting digital electronics and it was clear to us that we could surpass the performance of semiconductors, if we could make it work at sufficiently high frequencies and at temperatures easily achievable by cryocoolers, like 40 K or above. Learning from the materials science results of epitaxy on angled films, it occurred to me that by cutting a low-angle ramp in an $YBa_2Cu_3O_{7-\delta}$ film and then depositing a layer of (semiconducting) $PrBa_2Cu_3O_{7-\delta}$ on top followed by the deposition of a counter-electrode one could create a Josephson junction that had primarily a current-flow in the ab-plane of the c-axis oriented films. We tested the idea and it worked—the high-T_c ramp-type junction was born[51]. We used this Josephson junction technique together with our multilayer technique to fabricate simple digital circuits, e.g. a quasi-one-junction digitizer[52]. In Europe we were the only group with this technique at hand, later followed by a ramp-type junction technology at the Chalmers University of Technology, Sweden and a planar junction technology at DRA, Great Britain[53]. In Japan, a successful modification of this ramp-type junction, the "interface-engineered" junctions, soon appeared (see Section 3 in this chapter), followed by a similar technique at the Research Center Jülich, Germany. From the USA

[49] B. David, M. Muck and H. Rogalla, *Advances in Cryogenics Engineering*, A.F. Clark and R.P. Reed (eds.), Plenum Press, New York 32 (1986) 543

[50] J.W.M. Hilgenkamp, G.C.S. Brons, J.G. Soldevilla, R.P.J. Ijsselsteijn, J. Flokstra, H. Rogalla, *Appl. Phys. Lett.* 64 (1994) 3497

[51] J. Gao, W.A.M. Aarnink, G.J. Gerritsma, H. Rogalla, *Physica* C 171 (1990) 126

[52] E.M.C.M. Reuvekamp, P.A.A. Booi, M.A.J. Verhoeven, G.J. Gerritsma, H. Rogalla, *IEEE Trans. Appl. Supercond.* (1993) 2621

[53] P. J. Hirst, R. G. Humphreys, J. S. Satchell, M. J. Wooliscoft, C. L. Reeves, G. William, A. J. Pidduck, H. Willis, *IEEE Trans. Appl. Supercond.* 11 (2001) 143

exciting messages about complex digital high-T_c circuits based on high-T_c microbridges (e.g., long shift registers) appeared and vanished.

7.5.2 European Projects

Our first European program was the ESPRIT-2 project UNITED (January 1989 through 1991, coordinated by Thomson CSF)[54]. This project had the theme "HTS thin films and tunnel junction devices". Initilally we did not take part in this program because I did not believe in HTS tunnel junctions; in the final phase of the project, we joined in order to help with HTS thin films. Clearly UNITED did not reach its main goal, the HTS tunnel junction, and it was far from any application.

In June 1992 the EU ESPRIT-3 project UNITED II in the 3rd Framework Program started as a successor to the UNITED project. In contrast UNITED II was clearly dedicated to technology and application development. It addressed "... two main application areas for high-T_c superconductors: digital circuitry and magnetic field sensors ..." Denis Crete of Thomson CSF coordinated the project. In a stimulting atmosphere of industrial request, technological development and fundamental research, we developed first simple logic circuits and a 4-bit flash-type input stage for an ADC[52] (see Figure 7.31). The project was successfully completed in August 1995.

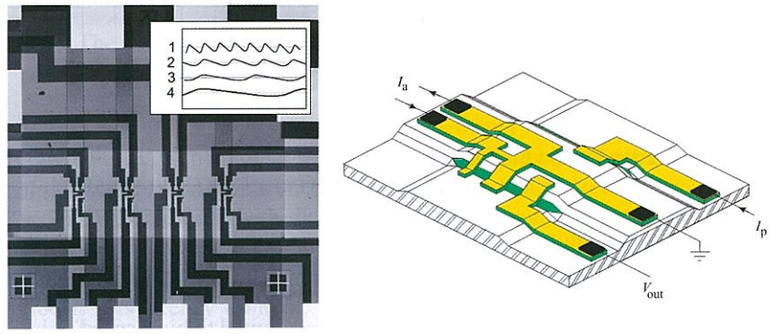

FIGURE 7.31: 4-bit flash converter with a R-2R network input and "quasi-one junction SQUID" digitizers.

Based on this success, we applied for a follow-up project, this time primarily focused on superconducting digital electronics. The program was called RSFQ-HTS and was coordinated by me. It was organized around a few groups with excellent HTS device experience: The Defense Research Agency (DRA), Great Britain brought in advanced evaporation techniques and a (planar) CAM junction process, the University of Twente–sputtering and in the ramp-type junction/multilayer process and Chalmers University of Technology/Sweden–a tri-crystal grain-boundary junction technique. The RSFQ-HTS program intended to establish a common design base for HTS digital circuits, further develop a HTS multilayer and Josephson junction technology, and demonstrate complete SFQ circuit functions. It started in January 1997 and finished at the end of 2000. In the course of the project a number of basic digital circuits were developed, among them a high-T_c T-flipflop that was operated up to 33 GHz. The main output of the project was a $\Sigma\Delta$-modulator that functioned up to an internal clock rate of 178 GHz (see Figure 7.32).

[54] for details of the European projects, mentioned here, search the European database CORDIS by acronym: http://cordis.europa.eu/search/index.cfm

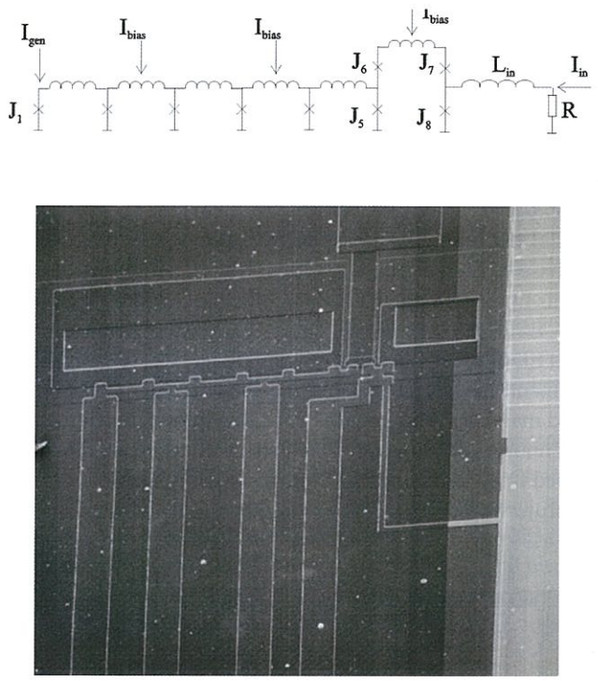

FIGURE 7.32: 1st order $\sigma\delta$-modulator.

In the meantime, the limitations of HTS Josephson junctions had become obvious: circuits with up to 10 Josephson junctions were "easy", circuits with more than 40-50 junctions were practically impossible to yield due to the wide spread of the current density in HTS Josephson junctions available at that time. So the high-T_c Josephson technology was limited to high-speed or high sensitivity frontends with a limited number of Josephson junctions.

The RSFQ-HTS project caught the attention of Erland Wikborg of Ericsson in Stockholm Sweden. Together we worked out a follow-up project, that would combine a second-order $\Sigma\Delta$-modulator at the input stage with a cold broadband amplifier interfacing with an InP-multiplexer and a CMOS decimation filter (see Figure 7.32). The low-temperature parts were all to be cooled by a specially developed cryocooler. The intention was to demonstrate the applicability of this technique to software-defined radios, which were of special interest to Ericsson. The application was successful and in January 2002 the project SUPER-ADC started.

At about middle of the project, Ericsson was forced to concentrate on its core business and sold our partner, the Ericsson Wireless Solutions to Infineon. The interest of Infineon in superconductivity was at best very small and, together with some fabrication problems of the fast electronics, the project did not reach its goal of testing all subunits together. However it succeeded in testing the major parts of the analog-to-digital converter successfully. The project finished end of June 2005.

In the early 2000s, the enthusiasm about high-T_c applications was gone—the materials science and preparation was much more difficult than many groups had anticipated and the overselling of high-T_c superconductivity now turned against the whole field: it was very difficult, nearly impossible to get funding for HTS projects. Nevertheless, after a number of attempts, we succeeded in getting funding for a project where the aim was to digitally read-out the state of a SQUID with high-T_c-electronics and then complete the data processing with semiconductor electronics at room temperature. Such a SQUID would have the advantage of a very high slew-rate and should thus

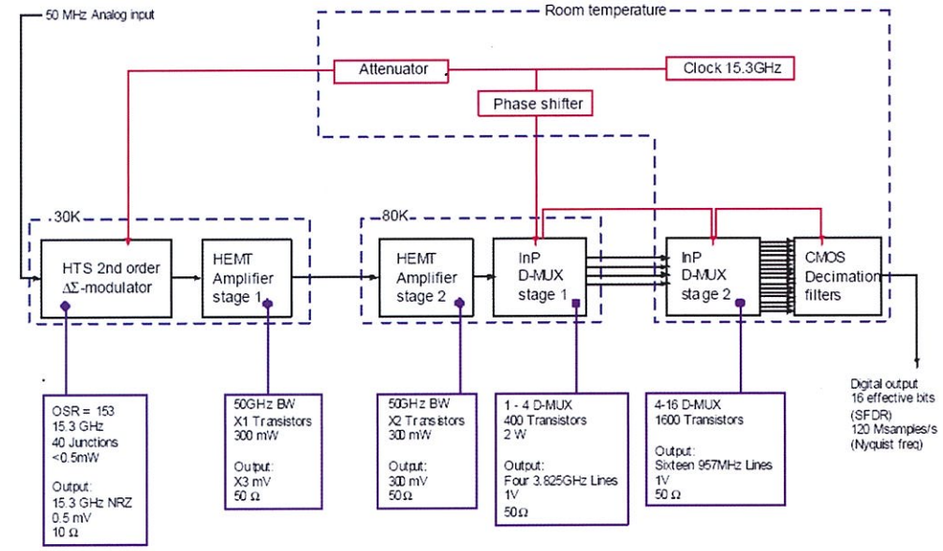

FIGURE 7.33: The ADC concept in the SUPER-ADC project.

be able to operate without shielding in an electromagnetically noisy environment. The project had the acronym DIGI-SQUID. The project started in October 2002 and it lasted until September 2006. Many parts of the whole system were successfully fabricated and tested. But changes in the participation and personnel, especially with the industrial partners and the withdrawing of Oxxel (after going out of business) as the fabrication source of the HTS circuits, resulted in big delays and insufficient budget to finish the project in time.

In this period it was already difficult, due to decreasing funding, to keep the quite expensive and knowledge-intensive high-T_c multilayer process up and running in Twente. We nevertheless stepped in and realized at least part of the high-T_c-circuit within a short time. In principle, this project marked the end of the involvement of my group at the University of Twente in this type of research and application development—neither national nor European funding were sufficient to continue.

In the late 1980s, 1990s and early 2000s Europe concentrated its superconducting electronics research almost entirely on HTS-superconductors, primarily because of an industry requirement of operation in liquid nitrogen or with one-stage low-power cryocoolers. It forced researchers to work on applications with a not-yet mature high-T_c technology instead of further improving the technology itself and performing the necessary fundamental research (e.g., the d-wave superconductivity in high-T_c was verified in 1993 (see Chapter 3 Section 3) and the mechanism for high-T_c is still unclear today). Instead, a balanced approach for low-T_c complex electronics and high-T_c technology development would probably have been much more productive. However, such advice was unheeded, both in Brussels and by national governments in Europe.

Luckily, some low-T_c digital research proceeded quietly in some places in Europe, such as at the PTB in Braunschweig, Jena and Karlsruhe (all in Germany), in Grenoble, France, in Naples, Italy and at the Chalmers University of Technology, Sweden, where Anna Herr set up a group to design and test complex low-T_c digital circuits. Together with Ericsson she worked on circuits for telecommunication, the most complex ones designed in Europe so far.

With the rise of quantum computing and qubits the idea came up to read out qubits with short coherence time using fast low-T_c RSFQ circuits. A consortium applied successfully for a European

project titled RSFQUBIT coordinated by Chalmers University of Technology, and work started in September 2004 and continued until the end of 2007.

7.5.3 Organization of Superconducting Electronics in Europe

Until 1996 there was no common body in Europe that represented applications of superconductivity at the level of the European Community or the national level. This low level of representation had impact on the political decisions of the different "Directorates" in Brussels and on the project/funding situation of superconductivity research and applications. A few attempts to realize such an infrastructure had failed until Massimo Marezio took the lead and with a number of colleagues we applied successfully for a Network of Excellence in the Information Society Technologies (ISCT) Program of the EU. This network started in October 1996 and brought together groups of superconducting electronics, superconducting materials, and large scale applications of superconductivity. It significantly strengthened the position of the superconducting electronics research in Europe. To receive funding from the European Community for digital superconducting electronics, this was an essential step: SCENET brought together research laboratories and interested industries Europe-wide, which was absolutely essential for European projects. Apart from the representation function towards the European Community, SCENET regularly organized meetings and summer schools, and supported the exchange of scientists between laboratories. This was an important step toward bringing together laboratories and people from different European countries and stimulating cooperation between scientists.

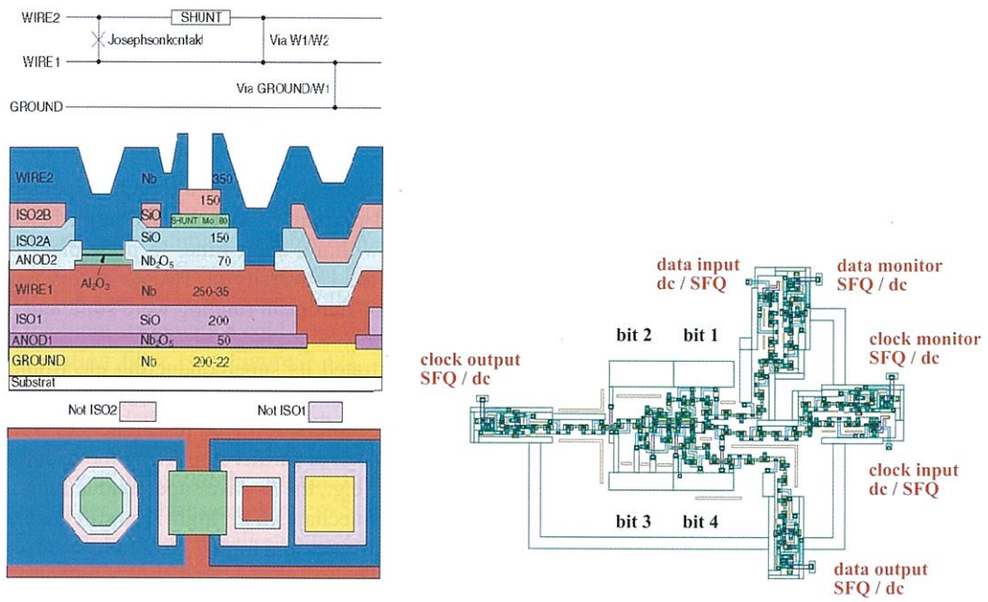

FIGURE 7.34: a) IPHT: multilayer process b) PTB: layout of a circular RSFQ shiftregister (courtesy FLUXONICS e.V.).

In the course of time, the organizational background of SCENET in the European Community

changed; the focus of SCENET became more materials and large scale oriented, but it remained an excellent platform for the applied superconductivity community in Europe. In cooperation with SCENET, I took the initiative to found, together with a number of colleagues, a European network for Superconducting Electronics, which was organized independently from the European Community as a society, according to German law, with seat at the PTB Braunschweig, Germany. The basic idea of this network was to bring together industry and research laboratories and create a "virtual" infrastructure for the design and fabrication of superconducting electronics circuits: a foundry network and a design network for analog and digital superconducting circuits.

After the formal end of SCENET in 2006, the general representation of superconductivity in Europe was taken over by the European Society for Applied Superconductivity (ESAS) and superconducting electronics by FLUXONICS. As the first director of FLUXONICS I initiated a European Roadmap for Superconducting Electronics, in which a number of colleagues wrote a common picture about the status and perspectives of superconducting electronics in Europe[55]. The second edition of this roadmap[56] was published recently as a part of the European project S-PULSE. Within FLUXONICS, superconducting digital electronics has always played an important role–the University of Ilmenau, Germany (Hannes Töpfer) has established a circuit and layout library, and regularly organized design courses for digital electronics. IPHT Jena, Germany took over the role as foundry for low-T_c circuits and a number of fabrication runs of test circuits have been made to verify its fabrication capability (see Figure 7.34). An overview of the role of FLUXONICS and Superconducting Electronics in Europe can be found in a Special Issue on Recent Progress in Superconducting Digital Electronics[57].

7.5.4 Road Ahead

Nearly all articles and talks on "alternative" digital techniques stress the fact that semiconductors "will hit a wall" soon, that Moore's law will come to an end, and that the "alternative" technique will take over. Until now the semiconductor industry has always found ways to extend Moore's law. It has to end some day for sure, not necessarily resulting in a replacement of the semiconductor technology with alternative technologies, but in complementing the existing technology with new technologies. Superconducting digital electronics is a very promissing alternative technology, with the big advantage of very low switching energy and very high speed. A huge knowledge base exists for superconducting digital circuits of some complexity; design, simulation and verification techniques and tools are available. Hundreds of thousands of Josephson junctions have been successfully fabricated on a chip for voltage standard applications. High-T_c circuits of low complexity with special functions for frontends have successfully been made. New Josephson junction technologies are being investigated and especially Nb/SiNb/Nb intrinsically shunted junctions[58] show superior perfomance in terms of yield, process compatibility and electrical properties. It seems very worthwhile to invest in this technology and make it ready to complement the semiconductor technology in areas where its limit will be reached. This will require further research and development in the area of compatible memory, low bias current operation and better cryocoolers for low-T_c and high-T_c circuit operation.

---

[55] H.J.M. ter Brake et al., *Physica* C 439 (2005) 1

[56] S. Anders et al., *Physica* C 470 23-24 (2010) 2079.

[57] H. Rogalla, *IEICE Trans. Electron.* E91.C (2010) 272

[58] D. Olaya, P.D. Dresselhaus, S. P. Benz, A. Herr, Q. P. Herr, A. G. Ioannidis, D. L. Miller, and A. W. Kleinsasser, *Appl. Phys. Lett.* 96 (2010) 213510

7.6 Integrated Circuit Fabrication Process

Mutsuo Hidaka

Superconducting integrated circuits, especially single-flux-quantum (SFQ) circuits[59], are ultimate high-speed and low-power electrical devices. These features are quite attractive for use as the main elements in supercomputers and network routers. These circuits are also lately getting much attention as the peripheral circuits of quantum-bits (Q-bit) and superconducting detectors. The fabrication process to implement superconducting integrated circuits started in the 1970s using Pb as the superconductor[60] and the initial types of logic and memory circuits[61,62] were fabricated by IBM. However, the soft and unstable nature of Pb resulted in fatal flaws regarding the long-term reliability and thermal contraction on cooling to 4 K. Nb was considered an attractive superconducting material from the early days, since it was harder and more stable than Pb. Nevertheless, Pb was used at first because the fabrication of a good quality Nb Josephson junction (JJ) was a difficult process[63]. Gurvitch et al. invented Nb/AlOx/Nb JJ [64], in which a thin Al layer was used to cover the surface of the Nb base-electrode and an AlOx tunnel barrier was formed through the oxidation of the Al layer surface. This method helped to eliminate any adverse effects on the JJ quality by the Nb sub-oxide at the junction interface and to create excellent quality Nb junctions. After that, Nb circuits based on the Nb/AlOx/Nb JJs became the mainstream of superconducting electronics devices as well as digital circuits. The JJ using other superconducting materials, such as NbN, MgB_2, and high-T_c superconductors, have also been investigated. However, the controllability and reliability of these JJs have not yet reached the necessary level for use in integrated circuits, although some small circuits were demonstrated using the NbN JJs[65] and high-T_c JJs[66]. Therefore, this article focuses on the fabrication process for Nb-based integrated circuits.

7.6.1 Circuit Elements

Josephson Junction

A JJ is the active element in superconducting circuits. A Nb/AlOx/Nb tunnel-type junction is generally used as the JJ in them. Figure 7.35 shows a schematic diagram of the Nb/AlOx/Nb JJ fabrication. Thin Al, which is typically 10 nm, is deposited on the base-electrode Nb, and the surface of the Al layer is thermally oxidized to form an AlOx tunnel barrier. A counter-electrode Nb is deposited on the tunnel barrier. The JJ region is patterned by using photolithography and the counter-electrode Nb except for the JJ region is etched away using reactive ion etching (RIE) with fluorine gas. In this method, part of the Al layer remains as normal metal. The residual Al layer has little impact on the JJ quality, since the residual Al layer has superconductivity due to the proximity effect from the base-electrode Nb. A cross-section TEM photograph (a) and the current-voltage characteristics (b) of an Nb/AlOx/Nb JJ are shown in Figure 7.36. The characteristics are of an under-damp nature, which has hysteresis in it, although the SFQ circuits require an over-damp JJ.

[59] K. K. Likharev and V. K. Semenov, *IEEE Trans. Appl. Supercond.* 1 (1991) 3
[60] J. H. Greiner, C. J. Kircher, S. P. Klecher, S. K. Lahiri, A. J. Warncke, S. Basavaiah, E. T. Yen, J. M. Baker, P. R. Broslous, H. C. W. Huang, M. Murakami and I. Ames, *IBM J. Res. Develop.* 24 (1980) 195
[61] T. R. Gheewala, *IBM J. Res. Develop.* 24 (1980) 130
[62] S. M. Faris, W. H. Henkels, E. A. Valsamakis and H. H. Zappe, *IBM J. Res. Develop.* 24 (1980) 143
[63] R. F. Broom, R. B. Laibowitz, Th. O. Mohr and W. Walter, *IBM J. Res. Develop.* 24 (1980) 212
[64] M. Gurvitch, W. A. Washington, H. A. Huggins, *Appl. Phys. Lett.* 42 (1983) 472
[65] H. Terai and Z. Wang, *IEEE Trans. Appl. Supercond.* 11 (2001) 525
[66] M. Hidaka, T. Satoh, M. Koike and S. Tahara, *IEEE Trans. Appl. Supercond.* 9 (1999) 4081

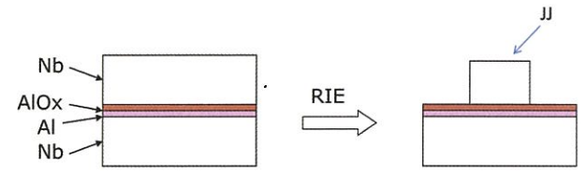

FIGURE 7.35: Schematic diagram of Nb/AlOx/Nb JJ fabrication.

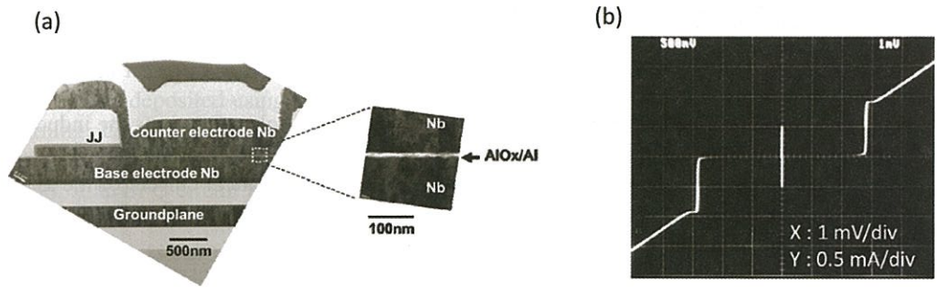

FIGURE 7.36: Cross-section TEM photograph and current-voltage characteristics of Nb/AlOx/Nb JJ.

Thus, the Nb/AlOx/Nb JJ is shunted by a resistor to change to the over-damp JJ in SFQ circuits.

The clock frequency of the SFQ circuits is proportional to $(J_c/C_0)^{1/2}$ when the McCumber coefficient of the JJ is constant, and inversely proportional to the JJ area. Here J_c is the critical current and C_0 is the characteristic capacitance of the JJ. The J_c is exponentially proportion to the tunnel barrier thickness. Figure 7.37 shows the J_c dependence on the Pt product. Here, P is the O_2 partial pressure and t is the oxidation time. The J_c can be well controlled by the self-limited logarithmic dependence on the thermal oxidation, as shown in Figure 7.37.

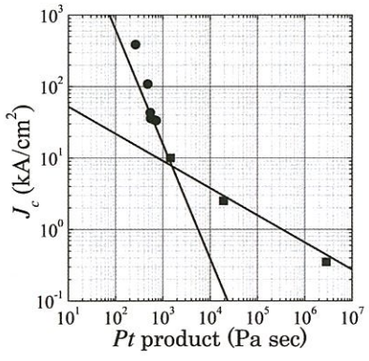

FIGURE 7.37: J_c dependence of product on O_2 partial pressure p and oxidation time t.

The basic technology for fabricating the Nb/AlOx/Nb JJs was established in the 1980s. Sustained efforts, however, have been devoted to improving the JJ quality, reliability, and controllability. For instance, Hinode et al. discovered from an I_c analysis of a huge number of JJs that the inclusion of hydrogen in the Nb electrodes affected the J_c of the JJ[67] and Noguchi et al. found that the contribution of the imaginary part of the superconducting gap energy, which was caused by incompleteness in the Nb superconductivity near the barrier interface and/or impurity in the barrier, on the JJ tunnel current[68]. Other barrier materials that can be used for a Nb JJ have been investigated. Among them, Nb_xSi_{1-x} [69] and AlN_x [70] are attractive because of their wide variety of electrical properties and excellent quality at a higher J_c, respectively. Some self-shunted JJs have been reported[71]. Some I_cR_n products from them have already been reported although they are relatively low. Here, R_n is the JJ normal resistance and the I_cR_n product represents the on-state voltage.

Wiring

Nb thin film is used as wiring material, and this wiring plays two roles. One is as the inductance element. The LI_c value is quite important in SFQ circuit, because SFQ loops are characterized by their LI_c values. Here, L is the inductance of SFQ loop and I_c is the critical current of the JJ. The wiring width, length, and insulator thickness underneath the wiring have to be well controlled to maintain a precise L value.

The other is for the interconnection between two elements. Passive transmission lines (PTL) are attractive interconnections because their SFQ pulses can propagate the speed of light. The impedance matching between the wiring and JJs at the ends of PTL has to be maintained. Microstrip line or strip line structures are adopted to define the impedance of the wiring[72].

Resistor

The typical values of resistors in integrated circuits are from a few Ω to a few tens of Ω. Mo is popular for implementing the resistors because its resistivity is appropriate for creating a 1-2 Ω sheet resistance within a 100-nm thickness. Pd is also popular because it is expandable for the Q-bit and detector peripheral circuits since it maintains a normal resistance below 1 K. Larger resistors, for instance 50 Ω in a terminate resistor for a high-speed signal line, are occasionally used. MoN_x or NbN_x, which have larger sheet resistances, are sometimes used in addition to the metal resistors to save resistor area[73].

Interlayer Insulator

SiO_2 is usually used as the interlayer insulator and dielectric material of superconducting circuits because of its high-reliability and ease of deposition and etching. Bias-sputter and PECVD (plasma enhanced chemical vapor deposition) are used for improving the step coverage of the interlayer insulator. Anodized films of Nb and/or Al are sometimes used for part of the insulator.

[67] K. Hinode, T. Satoh, S. Nagasawa and M. Hidaka, *J. Appl. Phys.* 104 (2008) 23909
[68] T. Noguchi, T. Suzuki, A. Endo and T. Tamura, *Physica* C 496 (2009) 1585
[69] D. Olaya, P. D. Dresselhaus, S. P. Benz, J. Bjarnason and E. N. Grossman, *IEEE Trans. Appl. Supercond.* 19 (2009) 144
[70] A. Endo, T. Noguchi, M. Kroug, T. Tamura and H. Inoue, *Physica* C 469 (2009) 1589
[71] M. Yu. Kupriyanov, A. Brinkman, A. A. Golbov, M. Siegel and H. Rogalla, *Physica* C 326-327 (1999) 16
[72] Y. Hashimoto, S. Yorozu, Y. Kameda and V. K. Semenov, *IEEE Trans. Appl. Supercond.* 13 (2003) 535
[73] L. A. Abelson, R. N. Elmadjian and G. L. Kerber, *IEEE Trans. Appl. Supercond.* 9 (1999) 3228

7.6.2 Integration of Circuit Elements

These circuit elements are integrated into a device structure consisting of a $Nb/AlO_x/Nb$ JJ layer, three or four Nb layers, and one or two resistor layers on a substrate with corresponding insulator layers between these metal layers. The lower three Nb layers and one resistor layer are a necessity for digital circuits and the top Nb layer and second resistor layer are options. Several institutes have developed fabrication processes for these devices[73,74,75,76]. Figure 7.38 shows a schematic cross-section diagram of an SFQ circuit fabricated by the International Superconductivity Technology Center (ISTEC) in Japan[74]. This device includes four Nb layers, such as for one groundplane and three wirings, a Mo resistor layer, and SiO_2 insulation layers between the metal ones; the device is fabricated on a 3-inch surface-oxidized Si wafer. $Nb/AlO_x/Nb$ JJs are placed between the second and third Nb layers. The minimum JJ size and wiring width are 2 μm×2 μm and 1.5 μm, respectively. The target J_c is 2.5 kA/cm^2. All the metal layers were deposited using DC magnetron sputtering and SiO_2 was deposited using biased RF magnetron sputtering. An i-line stepper was used for the patterning. Each layer was etched by an RIE in which several kinds of fluorine gas were used according to the etched materials. Figure 7.39 shows a top view, cross-section, and circuit diagram for part of an SFQ circuit fabricated by using the ISTEC process. The identical parts are indicated in this figure. The top Nb layer does not appear in it.

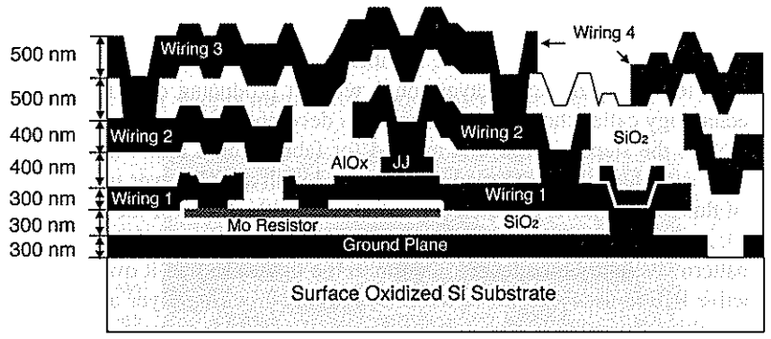

FIGURE 7.38: Schematic cross-section diagram of SFQ circuit fabricated by using ISTEC Nb four-layer process.

The circuit parameters in this process are sufficiently controlled. Run-to-run scattering of the J_c and Mo sheet resistance are both within ±10%. Many SFQ circuits consisting of more than 10,000 JJs fabricated by this process operated correctly using several tens of GHz clock frequency[77,78].

[74] S. Nagasawa, Y. Hashimoto, H. Numata and S. Tahara, *IEEE Trans. Appl. Supercond.* 5 (1995) 2447
[75] S. K. Tolpygo, D. Yohannes, R. T. Hunt, J. A. Vivalda, D. Donnelly, D. Amparo and A. F. Kirichenko, *IEEE Trans. Appl. Supercond.* 17 (2007) 946
[76] L. Grönberg, J. Hassel, P. Helistö and M. Ylilammi, *IEEE Trans. Appl. Supercond.* 17 (2007) 952
[77] A. Fujimaki, M. Tanaka, T. Yamada, Y. Yamanashi, H. Park, N. Yoshikawa, *IEICE Trans. Electron.* E91-C (2008) 342
[78] H. Park, Y. Yamanashi, K. Taketomi, N. Yoshikawa, M. Tanaka, K. Obata, Y. Ito, A. Fujimaki, N. Takagi, K. Takagi and S. Nagasawa, *IEEE Trans. Appl. Supercond.* 19 (2009) 634

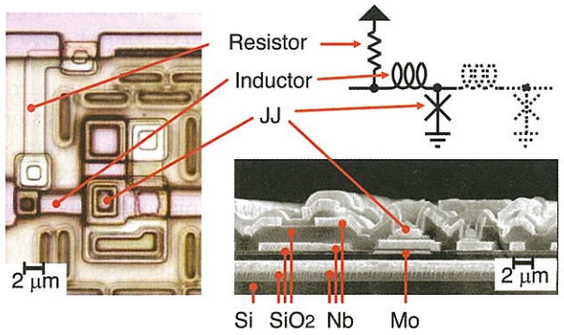

FIGURE 7.39: Top view, cross section, and circuit diagram of part of SFQ circuit fabricated by using ISTEC Nb four-layer process.

7.6.3 Planarized Multilayer Process

In order to fabricate faster and larger integration level SFQ circuits, ISTEC also developed a new fabrication process characterized by the planarized multilayer[79]. Increasing the number of Nb layers enables not only decreasing the circuit area but also increasing the design degree of freedom. However, it is difficult to further increase the number of Nb layers past four because the vertical steps are too large to create additional layers on it without producing defects. Therefore, a new planarization technology called the caldera method was developed[80].

Figure 7.40 shows the steps used in this method for fabricating a unit wiring level. (a): After a lower Nb wiring layer has been patterned, it is covered with a SiO_2 layer using bias sputtering. The thickness of this SiO_2 layer is adjusted depending on the thickness of the Nb wiring layer, i.e. 200-300 nm. (b): A photoresist layer is then formed in the reversed pattern of the Nb wiring layer. This reversed pattern is slightly broadened (300 nm in the figure) so that it overlaps the Nb wiring layer. (c): Selective RIE is used to remove the SiO_2 on the Nb wiring layer and stops the RIE on the Nb surface resulting from the overlap, leaving narrow, 1-μm-wide at most, convex SiO_2 regions shaped like caldera volcanoes along the edges of the Nb wiring layer. This remaining caldera-shaped SiO_2 is easily flattened using a conventional planarization method such as mechanical polishing planarization (MPP). (d): A very small amount of MPP is enough to obtain a smooth surface.

The planarized surface enabled us to add more Nb layers. The critical current density J_c of the JJ was increased to 10 kA/cm^2, which was four times larger than that of the previous process shown in Figure 7.38 and is expected to have twice the operation speed. The minimum JJ size was reduced to 1 μm×1 μm to maintain I_c value and the minimum line width also decreased to 1 μm.

Figure 7.41 shows a cross-sectional view of a device structure fabricated by using the multilayer process. The device has ten Nb layers. The role of the bottom Nb layer is as a DC bias current supply. The middle five layers are devoted to the X and Y direction PTLs, which have strip-line configurations. The SFQ gates were fabricated using the top four Nb, Mo resistor, and Nb/AlO_x/Nb JJ layers. This part is not planarized and is the same as that of the structure in Figure 7.38 to secure the design continuity. Vertically-stacked superconductive contact holes were also adopted into this process.

The multilayer process produced high-performance SFQ circuits; for example, an 8-bit shift regis-

[79] T. Satoh, K. Hinode, H. Akaike, S. Nagasawa, Y. Kitagawa and M. Hidaka, *IEEE Trans. Appl. Supercond.* 15 (2005) 78
[80] K. Hinode, S. Nagasawa, M. Sugita, T. Satoh, H. Akaike, Y. Kitagawa and M. Hidaka, *Physica* C 412-414 (2004) 1437

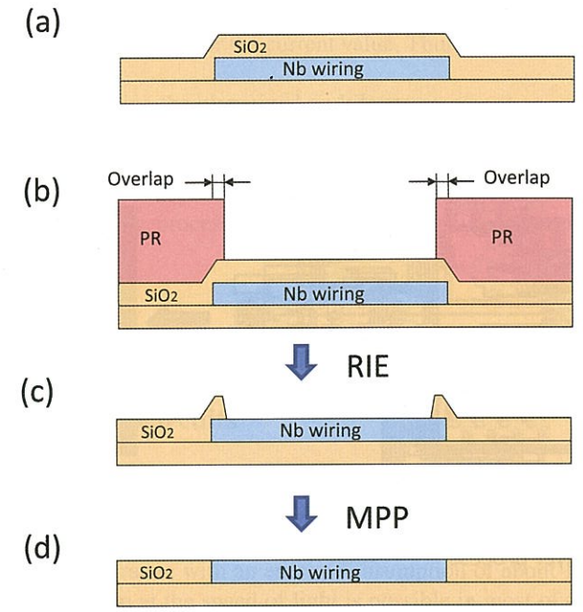

FIGURE 7.40: Steps in caldera method for fabricating unit wiring level.

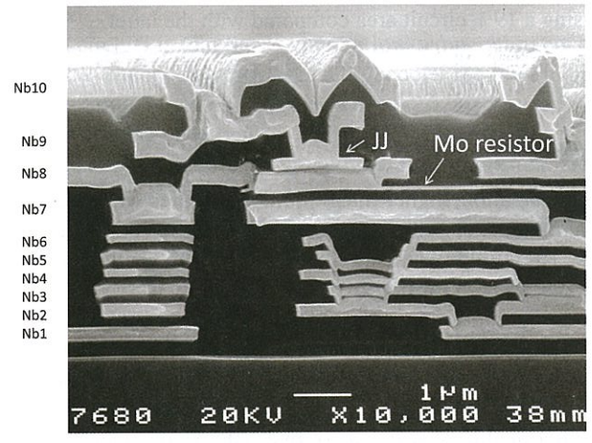

FIGURE 7.41: Cross-section SEM photograph of planarized ten Nb-layer device.

ter operated at up to 120 GHz [81] and a 16k-bit RAM consisting of 80,768 JJs at 3.8 mm×3.7 mm [82]. A 4×4 switch circuit fabricated by using the ten-layer process demonstrated a 112-GHz operation, which is more than twice that compared with the same circuit fabricated by using the four-layer

[81] H. Akaike, T. Yamada, A. Fujimaki, S. Nagasawa, K. Hinode, T. Satoh, Y. Kitagawa and M. Hidaka, *Supercond. Sci. Technol.* 19 (2006) S320
[82] S. Nagasawa, T. Satoh, K. Hinode, Y. Kitagawa and M. Hidaka, *IEEE Trans. Appl. Supercond.* 17 (2007) 177

process. Moreover, the circuit area of the ten-layer process could be reduced to 19% as shown in Figure 7.42[83].

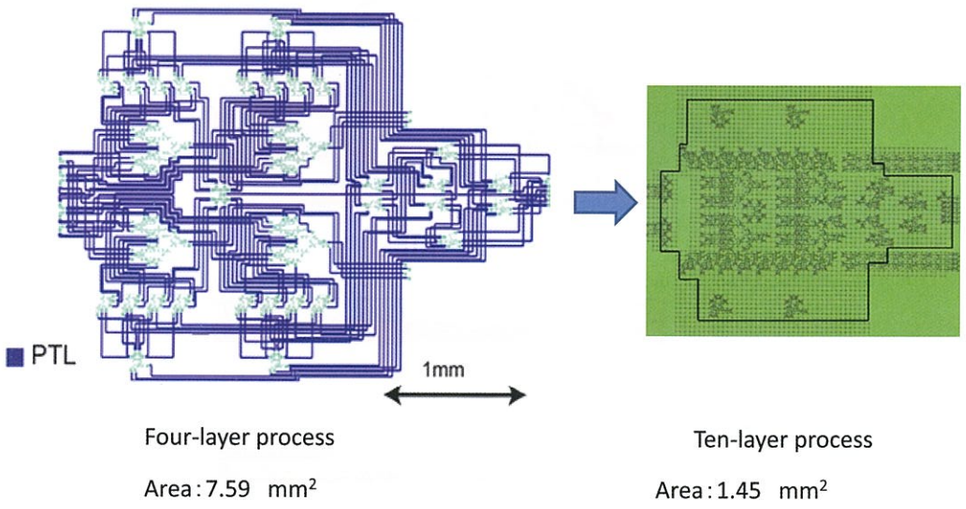

FIGURE 7.42: 4×4 switch circuit fabricated by using Nb ten-layer process and schematic circuit diagram of the same 4×4 switch based on four-layer processes. The former was operated at twice the clock frequency using a 19% circuit area compared with the latter.

7.6.4 Toward Further Progress

Faster, lower-power dissipation, higher-integration, and higher-yield are the main issues for consideration towards making further progress in the field of superconducting electronics devices as well as digital circuits. These improvements are necessary for superconducting devices to become widely used and there is still room for improvement.

In order to increase the operation speed by increasing the J_c, the thickness of the JJ tunnel barrier has to be decreased without degrading the JJ quality. Figure 7.37 shows that two different tendencies were observed in the J_c dependence on the *pt* product. This phenomena suggest that a micro-short in tunnel barrier may occur above 10 kA/cm^2 [84]. Therefore, the other tunnel barrier needs to be investigated to get a better quality JJ with a J_c of over 10 kA/cm^2 than the AlO_x barrier. The AlN_x barrier is a promising candidate that was demonstrated as an excellent quality JJ with a J_c of 33 kA/cm^2 [70]. The JJ area has to be reduced to become inversely proportional to the J_c increase.

A smaller JJ is also useful for drastically reducing the SFQ circuit power dissipation. Reducing the I_c is quite effective, since the dynamic and static power dissipations in SFQ circuits are proportional to $I_c\Phi_0$ and $I_c^2R_b$, respectively. Here, Φ_0 is an SFQ value (2.07×10^{-15} Wb) and R_b is a bias resistance. The minimum I_c in an SFQ circuit is decided by the tolerability against the thermal noise and the smallest makeable JJ area with a reasonable uniformity while maintaining the J_c value. The tolerability is not marginal for the current value. Thus, the I_c has the ability to be reduced by decreasing the JJ area.

The progress made when using the planarized multilayer process shows that the SFQ circuit can be improved by having a higher J_c and a larger number of Nb layers. The planarized surface shown in the multilayer process enables us to use advanced semiconductor fabrication technologies. The superconducting device fabrication process can be improved in collaboration with a deep understanding of the superconducting process and actively using advanced semiconductor fabrication technologies.

[83] M. Ito, I. Kataeva, R. Kasagi, M. Okada, T. Koketsu, M. Tanaka, S. Nagasawa, H. Akaike and A. Fujimaki, Demonstration of a 4x4 SFQ switch fabricated with a 10kA/cm2 Nb multi-layer process, Applied Superconductivity Conference (2010) 3EY-03

[84] Sergey K. Tolpygo and Denis Amparo, *J. Appl. Phys.* 104 (2008) 63904

7.7 High-Speed Digital Circuits

Akira Fujimaki

In this section, recent progress in single flux quantum (SFQ) circuits where an SFQ is employed as an information carrier is described. All the SFQ circuits have the special feature that the circuits can operate in a sub-terahertz range with an energy consumption of about 1 aJ/gate (10^{-18} J/gate). In addition, signal transmission at the speed of light is possible in most of the SFQ circuits. These features become increasingly important because society's digital infrastructure depends on semiconductor large-scale integration (LSI) devices. Increased heat density and increased interconnect delays make it more and more difficult to increase the performance of LSI circuits for operation at higher frequencies. SFQ circuits with their better performance are promising devices for use in future high-speed LSI devices.

One drawback of SFQ circuits is that they require a low-temperature environment. The cooling penalty of 1000–5000 W/W (the incident power of a cryocooler required to produce 1 W of cooling power at a 4 K operation temperature) has to be paid in systems based on SFQ circuits. One of the ways to overcome this cooling penalty is to design SFQ-circuit-based systems with high energy efficiency, which is defined as performance per unit power. This will be realized in upgraded network systems including baseband digital signal processors for wireless systems[85], high-end routers in backbone networks[86], and high-end computers[87,88], in which SFQ LSI circuits and their dense packaging are essential. A third important contribution to the total power of SFQ circuits is from current biasing. Section 7.7.4 describes efforts to minimize bias power, which may further improve the performance per unit power of SFQ LSI circuits.

[85] A. Herr, *IEICE Trans. Electron.* E91-C (2008) 293

[86] S. Yorozu, Y. Kameda, Y. Hashimoto, H. Terai, A. Fujimaki, and N. Yoshikawa, *IEEE Trans. Appl. Supercond.* 15 (2005) 411

[87] M. Dorojevets, P. Bunyk, and D. Zinoviev, *IEEE Trans. Appl. Supercond.* 11 (2001) 326

[88] M. Tanaka, T. Kondo, N. Nakajima, T. Kawamoto, Y. Yamanashi, Y. Kamiya, A. Akimoto, A. Fujimaki, H. Hayakawa, N. Yoshikawa, H. Terai, Y. Hashimoto, and S. Yorozu, *IEEE Trans. Appl. Supercond.* 15 (2005) 400

7.7.1 Principle of the Rapid Single Flux Quantum Circuit

The rapid single flux quantum (RSFQ) circuits proposed by Likharev, Mukhanov and Semenov[3,89] are the most notable circuits among a variety of SFQ circuits reported so far[90,91,92,93]. The coding of RSFQ circuits is defined by using clock signals. If an SFQ exists in a data path in the time interval between two adjacent clock signals, the SFQ can be interpreted as the logical "1". If there is no SFQ, it is the logical "0".

Figure 7.43 shows an equivalent circuit of a delay flip-flop (DFF), the basic element of an RSFQ circuit. The use of overdamped Josephson junctions, which have external shunt resistors, guarantees stable operation of the RSFQ circuits. In principle, the circuit is driven by a current source, and proper current distribution is achieved by bias resistor networks. The operation of the DFF begins with the arrival of an input signal at the "din" port. The data "flux quanta" is stored as a circulating current in the storage loop consisting of J_1, L, and J_2. Then the stored data is read out when a clock signal comes to the loop, and sent out at the "dout" port.

Storage loops employ the function of a latch or a memory. This function is essential for RSFQ logic gates with two inputs such as AND and XOR. Interconnects with unequal lengths are usually used to keep sufficient design flexibility, resulting in different arrival times of an SFQ at the two input ports. Thus, the input signal arriving first must wait for the other one in a storage loop.

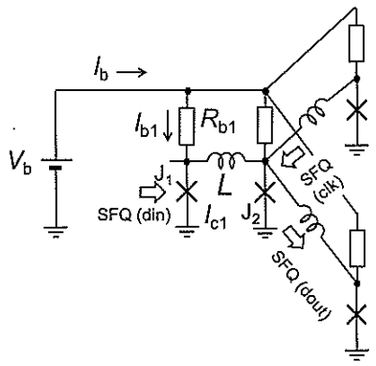

FIGURE 7.43: Equivalent circuit of a DFF cell. Bias currents are supplied to Josephson junctions through bias resistors.

The voltage impulse called an SFQ pulse is generated only when an SFQ crosses a Josephson junction. For a typical pulse width of a few picoseconds, an energy of about $I_c\Phi_0$ is consumed in the shunt resistor, that is connected in parallel to the junction, within I_c is the critical current of the junction and Φ_0 is the flux quantum. This feature enables high-speed signal processing with very low energy or power consumption.

Passive transmission lines (PTLs) with microstrip or strip line structures are used for long interconnects, where a voltage pulse can travel at the speed of light. For using a PTL, a transmitter is

[89] K.K. Likharev and V. K. Semenov, *IEEE Trans. Appl. Supercond.* 1 (1991) 3
[90] Y. Harada, E. Goto, and N. Miyamoto, *Technical Digest International Electron Devices Meeting* (1987) 389
[91] A. Silver and Q. Herr, *IEEE Trans. Appl. Supercond.* 11 (2001) 333
[92] Q. P. Herr and A. Y. Herr, 2008 *Applied Superconductivity Conference*, 3EY03, 2008
[93] O. A. Mukhanov, *IEEE Trans. Appl. Supercond.*, vol. 21, no. 3, Jun. 2011

placed between a logic gate and a PTL, and a receiver is placed between a PTL and a gate. Figure 7.44 shows operating margins in bias currents provided to a receiver for PTLs having different lengths. The PTLs under test had a microstrip line structure and were made on a single chip. Bias currents are normalized by the design value. Sufficiently wide margins exceeding ±20% are obtained for PTLs with a length shorter than 50 mm, and the margin even for a 100-mm-long PTL is still within an acceptable range. This feature means that large bandwidths can be achieved not only for on-chip (gate-to-gate) communication, but also for off-chip (chip-to-chip) communication.
In fact, 117 Gb, :C 10 kA/cm^2
Nb integrated-c

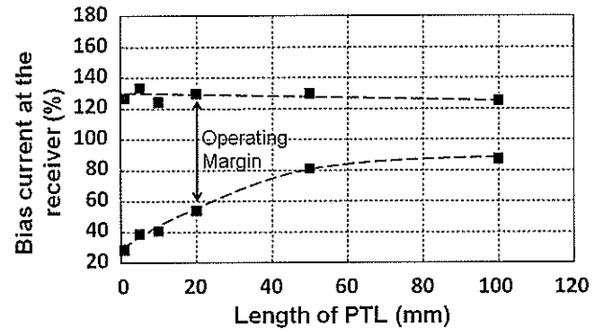

FIGURE 7.44: Length dependence of the operating margins in bias currents provided to a receiver.

7.7.2 LSI Design Technology

The sequence of arrival timing between a clock signal and a data signal has to be controlled in RSFQ circuits. In particular, timing control with pico-second order is essential for the operation under concurrent-flow clocking, which has an advantage over any other clocking method in speed of operation. Note that the delay time of a Josephson junction is sensitive to the bias current and that circuit parameters have a spread in actual chips. This makes the timing control difficult in large-scale circuits.

To overcome this situation, the introduction of computer aided design (CAD) including an analog simulator and an optimizer is necessary. The CONNECT top-down design is described here as a typical CAD for RSFQ circuits. The design is based on the CONNECT cell library[95]. Layouts of all the logic gates are designed in a square based on the 2.5-kA/cm^2 Nb/AlO_x/Nb LSI process called the standard process 2 (STP2)[96]. The unit length of the sides of the square is 40 μm. Input/output/clock ports are placed at designated spots inside the square. These layouts are called the logic cells. Josephson transmission lines (JTLs) and passive transmission lines (PTLs), which are used as interconnects, are also designed in a square because the standard process provides no layer dedicated to wiring.

Actual RSFQ circuits are designed by placing the logic cells and the wiring cells in the design

[94] Y. Hashimoto, S. Yorozu, T. Satoh, and T. Miyazaki, *Appl. Phys. Lett.* 87 (2005) 022502
[95] S. Yorozu, Y. Kameda, H. Terai, A. Fujimaki, T. Yamada, and S. Tahara, *Physica* C 378-381 (2002) 1471
[96] S. Nagasawa, S. Hashimoto, Y. Numata, and S. Tahara, *IEEE Trans. Appl.Supercond.* 5 (1995) 2447

area. Circuit parameters of the logic cells are optimized by using the circuit optimizer SCOPE[97] in order to exclude the interference between adjacent cells and to operate with a large margin even under parameter spread. The SCOPE optimizer can pick up the timing parameters such as setup time, hold time, delay, etc. The dependence of these parameters on the bias currents are examined and stored in the library. The timing design and verification of the RSFQ circuits are carried out in a digital domain using the stored timing parameters.

The initial CONNECT cell library was effective for circuits consisting of about 5000 Josephson junctions. However, increased bias currents in larger-scale integrated circuits induce relatively large magnetic fields themselves, and thus reduce operating margins. To suppress self fields, all the logic cells registered in the present CONNECT cell library have superconducting shields for the bias feed lines.

Recently, the 10 kA/cm^2 Nb/AlO$_x$/Nb LSI process called the advanced process 2 (ADP2) has been developed[98]. Increased critical current density enables operation at 50-100 GHz and a reduction of the width of PTLs. Moreover, the ADP2 provides 9 Nb layers. The bottom Nb layer is used for distributing bias currents, and the top 4 Nb layers are almost the same as that of the standard process. Two vertically stacked strip-line structures are formed by using the other 4 layers. The increased number of Nb layers leads to a remarkable reduction in the circuit area, because PTLs can be placed below Josephson junctions. So far, a 4×4-switch made with the ADP2 process has been demonstrated at 112 GHz using only 19% of the area of that made with the STP2[99].

Figure 7.45 (a) and (b) show a microphotograph of a DFF cell made with the STP2 and with the ADP2, respectively. In the cell with the ADP2, the unit length of the sides of the square is 30 μm. Pillars connected to the bottom layer are formed at each corner. Bias currents are provided to the circuits through these pillars. Moats are formed around the pillars.

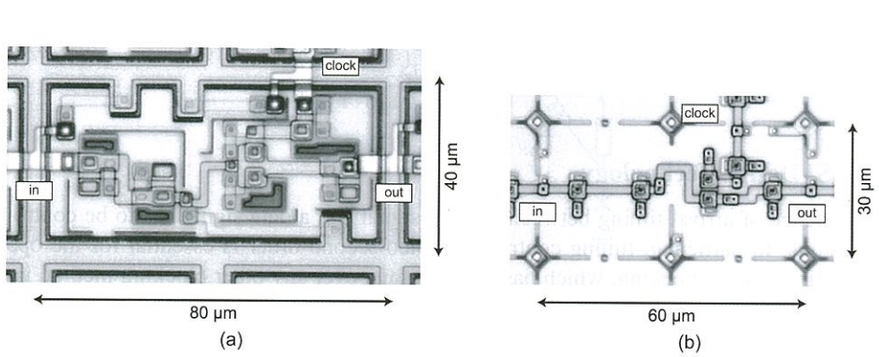

FIGURE 7.45: Microphotographs of basic cells (delay flip-flop, DFF) in the CONNECT cell library. (a) DFF cell made with the STP2. (b) DFF cell made with the ADP2.

Advanced CAD tools have been developed based on the ADP2. A new design flow and algorithms involving a PTL interconnect technique in a skewed clocking scheme were introduced. The clock frequencies of RSFQ circuits can be maximized by using these tools. The design flow is similar to that for a conventional semiconductor LSI design, and several dedicated steps are added to reinforce

[97] N. Mori, A. Akahori, T. Sato, N. Takeuchi, A. Fujimaki, and H. Hayakawa, *Physica* C 357 (2001) 1557

[98] S. Nagasawa, T. Satoh, K. Hinode, Y. Kitagawa, M. Hidaka, H. Akaike, A. Fujimaki, K. Takagi, N. Takagi, N. Yoshikawa, *Physica* C 469 (2009) 1578

[99] M. Ito, M. Tanaka, I. Kataeva, M. Okada, H. Akaike, S. Nagasawa, M.Hidaka, and A. Fujimak, 2010 Applied Superconductivity Conference, 3EY-03, 2010

it for an efficient design of RSFQ LSI circuits.

Figure 7.46 shows a design of an 8-bit carry look-ahead adder along with the new design flow[100]. In the first step, the "logic synthesis", DFFs are inserted to equalize the number of clocked gates on every data path because every RSFQ logic gate has also a latch functionality. The set of logic gates are partitioned into logic levels, where the level of the gate is defined as the number of gates on the path from the circuit input to that gate. Then, the timing of clock signals for each gate is scheduled, and the clock tree is synthesized by inserting some delay elements (JTLs) on the paths, which are required to adjust the timing[101,102]. The gate arrangement in each logic level is optimized to minimize the number of delay elements, and placement of the logic gates is roughly obtained. Figure 7.46(a) shows the schematic after the clock tree synthesis and the first rough placement.

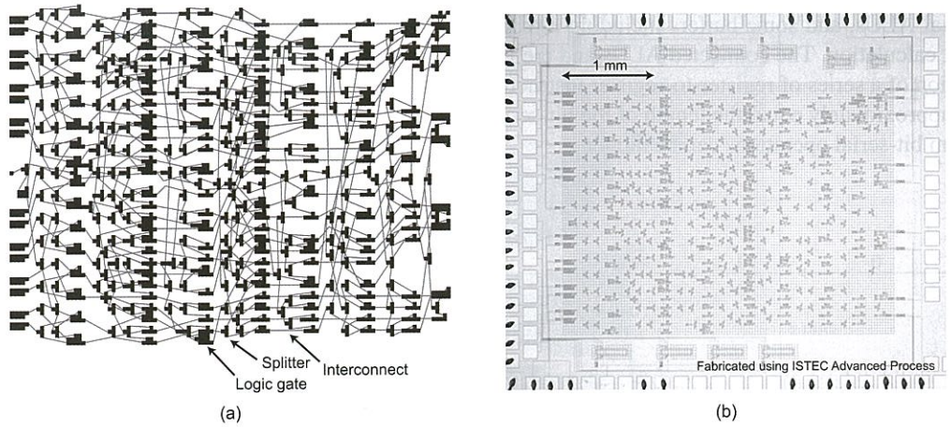

FIGURE 7.46: Design of a carry look-ahead adder with the advanced CAD tools. (a) Schematic diagram after placement of logic gates, and (b) microphotograph. Black squares and lines in the schematic represent logic gates and interconnects, respectively. PTLs are invisible in microphotograph due to planarization process. Layout size is 3.84 mm × 2.70 mm.

Using the feedback from the verification, the next steps, "place and route", are done not independently but simultaneously in order to satisfy timing requirements. After a first rough placement of logic gates and a rough routing of PTLs, a timing analysis is performed to find a critical timing path, and the detailed route of the path is determined. Repeating the analysis of timings and congestion degrees, PTLs are carefully routed one by one[103].

Figure 7.46(b) shows a microphotograph of the 8-bit adder fabricated using the ADP2. The target frequency is 50 GHz. The number of PTLs and Josephson junctions are 598 and 7,092, respectively. An actual circuit operated with a sufficient bias margin of ±20%. The routing of PTLs, which is one of the most time-consuming tasks in manual design, was done in 10 seconds.

[100] K. Takagi, N. Takagi, M. Tanaka, K. Obata, and Y. Ito, First Superconducting SFQ VLSI Workshop, A2-3, 2008

[101] K. Obata, K. Takagi, and N. Takagi, *IEICE Trans. Fundamentals* E91-A (2008) 3772

[102] K. Takagi, Y. Ito, S. Takeshima, M. Tanaka, and N. Takagi, submitted to *IEICE Trans. Electron.*

[103] S. Takeshima, K. Takagi, M. Tanaka, and N. Takagi, Second Superconducting SFQ VLSI Workshop, P5, 2009

7.7.3 Demonstration of RSFQ LSIs

So far, several RSFQ LSI circuits consisting of more than 10,000 Josephson junctions have been demonstrated. In this section, an RSFQ microprocessor based on the STP2 and an accelerator based on the ADP2 are shown as examples of RSFQ LSI circuits.

Figure 7.47 shows the microarchitecture of the RSFQ microprocessor named CORE1β. The CORE1β employed the instruction-set based on the DLX[104], a typical reduced instruction-set computer (RISC) architecture. For simplicity, the number of instructions is reduced to a minimum and only bit-serial data are handled. The lengths of data and instructions are 8 and 16 bits, respectively. The CORE1β targets almost the same performance as the semiconductor conventional one at the peak. To achieve the target, two techniques are employed. One is the introduction of a "forwarding architecture"[105], in which multiple arithmetic logic units (ALUs) are connected in cascade. As shown in Figure 7.47, the data path of the CORE1β is composed of a general register file, two bit-serial ALUs, and some buffers including a forwarding buffer (FB). The FB holds the value of the last calculation. The connected ALUs and the FB enable two calculations continuously by the execution of a series of register-to-register instructions. The latency of the cascaded ALUs is designed to approximately equal the length of the bit-serial data. As a result, the enlarged latency originating from bit-serial operations can be hidden.

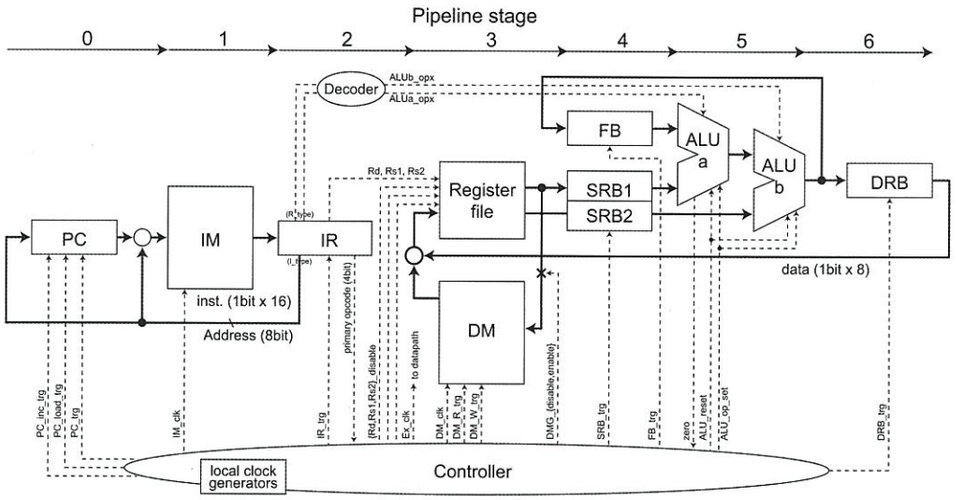

FIGURE 7.47: Microarchitecture of the CORE1β. The CORE1β is composed of a decoder, a program counter (PC), an instruction memory (IM), an instruction register (IR), a register file, two ALUs, two source register buffers (SRB1, SRB2), a destination register buffer (DRB), a forwarding buffer (FB), and a controller. The pipeline stages are shown at the top of the figure.

The other technique to obtain high performance is "pipelining". The CORE1β is made up of

[104] J. L. Hennessy and D. A. Petterson, *Computer Architecture, A Quantitative Approach*, 2nd ed. (San Francisco, CA: Morgan Kaufmann)

[105] M. Tanaka, T. Kondo, T. Kawamoto, Y. Kamiya, K. Fujiwara, Y. Yamanashi, A. Akimoto, A. Fujimaki, N. Yoshikawa, H. Terai, and S. Yorozu, *Physica* C 426 (2005) 1693

seven pipeline stages as indicated at the top of Figure 7.47. The master clock controls the pipeline execution and the local clocks. The master clock, corresponding to the so-called "clock" in a conventional semiconductor LSI, is generated in an independent clock generator with a frequency of 1–2 GHz. The local clocks with frequencies of 20–25 GHz are used for bit-serial processing. The details of the microarchitecture of the CORE1β are described in Ref. 106.

Figure 7.48 shows a microphotograph of the CORE1β. A large die with an area of 8 mm × 8 mm is used to reduce external magnetic fields generated by bonding wires or off-chip bias-feeding lines, while a typical die size is 5 mm × 5 mm. The CORE1β is composed of five main circuit blocks and consists of 10,995 Josephson junctions. Bias currents are individually supplied to each circuit block. The total bias current is 1,373 mA. The power consumption is estimated to be 3.4 mW.

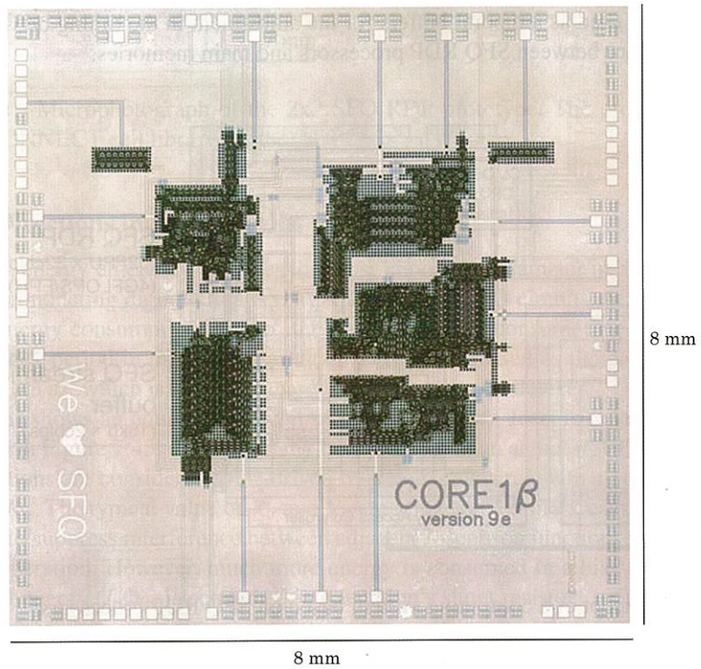

FIGURE 7.48: Microphotographs of the CORE1β. The CORE1β was designed based on the CONNECT cell library for the STP2.

The instruction memory (IM) and the data memory (DM) are made up of 16-bit and 8-bit shift registers, respectively. The designed local clock frequency is 25 GHz for the instruction fetch and 20 GHz for the bit-serial data operation. The master clock frequency is raised up to 1.4 GHz after careful timing adjustments between components. The peak performance is calculated to be 1,400 MOPS (million operations per second) because instructions are issued every two master clocks, and two operations are executed for one instruction in the cascaded ALUs.

The operation of the CORE1β was examined in liquid helium using an on-chip high-speed test method. The test sequence included multiple ADD operations. The correct operation was obtained

[106] M. Tanaka, T. Kawamoto, Y. Yamanashi, Y. Kamiya, A. Akimoto, K. Fujiwara, A. Fujimaki, N. Yoshikawa, H. Terai, and S. Yorozu, *Supercond. Sci. Technol.* 19 (2006) S344

up to 37 GHz for the instruction fetch and 18 GHz for the data operation.

Another example of RSFQ LSI circuits is a reconfigurable data path (RDP) processor, which is a compact, high-performance computation engine. The architecture of the RDP processor gives a solution to the memory-wall problem. The memory-wall problem is the problem that the memory bandwidth cannot be wide enough relative to the processor performance because of the difference between the operating speed of a processor and that of the memory limits the performance of a computer.

Figure 7.49 shows a concept of a computing system based on SFQ-RDP processors. The SFQ-RDP processors are used as accelerators, while the central processing units (CPUs), based on complementary metal-oxide-semiconductor (CMOS) devices, serve as main processors. An RDP is mainly composed of a 2-dimensional array of floating point processing units (FPUs). The output of each FPU can be fed to one or more FPUs via flexible operand routing networks (ORNs). Streaming buffers are used as temporal buffers for the adjustment in the timing between SFQ RDP processors and CPUs or between SFQ RDP processors and main memories.

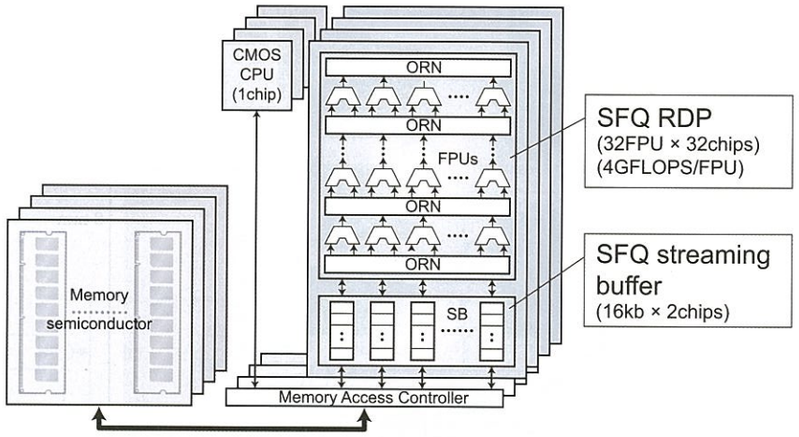

FIGURE 7.49: Concept of a computing system based on SFQ RDP processors.

In an RDP, a data flow graph (DFG) extracted from a target application program is mapped to a 2-dimensional FPU array. To enable the mapping, an ORN consists of programmable switches, while FPUs support multiple functions such as add, sub, and multiply. By means of setting the control signals provided to FPUs and ORN switches, the function of the RDP can be changed at run time.

Since the cascaded FPUs can generate a final result without temporally memorizing intermediate data, the number of memory load/store operations corresponding to spill codes is reduced. In other words, memory bandwidth required to achieve high performance can be reduced. Moreover, since a loop-body mapped into the FPU array is executed in pipeline fashion, RDP can provide high throughput computing.

A microphotograph of a prototype of a 2×2 (double stages of an array composed of dual ALUs) RDP processor is displayed in Figure 7.50. For simplicity, ALUs are employed instead of FPUs in this design. In addition, the ALUs and ORNs are designed to handle only bit-serial data. The RDP processor prototype was made up of 11,458 Josephson junctions and occupied an area of 5.61×2.82 mm^2.

All the instructions for each ALU and reconfiguration of the 2×2 RDP processor prototype were confirmed up to a frequency of 45 GHz. The power consumption is 3.4 mW.

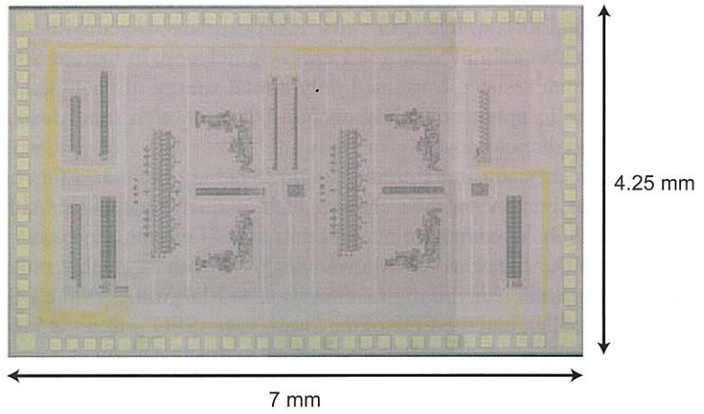

FIGURE 7.50: Microphotograph of the 2x2 SFQ RDP prototype. The prototype was designed based on the CONNECT cell library for the ADP2.

7.7.4 New Directions in SFQ Circuits

In these days, energy efficiency becomes the most important parameter in digital systems. Originally, the superconducting digital circuits, in particular the RSFQ circuits, have the special feature of low power/energy consumption. In fact, the intrinsic energy consumption of a Josephson junction within a clock period in the RSFQ circuit is roughly expressed as the product of $I_c\Phi_0$, and is estimated to be 0.3 aJ, which is small compared to semiconductor devices.

Figure 7.51(a) shows an equivalent circuit of a current-driven Josephson junction in RSFQ circuits. As shown in Figure 7.43, there are many bias resistors in an actual RSFQ circuits. As a result, Josephson junctions are considered to be driven by a voltage source with a voltage V_b through the bias resistance R_b. The typical value of R_b and V_b are 16 Ω and 2.5 mV, respectively. These values are determined to suppress interference between adjacent Josephson junctions through bias resistors in high-speed operation. However, much more energy is consumed in a bias resistor, while only a small amount of energy ($I_c\Phi_0$) is consumed in a junction's shunt resistor.

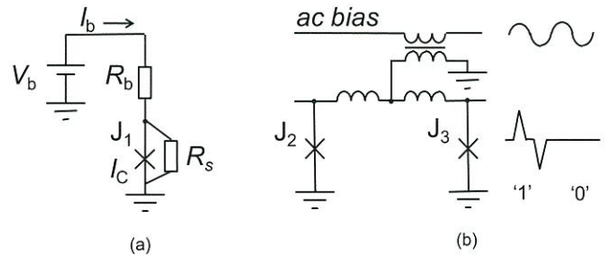

FIGURE 7.51: (a) Equivalent circuit of a current-driven Josephson junction in an actual RSFQ circuit. (b) Equivalent circuit of an RQL. No bias resistor is used.

An effective way to eliminate the energy consumption in a bias resistor is the employment of ac-biasing. The reciprocal quantum logic (RQL) is a typical model for ac-biasing[92]. An excellent summary including dc-biased energy-efficient circuits is given in Mukhanov[93].

Recently, it was found that low-V_b RSFQ circuits, RSFQ circuits driven with very low voltages such as a few tens of μV, also exhibit very good energy efficiency. In fact, at 20 GHz operation the bias resistor and the shunt resistor consumed only a total energy of about 0.1 aJ. This energy consumption is close to the Josephson coupling energy $I_c\Phi_0$, although small Josephson junctions with small critical currents were employed.

Figure 7.52 shows the energy consumption in a single switching event as a function of the clock period for different devices comprising LSI circuits such as microprocessors. Although the low-V_b RSFQ circuit described above cannot be classified as an LSI circuit, the corresponding energy consumption is marked in the figure as "low-power SFQ". The energy-delay product (EDP) is a good measure for the energy efficiency in digital circuits. The EDP values of the RSFQ circuits are 3-4 orders of magnitude smaller, and the EDP of the "low-power SFQ" circuit is 5–6 orders smaller than that of CMOS devices. This small EDP is a remarkable advantage over semiconductor devices even if the cooling penalty is taken into account.

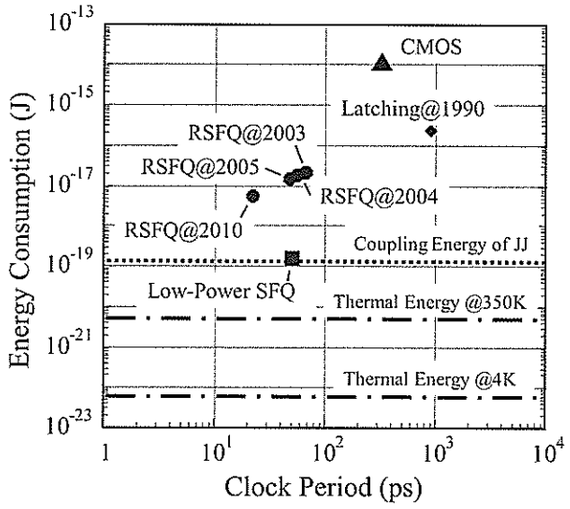

FIGURE 7.52: Energy consumption in a single switching event as a function of clock period for different devices comprising LSI circuits.

7.8 History of Superconductor Analog-to-Digital Converters

Oleg Mukhanov

An analog-to-digital converter (ADC) is a mixed-signal electronic circuit that converts an electrical signal from the analog domain to the digital domain, typically providing N binary bits at the sampling frequency f_s. The higher speed of superconducting circuits comparable to conventional circuits provided an initial interest in superconductor technology for ADC applications. One can find technical details of superconductor ADCs in earlier reviews[107,108]. In contrast here, we focus on a historical perspective of the ADC development identifying important trends and milestones as well as acknowledging main actors.

Similar to superconductor digital electronics, early superconductor mixed-signal circuits were based on cryotrons, pre-Josephson switching elements. A patent for the first superconductor analog-to-digital converter (ADC) was filed in 1960 [109], just in a few years after the initial cryotron-based digital circuit implementation. The projected speeds of the order of microseconds per ADC switching operation was rather attractive goal at that time. Several years later, the cryotrons were replaced by faster Josephson junctions in superconductor circuits including ADCs. The early Josephson-junction based ADC was a simple thermometer-code "totalizer" circuit patented in 1969 and presented an A-to-D conversion idea rather than a complete ADC circuit[110].

The first superconductor ADC circuit of a practical significance was a successive-approximation ADC invented in 1974 by M. Klein of IBM[111]. It consisted of a sample-and-hold circuit and four comparators made of serially connected Josephson junctions being switched to a voltage state at a predetermined control signal levels. This design was fabricated and tested in 1977 to show a 25 MHz bandwidth. In general, this ADC design was following semiconductor implementations using Josephson junctions. All early ADCs were focused on exploiting only the high switching speed of superconducting devices starting from cryotrons and then Josephson junctions. As in digital circuits, these first ADCs were viewed as a faster version of their semiconductor counterparts.

The realization that superconductivity offers much more than the higher speed led to innovations in ADC circuits. These new truly superconductive ADCs were exploiting fundamental features of superconductivity unavailable in other technologies: magnetic flux quantization, extremely high sensitivity, quantum accuracy, and low noise. For instance, the magnetic flux quantization provides a natural ruler which may be used to provide a large number of quantum-mechanically accurate thresholds for the ADCs.

Newer superconductor ADCs generally fall into two categories: *Nyquist-sampling parallel* ADCs and *oversampling* ADCs. An ideal Nyquist ADC samples a signal at a sampling rate $f_s = 2f_N$, where f_N is Nyquist frequency. The Nyquist ADCs are usually composed of a large number of *separate* quantizers arranged in parallel—each defining a single quantization level. The performance of such an ADC is limited by the precision of the quantization levels. These parallel-type ADCs are best for digitizing *high bandwidth* signals when a *moderate resolution* up to 8 bits is adequate.

In the oversampling ADCs, the signal is sampled at a frequency $f_s \gg 2f_N$ using a single quantizer. Then, feedback techniques and digital filtering are used to reduce or shape (move out of band) the quantization noise and enhance the effective dynamic range. Oversampling ADCs are built using a "delta" or more often a "delta-sigma" modulator (sometimes called "sigma-delta"). In semiconductor technology, more robust sigma-delta ADCs are overwhelmingly preferred to delta ADCs. In superconductor technology, the availability of a close-to-ideal integrator in the feedback loop makes delta ADCs practical. The oversampling-type ADCs are best for digitizing relatively *lower bandwidth* signals but with the *maximum possible resolution*.

[107] e.g., G. S. Lee and D. A. Petersen, *Proc. IEEE* 77 (1989) 1264

[108] e.g., O. Mukhanov, et al., *Proc. IEEE* 92 (2004) 1564

[109] H. T. Mann, D. G. Fladlien, Superconductive analog-to-digital converter, U.S. Patent 3 196 427, July 20, 1965 (Filed Nov. 14, 1960)

[110] M. D. Fiske, Superconductive totalizer or analog-to-digital converter, U.S. Patent 3 458 735, July 29, 1969 (Filed Jan. 24, 1966)

[111] M. Klein, Successive-approximation analog-to-digital converter using Josephson devices, U.S. Patent 3 949 395, Apr. 6, 1976 (Filed Aug. 28, 1974); M. Klein, ISSCC77, *Digest of Tech. Papers* (1977) 202)

7.8.1 Superconductor Parallel-Type ADCs

Early Superconductor Parallel ADCs

Historically, the very first true superconductor ADC was of the Nyquist type, more specifically a parallel-type Flash ADC. In 1975, H. Zappe of IBM pioneered the idea that periodic nature of superconducting quantum interference devices (SQUIDs) allows the formation of an n-bit flash ADC with only n comparators, rather than the $2n-1$ single-threshold comparators usually required in the conventional semiconductor flash ADCs[112]. It provides a unique solution for drastic reduction of a circuit complexity and, at the same time, allows faster sampling.

This ADC design signifies the first use of a superconductor's natural magnetic flux quantization. It also exploited the extreme field sensitivity of quantum interference devices, so that a very small analog signal could be converted. This was a truly pioneering invention. This first ADC design relied on the use of SQUID comparators with different inductance values and therefore was difficult for a practical ADC implementation. These difficulties were resolved by 1979, when R. Harris, C. Hamilton and F. Lloyd of NBS (now NIST) demonstrated a 200 MS/s 4-bit Flash ADC circuit using a Pb-alloy fabrication process[113]. They improved Zappe's design by using optimally designed identical SQUID comparators with variable the coupling of signal (Figure 7.53).

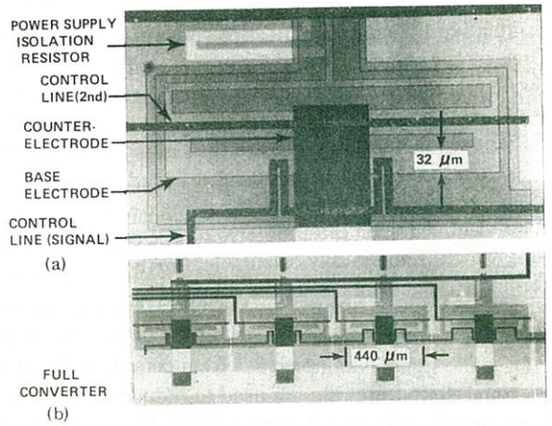

FIGURE 7.53: In 1979 the world's first implementation of superconducting flash ADC at NBS/NIST[113]: (a) microphotograph of one of 4 SQUID Flash ADC comparators. (b) microphotograph of a complete 4-bit ADC. (Reprinted with permission from 113. Copyright 1979, American Institute of Physics.)

This work inspired a significant activity aimed to improve the ADC accuracy-bandwidth performance. Hamilton and Lloyd proceeded to demonstrate a 6-bit ADC at 4 GS/s [114]. By 1988, S. Ohara, T. Imamura, and S. Hasuo of Fujitsu extended sampling rate to 5 GHz by implementing the ADC using a 3-μm Nb/AlOx/Nb process[115]. A great deal of the development took place at the University of California, Berkeley (UC Berkeley), NBS/NIST, and TRW, which aimed to develop a better SQUID comparator[107].

[112] H. H. Zappe, *IBM Tech. Discl. Bull.* 17 (1975) 3053
[113] R. E. Harris, C. A. Hamilton, F. L. Lloyd, *Appl. Phys. Lett.* 35 (1979) 720
[114] C. A. Hamilton and F. L. Lloyd, *IEEE Trans. Magn.* MAG-17 (1981) 3414
[115] S. Ohara, T. Imamura, and S. Hasuo, *Electron. Lett.* 24 (1988) 850

Quasi-One Junction SQUID (QOS) Comparator for Flash ADC

The most significant and influential flash ADC improvement was the 1988 invention of the Quasi-One junction SQUID (QOS) comparator by Ḣ. Ko and T. Van Duzer at UC Berkeley[116]. This new comparator had a greater than 5× improvement over the previous designs in analog bandwidth and sampling rate. The main design goal was to eliminate the hysteresis and dynamic distortions caused by the vortex-to-vortex transition in the two- and three-junction SQUID comparators. This was achieved by a low-inductance, one-junction SQUID. For signal sampling, an additional junction was inserted in the one-junction SQUID loop (Figure 7.54a). This QOS comparator set the design trend for many years. Even today, the QOS remains the basis for the latest ADC comparator designs.

In following years, the QOS-based flash ADCs were extensively developed for instrumentation applications, such as wideband transient digitizers. P. Bradley of HYPRES (originally from UC Berkeley) demonstrated a 6-bit Flash ADC with about 4 effective bits at 5 GHz and 3 effective bits at 10 GHz using a beat frequency test method[117]. The flash ADC consisted of a linear array of six active comparators with analog signal applied via an $R-2R$ ladder and producing a Gray-coded digital output. In 1993, this Flash ADC was cryopackaged within an APD Gifford-McMahon (G-M) cryocooler and successfully operated as a rack-mounted demo unit at HYPRES (Figure 7.54b,c). In fact, this was the first superconducting ADC (or any digital or mixed-signal LTS integrated circuit) operating on a 4 K closed-cycle refrigerator.

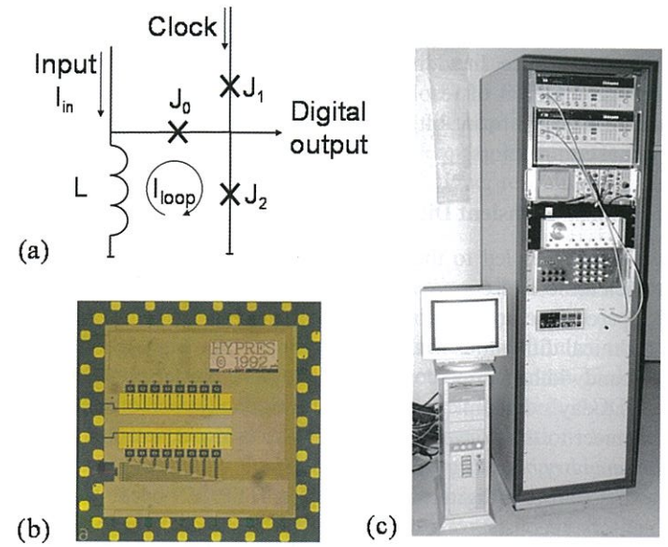

FIGURE 7.54: (a) Schematic of Quasi-Onejunction SQUID (QOS) comparator (1988)[116] (©1988 IEEE). (b) HYPRES 1992 4 GHz Flash ADC chip based on QOS comparators and fabricated using the 1993 standard HYPRES 3-μm process. (c) The demonstration setup of a cryocooled 4 GHz Flash ADC using a 3-stage APD HS-4 cryocooler with a 1 W capacity at 4.2 K. The cryocooler cold head occupied the bottom compartment while test equipment occupied the top compartment of the standard rack.

[116] H. Ko and T. Van Duzer, *IEEE J. Solid-State Cir.* 23 (1988) 1017
[117] P. Bradley, *IEEE Trans. Appl. Supercond.* 3 (1993) 2550

SFQ Flash ADC

The demonstrated flash ADC design was quite successful, although it suffered from so-called "duty cycle" problem when thresholds for the rising and falling edges appeared to be shifted for high slew rate signals. At that time, a paradigm shift from the latching type to non-latching single flux quantum (SFQ) logic influenced the designs of flash ADCs. Consequently, two new SFQ ADC comparators were proposed. One of these designs was based on Quantum Flux Parametron (QFP), which provided high accuracy although it was too complex. The alternative SFQ comparator design was introduced by S. Rylov of HYPRES in 1997 [118]. This SFQ comparator followed the general QOS basic design but was implemented using RSFQ design principles with shunted Josephson junctions and was integrated with a SQUID wheel (a phase tree). The duty cycle problem was compensated to a substantial degree by the insertion of a simple negative feedback resistor. This design became the comparator of choice for HYPRES transient digitizer.

Getting more Bits: Error-Correction and Interleaving

Like all parallel ADCs, the superconductor flash ADC is susceptible to fabrication mismatches in circuit components and conditions. This flaw can be corrected with a real-time digital error correction technique, called the look-back algorithm. This technique was developed by C. Anderson of IBM in the 1980s and then finally published in 1993 [119]. In this scheme, two comparators, offset from each other by a dc $\Phi_0/4$ flux bias, are used for each bit. This ensures that at most one comparator can be close to threshold for any input signal value. The look-back error-correction logic also converts the original Gray code output to standard binary. Furthermore, one can synthesize additional bits of lower significance. In addition to the error-correction, the bit-interleaving technique can be used to add one more bit of resolution without increasing the slew rate of a comparator. It adds an additional least significant bit (LSB) by XOR-ing outputs of 90-degree phase shifted (interleaved) additional comparators.

Flash ADC Applications: Transient Digitizer

Finally, all these techniques led to the development of a transient digitizer. There are several important areas of scientific and commercial instrumentation in which the precision, speed, and dynamic range of superconductor ADCs are of a great interest.

One of the key technical difficulties in the development of the high-speed flash ADC digitizers is the output interface bandwidth. A superconductor flash ADC produces digital output data at tens of Gbit/s which exceeds today's data link per line capabilities and speed of semiconductor electronics. The only way to connect to the conventional world is to slow down the data using two possible approaches: *on-chip memory buffering and demultiplexing*.

Figure 7.55 shows a transient digitizer developed at HYPRES by S. Kaplan et al. in 1998 [120] using an on-chip memory. It consists of a superconductor flash ADC, combined with fast RSFQ shift register memory circuits to store the digitized data for subsequent readout at much slower data rate. A prototype instrument, comprising a superconductor integrated circuit (Figure 7.55b) along with a room temperature interface and data acquisition electronics, was demonstrated for single-shot pulse capture. Each digitizer chip contained a 6-bit flash ADC coupled to a bank of 32-stage shift registers through a set of acquisition control switches. Despite the superior ADC performance compared to the semiconductor counterparts, the low capacity of the digitizer memory was the limiting factor for commercialization. As in the case of digital processors, the lack on a large capacity memory prevented the insertion of superconductor digitizers into a marketplace.

[118] P. Bradley and S. Rylov, *IEEE Trans. Appl. Supercond.* 7 (1997) 2677
[119] C. J. Anderson, *IEEE Trans. Appl. Supercond.* 3 (1993) 2769
[120] S. Kaplan, et al., *IEEE Trans. Appl. Supercond.* 9 (1999) 3020

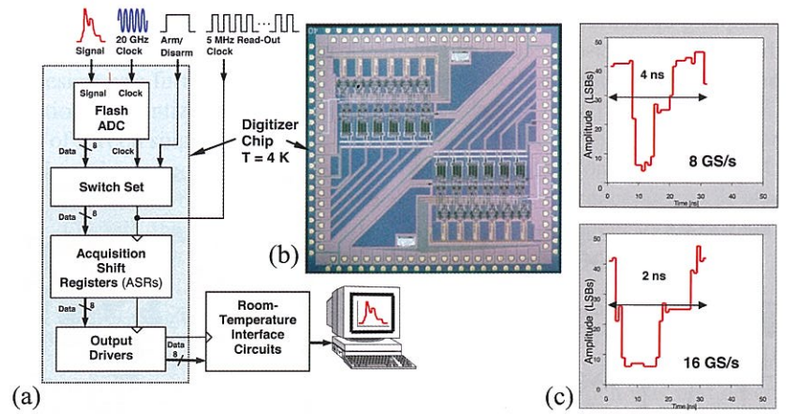

FIGURE 7.55: A 1998 HYPRES superconductor transient digitizer: (a) Block diagram. (b) A superconductor chip with two transient digitizers based on a 6-bit flash ADC and a 32-bit-deep memory. (c) A fast pulse capture: 4 ns for 8 GS/s (top) and 2 ns for 16 GS/s (bottom) (©2004 IEEE).

An alternative transient digitizer design proposed by M. Maezawa, et al. in AIST, Japan in 2001 was based on the use of demultiplexers[121]. The digitizer consisted of a 2-bit 16 GS/s flash ADC similar to the one described above. It was followed by a 1:16 RSFQ demultiplexer and output drivers. This demultiplexer-based architecture can avoid the superconductor memory bottleneck. However, the number of output lines are larger by the demultiplexing ratio (e.g., by 16), which presents a cryopackaging and cost challenge for faster and higher resolution ADCs.

Recent Flash ADCs: Complimentary QOS Comparator

Relatively fast development of parallel-type superconducting ADCs in the 1980s–1990s was considerably slowed after 2000 by the lack of dedicated government-sponsored development programs, requirements for the superfast transient measurements, and competition from conventional instruments. Similarly in the commercial marketplace, product development goals were shifted from instrumentation to wireless communications which required a different ADC type: oversampling ADCs. Fortunately, recent attention to ultra-fast optical communications has been renewed after several years of low interest caused by the "dark fiber" overcapacity problem. This has opened an attractive opportunity for flash ADCs in the optical communication systems and their measuring instruments. Sampling speeds exceeding 100 GS/s became a target for the flash ADCs. In 2008, H. Suzuki et al. from the SRL ISTEC, Japan, invented a new flash ADC comparator capable of operating with the required speed if fabricated with a 40 kA/cm2 critical current density process. The new comparator is the latest development of the famous QOS comparator, Complementary QOS (CQOS). It finally solved the long-standing "duty cycle" problem plaguing previous QOS designs. The new design is based on a differential pair of the identical SFQ QOSs connected at the decision-making part. The signal is applied to both QOSs complimentarily (Figure 7.56a) and cancels the asymmetrical distortions[122]. In 2010, a 4-bit CQOS comparator test circuit showed the 3-bit binary and 4-bit Gray-code operation at 15 GS/s in beat frequency tests. For low frequency input, correct

[121] M. Maezawa, et al., Analog-to-digital converter based on RSFQ technology for radio astronomy applications, in *Extended Abstracts of ISEC'01*, Osaka, Japan, (2001) 451
[122] M. Maruyama, et al., *IEEE Trans. Appl. Supercond.* 19 (2009) 680

high-speed sampling operation up to 50 GS/s at 10 kA/cm^2 were observed. A complete 5-bit flash ADC with the look-back error-correction and bit-interleaving circuits (Figure 7.56b) was assembled for testing on a 1 W G-M cryocooler[123].

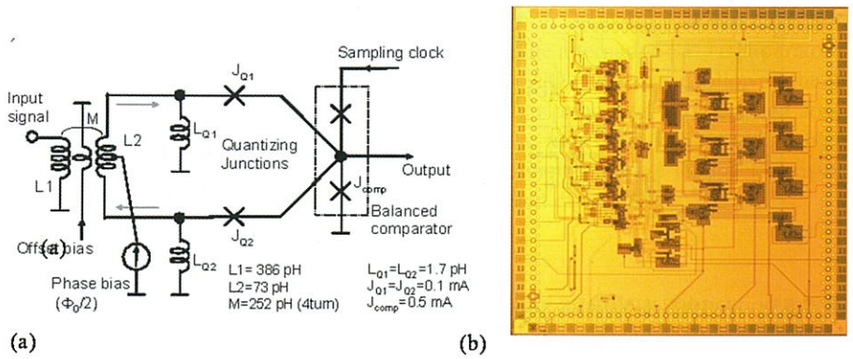

FIGURE 7.56: A 2008 Complimentary QOS comparator Flash ADC (ISTEC, Japan): (a) CQOS schematic. (b) Flash ADC chip (2010) with integrated error-correction and interleaving circuits[123] (©2009 IEEE, courtesy of H. Suzuki).

7.8.2 Superconductor Oversampling ADCs

The availability of fundamental flux quantization in superconductivity inspired several different oversampling delta and delta-sigma ADC designs. These are counting delta and sigma-delta type ADCs, a phase modulation-demodulation (PMD) delta ADC, and conventional delta and sigma-delta ADCs. While having quite different design approaches, most of them take advantage of the unique availability of *implicit feedback* and signal integration inherent to a SQUID loop, which is a result of fundamental conservation of flux in a superconducting loop. The SQUID loop automatically accumulates the total flux with opposite sign (sum of antifluxons) of all SFQ pulses (fluxons) emitted by the Josephson junction.

Counting V/F ADC

The first idea of superconductor oversampling ADC was suggested by McDonald of NBS/NIST at the 1976 Navy Summer Study on Superconductive Electronics. He proposed to use the ac Josephson effect to perform direct voltage-to-frequency (V/F) conversion. A single Josephson junction (Figure 7.57a) can act as a voltage-controlled oscillator (VCO) and produce an SFQ pulse train at a rate proportional to the applied analog voltage as $f = 2eV/h = V/\Phi_0$. The generated SFQ pulses representing threshold crossings are to be counted over a time interval. This critical ability to count low-power SFQ pulses was provided in 1978 when J. Hurrell and A. Silver invented a binary counter based on a two-junction SQUID with overdamped Josephson junctions[124,125]. The speed and simplicity of the counter circuit was a profound manifestation of the potential of superconductor circuits

[123] H. Suzuki, et al., *IEEE Trans. Appl. Supercond.*, vol. 21, no.3, Jun. 2011
[124] J. P. Hurrell and A. H. Silver, *AIP Conf. Proc.* 44 (1978) 437
[125] J. P. Hurrell, D. C. Pridmore-Brown, A. H. Silver, *IEEE Trans. Electron.* Dev. 27 (1980) 1887

utilizing SFQ switching. Amazing switching speed of 100 GHz was experimentally demonstrated by C. Hamilton and F. Lloyd of NBS/NIST in 1982 [126].

This basic design was further developed and improved to increase its performance. In order to increase resolution of quantization process, a multi-junction VCO was proposed at TRW. It is based on interleaving of several single-junction VCOs while maintaining a fixed phase shift of one junction to another[127]. In order to increase the sensitivity of the V/F ADC, one can use a SQUID with a sensitive input transformer biased into the voltage state as a pulse generator as it was proposed at HYPRES[128]. Overall, the V/F counting A/D conversion is equivalent to a low-pass first-order *sigma-delta modulation with implicit feedback*[108].

Counting Flux Quantizing (Tracking) ADCs

The fundamental linearity of flux quantization in a superconducting loop is used for constructing another counting ADC design a flux quantizing or tracking ADC which was first described by G. Lee of TRW in 1989 [129,107]. In this design, the input signal current is coupled into a SQUID loop, which generates one SFQ pulse for each Φ_0 change in flux. In contrast to the V/F ADCs, the SFQ pulses are generated in response to increments or decrements of the signal, i.e., only changes of signal are registered. Similarly to the V/F ADC, these SFQ pulses can be counted by using binary counters to reconstruct the signal. Each time the input increases the flux in the loop (Φ_{loop}) by Φ_0, the junction switches, creating a fluxon-antifluxon pair, one of which propagates as an SFQ pulse and the other decreases Φ_{loop} by Φ_0 (Figure 7.57b). This automatic subtraction of the output signal from the input makes it equivalent to low-pass first-order *delta modulation*, where the output is proportional to the signal derivative $d\Phi/dt$. Since RF signal is sensed by a SQUID transformer, this ADC has an extremely high sensitivity similar to that of a SQUID.

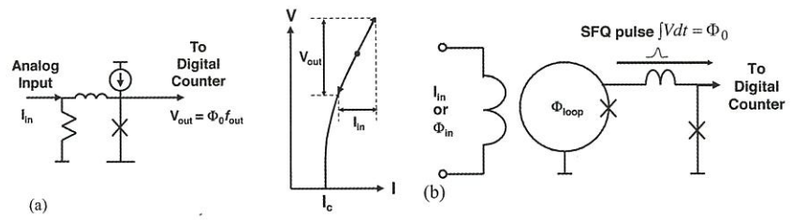

FIGURE 7.57: Basic oversampling Counting ADC modulators. (a) Voltage-to-frequency (V/F) sigma-delta ADC modulator and its operating region. (b) Flux quantizing unidirectional delta (Tracking) ADC modulator (©2004 IEEE).

This concept can be expanded to accommodate both polarities of input signal derivative. Figure 7.58a shows a scheme with a two-junction quantizer, biased such that one of them switches when the flux in the loop changes by $+\Phi_0$ and the other when it changes by $-\Phi_0$, followed by bi-directional (up and down) counting implemented using either two counters or a single bi-directional counter[107]. In 1990, the joint Moscow State University (MSU) and IREE, USSR group implemented the first RSFQ-based tracking ADC featuring bi-direction counter with non-destructive readout al-

[126] C. A. Hamilton and F. L. Lloyd, *IEEE Electron. Dev. Lett.* 3 (1982) 335
[127] M. W. Johnson, et al., *IEEE Trans. Appl. Supercond.* 11 (2001) 607
[128] O. A. Mukhanov, et al., *Physica* C 368 (2002) 196
[129] G. S. Lee, *IEEE Trans. Magn.* 25 (1989) 830

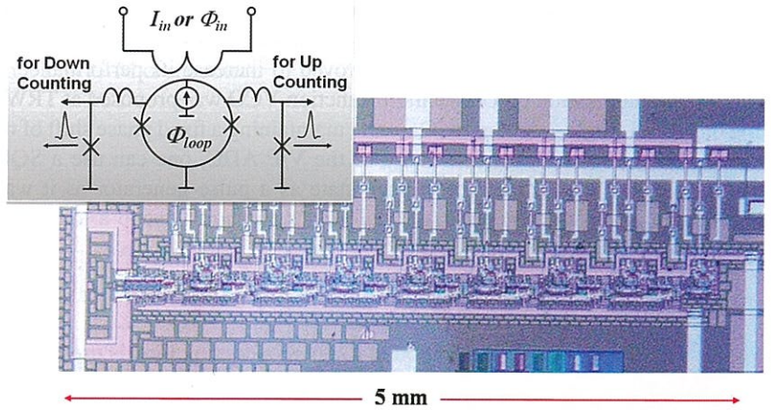

FIGURE 7.58: First RSFQ-based Tracking ADC with a bi-directional (Up/Down) counter (1990). It was fabricated with a 5-μm all-Nb process with 500 A/cm^2. Inset: Basic bi-directional ADC modulator schematic.

lowing uninterruptable signal tracking[130] (Figure 7.58b).

Phase Modulation-Demodulation (PMD) ADC

One of the problems associated with the flux-quantizing (tracking) delta ADCs is the hysteresis of the SQUID quantizer in response to changing polarity of the signal derivative. In order to solve this, a dc voltage-biased single-junction SQUID quantizer (Figure 7.59a) was introduced by S. Rylov, et al. of HYPRES in 1994 [131]. The voltage source (or phase generator) continuously pumps flux into a quantizer at a constant rate, which then leaves the quantizer via the only junction with the timing modulated by the derivative of the analog signal (Figure 7.59a). The modulated SFQ pulse train is passed for SFQ phase (time) demodulation to a synchronizer—a clocked sampling circuit generates a "1" or a '0" indicating whether or not an SFQ pulse arrived during that clock interval. Higher SFQ phase resolution can be achieved by either higher clock or by adding more channels of the synchronizer. Typical sampling clock of this PMD ADC is in tens of GHz limited by the speed of subsequent digital signal processing circuits.

Similarly to the flash ADC digitizers, the oversampling ADC produces digital output data at tens of Gbit/s which exceeds today's data link per line capabilities and speed of semiconductor electronics. There are two possible approaches to this interface problem: *on-chip digital filtering* and *demultiplexing*.

A digital decimation filter reduces the sampling rate, narrows output bandwidth, and generates additional bits. For oversampling superconductor ADCs, sinc-type digital filters were implemented using fast RSFQ logic capable of operating at the same speed as the sampling speed of the ADC. One of the key factors in successful development of the PMD ADCs was the adoption of a new design of the digital filter with programmable bandwidth developed by V. Semenov *et al.* in 1997 [132] and then perfected by T. Filippov et al. of SUNY Stony Brook[133]. By 2001, O. Mukhanov et al. of HYPRES

[130] L. V. Fillipenko, et al., *IEEE Trans. Magn.* MAG-27 (1991) 2464

[131] S. V. Rylov and R. P. Robertazzi, *IEEE Trans. Appl. Supercond.* 5 (1995) 2260

[132] V. Semenov, Yu. Polyakov, and A. Ryzhikh, Decimation filters based on RSFQ logic/memory cells in *Extended Abstracts of ISEC' 97*, Berlin, Germany, (1997) 344

[133] T. V. Filippov, et al., *IEEE Trans. Appl. Supercond.*, 11 (2001) 545

and SUNY team[134] demonstrated a PMD ADC (Figure 7.59b) with over 11 effective bits or 68 dB signal-to-noise ratio (SNR) for 145 MS/s output and maximum operation speed up to 19 GS/s. This was the world's fastest operation of the most complex (6,000 Josephson junctions) superconductor digital or mixed-signal RSFQ circuit of that time.

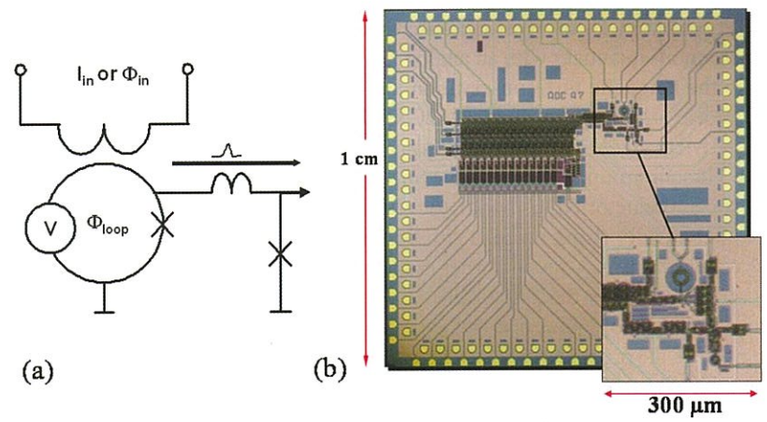

FIGURE 7.59: Phase modulation demodulation (PMD) delta ADC invented in 1994. (a) Flux quantizer for PMD ADC modulator. (b) Second-generation PMD ADC chip consisting of a low-pass PMD delta modulator (in the inset) and a 15-bit decimation digital filter operating at 19.6 GS/s. This chip contains ~6,000 Josephson junctions fabricated at 1 kA/cm^2 process in 2000 (©2004 IEEE).

A large variety of PMDs ADCs were developed including ADCs with serialized digital output, multi-rate ADC with doubled modulator sampling rate for communications and signal intelligence applications. The ADC fabrication using 4.5 kA/cm^2 allowed sampling rate up to 34 GS/s. In 2006, I. Vernik et al. of HYPRES[135] demonstrated 13.5 effective bits for 10 MHz signal with a PMD ADC chip cryopackaged onto Sumitomo G-M cryocooler. By 2008, A. Inamdar et al. of HYPRES[136] achieved 14.5 effective bits (SNR=89.2 dB) at 29 GS/s sampling clock, while the multi-rate PMD ADCs operated up to 46 GS/s. In order to increase dynamic range of the PMD ADC, a quarter-rate PMD quantizer (QRQ) was introduced by A. Inamdar and S. Rylov et al. in 2006 [137] to increase the maximum ADC slew rate and to add two more bits of resolutions.

Higher-Order Delta ADC

Improvement of ADC performance is expected with higher order ADC modulators. V. Semenov's group at SUNY developed a low-pass delta ADC modulator based on a synchronous quantizer with two feedback loops and two integrators: an implicit loop due the conservation of magnetic flux in the superconducting loop of the quantizer and an explicit loop formed with the Josephson amplification circuit and a low-pass filter. A complete ADC chip with decimation digital filter was

[134] O. A. Mukhanov, et al., *Supercond. Sci. Technol.* 14 (2001) 1065

[135] I. V. Vernik, et al., *IEEE Trans. Applied Superconductivity* 17 (2007) 442

[136] A. Inamdar, et al., *IEEE Trans. Applied Superconductivity* 19 (2009) 670

[137] A. Inamdar, et al., *IEEE Trans. Applied Superconductivity* 17 (2007) 446

demonstrated its operation at up to 10.5 GHz clock in 1998 [138]. Although the modulator has two loops, its performance was still similar to a first-order modulator. In order to obtain the second-order characteristics, it is necessary to increase the explicit feedback gain. Achieving higher gain is difficult in superconductor technology, since it requires the construction of SFQ amplifiers (drivers).

Sigma-Delta ADC

In 1992, J. Przybysz et al. of Westinghouse invented a low-pass sigma-delta ADC modulator based on a synchronous quantizer with an analog $L-R$ integrator (Figure 7.60a)[139]. It has an implicit feedback due to the magnetic flux conservation and demonstrates the sigma-delta "noise shaping", i.e. suppressed noise at low frequencies. By 2006, the first-order sigma-delta ADC has reached 77 dB SNR for a 10 MHz signal at 16 GS/s clock as it was demonstrated by A. Yoshida et al. of SRL ISTEC and the Hitachi group[140]. Demultiplexing was used in order to bridge the disparity in data rates between superconductor ADC modulator and semiconductor digital signal processing.

Due to the quadratically rising noise, a simple first-order decimation filter is insufficient to filter out the high-frequency noise. A second order modulator can improve SNR from 9 to 15 dB/octave of oversampling. However as for the delta ADC described above, the lack of broad-band amplification in superconductor technology makes construction of a second order sigma-delta ADC difficult. In 1994, J. Przybysz et al. proposed a two-loop modulator design employing an additional explicit feedback loop with the required substantial gain M (Figure 7.60b)[141].

There have been several attempts in the US and Japan to realize this challenging amplification task which has to deliver enough gain ($M \sim 64$) within a very short time, below the high-speed clock period. In 2003, S. Hirano et al. of SRL ISTEC, Japan demonstrated an amplifier based on a magnetically coupled Josephson transmission line (JTL) tree and serially connected SQUIDs demonstrated close to 12 dB/octave power spectrum characteristics although at a relatively low 1.2 GHz clock rate[142].

In 2004, realizing the difficulty of building a second-order sigma-delta ADC, A. Sekiya et al. of Nagoya University[143] found a way to increase first-order sigma-delta ADC SNR and sensitivity by using a multi-bit modulator following the PMD approach. The 4,000-junction ADC chip consisting of a modulator and decimation filter was demonstrated using NEC standard Nb process with 2.5 kA/cm^2.

Finally in 2008, Q. Herr et al. of Northrop Grumman[144] developed an SFQ amplifier with the required gain. A second-order sigma-delta ADC circuit featuring a high gain (50 Φ_0) quantum-accurate feedback amplifier (Figure 7.60c) was built using HYPRES' commercial 4.5 kA/cm^2 Nb process. It achieved 81 dB SNR or 13.1 effective bits over a 10 MHz band at a 5 GS/s sampling clock. Since the ADC chip did not have an on-chip digital filter, the sampling speed was limited by an output interface. The measured performance was in agreement with the linearized model which showed that the amplifier delay does not have to be shorter than the sampling clock period.

Band-Pass Sigma-Delta ADC

Superconductor technology is particularly suitable for implementing band-pass ADC designs exhibiting a peak performance around a particular frequency. Superconductivity features two major advantages: low-loss materials allowing very high Q resonators and high clock rates allowing direct

[138] V. K. Semenov, Y. A. Polyakov, and T. V. Filippov, *IEEE Trans. Appl. Supercond.* 9 (1999) 3026
[139] J. X. Przybysz, et al., *IEEE Trans. Appl. Supercond.* 3 (1993) 2732
[140] A. Yoshida, et al., *IEEE Trans. Appl. Supercond.* 17 (2007) 426
[141] J. X. Przybysz, D. L. Miller, and E. H. Naviasky, *IEEE Trans. Appl. Supercond.* 5 (1995) 2248
[142] S. Hirano, et al., *Physica* C 392 (2003) 1456
[143] A. Sekiya, et al., *IEEE Trans. Appl. Supercond.* 15 (2005) 340
[144] Q. Herr, et al., *IEEE Trans. Appl. Supercond.* 19 (2009) 676

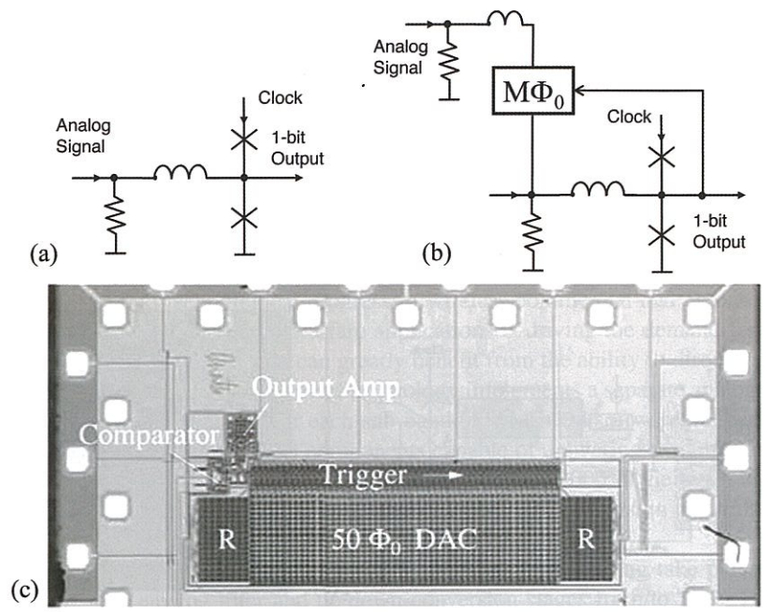

FIGURE 7.60: Superconductor low-pass sigma-delta modulator. (a) 1993 first-order modulator with implicit feedback and input $L-R$ integrator. (b) 1994 second-order modulator showing the critical feedback M Φ_0 amplifier. (c) Northrop Grumman 2-order sigma-delta ADC with a 50 Φ_0 feedback amplifier demonstrated in 2008 (©2009 IEEE).

sampling of multi-GHz RF signals. J. Przybysz and D. Miller of Westinghouse invented a first-order band-pass sigma-delta ADC modulator by replacing the front-end *LR* integrator with an *LC* resonator[145]. It suppresses the quantization noise around the resonant frequency f_{LC}, rather than at dc. The expected first-order noise shaping of sigma-delta modulator with lumped-element resonator was demonstrated by T. Hashimoto et al. of SRL ISTEC in 2001 [146]. In 2002, J. Bulzacchelli et al. of IBM[147] demonstrated a band-pass ADC with distributed microstrip-based resonators exhibiting the desired noise suppression around 2.2 GHz up to a sampling rate of 45 GHz. The demonstrated performance (SNR of 49 dB and dynamic range of 57 dB over ~20 MHz bandwidth at 2.2 GHz) exceeded that of semiconductor band-pass modulators at that time. Due to the lack of on-chip digital filters, the digitized data was stored using on-chip buffers for subsequent slow readout.

D. Kirichenko of HYPRES developed a family of continuous-time sigma-delta band-pass ADC modulators employing an implicit feedback and lamped-element resonators. Band-pass ADCs centered around various RF frequencies: 1 GHz, 4 GHz, 5 GHz, 7.5 GHz, and 20 GHz were demonstrated[148]. Similarly to the low-pass ADC, a first order sigma-delta ADC could provide sufficient performance desired for directly digitizing receiver architectures. In 2007, D. Kirichenko developed a second-order delta-sigma ADC modulator with two lumped *LC* resonators (Figure 7.61a) by introducing an explicit feedback loop using JTLs as active delay elements in addition to a D flip-flop

[145] J. X. Przybysz, D. L. Miller, Bandpass sigma-delta modulator for analog-to-digital converter, U.S. Patent 5 341 136, Aug. 23, 1994
[146] T. Hashimoto, et al., *Jpn. J. Appl. Phys.* 40 (2001) L1032
[147] J. F. Bulzacchelli, et al., *J. Solid State Circ.* 37 (2002) 1695
[148] D. Gupta, et al., *IEEE Trans. Applied Superconductivity* 17 (2007) 430

to control the phase of the feedback signal[149].

Typically, the clock frequency for a band-pass sigma-delta ADC is chosen to be $f_{clk} = 4f_0$, where f_0 is the center of the band of interest, e.g., 30 GHz for X-band. One can also use a lower clock frequency with some performance penalty. In this scheme, called RF undersampling, one can take advantage of the sampling process that replicates the input analog frequency band, centered at f_0, translated by multiples of the sampling frequency (f_{clk}). The world's first Ka-band ADC with a 20.362 GHz center frequency was tested in the RF undersampling mode using a 27.136 GHz clock[149].

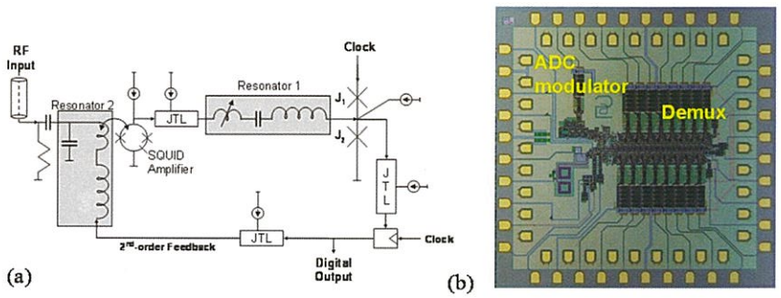

FIGURE 7.61: A 2007 HYPRES second-order band-pass sigma-delta ADC. (a) Schematics of ADC modulators with implicit and explicit feedback loops (©2009 IEEE). (b) X-band ADC chip consisting of second-order band-pass ADC modulator centered for 7.4 GHz and digital signal processor.

In 2008, D. Kirichenko invented an ADC modulator with two implicit feedback paths exhibiting a quasi-instantaneous feedback implemented by connecting two resonators directly to the comparator. The RF input was split and applied through inductive coupling to each resonator. In addition, a SQUID amplifier stage was used to connect two *LC* resonators in series to get the desired loop filter transfer function. Such a band-pass ADC equipped with a 1:16 deserializer was demonstrated with a 31.6 dB SNR in 660-915 MHz band at 10.24 GS/s clock[150].

Multi-Modulator ADC

Challenges in achieving higher performance encourage the adaptation of ADC architecture approaches known in conventional semiconductor ADC technology: time-interleaving, subranging, cascading, and others.

Time-interleaving allows the increase of effective sample rate by using several parallel comparators sampled by the same clock. The actual performance gain in the interleaved oversampling ADC depends on various factors, including feedback-loop delay in comparison to the effective clock period. In 1999, V. Semenov of SUNY[151] invented a time-interleaved delta modulator consisting of two delta modulators shifted by half a clock period, this requires interleaving both comparator and feedback functions. Since interleaving cannot be achieved with the implicit feedback of SQUID

[149] O. A. Mukhanov, et al., *IEICE Trans. Electron.* E91-C (2008) 306

[150] D. Kirichenko, T. Filippov, D. Gupta, Microwave receivers with direct digitization in *Proc. IMS'09*, Boston, USA, June 2009

[151] V. K. Semenov, Superconductor modulator with very high sampling rate for analog to digital converter U.S. Patent 6 608 581, Aug. 19, 2003

quantizers, separate explicit feedback loops are implemented using stacked SQUIDs.

Subranging is capable of significant increase of dynamic range by using several modulators to digitize different ranges of signal amplitude. This approach can be applicable for two-delta, two-sigma-delta, or combined delta and sigma-delta modulator combinations. A. Inamdar of HYPRES[136] showed that the two-delta subranging ADC based on the proven PMD ADC modulators is capable of a significant SNR improvement (23 dB) with a quite conventional 26 GS/s sampling clock.

Oversampling ADC Applications: Wideband Digital Receivers

Since the 1990s, rapid technological progress in wireless commercial and defense communications and related radar and electronic-warfare applications is driving the demand for much higher ADC performance. These applications can greatly benefit from the ability to directly digitize wideband RF signals. Conventional narrow-band technology implements a separate analog receiver with one or more down-conversion steps for each sub-band. A wideband software-defined radio (SDR) receiver needs mixed-signal and digital components capable of delivering extreme speed, linearity, dynamic range, noise, and sensitivity. As it was realized around 2000 in the USA, Japan, and Europe, the unique features of superconductor technology and ADC circuits, in particular, can make a true SDR possible[152,153,154].

In a *digital-RF architecture*[155], data conversion and digital processing take place at RF rather than at baseband – the analog filter and up/down-conversion stages from/to lower IF or baseband are eliminated (Figure 7.62). A wideband RF signal is applied directly to an ADC modulator producing an oversampled low-bit-width digital code at a very high data rate (tens of Gbps). This high-rate data stream is processed before down-conversion using a relatively low-complexity but very high-throughput processor, an *RF DSP*, to implement various functions such as digital signal—combining from multiple channels, true-time delay for digital beamforming, adaptive active cancellation of transmit channels, correlation-based digital filtering, etc. Finally, this high-rate data is down-converted to baseband using digital mixers and decimation filters for further processing and decoding. Back-end processing is implemented using conventional semiconductor parts and placed at ambient temperature.

The first practical implementation of the digital-RF architecture–superconducting digital-RF channelizing receivers extract different frequency bands-of-interest within the broad digitized spectrum. The single-bit oversampled data, from either a low-pass delta or band-pass delta-sigma modulator, are applied to one or more channelizers, each comprising digital **i**n-phase (I) and **q**uadrature (Q) mixers and decimation digital filters. On-chip digital channelization is followed by the lower-speed channelization using field programmable gate array (FPGA) chips at room temperature.

In 2004, the first digital-RF channelizing receiver chip was produced at HYPRES[155] (Figure 7.63a). It consisted of a 20 GS/s low-pass phase PMD ADC modulator. This ~11,000 junction chip was fabricated using a 1.0 kA/cm^2 process and tested up to 20 GHz clock rate. In 2005, the ADR chip was integrated onto a commercial Sumitomo SRDK 101D cryocooler capable of cooling 125 mW at 4.2 K. It was mounted into a standard 19-inch rack, which also housed a cryocooler compressor, interface and control hardware (Figure 7.63b). This world's first digital-RF receiver system was done under support and guidance from D. Van Vechten of the U.S. Office of Naval Research.

Satellite communications with high carrier frequencies and wide bandwidths (e.g., X-band: 500 MHz BW around 7.5 GHz; Ka-band: 1 GHz BW around 20.5 GHz) can benefit from wideband

[152] E. B. Wikborg, V. K. Semenov, and K. K. Likharev, *IEEE Trans. Appl. Supercond.* 9 (1999) 3615

[153] A. Fujimaki, et al., *IEEE Trans. Appl. Supercond.* 11 (2001) 318

[154] D. K. Brock, O. A. Mukhanov, and J. Rosa, *IEEE Commun. Mag.* 39 (2001) 174

[155] O. A. Mukhanov, Superconductor Digital-RF Electronics in: *Extended Abstracts ISEC'05*, Noordwijkerhout, the Netherlands, I-A.01, Sep. 2005

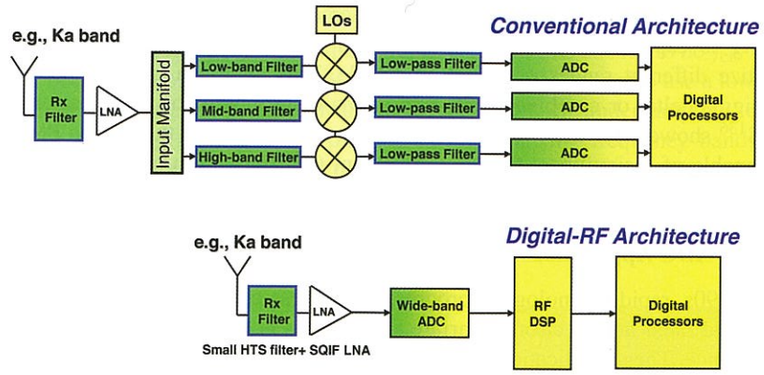

FIGURE 7.62: Comparison of conventional (top) and Digital-RF receiver (bottom) architectures. In the digital-RF architecture, data conversion is carried out directly at RF frequencies using a wideband oversampling ADC modulator. The digitized RF data stream is then processed at very high data rate in an RF DSP before being digitally down-converted and filtered to baseband for further processing.

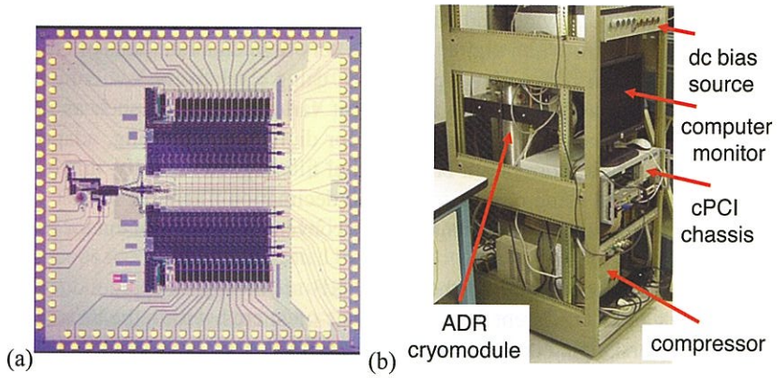

FIGURE 7.63: World's first digital-RF system: – 2005 HYPRES channelizing receiver: (a) Microphotograph of a single-channel all-digital receiver (ADR) chip based on the first-order low-pass delta ADC, digital in-phase and quadrature (I&Q) mixer, and decimation digital filters. This 1 cm×1 cm chip consists of ~11,000 JJs and dissipates ~3.5 mW. (b) Photo of the cryopackaged ADR test setup (ADR-0) using commercial Sumitomo 2-stage GM cryocooler mounted into the lower part of standard 19-inch rack.[155]

digital-RF channelizing receivers by eliminating balky analog channelizing and downconversion stages. In 2006, D. Gupta et al. of HYPRES[148,149] assembled and delivered an X-band digital receiver system to the Joint SATCOM Engineering Center (JSEC) in Ft. Monmouth, NJ to receive wideband X-band signals from the XTAR and DSCS satellites. The receiver was integrated with a digital I&Q MODEM, demonstrating demodulation of satellite signals including a video data transmission. In 2007, the ADR-1 system was upgraded with installing a faster 30-GHz chip fabricated 4.5 kA/cm^2 process (Figure 7.64a).

In subsequent years, more ADR systems based on low-pass PMD delta ADCs and band-pass

sigma-delta ADCs were assembled and delivered. In 2008, new-generation ADR systems featuring modular cryopackaging design were developed. These ADRs demonstrated the *hybrid temperature hybrid technology* (ht^2) system integration concept, where different components of the system are operated at different temperatures to optimize the overall performance. For example, such a system included a high-temperature superconductor (HTS) filter developed in University of Waterloo (Figure 7.64b) which was placed at 70 K on the first stage of the cryocooler and connected to the ADR chip located at the second (4 K) stage. In January 2009, the joint HYPRES, ViaSat, and Navy team demonstrated the world's first multi-net Link-16 data link in which analog outputs from two Link-16 terminals, operating with independent hopping patterns, were combined and applied to the superconductor chip with L-band sigma-delta ADC chip integrated with RSFQ 1:16 demux (Figure 7.64c, 7.64d)[156].

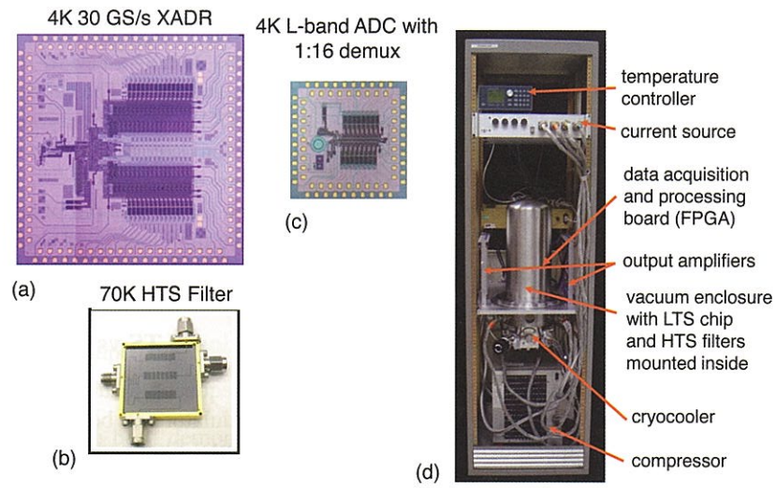

FIGURE 7.64: Digital-RF receiver and its key components: (a) World's first (2006) X-band single-chip digital-RF receiver (XADR) directly digitizes 7.5 GHz RF signal at 30 Gs/s. This 11,000-junction chip consists of a band-pass second-order continuous-time delta-sigma ADC modulator, digital I&Q mixer, and two digital filters; (b) L-band ADC integrated with a 1:16 RSFQ demux (2008); (c) HTS filter developed by University of Waterloo, Canada (2008); (d) HYPRES (2008) modular ADR system built using hybrid temperature hybrid technology (ht^2) approach.

By 2010, HYPRES ADR systems went through three generations. Third-generation ADR systems expanded to house two chip modules with 80 high-speed digital I/Os, up to four 17-channel interface amplifier assemblies and two current sources. The design is modular and allows for independent service of each chip module and quick field replacement when necessary. System reconfigurability enabled by the modular design allowed ADR-5 to be configured and used for different tasks. D. Gupta *et al.*[156] demonstrated operation with the XTAR satellite without utilizing a front-end low-noise amplifier usually required for this application. This was another step towards fully digital receivers. ADR-5 system worked up to 32 GHz clock frequency with a variety of phase and amplitude modulated waveforms at 30 Msymbol/s.

[156] D. Gupta, et al., Modular, multi-function Digital-RF receiver systems *IEEE Trans. Appl. Supercond.* 21 (2011)

The digital-RF channelizing receiver approach can be extended to include multiple ADC modulators and multiple channelizer units on a multi-chip module or a single chip. A chip integrating four ADC modulators (centered at 850 MHz, 4 GHz, 7.5 GHz and 12 GHz), a 1×4 digital switch matrix and a 1:16 demultiplexer was demonstrated in 2010 by S. Sarwana et al. of HYPRES[157].

ADC Applications: Sensor Readout

The inherent low noise, low power, high sensitivity, and radiation hardness of superconductor ADCs can be applied to many sensor applications especially for cooled detector arrays. Both flash-type and oversampling-type ADCs can be used for this application.

In 2001, A. Sun et al. of TRW[158] demonstrated a NbN 10 K V/F type ADC for cryocooled infrared (IR) focal plane detector arrays. In 2002, a Nb V/F type ADC with a SQUID-based VCO was used for measuring the integrated charge of a current pulse for superconductor tunnel junction (STJ) X-ray detector readout. Furthermore, this digital counter can also be used to count the number of SFQ clock pulses between successive time events to produce a time-to-digital converter (TDC) on the same chip. Such a dual-function signal and time digitizer was demonstrated in 2002 by joint US-Japanese team with 1 μA full-scale current and 30 ps time resolution[159]. The exceptionally low power of RSFQ technology allows integration of an ADC or TDC in a single cryopackage with the cooled detectors. The integration of the cooled semiconductor detector, visible light photon counter (VLPC) with Nb TDC, was demonstrated by O. Mukhanov et al. in 1998 [160]. The extreme radiation hardness of superconductor electronics was a motivation for the readout of a high-energy particle microstrip detector. A delta ADC based on a very sensitive flux-controlled comparator was demonstrated for CERN high-energy physics experiments by a joint US-Italian team[161].

7.8.3 Superconductor Materials for ADC Implementation: LTS vs HTS

Superconductor ADCs are medium-scale integrated circuits requiring a substantial number of Josephson junctions for complete systems. Even if an ADC modulator can be implemented with rather few junctions, the subsequent demultiplexer, drivers or digital filter can easily require hundreds or thousands of junctions. This requires well-controlled integrated circuit fabrication, with reproducible junction properties. Most of the complete ADC circuits have been demonstrated to date using low-temperature superconductor (LTS) niobium Josephson junctions, operating at about 4 K. Slightly higher temperate superconductors, NbN with T_c up to about 17 K, were used by TRW team to implement counting ADCs for operation at 10 K [158].

The possibility of a drastic reduction of size, weight and power (SWaP) of the cryocooler was the main motivation to implement high-temperature superconductor (HTS) ADCs. There have been major efforts to develop a reproducible technology for Josephson junctions based on $YBa_2Cu_3O_7$ (YBCO), although the high temperatures required for deposition of these materials makes a true multilayer process difficult to achieve. Several HTS ADC projects were active in Japan (Hitachi, SRL ISTEC), Europe (Twente University, Chalmers University, Karlsruhe University), and the USA (Conductus, TRW, Northrop Grumman) for a number of years. Some key components of ADCs, including a simple first-order sigma-delta oversampling ADC modulator, QOS comparator

[157] S. Sarwana, et al., Multi-band Digital-RF Receiver *IEEE Trans. Appl. Supercond.*, vol. 21, Jun. 2011.
[158] A. G. Sun, et al., *IEEE Trans. Appl. Supercond.* 11 (2001) 312
[159] S. Sarwana, et al., *Appl. Phys. Lett.* 80 (2002) 2023
[160] O. A. Mukhanov, et al., *IEEE Trans. Applied Supercond.* 9 (1999) 3619
[161] S. Pagano, et al., *IEEE Trans. Applied Supercond.* 9 (1999) 3628

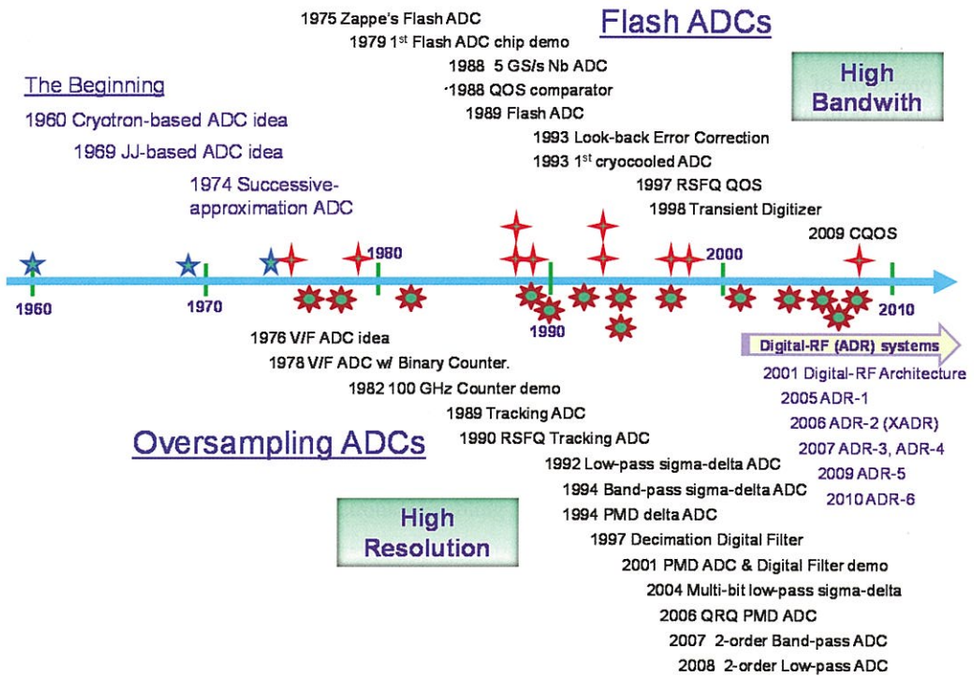

FIGURE 7.65: Superconductor ADC development timeline.

for flash ADC have been demonstrated[162,163,164,165,166]. In 1997, G. Gerritsma et al. of University of Twente[167] reported on the effort to build a 4-bit flash ADC based on QOS comparators using ramp junction technology. The functionality of QOS comparators was demonstrated at low speed. In 2004, H. Sugiyama et al. of SRL ISTEC[168] demonstrated high-speed operation of a QOS comparator based on high-T_c multilayer technology. A circuit containing 10 interface-engineered ramp-edge Josephson junctions was fabricated on a La-substituted $YBa_2Cu_3O_y$ ground plane. The output voltage as a function of the input current for the QOS indicated correct operation as a periodic comparator at clock frequency of 94 and 77 GHz at 35 and 40 K, respectively.

At this moment, it seems unlikely to have the HTS technology reach the required complexity in the near future. On the other hand, a progress in compact 4 K cryocoolers can make Nb-based ADCs useful for a wider range of applications.

7.8.4 Conclusions

We witnessed remarkable progress in superconductive ADCs over last several decades starting from early concepts to demonstrations of application systems performing satellite communication

[162] M. G. Forrester, et al., *Supercond. Sci. Technol.* 12 (1999) 698
[163] B. Ruck, et al., *Physica* C 326 (1999) 170
[164] A. Y. Kidiyarova-Shevchenko, et al., *Physica* C 326 (1999) 83
[165] A. H. Sonnenberg, et al., *IEEE Trans. Appl. Supercond.* 11 (2001) 200
[166] K. Saitoh, et al., *Physica* C 378-381 (2002) 1429
[167] G. Gerritsma, et al., *IEEE Trans. Appl. Supercond.* 7 (1997) 2987
[168] H. Sugiyama, et al., *Appl. Phys. Lett.* 84 (2004) 2587

tasks. Most influential ADC designs and development milestones are seen in Figure 7.65. The unique features of superconductivity, featuring the high speed of Josephson junctions and the quantum precision of magnetic flux quantization, produced a wide spectrum of superconductor ADC designs of both high-bandwidth Nyquist-sampling flash ADCs and high-resolution oversampling ADCs.

Acknowledgments

History of Superconductor Analog-to-Digital Converters

The author wishes to thank F. Bedard, D. Gupta, C. Hamilton, R. Harris, S. Hasuo, S. Kaplan, M. Ketchen, D. Kirichenko, V. Semenov, A. Silver and H. Suzuki for help and sharing their data and recollections.

8

Microwave Applications

Editor: D. E. Oates

8.1 Microwave Measurements of Fundamental Properties of Superconductors

D.E. Oates

8.1.1 Introduction

Why use microwaves to measure fundamental properties of superconductors? To understand the answer, one must consider that at microwave frequencies superconductors have finite resistance. The resistance is identically zero at dc and negligible at very low frequencies, so the superconductor does not interact with such probes. The origins of the finite resistance will be explained in Section 8.1.2. Microwaves interact strongly, and over the history of superconductivity microwave measurements have contributed considerable information to the understanding of the phenomenon. In the very early history of superconductivity, microwave technology was not developed enough to be of use in experiments of the fundamental properties. So it took the development of both the two-fluid model to illustrate the interaction of microwaves and the development of microwave technology immediately before and during World War II to make the realization of the microwave experiments possible. In this section, I use the broadest definition of microwave frequency range, from approximately 300 MHz to 300 GHz. However most of the experiments described here are in the range 1 to 20 GHz. In the microwave frequency range, one determines the resistance by measuring the quality factor Q of a microwave resonator and one determines the penetration depth by measuring the reactance of the resonator. More detail is presented below.

This section, like the whole book, is not intended to be comprehensive. It will present what I feel are the highlights of the development of microwave characterization and the findings that I think are the most important. In the more recent history, in which I have participated, the discussion will take a more personal perspective. I should add a few words on organization of Section 8.1. I will describe the two-fluid model is the basis for understanding the physics of the microwave measurements. That is followed in Section 8.1 by a brief description of the experimental techniques used in the microwave measurements. The historical highlights are then described in chronological order, Sections. 8.1.4 - 8.1.7.

8.1.2 Two-Fluid Model

To answer why microwaves, consider the existence of the finite resistance of a superconductor at microwave frequencies. The explanation invokes the two-fluid model, in which the superconductor is modeled as a mixture of normal electrons and superconducting electrons. The resistance arises because the superconducting electrons have inertia, and when the electromagnetic field reverses sign, the superconducting electrons cannot reverse direction immediately. This leads to a microwave current out of phase with the voltage, and is modeled as an inductance in an equivalent circuit model of the superconductor. An inductance generates a voltage across a sample when a time varying signal is applied. The voltage in turn will cause the normal electrons to flow and thereby generate dissipation. At dc, the superconducting electrons short out the normal electrons and no voltage or dissipation is generated. Figure 8.1 shows the resulting equivalent circuit for a piece of superconductor.

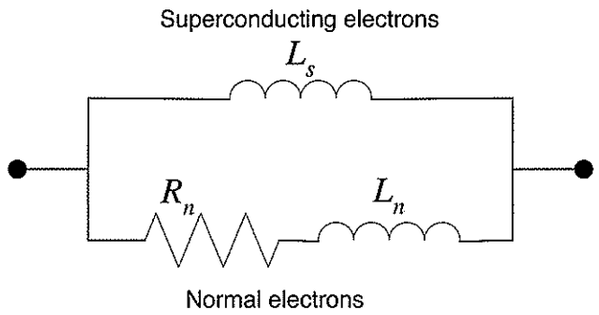

FIGURE 8.1: Equivalent circuit model for a piece of superconductor. The superconducting branch is represented by an inductance L_s, which reflects the inertia of the superconducting electrons. The normal branch is represented by a resistance R_n and inductance L_n reflecting the impedance of the normal electrons. At dc and very low frequencies the superconducting branch shorts out the normal branch, and effectively zero resistance is measured across the terminals. When a current of finite frequency is applied to the terminals a voltage develops because of the inductor, and the voltage developed induces current in the normal branch giving rise to dissipation.

An equivalent explanation of the ac losses begins with the finite penetration of the magnetic field, which is independent of frequency. Because the magnetic field is varying in time, an electric field is generated, and in the thin layer of magnetic penetration this electric field causes the normal electrons to flow and dissipate energy. The classical skin effect is similar in normal metals; for further explanation of the skin effect consult any text on classical electromagnetic theory. In superconductors the dissipation and thus resistance are very small compared with the normal resistance because

the penetration depth is short compared with a normal metal.

The usual way to describe the microwave properties of a superconductor is by a complex conductivity $\sigma = \sigma_1 - i\sigma_2$, which leads to a surface impedance Z_s given by

$$Z_s = \sqrt{\frac{i\omega\mu_0}{\sigma}} \tag{8.1}$$

where

$$Z_s = R_s + iX_s = R_s + i\omega L_s, \tag{8.2}$$

where R_s is the surface resistance and X_s is the surface reactance, which is inductive. Expressions for the surface impedance can be found in many books[1] and need not be derived here. The R_s is given by

$$R_s = \frac{\omega^2\mu_0^2\lambda^3\sigma_1}{2} \tag{8.3}$$

where λ is the London penetration depth, ω is the frequency in radians per second, μ_0 is the permeability of free space, and σ_1 is the real part of the conductivity given by

$$\sigma_1 = \frac{n_n\sigma_n}{n} \tag{8.4}$$

where σ_n is the normal state conductivity, and n_n/n is the ratio of normal to total electrons. The $n_n \to 0$ as $T \to 0$ and is often given by

$$n_n = \left(\frac{T}{T_c}\right)^4 n \tag{8.5}$$

where T is the temperature, and T_c is the critical temperature. The inductance is given by

$$L_s = i\omega\mu_0\lambda. \tag{8.6}$$

These are empirical formulas. A rigorous derivation of the surface impedance was presented by Mattis and Bardeen[2] using the BCS theory. Their derivation validated the expressions derived from the two-fluid model, which is more intuitive and in my opinion illustrates the physics pedagogically.

At frequencies higher than the microwave region, > 300 GHz, the two-fluid model is no longer valid. When the energy of a photon $\hbar\omega$ becomes comparable to the superconducting energy gap Δ, the excitation of quasiparticles by the photons becomes possible. In the high-frequency limit $\hbar\omega > \Delta(T)$, the resistance is equal to that of the normal state.

The two-fluid model gives a simple explanation of the microwave impedance at low levels of current. However in a superconductor, unlike in a normal conductor, the impedance is dependent on the microwave current; this is conventionally referred to as the nonlinear surface impedance. This dependence is quite complicated and cannot be given by a closed-form expression. In the simplest case, it is a matter of exceeding the critical current when the material is driven into the normal state. The dependence is also strongly influenced by the crystallinity and the nature of the superconductivity, by which we mean that the low-T_c superconductors behave differently from the high-T_c materials.

In the nonlinear case, the surface impedance can be written as

$$Z_s(I_{rf}) = R_s(I_{rf}) + iX_s(I_{rf}). \tag{8.7}$$

[1] For example, T. Van Duzer and C.W. Turner, *Principles of Superconductive Devices and Circuits* (Elsevier North Holland, New York, 1981)

[2] D.C. Mattis and J. Bardeen, *Phys. Rev.* 111 (1958) 412

The lowest-order approximation can describe many experimental results. For instance the nonlinear surface resistance is often accurately approximated by

$$R_s(I_{rf}) = R_{s0} + R_2 I_{rf}^2, \tag{8.8}$$

where R_{s0} is the surface resistance at very low current and R_2 is a constant that can in some cases be calculated from first principles. One expects no term in Eq. 8.8 depending on the I_{rf} because the impedance should not depend on the direction of current flow in the absence of a preferred direction. Below I explain how the nonlinearity can be used to determine some important fundamental properties.

8.1.3 Microwave Measurement Techniques

Before describing the important contributions of microwave measurements a few words about the experimental techniques are needed.

Linear Measurements

Most measurements have utilized resonator techniques, either bulk cavities or transmission-line resonators for the case of thin-film measurements where the material under test is made to be some part of the cavity or the transmission line. With the exception of the first measurements of London described in Section 8.1.4, the measured Q of the resonator can be used to determine the R_s by the relation $R_s = G/Q$ where G is a geometrical factor that can be calculated from the geometry of the resonator:

$$G = \frac{\omega_0 \mu_0 \int_V H^2 dV}{\int_s H_s^2 dS}, \tag{8.9}$$

where H is the volume magnetic field distribution in the resonator and H_s is the surface magnetic field distribution.

In general, the absolute value of λ cannot be determined from microwave measurements, but the fractional change in resonant frequency as a function of temperature $\Delta f(T)/f_0$ allows the change in penetration depth as a function of temperature to be determined by $\Delta\lambda(T)/\lambda_0 \sim \Delta f(T)/f_0$.

Nonlinear Measurements

As will be discussed in more detail below, the microwave surface impedance of superconductors shows a dependence on the microwave current I_{rf} or equivalently the microwave surface magnetic field H_{rf}. The nonlinearity is especially important in the high-T_c materials. An important consequence of the nonlinearity is the generation of higher-order harmonics, and when more than one frequency is present, intermodulation distortion (IMD) is generated. The third-order IMD is the most important and is measured in the usual way, in which two closely spaced tones of equal power at frequencies f_1 and f_2 are combined and applied to the resonator. The frequencies are centered about the resonant frequency 3-dB bandwidth. The nonlinearity of the material causes mixing products. The third-order products fall close to the fundamental frequencies and are easily observed even with narrowband devices such as high-Q resonators. The power P_{IMD} of the third-order mixing products at frequencies $2f_1 - f_2$ and $2f_2 - f_1$ is then measured in a spectrum analyzer as a function of the input power to the resonator. As discussed below the temperature dependence of this quantity yields information on the symmetry of the energy gap.

8.1.4 Early History

The first microwave measurements that I am aware of were made by Heinz London[3] and reported in 1940. The measurements were done on superconducting tin at 1.5 GHz in a split-ring resonator excited by a magnetron tube. He measured the microwave absorption and thus the resistance by a calorimetric method. The measurements were made as a function of temperature from above $T_c = 3.73$ K down to 2 K, thus also measuring the resistance in the normal state. He was able to measure the ratio of the microwave resistance in the superconducting state to that in the normal state R/R_n. This is shown in Figure 8.2. He noted that, unlike the dc resistance, R decreased gradually below the transition temperature. From this he deduced the number of the normal electrons as a function of temperature.

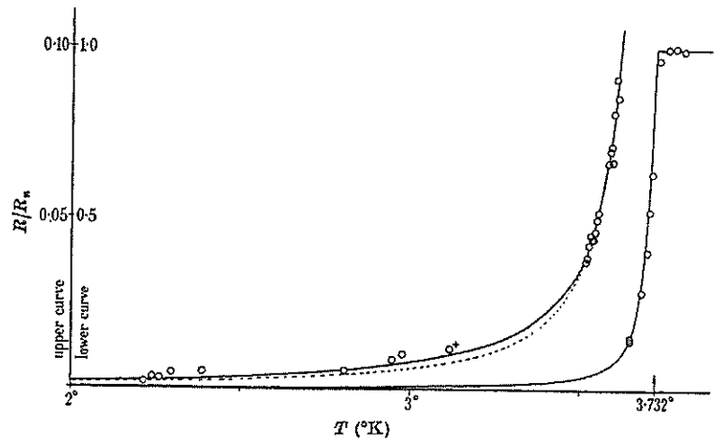

FIGURE 8.2: London's original results of microwave measurements of the resistance of a superconductor showing the gradual reduction in resistance that is the characteristic of the microwave resistance in contrast to the abrupt change in resistance for the dc case.

This experiment was the first measurement of ac resistance, provided the first verification of the two-fluid model, and supported the London theory of superconductivity. It also allowed the deduction of the temperature dependence of the number of normal electrons.

It is interesting to note that London first mentioned the possibility of measuring the microwave heating of a superconducting sample in a 1934 article, alluding to attempts that were interrupted after 1933 when he was forced to leave Germany.

8.1.5 Post World War II

The history continues after World War II. The development of microwave radar technology in the United States and Great Britain during the war transformed the experimental situation and made microwave experiments far more accessible. A. B. Pippard was one of the first to exploit the new technology following the war. Pippard had worked on radar development in England during the war, and following it was given access to much of the equipment that was then surplus[4]. In a series of

[3] H. London, *Proc. Roy. Soc.* A 176 (1940) 522

[4] B. Glowacki, Lectures on Superconductivity (2009) http://www.msm.cam.ac.uk/ascg/lectures/

important papers in the late 1940s and early 1950s[5], Pippard measured the microwave resistance of mercury and tin in resonators at 1.5 GHz and at 9.4 GHz. His findings agreed qualitatively with those of London mentioned above. Pippard also was able to measure the penetration depth by measuring the reactance of his resonators as a function of temperature and applied magnetic field. His values for the penetration depth agreed with those measured earlier by a completely independent method and provided validation of the numbers.

Pippard found that the measurements of penetration depth did not agree with the existing London theory, especially in impure samples and found that losses were larger than would be predicted by the London theory. He observed that the London theory is a local description of the electrodynamics where the current $\vec{j}_s$ and vector potential $\vec{A}$ are related by

$$\vec{j}_s(\vec{r}) = \frac{\vec{A}(\vec{r})}{\mu_0 \lambda^2}. \tag{8.10}$$

and his data are better fit with a nonlocal electrodynamics, where the current is that given by the vector potential averaged over a length scale which he introduced and called the coherence length ξ. The coherence length is given by

$$\frac{1}{\xi} = \frac{1}{\xi_0} + \frac{1}{\ell}, \tag{8.11}$$

where ξ_0 is an intrinsic coherence length particular to the pure material and ℓ is the mean free path of the electrons. This coherence length turns out to be identical, in the case of pure material, to the coherence length derived in the BCS theory. It is usually interpreted to be the diameter of a Cooper pair[1]. Bardeen was aware of Pippard's work when he together with Cooper and Schrieffer formulated the famous theory of superconductivity.

Pippard also discovered, as others before him had, that in the normal state, metals at low temperatures exhibit much larger losses than expected from the theory of the skin effect. This excess loss results from the mean free path being larger than the skin depth, thus making the effective skin depth larger than that calculated from the standard formulas. This effect is now known as the anomalous skin effect[2]. A similar situation arises in superconductors, as Pippard found, when the mean free path is larger than the coherence length $\ell \gg \xi_0$.

8.1.6 1960s and 1970s

Following the work of Pippard, considerable work on measuring the surface impedance of various materials continued.

Energy Gap Measurements

In the late 1950s, nearly coincident with the appearance of BCS theory, some measurements at the upper edge of what can be called microwave frequencies were reported[6] demonstrating a finite energy gap. They showed increased absorption of microwave energy when the frequency is raised above the values such that $\hbar\omega \approx kT_c$. Other data supported this and the definitive experiments of direct measurement of the energy gap were carried out in the far infrared. The development of the BCS theory gave a theoretical basis to these ideas.

Measurement in the Mixed State

Following the proposal by Abrikosov in 1958 that type II superconductors can support quantized vortices, microwave measurements played a role in the indirect verification of the proposal, before

[5] A. B. Pippard, *Proc. Roy. Soc. Lond.* A 216 (1953) 547
[6] M.A. Biondi et al., *Phys. Rev.* 108 (1957) 495

the later direct verification by magnetic decoration. Not only did microwave measurements support the idea of quantized vortices, but also they were able to measure the properties of the vortices, such as pinning strength and viscosity. Microwave measurements are unique in this capability, again because they interact with the superconducting state in a way that dc measurements do not. In my opinion the highlight of the effort to understand vortices is a classic series of experiments by Gittleman and Rosenblum[7], who measured the resistance from low frequencies up through the microwave region. The results are shown in Figure 8.3 where the relative power absorbed by various superconductors is plotted as a function of a reduced frequency f_0 defined as the frequency where the relative power absorbed is one half.

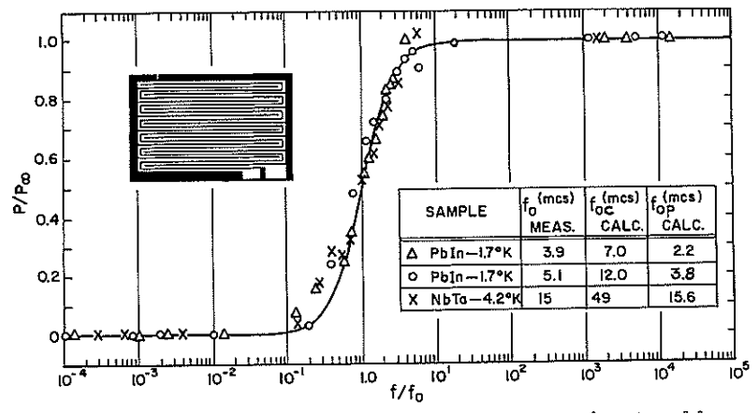

FIGURE 8.3: Relative power absorbed in the mixed state as a function of reduced frequency.

Gittleman and Rosenblum were able to understand these results using a very simple and elegant harmonic oscillator model of the vortices and pinning centers. Because the vortex-vortex interaction energy is larger than the pinning energy, the vortex lattice can be considered rigid. The vortices are driven by the microwave current, and the force constant k of the harmonic oscillator model, given by

$$k = \frac{2\pi\alpha_c\varphi_0^{1/2}}{cH_0^{1/2}}, \tag{8.12}$$

is identified as the pinning strength. In Eq. 8.12 α_c is a constant whose dependence on applied magnetic field H_0 is given explicitly and φ_0 is the flux quantum. The viscosity η of the vortex motion provides the damping term. Thus, the equation of motion for small currents and small displacements is

$$m\ddot{x} + \eta\dot{x} - kx = \frac{J\varphi_0}{c}, \tag{8.13}$$

where m is the effective mass of the vortex and J is the ac current. At low frequencies near dc the vortices are pinned, and the losses are very small. At microwave frequencies the vortices oscillate about the pinning sites freely with the losses determined by the viscosity. The vortices are essentially free at these frequencies. The transition frequency f_0 where the losses are one half of the high frequency values is given by $2\pi f_0 = k\eta$.

[7] J.I. Gittleman and B. Rosenblum, *Phys. Rev. Lett.* 16 (1966) 734

The agreement with a number of materials is excellent when plotted as in Figure 8.3. Although more sophisticated models have been subsequently developed, this model is still used today to understand the dynamics of vortex motion and the paper[7] is quite often cited, a quite remarkable fact considering the model was proposed even before vortices had been observed directly.

8.1.7 High-T_c Era

The discovery of the high-transition temperature superconductors (HTS) in 1986 caused a large increase in the study of the microwave properties of superconductors. This was due to the potential applications in microwave devices such as filters and delay lines. In the microwave region and at 77 K, the HTS materials have a surface resistance as much as two orders of magnitude lower than that of copper at the same temperature, the most commonly used normal metal for microwave devices. The older low-T_c materials, while possessing comparably low surface resistance, had never generated the same level of interest in microwave applications because of the low operating temperatures required. Microwave characterization of HTS was of interest not only for exploration of fundamental properties but also for the relevance for applications. The use of HTS for practical microwave devices is detailed in the chapter by Hammond (see Section 8.2) and will not be discussed further in this chapter.

With the HTS materials, the primary methods used for microwave characterization of fundamental properties changed from measurements on bulk samples to measurements of thin films and single crystals. Because the HTS materials are ceramics, and bulk samples are fabricated by ceramic processes such as sintering of powders, the microwave properties of the bulk ceramic samples are dominated by the grain boundaries, which are an unavoidable consequence of the sintering process. Because of the short coherence length ξ of the HTS materials, approximately 1 nm, the grain boundaries, which are of comparable size, act like weak-link Josephson junctions, and thus dominate the microwave losses because of the significantly lower critical current of the junction compared with the bulk. When the grain-alignment angles are greater than approximately 2° the critical current is severely reduced[8,9]. In the microwave region this is manifest as a very strong power dependence in the ceramics. This power dependence can also be evident in thin films that contain large-angle grain boundaries. An example of the effects of grain boundaries is shown in Figure 8.4. This is from some of my early measurements. Shown are the results for two different films. Plotted is $1/Q$ of a stripline resonator, which is proportional to R_s, *vs* the microwave current I_{rf}, which is varied by varying the input power to the resonator. These films, one made by postannealing of a precursor film, which leaves high-angle grain boundaries in the film, and the other made by in-situ deposition of YBCO, which produces only low-angle grain boundaries, show similar values of Q at low current but differ markedly as the current is raised.

These findings were quite puzzling at first because such behavior had not been observed in the low-transition-temperature (LTS) materials. However, at the urging of several people, especially Jürgen Halbritter[10] of the Karlsruhe Research Center in Germany (now Karlsruhe Institute of Technology), I and others became convinced that the grain-boundary explanation was correct. It is now widely accepted that the grain boundaries are the cause of the strong power dependence in HTS films and ceramics. I should, however, add that as deposition methods and characterization advanced, it became clear that films with very low angle grain boundaries could be produced on lattice-matched substrates by a variety of deposition methods[11]. As mentioned above[8,9], experiments to directly measure the effects of grain boundaries on microwave surface impedance are the most convincing

[8] Y.M. Habib et al., *Phys. Rev.* B 57 (1998) 13833
[9] Y.M. Habib et al., *Appl. Phys. Lett.* 73 (1998) 2200
[10] J. Halbritter, *J. Appl. Phys.* 71 (1992) 339
[11] D.E. Oates, *J. Supercond. Novel Magn.* 20 (2007) 3

evidence in support of the grain-boundary explanation.

That films can be grown without high-angle grain boundaries is fortunate for the applications discussed in Section 8.2 by Hammond et al., because otherwise, the power-handling capability of filters would be insufficient for most applications. However the third-order intermodulation discussed in the subsection on nonlinear measurements in Section 8.1.3 is still present and the role of IMD in fundamental measurements will be discussed below in Section 8.1.7.

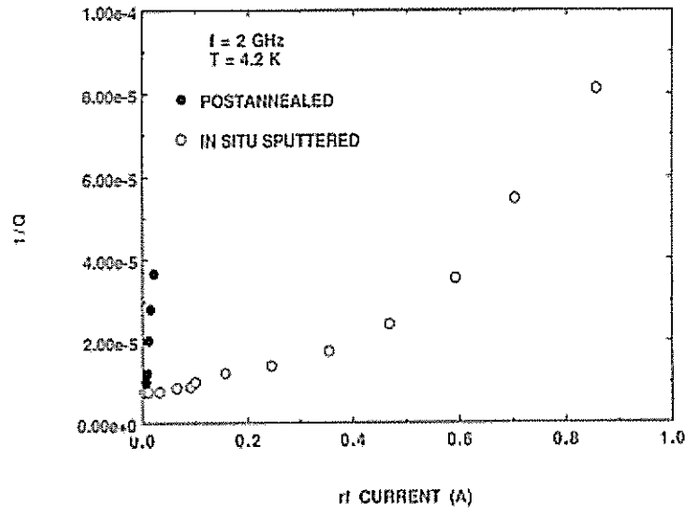

FIGURE 8.4: $1/Q$ (proportional to surface resistance) vs current for two different thin-film samples, one a postannealed film containing high-angle boundaries and an in-situ grown high-quality epitaxial film.

Microwave Determination of Penetration Depth in HTS

Early in the HTS cuprate era, it was proposed that the symmetry of the energy gap in these materials was unconventional. Whereas the symmetry of the LTS materials was s-wave, that is, spherically symmetric in momentum space, the HTS materials were, from theoretical considerations, proposed to exhibit d-wave symmetry[12]. That is,

$$\Delta(T) = \Delta_0(T)\cos(2\theta), \tag{8.14}$$

where Δ_0 is a constant and θ is the angle in momentum space. However experimental evidence for the d-wave symmetry was at best ambiguous[12]. To help clarify the issue, it was predicted that the temperature dependence of the penetration depth at low temperatures $\lambda(T)$ could give a definitive answer to the symmetry question, because the difference between s- and d-wave symmetries is distinctive. For YBCO, low temperature is between 1.3 and about 10 K. For s-wave symmetry the

[12] D.J. Scalapino, *Phys. Rep.* 250 (1995) 329

temperature dependence is fairly flat at low temperature, with the expression from BCS theory

$$\frac{\Delta\lambda(T)}{\lambda(0)} \cong \left(\frac{2\pi\Delta}{T}\right)^{1/2} \exp(\Delta/T), \tag{8.15}$$

where $\Delta\lambda(T) = \lambda(T) - \lambda(0)$. On the other hand for d-wave symmetry, a power law applies:

$$\frac{\Delta\lambda(T)}{\lambda(0)} \cong \ln(2)\frac{T}{\Delta_0}. \tag{8.16}$$

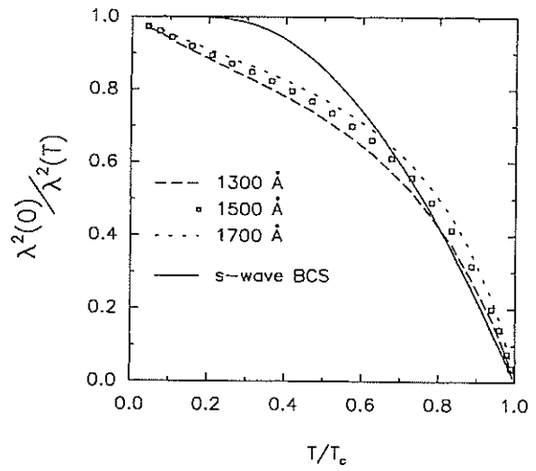

FIGURE 8.5: The quantity $(\lambda(0)/\lambda(T))^2$ *vs* T/T_c which is a measure of the superfluid density for a $YBa_2Cu_3O_{6.95}$ single crystal. The solid line is the same quantity for an s-wave superconductor. The broken lines are for different absolute values of the zero-temperature λ.

The group at the University of British Columbia led by Hardy[13] reported measurements of $\Delta\lambda$ on very high quality single crystals of $YBa_2Cu_3O_{6.95}$ free of impurities and weak links. They used a split-ring resonator at 900 MHz to make the measurements. The use of single crystals in this experiment is important because the $\Delta\lambda(T) = \lambda(T) - \lambda(0)$ changes from a linear dependence in T to a quadratic dependence $\sim T^2$ due to impurity scattering or weak links. Most measurements on thin films had shown the $1/T^2$ dependence. The results of the UBC experiments are summarized in Figure 8.5 which shows plotted vs T the quantity $\lambda^2(0)/\lambda^2(T)$ which is proportional to the fractional superfluid density n_s/n. Also shown is the predicted s-wave behavior. Clearly the d-wave nature of the YBCO sample is demonstrated. As noted above, the microwave resonator method can only measure changes in λ, not the absolute value $\lambda(0)$. The dotted and dashed lines are for different assumptions of the value of $\lambda(0)$. These results were at the time one of the most convincing pieces of evidence for the then-controversial but now widely accepted d-wave symmetry of the cuprate HTS materials.

[13] W.N. Hardy et al., *Phys. Rev. Lett.* 70 (1993) 3999

Intermodulation Distortion

Measurements

As already mentioned in the discussion of experimental methods, Section 8.1.3, IMD is a consequence of the nonlinear surface impedance. IMD is present in all superconductors but it took on new prominence in the HTS materials because of the importance in applications. As with the question of power dependence, the early measurements of IMD were puzzling, perhaps more so, and although some aspects of IMD are now well understood, as presented in the following, even now there is no comprehensive theory of IMD that explains the entirety of the measurements. One great mystery in the early development was the dependence of IMD on power. We are considering the third-order IMD, and it is expected that it arises from the quadratic dependence of the Z_s on current, Eq. 8.8. For instance if Eq. 8.8 holds then the voltage V generated by the current I_{rf} is

$$V \sim I_{rf}R_s = I_{rf}R_{s0} + I_{rf}^3 R_s. \tag{8.17}$$

The term cubic in the rf current is the source of the IMD and produces the mixing products mentioned above. The IMD voltage is proportional to the cube of the current. This implies that the IMD power P_{IMD} is proportional as well to the cube of the input rf power. On a double logarithmic plot this yields a slope of three. The early measurements produced many instances of slopes different from three. Slope 2 was observed often and a mix of slopes was frequently found. For some regions of power, slope 3 was observed and in others slope 2 or less was observed. The observation was also made that a Z_s proportional to $|I_{rf}|$ could produce the slope of two, but there was no theoretical basis. Some of these apparent anomalies have been explained by the theory presented in the next section.

Nonlinear Meissner Effect

In the midst of the efforts to understand IMD, important papers were published by Thomas Dahm and Douglas Scalapino[14,15]. This work observed that in a d-wave superconductor the nonlinear Meissner effect (NLME) would produce IMD. The NLME refers to the breaking of Cooper pairs by a magnetic field, in this case the magnetic self-field of the microwave current. For fields small compared with the critical field, this effect is negligible in s-wave materials, like the classical LTS materials, vanishing exponentially at temperatures below T_c. However, in d-wave superconductors, or any other symmetry with nodes in the energy gap, the NLME can be appreciable, and Dahm and Scalapino showed that it increases sharply at low temperatures. This is counterintuitive, but it turns out that it is easier to break pairs at low temperatures. The pair breaking manifests itself as an increase in penetration depth. Thus, as derived by Dahm and Scalapino,

$$\lambda(j,T) = \lambda(T)[1 + \frac{1}{2}b(T)\left(\frac{j}{j_{pb}}\right)^2 + \ldots], \tag{8.18}$$

where j_{pb} is the pair-breaking critical current given by $ne\Delta_0/p_F$ and p_F is the Fermi momentum.

Figure 8.6 shows the results of the calculation by Dahm and Scalapino. As is obvious in the figure the difference between s- and d-wave is large. Since the nonlinearity *increases* at low temperatures this predicts that the IMD will also increase at low temperatures. When Dahm and Scalapino published the papers all attempts to observe the NLME in static fields had been unsuccessful.

My initial impression had been that the NLME would not be observable in the IMD either, because the weak links and other defects in the films would dominate over this intrinsic effect. That

[14] T. Dahm and D.J. Scalapino, *Appl. Phys. Lett.* 69 (1996) 4248
[15] T. Dahm and D.J. Scalapino, *Phys. Rev.* B 60 (1999) 13125

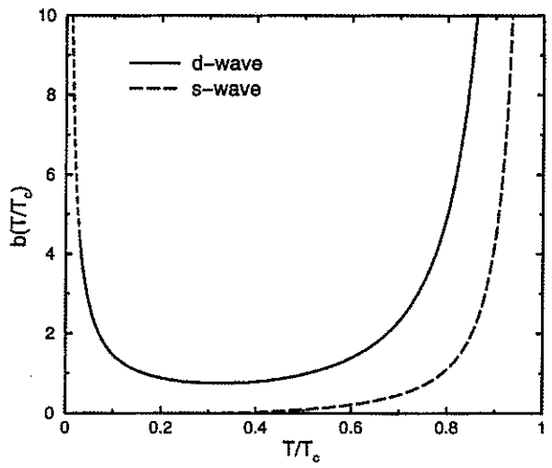

FIGURE 8.6: The leading order nonlinear coefficient $b(T/T_c)$ for the intrinsic nonlinear response of an s-wave (dashed line) and a d-wave superconductor (solid line). Here $2\Delta_0/kT_c = 6$ and currents running along the CuO bonds of the high-T_c cuprates have been assumed. The increase at low temperatures for the d-wave case will be cut off, if T/T_c falls below j/j_c .

is, the IMD was due to extrinsic effects and this intrinsic effect would be masked. Indeed many experiments had confirmed this view. A typical example is given in Willemsen et al.[16]

In spite of my doubts, with the aid of my student Sang-Hoon Park, I attempted to observe the low-temperature increase in IMD by measuring at lower temperatures than we had measured previously and using a very high quality film made by laser ablation by Gad Koren of the Technion in Israel. To my surprise we observed the effect quite clearly[17]. The results are shown in Figure 8.7. The NLME was observed this time because of the high-quality film that was used. Subsequently I have observed the same effect in many other films made by different deposition methods[11]. Although HTS films are known to contain various defects, in high-quality epitaxial films only very low angle grain boundaries are present and apparently other defects do not contribute significantly to the IMD so that the intrinsic d-wave properties dominate the IMD at low temperatures and low powers. Other researchers including the group led by Jim Booth at NIST Boulder[18] and the group of Antonello Andreone at the University of

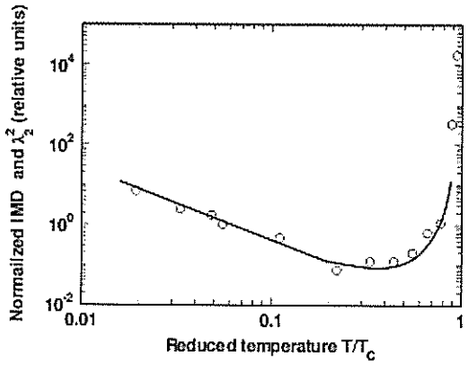

FIGURE 8.7: Comparison of data and theory. The empty circles are the IMD data from a high-quality film of $YBa_2Cu_3O_{7-\delta}$. The solid line is the calculation of d-wave theory.

[16] B.A. Willemsen et al., *Phys. Rev.* B 58 (1998) 6650
[17] D.E. Oates et al., *Phys. Rev. Lett.* 93 (2004) 197001
[18] K.T. Leong et al., *IEEE Trans. Appl. Supercond.* 15 (2005) 3608

Naples Italy[19] have observed the NLME in IMD measurements. The measurements of Andreone also included IMD of single crystals in which the NLME was observed.

Subsequently, another formulation of the theory of the NLME was developed by Dan Agassi of the Naval Surface Warfare Center in Bethesda MD. This theory was able to predict some further aspects of the NLME such as its nonlocal nature, but a full discussion is beyond the scope of this book. For detail see Agassi and Oates[20] and Oates et al.[21]

The IMD measurement of the NLME confirmed that IMD is an intrinsic effect in the cuprate HTS materials, thus leading to a better understanding of the IMD. In addition, the previous lack of success in observing the NLME was an outstanding missing piece in the d-wave hypothesis for the cuprates. The reason for the success of the IMD in observing the NLME is that the IMD is far more sensitive to changes in penetration depth than direct measurements. A value of $\Delta\lambda/\lambda$ of order 10^{-6} produces easily measurable IMD.

8.1.8 Summary and Future Prospects

I hope that I have provided some interesting examples of microwave measurement techniques that have illustrated the value of these techniques for exploring the fundamental properties of superconductors. Both historically and in the very recent past microwaves have proven to be a valuable technique in superconductivity. This was not intended to be an exhaustive listing of microwave measurements, but examples that I find particularly important.

I think that microwave techniques will continue to prove useful in characterizing superconductors. There are several very recent examples of publications dealing with the microwave properties of some of the newly discovered superconductors such as MgB_2 and the iron-pnictide materials. For example, a recent paper[22] presents measurements of MgB_2 showing evidence for unconventional symmetry as measured by microwave IMD. Also papers reporting measurements in the recently discovered pnictide superconductors are beginning to appear[23]. New explorations of the older materials will also undoubtedly continue. I cite a recent paper on the NLME in dirty s-wave superconductors, specifically niobium[24]. I expect the future of microwave characterization of superconductors to be as rich as the past has been. The situation can only improve as the technology of microwave measurements becomes more advanced and less expensive as is inevitable because of the intense interest in microwave wireless communication systems.

8.2 Applications of Passive Microwave Filters and Devices in Communication and Related Systems

R. B. Hammond, N. O. Fenzi and B. A. Willemsen

[19] A. Andreone et al., *IEEE Trans. Appl. Supercond.* 17 (2007) 3640
[20] D. Agassi and D.E. Oates, *Phys. Rev.* B 72 (2005) 14538
[21] D.E. Oates et al., *Phys. Rev.* B 77 (2008) 214521
[22] Y.D. Agassi et al., *Phys. Rev.* B 80 (2009) 174522
[23] T. Shibauchi et al., *Physica* C 469 (2009)590
[24] N. Groll et al., *Phys. Rev.* B 81 (2010) 020504

8.2.1 Introduction

This section focuses on the development and commercialization of HTS microwave filters for cell-phone base stations. This includes development of low-cost HTS film manufacturing and practical cryogenic systems.

In this short section we will try to address all the dimensions of a diverse subject—superconducting passive microwave devices—and we will provide suggested reading for readers interested in more detail. Most of our story will relate to the development and use of HTS filters for cellular telephone base stations. This became the primary focus of a great deal of research and technology development in HTS as well as several related fields. It also became a principal focus of commercial interest and investment in HTS during the mid-to-late 1990s. In addition, it is mostly a story that unfolded outside the public domain, mostly among the HTS companies and their wireless-industry customers. Here we attempt to reconstruct the key elements and events of that story.

Superconducting materials have been of interest for several decades to possibly replace the copper or silver used in radio frequency (RF) and microwave passive circuits where conductor loss and device size are the primary limitations to device performance and practicality. Candidate devices are primarily antennas, filters, and delay lines. Before the discovery of HTS very little development work was done. Design studies were performed for compact low-temperature-superconducting (LTS) antennas, and LTS microwave filters and delay lines were successfully demonstrated in the lab. No products resulted, however, due to the size, power requirements, reliability, and cost of the cryogenics needed to support these devices. The advent of HTS materials changed this, since operation at 77 K versus 4 K promised far more acceptable cryogenics.

Following the discovery of $YBa_2Cu_3O_7$ (YBCO) in early 1987, governments in the US, Europe, and Japan became substantial drivers in the definition of applications and funding the development of HTS materials and devices. Many large established companies became involved in the development efforts, facilitated by government funding. In addition, the excitement generated in the capital markets for the potential of HTS in the marketplace led to many new companies being formed, ultimately dozens around the world.

As early as 1987, HTS passive RF/microwave devices offered the potential for high value in a small size, since even the earliest bulk polycrystalline HTS materials showed substantially lower conductor loss than copper and silver, particularly at the lower microwave frequencies $\leq$10 GHz, and the potential reduction in size or the improvement in performance might be worth the cost of 77 K cryogenics for many applications. There were early demonstrations of high-quality-factor (Q) resonators and filters using these early materials. By April, 1990, 4 years after the discovery of HTS and 3 years after YBCO, the US Office of Technology Assessment had concluded that by ~1995 the early applications for HTS would be these devices or superconducting quantum-interference device (SQUID) sensors. Shortly thereafter it became understood that the passive microwave devices offered large existing applications and markets to justify a significant commercial investment.

Initially the market interest was for military and space applications. These both offered a wealth of diverse potential applications, where HTS passive microwave devices might provide better performance, smaller size, or both, and where those features were highly valued. By the early 1990s the explosive growth in cellular telephone networks offered another potential market.

Over about a decade from the early 1990s to the early 2000s, the cell-phone infrastructure market became the principal driver for what was ultimately the successful development of volume manufacturing of high-performance HTS materials and devices, as well as the development and volume manufacturing of reliable, maintenance-free cryogenic systems suitable for unattended operation in remote environments over many years. It is a story that grew out of the coincidence that HTS was discovered when cell-phone networks were just beginning a multi-decade period of extremely rapid growth and innovation. It involves famous people, became the focus of hundreds of millions of dollars in private sector investment, and helped some HTS start-up companies to briefly reach market capitalizations over a billion dollars in 2000.

The enormous worldwide excitement and enthusiasm generated by the discovery of the copper oxides and particularly YBCO in early 1987 led to a search for investment opportunities by large companies, investment companies, as well as private investors. New companies were started, and large companies began major R&D efforts. World-renowned scientists and engineers as well as highly successful technology entrepreneurs participated, a few directly as employees at new companies, but most as senior advisors, consultants, or board members. Two Nobel prize winners in superconductivity and the co-inventor of the integrated circuit all participated as board members. Of most relevance to this story were four new companies in the US, one in Germany, and one large company R&D effort in the US, all started within a year or two of the YBCO discovery. These attracted more than a decade of continuing investment funding, grew to efforts with ~50 or more full-time employees, with their principal focus becoming HTS passive microwave devices. Each ultimately developed and successfully trialed prototype HTS filter products in cell-phone base stations. Three of these companies established manufacturing and had their products purchased and installed into more than 100 base stations. Today there are HTS filters in approximately 10% of the 70,000 800-MHz cell-phone base stations in the US. That is about 40,000 HTS microwave filters and about 7,000 cryocoolers running continuously today in unattended locations. These HTS systems represent more than $150M in HTS product sales. They also represent the only broad application of superconducting or cryogenic systems in remote, unattended environments without requiring maintenance and with failure rates of 1% per year.

8.2.2 HTS Filters for Cellular Telephone Base Station Receivers

Background

After 1990 the search for products and markets for HTS continued unabated, particularly at the start-up companies that had to satisfy their investors to continue to receive funding. As time passed and the magnitude of the total private sector investment continued to rise, investors wanted products and markets that offered greater and shorter-term sales and profit potential.

By 1992–93, the wireless cellular telephone infrastructure original equipment manufacturers (OEMs) became important drivers for HTS-related technology development and innovation, sometimes with direct investment, but commonly and more importantly with clear, demanding application requirements: RF performance, size, reliability, manufacturing volume, and price.

The wireless opportunity for HTS narrowed fairly quickly to providing better microwave preselector filters for cell phone base-station receivers. Every cell phone base-station receiver had a preselector microwave filter at the time, which was usually a large silver-plated aluminum cavity filter, and very occasionally a dielectric-loaded cavity filter for higher performance.

It was argued that HTS filters would provide lower loss and noise, greater frequency selectivity, and/or smaller physical size than these alternatives. Thus, the geographic coverage area of the base station would be increased, adjacent band interference would be blocked, and less space would be consumed by the filters in the base station. In 1994–96, all the companies showed—in the lab—that they could make filters that did this. They used differing HTS materials and manufacturing methods, different substrates, different approaches to filter design, and different cryocoolers in their filter systems, which also began to be field tested at this time. By the late 1990s, the product focus became what was dubbed a "cryogenic receiver front-end" (CRFE) by Nippon Telegraph and Telephone (NTT) DoCoMo in Japan. NTT was a strong proponent of a CRFE solution for its planned new third-generation wireless (3G) network, which would start to roll out in 2000. The CRFE includes a high selectivity HTS filter followed immediately by a cryogenic low-noise amplifier. With this powerful combination the sensitivity of the base station receiver could be significantly improved, particularly in environments with significant adjacent-band interferors such as NTT faced with its 3G band assignment, and the US operators faced with their 800-MHz cellular band assignments.

One of the start-up companies in the US (Illinois Superconductor) became the first to consider

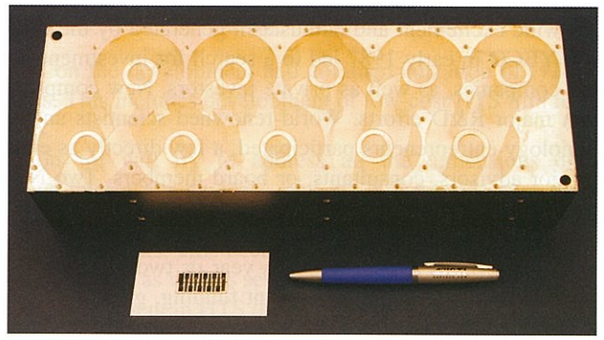

FIGURE 8.8: High performance conventional base station filter (top). Size comparison to HTS base station filter (bottom).

the cell-phone base-station market. Through ties with AT&T Bell Labs, it succeeded in getting a NIST Advanced Technology Program (ATP), funded in 1992. A second company (Superconductor Technologies Inc., STI, in Santa Barbara) at about the same time found interest from base-station OEMs Motorola and Ericsson, in this application, and Motorola funded them to develop a prototype starting in 1993. A third company (Conductus in Sunnyvale), also with ties to AT&T Bell Labs, began to look at this opportunity in 1993, exploring both HTS transmitter filters and receiver filters. A fourth company (Superconducting Core Technologies, SCT, in Colorado) began to work in this area in 1994, and focused on receiver filters primarily for increasing coverage.

Three of the US HTS start-up companies went public in 1993, mostly based on relatively broad-based stories regarding product and market opportunities for HTS; these included extremely fast fluxon-based digital electronics, SQUID sensors, magnetic resonance (MR) RF pick-up coils, RF and microwave filters for defense applications, and—most often—filters for cell-phone base stations. By about 1996, the main focus of the companies had narrowed to the cell-phone base-station opportunity, although the best funded kept some efforts going in other areas: defense/space electronics and digital electronics.

Markets

Cellular telephone systems began to appear in the early 1980s. By 1990, cell-phone networks were growing rapidly in the developed world, and continued to grow at an exponential pace throughout the 1990s and well into the 2000s. The uplink, the radio link from the cell phone to the base station, is the weaker of the two links supporting a two-way conversation, because the microwave transmit power of the cell phone is lower than the microwave transmit power of the base station. As cell phones became steadily smaller in size, cell-phone transmit power was reduced even further to maximize battery life. (Users become very annoyed when their cell phone batteries run out of juice!) This has driven a need for more sensitive base-station receivers. The CRFE provides unique benefits to cellular network performance as a simple add-on to an existing base station or as a designed-in subsystem. A CRFE is a high-selectivity, low-insertion-loss HTS filter followed by a high-linearity, cryogenic, ultra-low-noise amplifier (LNA) placed between the base-station receive antenna and the base-station receiver. The very low loss of the filter combined with the very low noise of the cryogenic amplifier combine to substantially reduce overall receiver noise level, typically by about a factor of two, thus extending uplink range and the geographic area covered by a base station. In addition, the high frequency selectivity of the HTS filter can reject large adjacent-frequency-band interfering signals that produce distortion in the base-station receiver. An added benefit is that the entire CRFE can be significantly smaller in size than conventional high-selectivity filters that might

otherwise be used to provide interference protection at the expense of added loss and noise.

In the 1990s, cellular base station manufacturers and cellular network operators expressed a variety of reasons for using the CRFE, always some combination of the three benefits described above. Four are worth particular mention because of their importance to the development and sales of CRFE products. In the mid-1990s, one base station manufacturer (Motorola in the US) was interested in reducing the size of filters for its 800-MHz base stations. These were starting to dominate the base station size and were resistant to further size reduction, unlike the rest of the base station components. Also beginning in the mid-1990s and continuing right up to the present day, several US operators have been interested in a combination of uplink range extension and interference rejection in their 800-MHz base stations. In the late 1990s through early 2000s NTT DoCoMo in Japan was interested in blocking interference to the Japanese 1900-MHz 3G bands. Most recently, in the late 2000s and into the 2010s, some US carriers are interested in the CRFE to block adjacent-band interference in their new 700-MHz fourth-generation wireless (4G) bands.

OEM sales (as opposed to network-operator sales) of CRFEs are most sought after because of the opportunity offered for high-volume sales, typically tens of thousands of base stations for a single product. Despite some near misses this has not yet happened for CRFEs. (Just such an opportunity seems to be emerging in the 4G 700-MHz networks being in the US though!) Motorola's interest in reducing filter size in the mid-1990s resulted in a CRFE prototype (developed by STI) that met its most demanding requirements for frequency selectivity and would fit in one tenth the volume of its existing conventional filter product. This reduced size included the cryocooler, cryogenic package, and control electronics—the HTS filters themselves are much smaller. The CRFE prototype was qualified by Motorola for network deployment in 1996, but the HTS industry was not able to respond with sufficient manufacturing capacity to meet Motorola's needs at that time. It would take ~5 years for the HTS industry to close this gap in manufacturing capacity, but by then it was too late; that market window had closed. In the late 1990s and early 2000s NTT pushed its OEM suppliers (such as Matsushita (MCI)) to provide extremely sharp HTS filters in their 3G base stations for interference protection. Again, a product was qualified for the application and for network deployment, but this time the industry could not meet the selling price required by the OEM. Most recently a US operator has pushed its OEM suppliers to provide extremely sharp HTS filters in their new 4G base stations. Once again, a product has been qualified, and sales are expected to begin in 2012. To date, although products have been successfully developed and qualified, there have been no sales to OEMs of CRFE products besides a few dozen test and qualification units. Despite the variety of the early interests expressed by major wireless industry players in potentially using the CRFE, it has been the presence of strong adjacent-band interference in some cell-phone services that became the primary sustained driver for the development and sales of CRFE products. By far the most important, and responsible for virtually all CRFE sales to date, is the 800-MHz cellular band in the US. There are several significant sources of adjacent-band interference, as indicated in Figure 8.9.

Another important source of adjacent band interference to cell phones that drove substantial CRFE development is in the 3G bands in Japan, indicated in Figure 8.10.

In the mid-to-late 1990s when no OEM, network-designed-in, opportunities for CRFE had materialized, most of the companies had started to market their CRFE products directly to the network operators, the wireless telephone companies. It is these cellular phone service providers, close to the cell phone user's experience and thus concerned about improving service, that have proved the largest customers for HTS filter systems to date. Going this route allowed higher prices, but much smaller unit orders, lower total sales volume and higher cost of sales. Actual sales of CRFEs began with small local operators in the US, some with as few as a dozen base stations. This provided a much easier sales channel than the OEMs or even the large network operators, and the timing was right because these mostly rural carriers were experiencing the shift from car phones to handheld cell phones which had much lower transmit power. Network geographic coverage typically dropped by more than 50%. In many cases, the addition of the CRFE brought most of that back, and the chal-

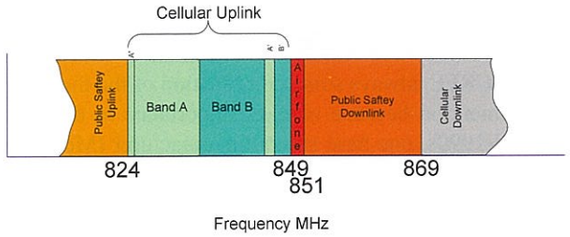

FIGURE 8.9: The 800-MHz cellular uplink bands in the US (light green A; blue B) were initially 10 MHz each. Then the A' and B' frequencies were added to make the total 12.5 MHz each and resulted in the unusual split shown in the figure. There are three sources of interference to the base-station receiver. The first is the close interleaving of the two operators' spectrum assignments which creates an unusually severe "near-far" interference. This type of interference occurs when a competing service's cell-phone user is close to your base station and far from its own base station and thus is transmitting at high power. The second is the Airfone service: high-power, always-on transmitters located near airports to provide telephone service on commercial flights (mostly not in use since ~2005). The third is high-power, always-on, public-safety transmitters that provide two-way radio voice communications for police, fire, and other emergency services.

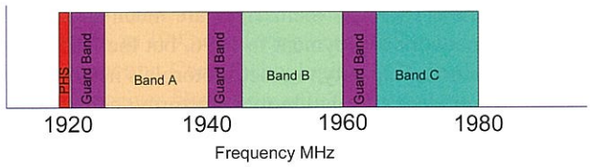

FIGURE 8.10: Personal Handyphone Services, PHS, widely used for data services in Japan, prevent the use of the first 5-MHz 3G channel in the KDDI band assignment unless an HTS filter is used. The Japanese government has prevented the other two carriers from using their first channel assignment as well, just to be fair to all.

lenge for the HTS companies was to offer a reliable product fairly quickly to capture the opportunity at the $20K to $30K per base station that the market was ready to pay.

Between 1996 and 1998, CRFE systems were sold to a number of operators in the US, totaling about 100 base stations. The first large single order was announced in 1999 (CRFE systems for 500 base stations) to a large regional cellular operator in the US (US Cellular). Another large order of 160 sites to Alltel, another large regional operator, was made by another CRFE supplier in the US at about the same time. Larger CRFE orders for 1,000 base stations by Alltel were announced during the following 3 years. Sales peaked in 2003 with CRFE systems sold and installed that year into 2,000 base stations in the US. At this point, sales dropped to under 1,000 per year, where they remain today. The early growth and the peak in 2003 was encouraged by the December, 2003, FCC-mandated change to local number portability (LNP). This would allow US cellular phone customers for the first time to retain their phone number when they changed phone companies. The change had been announced years in advance and the carriers had responded by investing in their existing network performance to give their existing customers the best possible service in advance of the deadline, hoping to reduce their motivation to switch to another carrier. In 2004, and for several years after that, the carriers focused on building out their 1900-MHz networks to expand capacity, and to utilize the spectrum bands which they had invested billions of dollars in acquiring/licensing in the late 1990s. The network build in 1900 MHz proved not to be a CRFE opportunity due to lack

of adjacent band interference.

Since 2003, the US network operators have continued to rely on their 800-MHz networks as the backbone of their services for both voice and data, due to the much better propagation of the wireless signals in the atmosphere and better penetration of buildings and other physical obstacles. The CRFE has continued to be used as a tool to fix weak sites in their networks, and sales continue at several hundred sites per year.

In 2008, new spectrum was auctioned at 700 MHz in the US. Major carriers such as Verizon and AT&T invested more than $20B in the new spectrum to provide new 4G services. Some of the new bands, as was the case for the original 800-MHz bands assigned in the 1980s, suffer from strong adjacent band interference, as indicated in Figure 8.11.

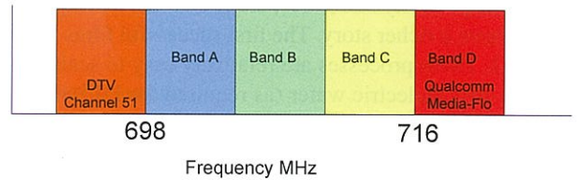

FIGURE 8.11: Broadcast services such as MediaFLO and UHF digital television provide strong interference in the lower 700-MHz bands, A thru C.

A CRFE product has been designed into the base station by one of the two major OEMs that are be building these networks. So the long-sought-after OEM opportunity for HTS filters for designed-in, initial deployment in base stations for new network roll-out may finally be on the verge of happening. Stay tuned.

HTS Film Production

Base-station RF receiver filter requirements drive the requirements on the HTS materials and filter structures utilized for HTS base-station filters. The filter microwave performance requirements are best summarized in two parameters: quality factor (Q), and third-order intermodulation-distortion intercept point (IP3). Q is a measure of the loss in the resonators in the filter and determines both the loss and frequency selectivity achievable. IP3 is a measure of the linearity of the filter response, i.e., its ability to pass signals or block interference without adding distortion to the wireless signal of interest. HTS filter resonator Q's must be ~100,000 or higher, and filter IP3 must be ~100 mW or higher for base station filter applications. These filter characteristics are determined by the surface resistance of the superconductor (Rs), any losses added by the HTS substrate material (dielectric loss tangent), the resonator structure chosen, and the microwave critical-current density of the superconductor (J_{IMD}).

The early, bulk, polycrystalline HTS materials were soon improved upon by other synthesis approaches for making practical microwave filters. Demonstrations of many approaches were successfully performed in the lab during the period 1987–90. Thick-film, melt-processed, polycrystalline YBCO films can be formed on refractory metal substrates (or ceramics) and achieve sufficient properties for filters if relatively large, 3-dimensional resonator structures are used. These also are relatively easy to put into production at low cost. Thin films of single-crystal HTS materials can be formed on single-crystal oxide wafers ($LaAlO_3$, MgO, sapphire) most often with much better microwave properties than the polycrystalline films, but the single-crystal substrates are expensive. These can often achieve sufficiently low loss for filters in small 2-dimensional microstrip-resonator

structures (which require HTS films on both sides of a dielectric substrate/wafer), if the substrate has low microwave loss like $LaAlO_3$, MgO, sapphire. There are two basic approaches to forming these films. Ex-situ films are formed by depositing at room temperature a layer on a wafer with the appropriate mix of metals (Y, Ba, Cu), usually in oxide form. Then the wafer is placed in an oven in a controlled atmosphere at ~ 800 °C, for tens of minutes to grow an HTS single-crystal film from the single-crystal substrate template beneath. In-situ films are formed by depositing the appropriate mix of metals (Y, Ba, Cu) onto a single-crystal wafer heated to 800 °C in the presence of oxygen. The HTS single-crystal film grows epitaxially on the single-crystal wafer, layer by layer, while the metals are being deposited. Commonly there is a subsequent heating of the final HTS film in oxygen to complete the film synthesis.

Thick-film YBCO processes were successfully developed at a large chemical company in the UK (ICI), put into production by Illinois Superconductor, and used to develop three dimensional (3-D) HTS filters, first with fairly large cavity structures, later with more compact split-ring resonators.

Thin-film processes represent a richer story. The first successful films were formed in 1987 using ex-situ methods with YBCO. These processes are relatively easy to scale to large wafer areas, with films on both sides of a low-loss dielectric wafer (as required for HTS filters and other passive microwave devices); however, sufficient quality material could not be formed in thicknesses more than about half the penetration depth at 77 K, insufficient for devices that rely on very low microwave loss. In-situ YBCO processes received intensive development in the period 1987–92. Virtually every known technique for forming in-situ epitaxial thin films was tried. Many of these were successful in forming single-crystal films with low enough loss. However, all these techniques ultimately proved to be too expensive to scale to the manufacture of the minimum 2-inch, double-sided wafers needed for devices.

Successful in-situ growth of YBCO films requires three conditions to be met during the entire growth of the film: a) maintain a temperature of ~800 °C with ±1 K stability, b) maintain specific ratios of Y, Ba, and Cu, stable to ±2%, and c) provide an oxygen pressure at the film growth interface of >~ 100 mT. This was known by the early 1990s. It was due to this new and unique combination of requirements that no pre-existing epitaxial-growth process proved scalable at low cost for 2-inch double-side wafer manufacturing. A new type of process appeared in the early 1990s that was developed specifically to meet YBCO's special epitaxial-growth requirements.

In 1992–93 a novel in-situ process was developed to form YBCO thin films which proved to be scalable for low-cost production. The basic concepts were developed at the Technical University of Munich. A company was formed, THEVA, which became the first (in 1995) successful supplier of YBCO-coated 2-inch, double-side wafers with low loss for microwave devices and other applications. Conductus adopted and adapted this approach for manufacturing YBCO wafers.

In early 1988 the thallium barium calcium copper oxide (TBCCO) family of HTS materials was discovered. For these materials ex-situ processes did prove to be successful in forming single-crystal films with low enough loss for devices. In the early 1990s DuPont Superconductivity and STI put the $Tl_2Ba_2CaCu_2O_8$ on $LaAlO_3$ material into production, manufacturing 2-inch, double-side HTS wafers with low microwave loss. Both companies offered these wafers for sale and also used them internally to develop devices.

In 1994 it was discovered that the existing film manufacturing processes did not meet requirements for base station filters. In 1994, Ericsson and Motorola tested early HTS base-station filters and found that they met Q requirements but not IP3 requirements. This drove the film manufacturing processes further. Beginning in 1995, a new process for ex-situ TBCCO was developed on buffered MgO wafers, first at STI then later at DuPont Superconductivity that met all the base-station filter requirements. Meanwhile, base-station filter IP3 requirements drove improvements to the in-situ YBCO wafer manufacturing that were ultimately successful first at Conductus (late 1990s) and later at THEVA at meeting filter IP3 requirements. The filter IP3 requirements also drove accurate electromagnetic analysis of superconducting microstrip structures in order to infer the limiting RF critical current density of the superconducting material from the intermodulation distortion (IMD)

measurements. These studies resulted in the notation J_{IMD} for the limiting RF critical current density J_c in the superconductor. In general it was found that this critical current cannot be inferred from dc critical current density—different physics is responsible for these two limits. Thus, measurement of filter IMD became necessary to guide HTS material process development. As noted, this was accomplished successfully in both TBCCO and YBCO.

In December 2002, Conductus and STI merged. To achieve both the lowest manufacturing cost and the highest RF performance, in 2004 the merged company discontinued TBCCO production and changed over completely to the Conductus YBCO process, which was then scaled to high volume, semi-automated production of 2-inch double-sided YBCO wafers for filters. Interestingly, this process produces both the best RF properties for HTS films and by far the lowest manufacturing cost of any HTS film production process. The current production machine produces 22 2-inch wafers per run, and has capacity for 15,000 double-side wafers per year.

Of the 40,000 or so HTS filters in base stations today about two thirds are TBCCO and one third are YBCO.

HTS Filter Designs and Performance

The first CRFEs were built with 3-dimensional cavity resonators utilizing thick-film YBCO. These were also the first systems sold and installed into cell-phone base stations. Later the market required smaller filter systems than the multiple cubic meters required for these designs. These thick-film filters evolved to using split-ring resonators, much more compact designs, allowing systems comparable in size to that permitted by the thin film microstrip HTS filters.

Microstrip HTS filters required the development of novel resonator structures to enable the complex, high-selectivity HTS filters that were developed to be realized on compact chips. Many types of resonators were used. These evolved initially from simple half-wavelength lengths of microstrip transmission line that were edge coupled in a classic configuration for thin metal films. To reduce chip area, these structures were subsequently folded and wrapped in a variety of ways to make compact resonators that would achieve high Qs and be easily coupled with similar resonators in a controlled manner on the same chip. Figure 8.12 shows an example of an early HTS filter chip. Figures 8.13 and 8.14 show the measured insertion loss versus frequency of production HTS filters.

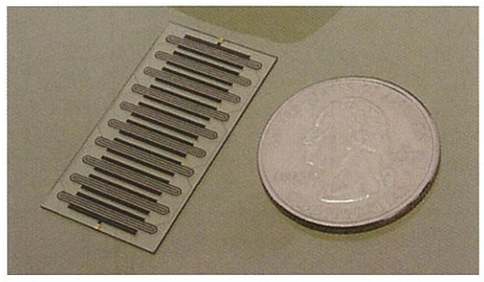

FIGURE 8.12: HTS filter chip compared in size to a US coin. The filter is 34 mm×18 mm×0.5 mm in size.

Other New Technologies for CRFE

Cryocooler—Long-life, no-maintenance, low-cost cryocoolers were developed.

Cryo-LNA—Low-noise, high-linearity, cryogenic, microwave semiconductor amplifiers were developed.

Cryo-cables—Low thermal conductance, low-RF-loss transmission lines were developed.

Dewars—Large, permanently sealed, long-life dewars were developed.

Automation—Automated frequency setting/tuning for manufacturing filters was developed.

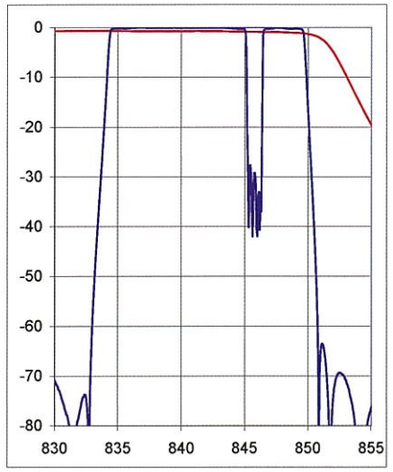

FIGURE 8.13: Measured insertion loss of a production HTS filter pair for a US 800-MHz B-Band base-station receiver. Two filters are cascaded in series: a bandpass filter followed by a bandreject filter. The red line shows the response of the standard base station receiver filter for comparison.

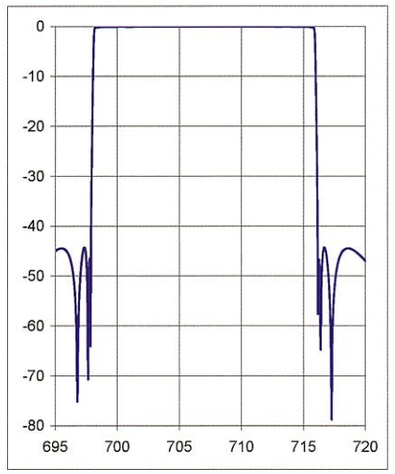

FIGURE 8.14: Measured insertion loss of a prototype HTS filter for US lower 700-MHz A,B, or C Band base station. The filter protects the base-station receiver from the digital television broadcast services at channel 51 and below and channel 55 (MediaFLO).

CRFE Products

Illinois Superconductor was the first to market with a CRFE product. It used thick film YBCO cavity resonators cooled with an off-the-shelf Gifford-McMahon (G-M) cryocooler. The filter provided very high selectivity. In the late 1990s they converted their HTS filters to a much more compact split-ring-resonator design and named the new CRFE the "ATP" (all temperature product) since

TABLE 8.1: Summary of CRFE Cryocoolers Designed Specifically for CRFE Products

Cryocooler Name	Company	Cycle	Lift, 77 K	Power	Weight	CRFE
Cryodyne M-22	CTI Cryogenics	G-M	11 W	250 W	20 kg	ClearSite
Polar SC7	Leybold	Stirling	8 W	250 W	8 kg	DE, CO, IL
Sapphire	STI	Stirling	5 W	120 W	3 kg	SuperLink

it was designed to maintain some filtering even at room temperature, in case the cryogenics failed. It utilized the Leybold cooler.

SCT was also early to market with a CRFE product. They had a system designed to be mounted on the antenna tower with an off-the-shelf G-M cryocooler. The cryocooler compressor was placed on the ground and the cold head at the top of the tower with the thin-film TBCCO filters. They transitioned this to a Stirling-cryocooler-based system at about the time the company shut down, and its technology and key staff were picked up by a new company, Spectrum Solutions Inc. (SSI) also in Colorado, which marketed the new CRFE.

TABLE 8.2: CRFE Prototypes and Products

CRFE	Company	HTS	Cooler	Power (W)	Sales (sites)
SpectrumMaster	Illinois	Thick Film Y123	G-M	2,000	200
ATP	Illinois	Thick Film Y123	Leybold	250	N/A
REACH	SCT	Thin Film Tl2212	G-M	2,000	N/A
SC200	SSI	Thin Film Tl2212	Leybold	250	~10
ClearSite	Conductus	Thin Film Y123	CTI	550	~200
SuperFilter	STI	Thin Film Tl2212	Sapphire	120	~1000
SuperLink	STI	Thin Film Tl2212/Y123	Sapphire	120	>5,000
CRFE D8	Cryoelectra	Thin Film Y123	Leybold	250	N/A

Conductus and STI both came to market with CRFE offerings in the 1996–97 timeframe. Conductus used the new G-M cryocooler from CTI designed specifically for the application. STI used an in-house developed Stirling cryocooler named "Sapphire".

Cryoelectra built several prototype CRFE systems in the mid-2000s and some were trialed in cell phone base stations in China. They also used the Leybold cryocooler.

CRFE Reliability

In the case of LTS, it had been the cost and reliability of the cryogenics that had kept superconducting passive microwave devices from being used in practical applications. With the discovery of HTS and the advent of devices operating at 77 K, the hope was that the cryogenics would be far cheaper and more practical. And indeed it was and is. However, despite that, for the companies developing CRFE products and marketing them to wireless companies, it was the poor reliability of their cryogenic systems, far more than any other factor, that became the primary stumbling block to commercial success. Several significant sources of failure had to be overcome successfully. The combination proved to be extremely challenging, and ultimately only one product line emerged successfully.

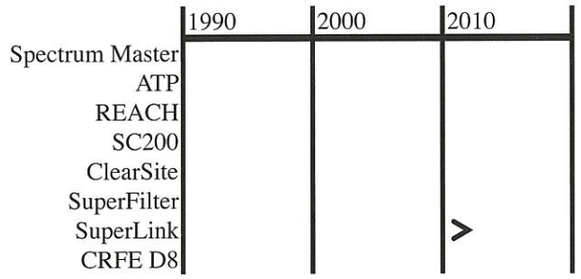

FIGURE 8.15: CRFE product timeline.

FIGURE 8.16: 3 CRFE systems shown with one another; each servicing a single 3-sector base station with 6 base station receivers for the US 800-MHz market. ClearSite (lower right), SuperFilter (upper right), and SuperLink (upper left).

OEM requirements for base-station subsystem reliability and service (250,000-hour mean time between failures, MTBF, no maintenance) became a major challenge to CRFE companies. The CRFE is a complex system requiring a reliable cryocooler, a reliable long-life dewar, and reliable power supplies and system control electronics. Only one CRFE was qualified for OEM use in the 1990s primarily for this reason.

Operators did not qualify products rigorously like the OEMs. They were willing to try new products to see if they provided the benefits they were looking for, and then would test reliability against actual performance in the field combined with the support provided by the vendor company supplying the product. Because CRFE companies focused their attention on selling to operators, several companies made at least a few CRFE units that were tested in base stations by operators. Two companies were successful in getting orders for ~200 sites, and ultimately shipping and installing CRFE systems into those sites. None of these products though proved to be reliable enough to last more than a few months to a year or so in the field. Ultimately they were all taken out by the operators due to poor system reliability. The reasons for failure of course included the cryocoolers and the dewars, but system power supplies and control electronics also proved to be major sources of failure; these too are part of the cryogenics support system for the HTS filters. One CRFE company was successful in meeting the reliability needs of the operators. It is this company, STI, that succeeded in manufacturing reliable CRFE systems, that has sold thousands of systems and remains in this business today.

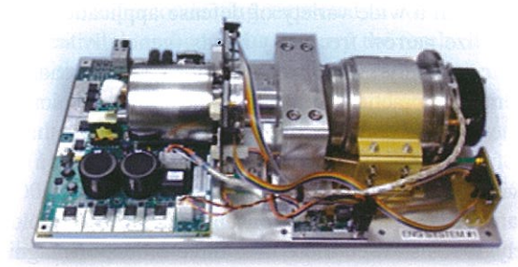

FIGURE 8.17: CRFE system designed into the base station of one of the two primary OEMs for the 700-MHz 4G network roll-out in the US beginning in late 2010.

8.2.3 Other SC Passive Microwave Devices

A wide variety of HTS passive microwave devices have been successfully demonstrated in the lab over the past 2+ decades. These include antennas, filters, delay lines, multiplexers, etc. (The suggested reading provides good information on these devices.) Two are worth more detailed mention here: commercial satellite communications filters and switched-tuned filters for defense receiver applications.

COMDEV and DuPont collaborated on a program in the late 1990s, early 2000s, to develop and demonstrate HTS output-multiplexer filters for satellite-based communication transceivers. A thorough design and cost analysis was completed and lab prototypes were successfully built and tested. This is an application where there is a high premium on system weight because of the high cost of launching satellites into orbit around the earth. The microwave filters in a communications satellite comprise most of the weight of the transceiver systems and thus for decades have been an area of intense technology development and innovation. The low weight of HTS filters, even when combined with the required cryogenics systems to cool them, offers the promise of reduced total system weight and volume; additionally since the application can support relatively high cost, that is not expected to be a major barrier to broad usage. The COMDEV/DuPont joint program concluded that for the lower communications bands, e.g., C-Band (~ 4 GHz), that HTS filters could be lower weight and thus attractive compared to the best conventional solutions. At the higher frequency bands, e.g., Ku-Band (~ 12 GHz), and above, the conventional approaches would still be preferred simply on a performance/weight basis. Please see the review paper by R. Mansour in the suggested reading for a detailed review of this excellent work.

Extremely compact, high-selectivity, fixed-frequency HTS filters were demonstrated in thin-film form as early as the late 1980s. The possibility of using efficiently switched or tuned arrays of

such filters offered the potential to provide extremely effective protection not otherwise possible for microwave receivers used in a wide variety of defense applications. Unlike most commercial microwave systems that utilize narrow frequency bands (generally $\ll 10\%$ total bandwidth), defense microwave systems commonly utilize frequency bands far broader in frequency ($\gg 10\%$). Because of this it is generally impractical to use high-performance microwave filters ($Q > 1{,}000$) in these systems due to the size and complexity of the arrays of filters that would be required to be useful. With the advent of extremely compact HTS filters, this situation changed. The volume required for a high-selectivity HTS filter at microwave frequency ($Q \gg 1{,}000$) could be many orders of magnitude smaller than any high-selectivity conventional filter technology. Lab demonstrations of HTS filters in the early 1990s showed more than three-orders-of-magnitude volume reduction. This sparked considerable interest and many DoD-funded development programs throughout the 1990s and well into the 2000s. An enormous variety of HTS filter switching approaches were tried. These included cryogenic semiconductor switches, photoconductors, and microelectromechanical systems (MEMS); each was implemented in a variety of circuit configurations to achieve the lowest loss and greatest linearity. In addition, a wide variety of mechanisms were tried to provide continuous frequency tuning of the HTS filters, e.g., semiconductor varactors, ferroelectric materials, magnetic materials, MEMS capacitors, micro-stepping-motor-driven HTS plates. Many impressive lab demonstrations were performed. These achieved broad tuning ranges ($> 20\%$), high Qs($\sim 100{,}000$), high tuning speeds (microseconds), and sometimes high linearity. No products have yet appeared, but this remains an area of great interest and potential for HTS microwave devices.

8.2.4 Summary and Looking Ahead

HTS opened the door for market entry of superconducting passive microwave devices. It simultaneously provided an impetus for the development and production of commercially viable HTS thin-film materials and reliable cryogenics systems. There is a market opportunity at this writing (October, 2010), for the emergence of the first designed-in HTS filter systems in cell phone base stations in the 700-MHz 4G roll-out in the US. In addition, in-situ YBCO manufacturing processes developed for low-cost wafers may in the future provide the foundation for low-cost HTS wire. Finally, the independent development of ion-beam-assisted-deposition (IBAD) of single-crystal MgO films on noncrystalline substrates can offer the chance to remove the last major cost element of HTS wafers — the single crystal substrate. This would open the door to the development of low cost HTS transmit filters with $Q \sim 10^6$ for high power (100s of watts or more) applications in cell phone base stations and other RF/microwave applications.

8.3 Superconducting Quantum Electronics Enabling Astronomical Observations

T. M. Klapwijk

On May 14th 2009 the Herschel Space telescope was launched from Kourou, French Guyana, to the 2nd Langrangian (L2) orbit with enough helium on board for a period of about 3 years to perform heterodyne spectrosocopy[25] of the interstellar gas with the Heterodyne Instrument for the Infrared (HIFI). While we commemorate the discovery of superconductivity 100 years ago, superconductivity plays an active role at a distance varying between 1.2 and 1.8 million kilometers from

[25] T. de Graauw et al., *Astronomy and Astrophysics* 518 (2010) L6

the planet Earth to unravel the evolution of the interstellar matter (Figure 8.18). When the superconductors in Herschel cease to be superconducting, expected in 2012, the Atacama Large Millimeter Array (ALMA) will be operational, and continue to carry the torch of the astronomical use of the superconducting state. It is the culmination of detector-research started around 1975, based on a phenomenon discovered in 1962 by Dayem and Martin[26] and subsequently called photon-assisted tunneling in the theoretical interpretation offered by Tien and Gordon[27]. HIFI was optimized to perform three key-tasks: (1) observations of water lines ending in the ground states, which are essential for absorption studies of cold water (557 GHz, 1.11 THz, and 1.67 THz), (2) a survey of the molecular complexity of the Universe and (3) observation of red-shifted ionized carbon[CII] at 1.9 THz. These astronomical frequencies indicate that the photon-energies are stretching the limit of the superconducting material, set by the energy gap of niobium at 700 GHz.

8.3.1 The Electrodynamics of Superconducting Films

The absorption of far-infrared radiation in thin superconducting films is one of the striking direct indications of the existence of an energy gap Δ in the electronic states of a superconductor[28,29]. The early observations even preceded the theoretical interpretation known as the BCS-theory[30] and were rapidly incorporated in the theory for the electrodynamics of superconductors by Mattis and Bardeen[31]. The real, σ_1, and imaginary, σ_2, parts of the complex impedance are given by:

$$\frac{\sigma_1}{\sigma_n} = \int_{\Delta}^{\infty} dE[f(E) - f(E+\hbar\omega)] \frac{2(E^2+\Delta^2+\hbar\omega E)}{\hbar\omega\sqrt{E^2-\Delta^2}\sqrt{(E+\hbar\omega)^2-\Delta^2}} + \int_{\Delta}^{\hbar\omega-\Delta} dE[1-2f(\hbar\omega-E)] \frac{\hbar\omega E - E^2 - \Delta^2}{\hbar\omega\sqrt{E^2-\Delta^2}\sqrt{(\hbar\omega-E)^2-\Delta^2}} \tag{8.19}$$

and

$$\frac{\sigma_2}{\sigma_n} = \int_{\Delta-\hbar\omega}^{\Delta} dE[1-2f(E+\hbar\omega)] \frac{E^2+\Delta^2+\hbar\omega E}{\hbar\omega\sqrt{E^2-\Delta^2}\sqrt{(E+\hbar\omega)^2-\Delta^2}} \tag{8.20}$$

with σ_n the normal state conductivity. In thermal equilibrium, the complex impedance is determined by the temperature through the Fermi-Dirac distribution function $f(E)$ and depends on the frequency ω. The integral runs over the energies E. For $\hbar\omega \geq 2\Delta$, where the photon energy exceeds the energy gap 2Δ, the loss rapidly increases because of the creation of quasiparticles. These expressions assume uniform superconducting properties, although in practice the superconducting films may be bilayers of niobium and aluminium or consist of material with properties that vary over the thickness of the film[32]. In both cases the energy terms will be modified and will depend on the material characteristics[33].

At low frequencies down to $\omega = 0$ the superconducting film is lossless. However, with increasing electron temperature dc resistance gradually emerges, in particular close to the critical temperature

[26] A.H. Dayem and R.J. Martin, *Phys. Rev. Lett.* 8 (1962) 246
[27] P.K.Tien and J.P.Gordon, *Phys. Rev.* 129 (1963) 647
[28] M. Tinkham, *Phys. Rev.* 104 (1956) 845
[29] R.E. Glover and M. Tinkham, *Phys. Rev.* 104 (1956) 844
[30] J. Bardeen et al., *Phys. Rev.* 108 (1957) 1175
[31] D.C. Mattis and J. Bardeen, *Phys. Rev.* 111 (1958) 412
[32] S.C. Zhu et al., *Appl. Phys. Lett.* 95 (2009) 253502
[33] S.B. Nam, *Phys. Rev.* 156 (1961) 470

T_c, due to time-dependent changes of the macroscopic quantum phase of the superconductor (See for a recent review Halperin *et al.*[34]). These processes play a stronger role in materials with a high level of disorder and they are particularly relevant for hot-electron bolometers discussed in Section 8.3.8.

8.3.2 Photon-Assisted Tunneling with Superconductors

Early on it was proposed by Burstein et al.[35] that the absorption of photons in superconducting films can be used, analogously to photo-excitation in semiconductors, to detect radiation in the submillimeter range. The created excess quasiparticles should be measured with a superconducting tunnel-junction[36], which carries a quasiparticle current I_{qp} given by

$$I_{qp} = \frac{1}{eR_N}\int_{-\infty}^{\infty} dE N_1(E)N_2(E+eV)[f(E)-f(E+eV)] \tag{8.21}$$

with N_1 and N_2 the usual BCS density of states of the two superconductors, being 0 for $|E| < \Delta$ and equal to $E/\sqrt{E^2-\Delta^2}$ for $|E| > \Delta$. V is the applied dc voltage and E the quasiparticle energies. Such a detection mechanism, due to absorption in one of the superconducting films, would have a low-frequency cutoff given by the energy gap and only be relevant for frequencies in the submillimeter range and higher. The tunnel current (Eq. 8.21) is merely a probe of the absorbed quasiparticles in the superconducting film and assumed to be not effected by the microwave field.

In reality, the quasiparticle tunnel current itself responds directly to the electromagnetic field. Dayem and Martin [26] discovered experimentally that the quasiparticle current of a tunnel junction increases strongly by photons with energies far below 2Δ. They find stepwise increases of current for voltages given by $eV = 2\Delta - n\hbar\omega$, with n an integer. Obviously this cannot be understood as due to photo-excitation of quasiparticles in the superconductor.

An explanation has been provided by Tien and Gordon[27], who assume that the electromagnetic field sets up a potential difference across the tunnel barrier between the superconducting electrodes given, for example, by

$$V_{rf}\cos\omega t \tag{8.22}$$

with V_{rf} the amplitude of the voltage across the barrier and ω the radial frequency of the incoming signal. This time dependent voltage modulates the energy levels in electrode 1 with respect to electrode 2. The single-particle wave functions in electrode 1 with the microwave field are given by:

$$\psi(\mathbf{r},t) = \psi(\mathbf{r})e^{-\imath Et/\hbar} \tag{8.23}$$

with the energy E referred to $V_{rf}\cos\omega t$. This leads effectively to a modification of the density-of-states to

$$N_1'(E) = \sum_{n=-\infty}^{\infty} N_1(E+n\hbar\omega)J_n^2(\alpha), \tag{8.24}$$

with $\alpha = eV_{rf}/\hbar\omega$, J_n the n-th order Bessel-functions, and N_1 the undisturbed BCS density of states. By substituting this new expression for the density of states into Eq. 8.21, Tien and Gordon find a natural explanation for the observations of Dayem and Martin. The photon-assisted tunneling curve $I_{qp}(V)$ is given by

$$\frac{1}{eR_N}\sum_{n=-\infty}^{\infty} J_n^2(\alpha)\int_{\infty}^{\infty} dE N_1(E+n\hbar\omega)N_2(E+eV)[f(E+n\hbar\omega)-f(E+eV)]. \tag{8.25}$$

[34] B.I. Halperin et al., arXiv:1005.3347v1 (2010)
[35] E. Burstein et al., Phys. Rev. Lett. 6 (1961) 92
[36] I. Giaever, *Phys. Rev. Lett.* 5 (1960) 147

Note that the theoretical approach taken by Tien and Gordon (Eqs. 8.22–8.24) is not unique to superconductive tunnel junctions. It is applicable to any quantum conductor in which the energy is conserved in a conductor coupled to two well-defined equilibrium reservoirs of electrons. However, the sharp nonlinearity resulting from the superconducting density-of-states leads to the very useful strong signatures of the photon-assisted tunneling process in the I,V curve.

This important insight into quasiparticle tunneling in the presence of microwave potentials was soon overshadowed by the subsequent developments in pair tunneling by Josephson[37].

8.3.3 Dynamic Pair Currents: Josephson Tunneling

In 1962 Josephson predicted that a tunnel barrier will also carry a zero-voltage pair current with an amplitude about equal to the quasiparticle current. The Josephson current is dependent on the differences between the macroscopic quantum phases of the two superconductors. After the initial prediction and verification it was soon realized that such a phase-dependent Josephson current is of a much more general nature than the quasiparticle current and occurs in any kind of "weak link": point contact, microbridge, normal metal, semiconductor, etc., and for an applied voltage one will get an oscillating supercurrent running in parallel with a normal current. In order to account for this complex voltage-carrying state, the resistively shunted junction (RSJ-) model was developed. In this model a Josephson element, carrying the supercurrent I_s, is described by two equations

$$I_s = I_0\sin\phi \tag{8.26}$$

$$\frac{d\phi}{dt} = \frac{2eV}{h} \tag{8.27}$$

and in parallel a quasiparticle current I_{qp} modeled as a voltage-independent resistor

$$I_{qp} = \frac{V}{R}. \tag{8.28}$$

In this set of equations ϕ is the difference in quantum phase of the two superconductors coupled by the weak link. Both I_0 the amplitude of the Josephson current and the normal resistance R are assumed to be voltage- and hence frequency-independent. This model emphasized the unique and universal properties of the Josephson currents irrespective of the kind of weak link and came to dominate also the analysis of the response to radiation.

Heterodyne mixing is the preferred technique to obtain spectral lines revealing rotational transitions in the interstellar matter. Very high resolutions $\lambda/\Delta\lambda \approx 10^6$ are needed to measure Doppler shifts and spectral-line profiles. A signal of a local oscillator is combined with the signal to be detected in a nonlinear mixing element and the difference frequency is amplified. Several groups studied the possibility to use the Josephson current for heterodyne mixing by driving a point contact junction and studying the RSJ-model with a dc and an rf-current (for example[38,39]). Unfortunately the results were hardly any better than the best semiconductor Schottky diode devices. The noise for a driven Josephson junction turned out to be higher than expected[40,41]. This observed excess noise was subsequently[42] shown to be intrinsically due to the nonlinear and deterministic junction dynamics, exhibiting chaotic solutions associated with the appearance of strange attractors in phase space. The dynamic nature of the Josephson effect itself had shown its limitations for practical use and a return to the less universal aspects of the quasiparticle current in a tunnel junction was imminent.

[37] B.D. Josephson, *Phys. Lett.* 1 (1962) 251
[38] C.C. Grimes et al., *Phys. Rev. Lett.* 17 (1966) 431
[39] P.L. Richards and S.A. Sterling, *Appl. Phys.* Lett. 14 (1969) 394
[40] J.H. Claassen et al., *J. of Appl. Phys.* 49 (1978) 4117
[41] J.H. Claassen et al., *Appl. Phys. Lett.* 25 (1974) 759
[42] B.A. Huberman et al., *Appl. Phys. Lett.* 37 (1980) 250

8.3.4 Passive Nonlinear Device: Quantum Mixing

In 1973 it was recognized by McColl et al.[43] that the commonly used normal-metal-semiconductor Schottky diode could be modified in a straightforward way. By replacing the normal metal by a superconductor and by doping the semiconductor heavily, transport would be predominantly by electron tunneling, in contrast to thermionic emission. The current-voltage characteristic would be analogous to a normal-metal-insulator-superconductor (NIS) device, while maintaining, in contrast to point contacts, the stable properties of a thin-film device. In a theoretical and experimental analysis the superior properties as a video detector were demonstrated as well as in the heterodyne mode of operation[44]. Whereas in the ordinary Schottky diode the nonlinearity is due to the semiconductor, with the super-Schottky diode the nonlinearity is due to the superconducting gap and the BCS density of states. The responsivity, using classical mixing theory is given by

$$R = \frac{1}{2}\frac{d^2I/dV^2}{dI/dV} \tag{8.29}$$

which with the appropriate expression for the nonlinearity

$$I_{\mathrm{dc}}(V) = I_0 e^{eV/kT} \tag{8.30}$$

is predicted to lead to a responsivity given by

$$R \approx \frac{e}{2kT} \tag{8.31}$$

with e the electron charge and kT the temperature multiplied by Boltzmann's constant. Video detection at 10 GHz was reported in 1973 followed by mixing results in 1975. The super-Schottky was demonstrated to be far superior to the available alternatives, despite the fact that the semiconductor will contribute to the loss of the signal by absorbing part of the radiation[45].

The implicit consequence of Eq. 8.31 is that the responsivity will rise to infinity with decreasing temperature. This observation led Tucker[46] as early as 1975 to the insight that these resistive mixers could act as photon detectors in the millimeter spectral regions. This is first pointed out in his contribution to the Helsinki 14th Low Temperature Conference (14–20 August 1975), which closes with the sentence: "The technical problems will no doubt prove challenging, but the prospect is an extremely interesting one in our opinion". Tucker and Millea[47] proceed by analyzing the situation in which the photon energy would exceed the voltagescale over which the dc current rises rapidly (i.e., the strength of the nonlinearity). The analysis means a return to the concept of photon-assisted tunneling[27] and the development of a full quantum mixer theory. In a paper presented at the Applied Superconductivity Conference in 1978, the authors[48] applied their newly developed quantum mixer theory, as an example, to the super-Schottky diode but point out that the theory applies equally well to the superconductor-normal-metal tunnel junction (SIN) and the superconductor-insulator-superconductor junction (SIS). The full theory[49] was published in 1979, leading to the quantum responsivity in video detection of

$$R = \frac{e}{2kT}\frac{\tanh(\hbar\omega/2kT)}{\hbar\omega/2kT} \tag{8.32}$$

$$\approx \frac{e}{\hbar\omega}(\hbar\omega \gg k_{\mathrm{B}}T) \tag{8.33}$$

[43] M. McColl et al., *Appl. Phys. Lett.* 23 (1973) 263
[44] M. McColl et al., *Appl. Phys. Lett.* 28 (1976) 159
[45] E.A. Bergin et al., *Astrongomy and Astrophysics* 521 (2010) L20
[46] J.R. Tucker, *Proc. 14th Int. Conf. Low Temp. Phys.* Vol. 4 (1975) 180
[47] J.R. Tucker and M.F. Millea, *Appl. Phys. Lett.* 33 (1978) 288
[48] J.R. Tucker and M.F. Millea, *IEEE Trans. Magn.* MAG-15 (1979) 288
[49] J.R. Tucker, *IEEE J. Quantum Electron.* QE-15 (1979) 1234

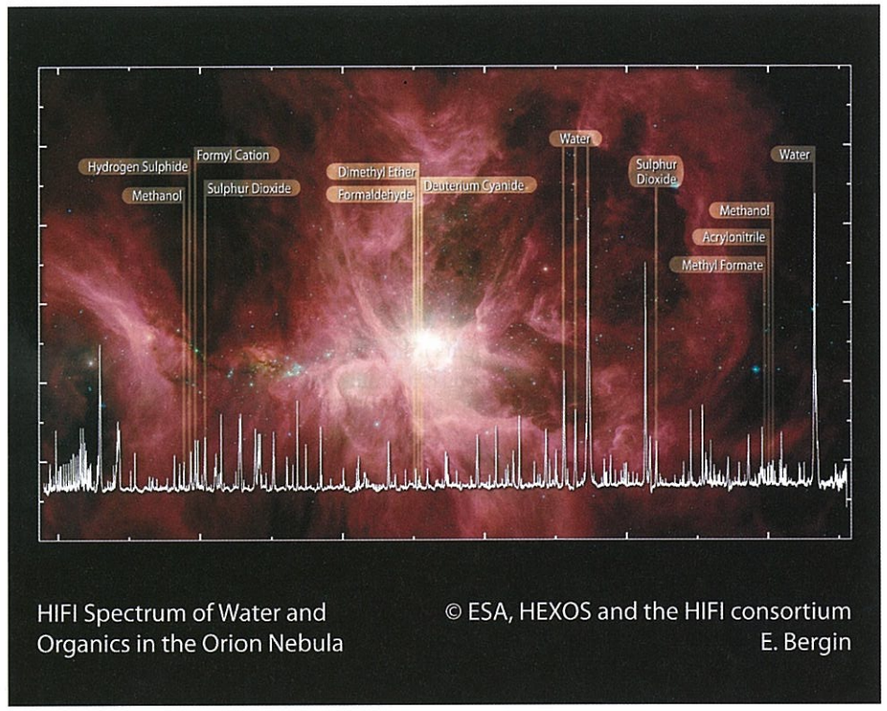

FIGURE 8.18: One of the first results of HIFI: a high resolution spectrum of water and organic molecules in the Orion nebula in the frequency range from the hitherto invisible frequency range of 1.06 to 1.12 THz. For details see Bergin et al.[45]

for a sufficiently nonlinear I,V curve. In subsequent theoretical work[50] it was demonstrated that, for heterodyne detection, the expected lower limit for the noise temperature is given by $\hbar\omega/k_{\mathrm{B}}$, which implies that photon absorption is the only noise source in an ideal SIS mixer.

8.3.5 First Experimental Demonstration: Technology Base

Inspired by the experimental progress in the super-Schottky diode and taking advantage of the emerging thin-film technology for superconducting tunnel junctions, Richards et al.[51] and Dolan et al.[52] developed and studied SIS devices and demonstrated heterodyne mixing at respectively 35 and 110 GHz. After many years of focus on utilizing the Josephson effect, the field had abandoned the Josephson effect, considered it a source of unwanted noise, and returned to the Dayem-Martin effect[53] as the desired detection principle.

A very important condition was the emerging technology of making lithographically structured superconducting tunnel junctions, since those were the only superconducting weak links with a usable nonlinearity. In 1964 Matisoo[54] had proposed the use of Josephson junctions as digital switch-

[50] M.J. Wengler and D.P. Woody, *IEEE J. Quantum Electron.* QB-23 (1987) 613
[51] P.L. Richards et al., *Appl. Phys. Lett.* 34 (1979) 345
[52] G.J. Dolan et al., *Appl. Phys. Lett.* 34 (1979) 347
[53] T.G. Phillips et al., *IEEE Trans. Magn.* MAG-17 (1981) 684
[54] J. Matisoo, *Appl. Phys. Lett.* 9 (1966) 167

ing element with a low power consumption and fast switching speed. It led to extensive programs to develop a superconducting junction technology at IBM, Bell Laboratories, NIST and in Japan. The programs came to an end in the early 1980s but had laid the groundwork for a thin-film technology of superconducting tunnel devices, including the need to develop metallurgically stable materials such as PbBi alloys and PbInAu-alloys. A very useful invention, enabling very small scale tunnel junctions, was the Dolan-Dunkleberger stencil lift-off technique or shadow-evaporation[55,56]. The technology push towards the Josephson computer was ready to be used for astrophysics.

Just at the end of this program a major new step was provided by Gurvitch et al.[57] who found a path, based on earlier work by Rowell et al.[58], to make robust niobium tunnel junctions using aluminium-oxide barriers grown on a thin layer of aluminium on top of niobium. The superconducting proximity-effect ensured that the aluminum acted as if it had the superconducting properties of the niobium. Although the early mixer experiments relied on the soft "old materials", the subsequent developments were going to rely on this new robust niobium-based technology, which also enabled the highest possible frequency reachable with the elemental superconductors. All the submillimeter telescopes currently equipped with superconducting technology are based on this niobium technology, first realized for astrophysics by Inatani et al.[59]

8.3.6 Submillimeter-Wave Astronomy

Millimeter-wave astronomy has grown rapidly since the discovery of the cosmic microwave background radiation in 1965. Currently it has become a broad exploration of the interstellar medium. The interest in understanding this interstellar medium has increased enormously due to studies of interstellar molecule-rotation transitions. It has become possible to determine the compositions, density, temperature, velocity, and the type of the molecules (Figure 8.18). It has led to improved understanding of the galactic structure, star formation and stellar mass-loss processes. Against this background it is understandable that rather than stretching the limits of the existing radio observatories, a new generation of millimeter-wave telescopes was developed in the early 1980s. In a 1982 review by Phillips and Woody[60] the progress made in superconducting tunnel devices is communicated to the astronomical community with the unequivocal recommendation to equip the new observatories with superconducting receivers and even to consider "someday to place a large submillimeter-wave band telescope in space".

One of the first experimental papers using superconducting devices[61] identified a particular radio source (1413+135) as a far-infrared extragalactic object. New observatories were created by Caltech's Submillimeter Observatory (CSO), the UK/NL's James Clerk Maxwell telescope, the French-German IRAM 345 GHz telescope at Pico Veleta in Spain, and the Japanese Nobeyama observatory. All of them providing lots of interesting data, but limited by atmospheric transmission to a few windows at the lower frequencies and also without the possibility to enhance the spatial resolution using interferometry.

In the past decade we have witnessed the step into space with the instrument HIFI on board the Herschel Space telescope. In the next decade the step to an enhancement of the spatial resolution will be taken by the completion of Atacama Large Millimeter Array (ALMA).

[55] G.J. Dolan, *Appl. Phys. Lett.* 31 (1977) 337
[56] L.N. Dunkleberger, *J. Vac. Sci. Technol.* 15 (1978) 88
[57] M. Gurvitch et al. *Appl. Phys. Lett.* 42 (1983) 472
[58] J.M. Rowell et al., *Phys. Rev.* B 24 (1981) 2278
[59] J. Inatani et al., *IEEE Trans. Magn.* MAG-23 (1987) 1263
[60] T.G. Phillips and D.P. Woody, *Ann. Rev. Astron. Astrophys.* 20 (1982) 285
[61] C.A. Beichman et al., *Nature* 293 (1981) 711

8.3.7 From Proof-of-Principle to Demanding Use

In order to use superconducting tunnel junctions in these very demanding applications, two components needed careful research to exploit the ultimate possibilities. One of them, the local oscillator, is outside the scope of this chapter because it does not use superconductivity. However, the improvements in local oscillators operating up to 1.9 THz has been tremendous in the last decade. The other component, the superconducting tunnel junction, has moved forward in an equally impressive way, yet no longer being able to benefit from the Josephson computer projects (mostly terminated around 1983).

A first requirement is band coverage. The *RC* time constant of a tunnel junction should be as small as possible. Since the capacitance increases linearly as the thickness of the dielectric decreases, i.e. the tunnel barrier, and the resistance decreases exponentially with the thickness, one prefers a tunnel barrier as thin as possible (about 2 nm). In practice this means for aluminum-oxide a minimum value of 14 Ω for an area of 1 μm^2, which implies a bandwidth of about 150 GHz. A further reduction in thickness leads to a breakdown of the tunnel barrier allowing for higher order tunnel processes leading to excess shot noise[62]. Only recently, a strong improvement in bandwidth has been obtained by the introduction of much more uniformly transmissive AlN tunnel barriers[63].

A second requirement is the suppression of the Josephson current. Any tunnel junction will also carry a Josephson current. This current is suppressed with a magnetic field in order to prevent excess noise coming from the Josephson currents.

A third requirement is adequate impedance matching to the outside world. Although, in an early phase, it was customary to use mechanical tuning stubs to create optimum signal transfer, they were replaced by integrated tuning structures consisting of superconducting striplines.

A fourth requirement was to exploit as much of the frequency band as possible with a single superconducting mixing device. Since in a spacecraft the Earth's atmosphere is no longer determining the possible frequency bands, the technology can be pushed to exploit the highest possible frequencies. Since the tunnel barriers should be as thin as possible, a robust tunnel junction technology together with a high-gap superconducting material was needed. The only realistic candidate was niobium with the AlOx (or now also AlN) technology. The energy gap of niobium is at 700 GHz. Given the nature of photon-assisted tunneling this would allow the use of tunnel devices for mixing up to 1.4 THz. However, losses would occur in the striplines used for the tuning circuits. This was solved by using striplines with the high-gap superconducting material NbTiN on one side and good conducting Al on the other side.

Given these considerations the HIFI instrument (Figure 8.18) was equipped with different technologies for the different frequency bands, leading to a natural division of labor between the contributing institutes (most of them European): 450–640 GHz (the French Institutes LERMA and IRAM), 640–800 GHz (the German Institute KOSMA), 800–960 GHz (the Dutch collaboration of SRON with TUDelft), 960–1120 GHz (idem), and 1120–1250 GHz (the US collaboration of CalTech with JPL). In all cases a performance close to the quantum limit was achieved.

8.3.8 Nonequilibrium Mixers: Hot-Electron Bolometers

Beyond the upper-frequency limit of $4\Delta/\hbar$, niobium superconducting tunnel junctions no longer provide a usable signal. Unfortunately, a new tunnel barrier technology for materials with a higher superconducting gap has not yet emerged. An alternative strategy for heterodyne mixing is based on nonequilibrium hot electrons. It was first introduced by Phillips and Jefferts[64] using the temperature dependence of the resistance of the low-bandgap semiconductor InSb and used in the 100-GHz

[62] P. Dieleman et al., *Phys. Rev. Lett.* 79 (1997) 3486
[63] T. Zijlstra et al., *Appl. Phys. Lett.* 91 (2007) 233102
[64] T.G. Phillips and K.B. Jefferts, *Rev. Sci. Instrum.* 44, (1973) 1009

range before the emergence of superconducting mixers. The principle of hot electron bolometers was picked up again for the higher frequencies, but now based on nonequilibrium superconductivity, by Gershenson et al[65]. It uses the electrical response of a thin superconducting film to two coherent signals with a frequency higher than the energy gap. The photon energy from the local oscillator, $\hbar\omega_{LO}$, and of the signal to be detected, $\hbar\omega_s$, will break Cooper-pairs resulting in an electronic system with an enhanced electron temperature, hence the name hot-electron bolometers (HEBs). The LO-power is high enough to bring the electron temperature up to a level that the superconducting state gets close to the resistive transition, where small changes in electron temperature lead to strong changes in resistance, essentially due to the increased occurrence of phase-slip events[66]. The interesting physics of the device is contained in the time-response of the electron temperature and hence of the resistance. The hierarchy of times is given by

$$\omega_{\rm IF} < 1/\tau_{\rm el} < 2\Delta/\hbar < \omega_{\rm LO} \tag{8.34}$$

with $1/\tau_{\rm el}$ the time response of the electron system. The two oscillating fields at superTHz frequencies ($\omega_{\rm LO}$ and $\omega_{\rm s}$) contain a component at the intermediate frequency (IF). The electron temperature at this $\omega_{\rm IF}$ is coherently related to the signals at superTHz frequencies and leads to a modulation of the electron temperature and hence the resistance at $\omega_{\rm IF}$, provided $\omega_{\rm IF} < 1/\tau_{\rm el}$ is satisfied. In principle, one would like to have a large value for $\omega_{\rm IF}$, which requires a large value for $1/\tau_{\rm el}$. For the latter condition three processes must be distinguished. First, the diffusion time $\tau_{\rm D} = L^2/D$, with L the length of the device and D the diffusion constant. It is assumed that the sensitive superconducting film is connected to thermal equilibrium reservoirs. Second, the transfer of energy from the electrons to the phonon bath, characterized by $\tau_{\rm e-ph}$. This value is determined by the choice of materials, and materials with a strong electron-phonon interaction are preferred. Empirically it has been found that a thin film of NbN is most suitable; Third, the phonons in the film should be tightly coupled to the phonons of the substrate. Given the unavoidable acoustic mismatch between different materials this has been achieved by making the films as thin as possible (a few nanometers) in order to maximize the chances for phonon-escape, characterized by $\tau_{\rm esc}$.

These devices have been successfully included in HIFI of the Herschel Space telescope, providing data around the ionized carbon 1.9-THz line. Since HEB's are advantageous only at superTHz frequencies, where the atmosphere is opaque, they can be used only in experiments in the stratosphere or in space. In subsequent experiments their potential has been demonstrated up to an impressive 6.5 THz, while also the limiting factor of quantum noise has come into sight[67]. An interesting aspect is also that a very compact package has been developed by the inclusion of the newly developed quantum cascade lasers (QCL's) as a local oscillator[68]. It is very likely that this combination will within a few years be used at an observatory to be built at Dome A on Antarctica, one of the other remote places to let superconductivity function[69] for astronomy.

8.3.9 Conclusions

The unique properties of the superconducting state, as identified in the BCS-theory, have provided the extremely sharp nonlinearities in the current-voltage characteristics of superconducting tunnel junctions, which enabled quantum-limited heterodyne detection. The emerging thin-film technology, the rise of interest in millimeter and submillimeter astronomy, and the acceptance that, despite its beauty, the Josephson-effect should be suppressed to exploit fully the process of photon-assisted tunneling have conspired to the instrument Heterodyne Instrument for the Far-Infrared (HIFI) at

[65] E.M. Gershenson et al., *Sov. Phys. Superconductivity* 3 (1990) 1582
[66] R. Barends et al., *Appl. Phys. Lett.* 87 (2005) 263506
[67] W. Zhang et al., *Appl. Phys. Lett.* 96 (2010) 111113
[68] J.R. Gao et al., *Appl Phys. Lett.* 86 (2005) 244104
[69] Y. Ren et al., *Appl. Phys. Lett.* 97 (2010) 161105

the Herschel Space telescope and to the soon-to-be completed Atacama Large Millimeter Array in Chili.

8.4 Microwave Cooling of Superconducting Quantum Systems

W. D. Oliver

8.4.1 Introduction

Superconducting artificial atoms (qubits) are solid-state quantum systems, comprising lithographically defined Josephson tunnel junctions and superconducting interconnects. When cooled to milli-Kelvin temperatures, these qubits exhibit quantized states of charge, flux, or junction phase depending on the circuit design parameters[70]. Associated with these quantized states is a spectrum of energy levels, tunable via an external control parameter, e.g., an applied electric or magnetic field. Although generally only the lowest two energy eigenstates are utilized for quantum information science applications, the energy spectrum indeed extends to higher-energy levels corresponding to higher-excited states of the circuit. The separation between pairs of energy levels typically falls in the radio frequency and microwave regimes, and resonantly driving the artificial atom with a harmonic field can couple and induce quantum-state transitions.

There are several features that make superconducting artificial atoms excellent candidates for quantum information science applications[71]. Superconductors are intrinsically low-loss materials, enabling coherence times (both energy relaxation and dephasing) that are presently at the 1–10 μs level, limited primarily by losses in the junction, metal surfaces, and ancillary passive components (e.g., capacitor dielectrics). Furthermore, due to their relatively large size, critical dimensions ~1 – 10μm, superconducting artificial atoms can be strongly coupled to their external microwave control fields. Consequently, gate operations with superconducting qubits can be performed on the ~1 – 10ns time scale, a factor 10^3–10^4 faster than the coherence times. These numbers are reflective of the field as of 2010. As coherence times are improved, this factor will continue to increase and ultimately reach levels required for fault-tolerant quantum error correction protocols. The states of superconducting artificial atoms can be read out efficiently and with high visibility (presently as high as ~99%) using superconducting SQUIDs, cavity-quantum electrodynamics (C-QED) techniques, and superconducting microwave amplifiers (both phase sensitive and phase preserving).

In most QIS applications, high-fidelity state preparation is the starting point for high-fidelity gate operations. While a standard approach is simply to wait for the qubit to relax to its ground state, this imposes the constraint that state preparation will occur on the same time scale as the lifetime of the quantum system. While adequate for many of today's experiments, this approach is not conducive to future multi-qubit applications. For example, error correction protocols rely on ancillary qubits to perform syndrome measurements, and these ancillae must be rapidly refreshed each time the protocol is repeated. Another proposed technique is the use of ideal projective measurements (QND-type measurements) to put the qubit into its ground state, and this is an active area of research.

A third approach is actively cooling a quantum system using optical pumping techniques analogous to those introduced in natural atomic systems. By coupling the artificial atom to rapidly decaying energy levels, either internal levels of the atom or external levels such as as a harmonic

[70] J. Clarke and F.K. Wilhelm, Superconducting quantum bits, *Nature* 453 (2008) 1031; see also in this book Chapter 6 on superconducting qubits.
[71] D.P. DiVincenzo, *Fortschr. Phys. Progress of Physics* 48 (2000) 771

oscillator, energy is effectively pumped out of the quantum system of interest. In this section, we review the use of microwaves to cool superconducting artificial atoms actively to their ground state.

8.4.2 Superconducting Artificial Atoms

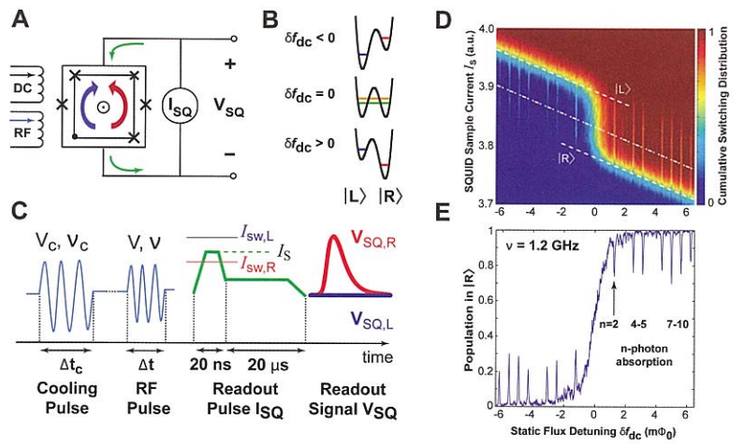

FIGURE 8.19: Artificial atom (persistent current qubit) and measurement set-up. A schematic of the qubit and surrounding DC SQUID readout. B Double well qubit potential comprising energy levels for static magnetic flux bias δf_{dc} about $\Phi_0/2$, where Φ_0 is the superconducting flux quantum. Diabatic states of the left (right) well corresponds to a persistent current with clockwise (counterclockwise) circulation. At detuning $\delta f_{dc} = 0$, the double-well potential is symmetric and the diabatic-state energies are degenerate. Tunnel coupling opens an avoided crossing Δ. C Qubit excitation and read-out pulse sequence. The qubit is first prepared in its ground state with a harmonic cooling pulse with amplitude V_c and frequency ν_c. Quantum-state transitions are induced with a subsequent harmonic RF pulse with amplitude V and frequency ν. The qubit state is read-out using the DC SQUID switching response. D Qubit step. Cumulative switching current distribution of the SQUID for each δf_{dc} value following a 3-μs RF driving pulse at 1.2 GHz applied to the qubit (the cooling pulse was not used here). Resonant multiphoton transitions (of order n) are observed between states $|L\rangle$ and $|R\rangle$. The switching distribution along the dashed-dotted line discriminates between states $|L\rangle$ and $|R\rangle$ (E).

We illustrate microwave cooling of a quantum system using the specific example of a superconducting persistent-current qubit[72,73]. The persistent-current qubit is a superconducting loop interrupted by three Josephson junctions (Figure 8.19A). When biased with a static magnetic flux $f_{dc} \sim \Phi_0/2$, where Φ_0 is the superconducting flux quantum, the system assumes a double-well potential profile (Figure 8.19B). The diabatic ground state of the left (right) well corresponds to a persistent current I_q with clockwise (counterclockwise) circulation. These two diabatic energy levels have an energy separation $\varepsilon = 2I_q\delta f_{dc}$ linear in the flux detuning $\delta f_{dc} \equiv f_{dc} - \Phi_0/2$. Higher-excited states of the double-well potential (see Figure 8.20A) will be used to cool the qubit to its ground

[72] J. E. Mooij, T. P. Orlando, L. S. Levitov, L. Tian, C. H. van der Wal, S. Lloyd, *Science* 285 (1999) 1036;

[73] T. P. Orlando, J. E. Mooij, L. Tian, C. H. van der Wal, L. S. Levitov, S. Lloyd, and J. J. Mazo, *Phys. Rev.* B 60 (1999) 15398

state.

The two-level system Hamiltonian near $\delta f_{dc} = 0$ for the lowest two energy

$$\mathcal{H} = -\frac{1}{2}(\varepsilon\sigma_z + \Delta\sigma_x), \tag{8.35}$$

where σ_z and σ_x are Pauli matrices. At detuning $\delta f_{dc} = 0$, the double-well potential is symmetric and the diabatic-state energies are degenerate. At this "degeneracy point," resonant tunneling between the diabatic states opens an avoided level crossing of energy Δ. Here, the qubit states are σ_x eigenstates, corresponding to symmetric and antisymmetric combinations of diabatic circulating-current states. Detuning the flux away from this point tilts the double well, allowing us to tune the eigenstates and eigenenergies of the artificial atom. Far from the degeneracy point the qubit states are approximately σ_z eigenstates, the diabatic states with well-defined circulating current. The qubit is read out using a hysteretic DC SQUID (superconducting quantum interference device), a sensitive magnetometer that can distinguish the flux generated by circulating current states.

In addition to the static flux biases, the artificial atom is controlled and read out using the harmonic RF/microwave pulses illustrated in Figure 8.19C. As we describe below, the qubit is first prepared in its ground state using a harmonic cooling pulse with amplitude V_c and frequency ν_c. Quantum-state transitions are then driven using a harmonic RF/microwave pulse with amplitude V and frequency ν. These fields are mutually coupled to the qubit through a small antenna. This is followed by a SQUID readout current pulse using the "sample and hold" technique. If the sample current exceeds the SQUID switching current, a voltage pulse will appear at the output during the hold phase. Threshold detection looks for the presence or absence of a SQUID voltage, and this constitutes a digital measurement of the qubit state. Alternatively, although not used in these experiments, we have incorporated the SQUID into a resonant circuit and realized qubit readout via the shift in resonance frequency and phase for both the linear and nonlinear resonance regimes.

The "qubit step," the readout of qubit in equilibrium with its environment, is shown in Figure 8.19D as a function of the SQUID sample current and the flux detuning. The diabatic states $|L\rangle$ and $|R\rangle$ correspond to different levels of sample current (dashed lines) located symmetrically about their energy degeneracy point at δf_{dc}=0. This plot constitutes a cumulative switching current distribution of the SQUID for each δf_{dc} value. Additionally, a 3-μs pulse at 1.2 GHz is applied to the qubit, and resonant transitions can be observed as fingers extending down (up) from state $|L\rangle$ ($|R\rangle$) when n×1.2 GHz becomes resonant with the energy-level separation. A best-estimator (dashed-dotted line) can be determined to provide the best statistical discrimination between states $|L\rangle$ and $|R\rangle$. The resulting qubit step with its saturated n-photon resonances along the best estimator line is shown in Figure 8.19E.

Note that in the cooling discussion in the next section, we label the multilevel energy diagram (Figure 8.20C) by the diabatic states of the left well ($|0L\rangle$ and $|1L\rangle$) and the right ($|0R\rangle$ and $|1R\rangle$). This corresponds to the energy levels of isolated wells and not the system eigenenergies. In general, the uncoupled well states have energies that are linear in flux: in Figure 8.20C energies of the states in the left well have positive slopes, while those in the right well have negative slopes. When the energy levels of these diabatic states cross, an avoided crossing opens labelled by $\Delta_{n,m}$ where n and m correspond to the level number in the left and right well respectively. For example, the state $|0L\rangle$ is the ground state at negative flux detuning in (Figure 8.20C). Following this diabatic energy as the flux is increased, it increases in energy until it becomes degenerate with the $|0R\rangle$ energy level, where an avoided crossing $\Delta_{0,0}$ opens. Continuing to increase the flux, the energy of state $|0L\rangle$ continues to increase, eventually crossing the $|1R\rangle$ energy level, where an avoided crossing $\Delta_{0,1}$ opens. Continuing further, the energy of level $|0L\rangle$ becomes becomes the second excited state on the right side of Figure 8.20C, above the states $|0R\rangle$ and $|1R\rangle$.

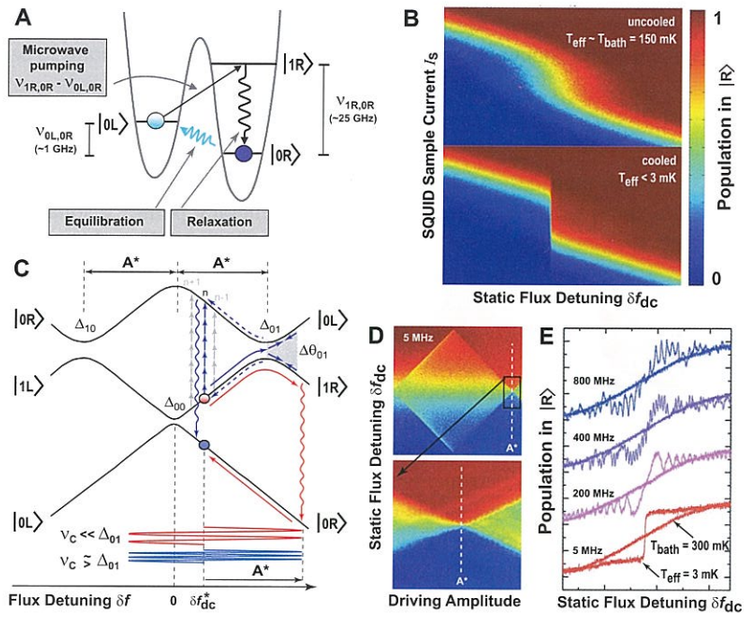

FIGURE 8.20: Cooling of an artificial atom via an ancillary excited state. A External excitation transfers the thermal population from state $|0L\rangle$ to state $|1R\rangle$ (straight line) from which it decays into the ground state $|0R\rangle$. Wavy lines represent spontaneous relaxation and absorption leading to equilibration. B Qubit step at $T_{bath} = 150$ mK in equilibrium with the bath (top) and after a 3-μs cooling pulse at 5 MHz (bottom). The average level populations exhibit a qubit step about $\delta f_{dc} = 0$, with a width proportional to T_{bath} (top) and $T_{eff} \ll T_{bath}$ (bottom). C Schematic level diagram illustrating resonant and adiabatic cooling. $|0L\rangle \rightarrow |1R\rangle$ transitions are resonant at high driving frequency ν (blue lines) and occur via adiabatic passage at low ν (red lines). Δ_{00} and Δ_{01} are the tunnel splittings between $|0R\rangle$ - $|0L\rangle$ and $|0L\rangle$ - $|1R\rangle$. D Optimal cooling parameters. State $|0R\rangle$ population *vs.* flux detuning δf_{dc} and driving amplitude A with $\nu = 5$ MHz, $\Delta t_c = 3\mu$s, and $T_{bath} = 150$ mK. Optimal conditions for cooling are realized at $A = A^*$, where A^* is defined in C. E Cooling at driving frequencies $\nu = 800$, 400, 200 and 5 MHz. State $|0R\rangle$ population *vs.* δf_{dc} for the cooled qubit and for the qubit in thermal equilibrium with the bath (black lines, $T_{bath} = 300$ mK). Measurements for $\nu = 800$, 400, 200 and 5 MHz are displaced vertically for clarity. A cooling factor of 100, independent of detuning, is obtained in the adiabatic limit (5 MHz).

8.4.3 Microwave Cooling

Quantum operations in single qubits generally involve driving transitions within a manifold of the lowest two energy levels in the double-well potential (Figure 8.20A), which constitute the two-level qubit subsystem of a more complex energy level diagram. When higher-excited states are accessed, the driven system behavior can be markedly different from the population saturation observed when only two levels are involved (for example, as in Figure 8.19E). For example, at least three levels are required to achieve incoherent population inversion, and such a multilevel artificial atom coupled to a microwave cavity has recently been used to demonstrate masing (microwave lasing)[74]. In that work, Josephson quasi-particle states were driven to achieve inversion. Alternatively, population

[74] O. Astafiev, K. Inomata, A.O. Niskanen, T. Yamamoto, Yu. A. Pashkin, Y. Nakamura, J.S. Tsai, *Nature* 449 (2007) 588

inversion can be established by accessing an ancilliary excited state via direct or LZS transitions[75].

Here, by reversing the cycle that leads to population inversion, we show that one can pump population from the qubit excited state $|0L\rangle$ to the qubit ground state $|0R\rangle$ (Figure 8.20A) via an ancillary energy level $|1R\rangle$[76]. In the case where the population in $|0L\rangle$ results from thermal excitation, the transfer of population to $|0R\rangle$ effectively cools the qubit by lowering its effective temperature. This kind of active cooling represents a means to initialize and reset qubits with high fidelity, key elements for quantum information science and technology. Alternatively, in addition to the quantum system itself, the pumping mechanism can be used to refrigerate environmental degrees of freedom[77] or cool neighboring quantum systems[78,79,80].

For a qubit in equilibrium with its environment, the population in $|0L\rangle$ that is thermally excited from $|0R\rangle$ follows the Boltzmann relation

$$p_{0L}/p_{0R} = \exp[-\varepsilon/k_B T_{bath}], \tag{8.36}$$

where $p_{0L,0R}$ are the qubit populations for energy levels $\varepsilon_{0L,0R}$, $\varepsilon = \varepsilon_{0L} - \varepsilon_{0R}$, k_B is the Boltzmann constant, and T_{bath} is the bath temperature. To cool the qubit subsystem below T_{bath}, a microwave magnetic flux of amplitude A and frequency ν targets the $|0L\rangle \rightarrow |1R\rangle$ transition, driving the state-$|0L\rangle$ thermal population to state $|1R\rangle$, from which it quickly relaxes to the ground state $|0R\rangle$. Efficient cooling occurs only when the driving-induced population transfer to $|0R\rangle$ is faster than the thermal repopulation of $|0L\rangle$. The hierarchy of relaxation and absorption rates required, $\Gamma_{0R,1R} \gg \Gamma_{0L,1R}, \Gamma_{0L,0R}$, is achieved in our system owing to a relatively weak tunneling between wells (states connected quantum mechanically through a tunnel barrier), which inhibits the inter-well relaxation and absorption processes $|1R\rangle \rightarrow |0L\rangle$ and $|0R\rangle \rightarrow |0L\rangle$, compared with the relatively strong intrawell relaxation process $|1R\rangle \rightarrow |0R\rangle$ (states connected within an approximate harmonic oscillator).

Figure 8.20B shows the qubit step at $T_{bath} = 150$ mK in equilibrium with the bath (top) and after a 3-μs cooling pulse at 5 MHz (bottom). Under equilibrium conditions, the average level populations exhibit a thermally-broadened qubit step about $\delta f_{dc} = 0$, with a width proportional to T_{bath}. The presence of microwave excitation targeting the $|0L\rangle \rightarrow |1R\rangle$ transition, followed by relaxation, acts to increase the ground-state population and, thereby, sharpens the qubit step. Cooling can thus be quantified in terms of an effective temperature $T_{eff} < T_{bath}$, a signature that is evident from the narrowing of the qubit steps in Figure 8.20B after cooling. Using the notation from Figure 8.20, the effective qubit temperature is obtained by fitting the temperature T_{eff} that would have been required in equilibrium to achieve the observed qubit population p_{0R},

$$p_{0R} = \frac{\varepsilon}{\sqrt{\varepsilon^2 + \Delta^2}} \left[\tanh\left(\frac{\sqrt{\varepsilon^2 + \Delta^2}}{2k_B T_{eff}} \right) + 1 \right]. \tag{8.37}$$

Universal cooling (cooling that is independent of flux detuning) occurs near an optimal driving amplitude A^* (Figure 8.20C). This is demonstrated in Figure 8.20D where we present the $|0R\rangle$ state population P_{sw} measured as a function of the microwave amplitude A and flux detuning δf_{dc} for $\nu = 5$ MHz. Cooling and the diamond feature can be understood in terms of the energy level diagram (Figure 8.20C). As the amplitude of the microwave pulse is increased from $V = 0$, population

[75] D.M. Berns, M.S. Rudner, S.O. Valenzuela, K. K. Berggren, W. D. Oliver, L. S. Levitov, T. P. Orlando, *Nature* 455 (2008) 51

[76] S. O. Valenzuela, W. D. Oliver, D. M. Berns, K. K. Berggren, L. S. Levitov, T. P. Orlando, *Science* 314 (2006) 1589

[77] A.O. Niskanen, Y. Nakamura, and J.P. Pekola, *Phys. Rev.* B 76 (2007) 174523

[78] J.Q. You, Yu-xi Liu, and Franco Nori, *Phys. Rev. Lett.* 100 (2008) 047001

[79] M. Grajcar, S.H.W. van der Ploeg, A. Izmalkov, E. Il'ichev, H.-G. Meyer, A. Fedorov, A. Shnirman, and G. Schön, *Nature Phys.* 4 (2008) 612

[80] S. Kafanov, A. Kemppinen, Yu. A. Pashkin, M. Meschke, J.S. Tsai, J.P. Pekola, *Phys. Rev. Lett.* 103 (2009) 120801

transfer first occurs when the $\Delta_{0,0}$ avoided crossing between the lowest two states is reached, i.e., $A > |\delta f_{dc}|$; this defines the front side of the observed diamond, symmetric about the qubit step. For amplitudes $A^*/2 \leq A \leq A^*$, the $\Delta_{0,1}$ ($\Delta_{1,0}$) side avoided crossing dominates the dynamics, resulting in a second pair of thresholds $A = A^* - |\delta f_{dc}|$, which define the back side of the diamond. In the region outside of the diamond's backside, the qubit is cooled. As the diamond narrows to the point $A = A^*$, the sharpest qubit step is observed. This is the universal cooling condition: only one of the two side avoided crossings ($\Delta_{0,1}$ or $\Delta_{1,0}$) is reached and, thereby, strong transitions with relaxation to the ground state result for a wide range of δf_{dc}. In contrast, for $A > A^*$, both side avoided crossings ($\Delta_{0,1}$ and $\Delta_{1,0}$) are reached simultaneously for $|\delta f_{dc}| < A - A^*$, leading once again to a large population transfer between $|0R\rangle$ and $|0L\rangle$, and opening the front side of a second diamond feature (Figure 8.20D).

The cooling exhibits a rich structure as a function of driving frequency and detuning, resulting from the manner in which state $|1R\rangle$ is accessed (Figure 8.20C). Transitions occur via a (multiphoton) resonant or adiabatic passage process when the driving frequency is high or low enough, respectively[81,82]. At high frequencies (800 and 400 MHz in Figure 8.20E) well-resolved resonances of n-photon transitions are observed and cooling is thus maximized near resonances. At intermediate frequencies (400 and 200 MHz), Mach-Zehnder interference at the side avoided crossing Δ_{01} becomes more prominent and modulates the intensity of the n-photon resonances. Below $\nu = 200$ MHz, individual resonances are no longer discernible, but the modulation envelope persists. At the lowest frequencies ($\nu < 10$ MHz), state $|1R\rangle$ is reached via adiabatic passage through the Δ_{01} crossing (Figure 8.20C), and the population transfer and cooling become conveniently independent of detuning (see $\nu = 5$ MHz in Figure 8.20E). As shown in Figure 8.20E, we achieve an effective qubit temperature $T_{eff} = 3$ mK, even for $T_{bath} = 300$ mK. In our qubit, our determination of T_{eff} was limited primarily by decoherence (linewidth), which limited the resolution with which we could distinguish the states $|0R\rangle$ and $|0L\rangle$ near degeneracy. Nonetheless, we can estimate the ideally resolvable cooling factor α_c for this type of cooling process using Eq. 8.36,

$$\alpha_c \equiv \frac{T_{bath}}{T_{eff}} = \frac{\varepsilon_{1R\to 0R}}{\Delta}, \tag{8.38}$$

where $\varepsilon_{1R\to 0R} \approx h\times 25$ GHz is the energy separation where the relaxation $|1R\rangle \to |0R\rangle$ occurs and $\Delta \approx h\times 0.01$ GHz for our qubit, yielding a cooling factor $\alpha_c \sim 2500$. For a bath temperature $T_{bath} = 50$ mK, this would correspond to an effective temperature $T_{eff} = 20$ μK in our qubit.

Cooling a qubit in equilibrium with the bath requires a characteristic cooling time. In turn, a cooled qubit will thermalize to the environmental bath temperature over a characteristic equilibration time. The relationship between these two times determines if it is possible to drive the qubit while it is still cold. We found in this qubit that equilibration times are at least one order of magnitude larger than cooling times at $T_{bath} < 250$ mK and up to three order of magnitudes larger at $T_{bath} < 100$ mK. This allowed us ample time to drive the qubit after cooling it. The implementation of an active cooling pulse prior to a generic driving pulse is highly advantageous. It sensibly shortens measurement times, enabling us to acquire data at repetition rates that far exceed the intrinsic equilibration rate due to interwell relaxation after each measurement trial. By adopting active cooling, we gained a factor 50 in data acquisition speed, limited by the bandwidth of our readout circuit. Furthermore, active cooling greatly reduces thermal smearing, allowing us to analyze features in the data that would have been hidden otherwise.

[81] W. D. Oliver, Y. Yu, J. C. Lee, K. K. Berggren, L. S. Levitov, T. P. Orlando, *Science* 310 (2005) 1653

[82] D.M. Berns, W.D. Oliver, S.O. Valenzuela, A.V. Shytov, K.K. Berggren, L.S. Levitov, T.P. Orlando, *Phys. Rev. Lett.* 97 (2006) 150502

8.4.4 Summary

We reviewed implementation of active cooling of a quantum system, a superconducting qubit. By applying microwave pulses, we pumped population from an excited state within the qubit manifold to a higher excited state, from which it quickly relaxed to the qubit qround state. This process is an example of an entropy pump, essentially, a qubit refrigerator. Using this technique, we have achieved effective qubit temperatures as low as 0.5 mK, a factor $\sim 10-100\times$ colder than the dilution refrigerator itself. The use of active cooling techniques in QIS will become more prominent as superconducting qubit coherence times increase. From a practical point of view, it reduces the amount of time one must wait between experiments to reset the qubit. Furthermore, this type of pump can be used to cool systems connected the qubit, e.g., resonators, SQUIDs, or other restricted environmental degrees of freedom. More fundamentally, active cooling has an important role in future QIS applications, enabling the rapid and high-fidelity state initialization of logical qubits as well as the ancillae required for syndrome measurements in quantum error-correction protocols.

8.5 Applications of Superconducting Microresonators

Jonas Zmuidzinas

8.5.1 Introduction

Over the past decade, interest in superconducting microresonators has risen dramatically as a result of the wide variety of emerging application possibilities. Various versions of these simple devices, produced by thin-film deposition and lithographic patterning, are now being developed for photon and dark matter detection, neutrino mass experiments, frequency-multiplexed readout of cryogenic detector arrays, quantum information experiments, coupling to nanomechanical systems, and ultra-low noise parametric amplifiers. These devices exploit a broad range of phenomena in superconductivity, including ultra-low dissipation, the kinetic inductance effect, nonlinear response, and non-equilibrium dynamics. In addition, the physics of superconducting microresonators touches on other fields of condensed matter physics, especially two-level systems in amorphous materials. To provide the necessary background, I will first briefly review the basics of superconductor electrodynamics and its historical development. I will then turn to a discussion of superconducting microresonators, with a primary focus on detector applications.

8.5.2 Linear Electrodynamics: A Brief Review

Two decades after Onnes' 1911 discovery, experiments had shown that the hallmark of superconductivity—the disappearance of the electrical resistance below the transition temperature T_c—could be seen not only using direct currents, but also with alternating radio-frequency (RF; 1-10 MHz) currents.[83] By 1940 this work had been extended into the microwave region (1.5 GHz).[84] Meanwhile, at much higher frequencies—at visible and infrared wavelengths—no significant change in the optical absorption was observed upon passing through the superconducting transition.[85] Indeed, the two effects were soon employed together to make the first superconduct-

[83] F. B. Silsbee et al., Phys. Rev. 39 (1932) 379; J. C. McLennan et al., *Proc. Roy. Soc.* 136 (1932) 52

[84] H. London, *Proc. Roy. Soc.* A176 (1940) 522

[85] J. G. Daunt et al., *Phil. Mag.* 23 (1937) 264

ing infrared bolometers.[86] Thus, it was apparent that the electrical conductivity $\sigma(\omega)$ must exhibit a change from superconducting behavior to normal-metal behavior at frequencies ω between the microwave and infrared bands. This transition was eventually shown to occur in the millimeter through far-infrared wavelength range,[87] consistent with a temperature-dependent electron energy gap of $2\Delta(T)$ (with $2\Delta \approx 3.5\ kT_c$ for $T << T_c$) that was a key feature of the BCS theory published shortly thereafter.[88]

Well before the electron-pairing BCS theory was proposed, Heinz London had understood a more subtle aspect of the electrodynamic behavior of superconductors.[89] London predicted that a superconductor should in general have a small but nonzero dissipation for AC currents, in contrast to the DC case for which the resistance and associated dissipation vanish entirely at $T < T_c$. The dissipation arises because the finite inertia of the superconducting electrons allows AC electric fields to exist inside a superconductor, and therefore the presence of normal electrons–expected for temperatures above absolute zero–leads to, in London's words, "production of heat". See Section 8.1.2 for a discussion of the two-fluid model proposed by London. The subsequent application of the BCS theory to the calculation of the electrical conductivity of superconductors yielded results consistent with London's insight; the Mattis-Bardeen expressions for the complex conductivity of superconductors are given in Section 8.3.1 as Eqs. 8.19 and 8.20).

In most cases, the complex conductivity is not directly accessible experimentally; instead, the complex surface impedance $Z_s = R_s + iX_s$ is the quantity being probed. For thick films in the local limit, the surface impedance and complex conductivity $\sigma(\omega, T)$ are related by[90]

$$Z_s(\omega,T) = \sqrt{\frac{i\mu_0\omega}{\sigma(\omega,T)}} = \frac{Z_s(\omega,0)}{\sqrt{1 + i\delta\sigma(\omega,T)/\sigma_2(\omega,0)}} \tag{8.39}$$

where $\delta\sigma(\omega,T) = \sigma(\omega,T) - \sigma(\omega,0) = \sigma_1(\omega,T) - i\delta\sigma_2(\omega,T)$. The theoretical surface impedance at zero temperature is purely reactive and may be expressed in terms of the penetration depth λ

$$Z_s(\omega,0) = i\mu_0\omega\lambda \tag{8.40}$$

where, in the local limit, $\lambda_{local} \approx 105\,\text{nm} \times \sqrt{(\rho_n/1\,\mu\Omega\,\text{cm})(1\,\text{K}/T_c)}$. Similar equations may be written for thick films in the "extreme anomalous" regime, and for films that are thin compared to the penetration depth.

These results may be summarized by relating the first-order fractional perturbation in the surface impedance to the fractional perturbation in the conductivity,

$$\frac{\delta Z_s(\omega,T)}{Z_s(\omega,0)} \approx -\gamma\frac{\delta\sigma(\omega,T)}{\sigma(\omega,0)} \tag{8.41}$$

where $\delta Z_s(\omega,T) = Z_s(\omega,T) - Z_s(\omega,0)$, and with $\gamma = 1$, $1/2$, and $1/3$ for the thin film, local, and extreme anomalous limits, respectively. If we introduce the conductivity quality factor as $Q_\sigma = \sigma_2(\omega,0)/\sigma_1(\omega,T)$, and similarly the surface impedance quality factor $Q_s = X_s(\omega,0)/R_s(\omega,T)$, Eq. (8.41) shows that they are related by $Q_s = Q_\sigma/\gamma$.

At low frequencies and temperatures, $\hbar\omega << \Delta_0$ and $k_B T << \Delta_0$, we may use the approximation[91]

[86] D. H. Andrews et al., *Phys. Rev.* 59 (1941) 1045

[87] G. S. Blevins et al., *Phys. Rev.* 100 (1955) 1215; R. E. Glover and M. Tinkham, *Phys. Rev.* 104 (1956) 844; *Phys. Rev.* 108 (1957) 243

[88] J. Bardeen et al., *Phys. Rev.* 106 (1957) 162; *Phys. Rev.* 108 (1957) 1175

[89] H. London, *Nature* 133 (1934) 497

[90] Accessible reviews of superconductor electrodynamics including references to authoritative and original papers may be found in J. P. Turneaure et al., *J. Supercond.* 4 (1991) 341 ; P. J. Walsh and V. P. Tomaselli, *Am. J. Phys.* 58 (1990) 644; and J. Gao, Ph.D. thesis, Caltech, Pasadena CA (2008), http://thesis.library.caltech.edu/2530.

[91] J. Gao et al., *J. Low Temp. Phys.* 151 (2008) 557

$$Q_\sigma(\omega,T) \approx \frac{\pi}{4}\frac{e^{\Delta_0/k_B T}}{\sinh(\hbar\omega/2k_B T)\,K_0(\hbar\omega/2k_B T)}, \tag{8.42}$$

which explicitly[92] shows the exponential rise with decreasing temperature.

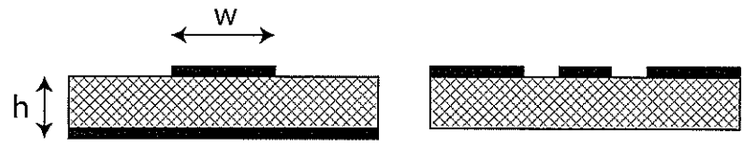

FIGURE 8.21: Left: a microstrip transmission line consists of a conducting strip of width w on the surface of a dielectric slab of thickness h backed by a conducting ground plane. The coplanar waveguide (CPW) line, illustrated on the right, has conductors only on the top surface of the dielectric, and consists of a center strip of width w separated from ground planes on either side bygaps of width g.

8.5.3 Superconducting Microresonators

Pippard[93] understood that the use of a superconductor in a parallel-strip transmission line—similar to what is today known as a microstrip line (see Figure 8.21)—would result in a change of the phase velocity due to the inductance contributed by the inductive surface impedance, $Z_s(\omega,0) = iX_s = i\omega L_s = i\omega\mu_0\lambda_{sc}$. Indeed, the inductance per unit length of a line made using a perfect conductor ($\sigma \to \infty$) is approximately given by $\mathcal{L} = \mu_0 h/w$, where h is the dielectric thickness and w is the microstrip width, provided that $w >> h$. The capacitance per unit length is approximately $C = \epsilon_r\epsilon_0 w/h$, where ϵ_r is the relative dielectric constant of the substrate. The phase velocity of the fundamental TEM-like mode is $\bar{c} = 1/\sqrt{\mathcal{L}C} = c/\sqrt{\epsilon_r}$. As discussed by Pippard and others,[94, 95] the use of a superconductor causes an increase in the inductance, $\mathcal{L} = \mu_0(h + 2\lambda_{sc})/w$, as if the spacing between the superconducting films had increased by $2\lambda_{sc}$. The capacitance remains unchanged. The fraction of the total inductance of the line that is contributed by the superconductor is

$$\alpha_{ms} = \frac{2\lambda_{sc}}{h + 2\lambda_{sc}}. \tag{8.43}$$

The increased inductance causes a reduction in the phase velocity by the factor $\sqrt{1-\alpha_{ms}}$, to $\bar{c} = (1 + 2\lambda_{sc}/h)^{-1/2} c/\sqrt{\epsilon_r}$. More accurate expressions for the properties of superconducting microstrip lines that include the effects of fringing fields may be found in the literature.[96] Alternatively, microstrip properties may be quickly calculated using modern electromagnetic simulation software.

Microstrip lines may be fabricated by depositing three film layers (superconductor, insulator, superconductor) on a substrate, and patterning the top superconductor layer. In this case, the dielectric thickness h would typically lie in the range $0.1 - 1\ \mu$m. Alternatively, the substrate may itself serve

[92] Note that $\sinh(x)K_0(x) \sim \sqrt{\pi/8x}$ as $x \to \infty$.

[93] A. B. Pippard, *Proc. Roy. Soc.* A191 (1947) 399

[94] J. C. Swihart, *J. Appl. Phys.* 32 (1961) 461; P. V. Mason and R. W. Gould, *J. Appl. Phys.* 40 (1969) 2039; R. L. Kautz, *J. Appl. Phys.* 49 (1978) 308

[95] J. M. Pond et al., *IEEE Trans. Magn.* 23 (1987) 903

[96] W. H. Chang, J. Appl. Phys. 50 (1979) 8129; G. Yassin and S. Withington, *J. Phys.* D28 (1995) 1983

as the microstrip dielectric, with superconducting films deposited on the top and bottom surfaces, in which case $h \sim 100-500\,\mu$m. In both cases h is quite small compared to the free-space wavelength $\lambda_{RF} \approx 30$ cm $\times$ (1 GHz/ν), so $\alpha_{ms} >> \lambda_{sc}/\lambda_{RF}$. Compared to a cavity resonator, a microstrip resonator limited by conductor losses has a considerably lower internal quality factor $Q_i = \alpha_{ms}^{-1} Q_s$ for the same value of Q_s. As Pond et al.[95] point out, the kinetic inductance fraction can even approach unity if a thin superconducting film with a high normal-state resistivity ρ_n is used.

The coplanar waveguide (CPW; Figure 8.21) is another popular superconducting transmission line structure. One advantage of CPW as compared to microstrip is that only one superconducting film layer is required. However, the kinetic inductance fraction of CPW is generally smaller than for thin-film microstrip. This can be seen from the crude estimate $\alpha_{CPW} \sim \lambda_{sc}/w$, and by noting that typical CPW center strip widths $w \sim 2-10\,\mu$m are larger than the $0.1-1\,\mu$m film thickness of deposited dielectrics used for microstrip lines. The kinetic inductance fraction of superconducting CPW lines may be accurately calculated using analytical formulae[97], conformal mapping methods,[98] or direct electromagnetic simulation, and these methods generally yield results consistent with measurements.[99]

Early Studies

Mason and Gould (1969) studied In/Ta_2O_5/Ta microstrip resonators in the 50–500 MHz range. The microstrips were made using evaporated thin In films on anodized Ta substrates. The highest resonator quality factors achieved were $Q_r \sim 1.7\times10^3$. Mason and Gould's results showed that a surface impedance quality factor of at least $Q_s \geq \alpha_{ms} Q_r \sim 8\times10^2$ was possible, a limit that was three orders of magnitude lower than contemporary cavity measurements. DiNardo et al.[100] obtained much higher quality factors, around $Q_r = 5\times10^5$ at 14 GHz, using thin-film lead microstrips on alumina substrates. However, the relatively thick substrates used yield low values of α_{ms}, so the inferred value of $Q_s \sim 5\times10^2$ is actually similar to the limit set by Mason and Gould. About a decade later, Pöpel[101] studied the losses of PbAu/SiO/Pb microstrip resonators, finding minimum losses at $T = 1.7$ K of 0.04 dB/m at 0.09 dB/m at 9.1 GHz and 27.3 GHz, corresponding to quality factors of $\sim 6\times10^4$. Given the the 880 nm thickness of the SiO dielectric, the kinetic inductance fraction was around $\alpha_{ms} \approx 0.12$, so a value of $Q_s \sim 7\times10^3$ was achieved, a significant step forward and not far from the Mattis-Bardeen value at $T_c/T = 4.2$. Pond et al.[95] studied NbN/Si:H/NbN microstrip resonators in the 0-2 GHz frequency range. Using magnetron sputtering, rather thin films (150 Å, 400 Å, 140 Å) were deposited, and the measured phase velocity $\bar{c}/c = 0.016$ was very low, indicating a kinetic inductance fraction close to unity as would be expected. The line loss was also measured, and indicated $Q_s \sim 3-6\times10^3$. As a final example, Andreone et al. (1993)[102] studied microstrip resonators made by depositing and patterning both Nb ($\rho_n = 2.6\,\mu\Omega$cm) and NbTiN ($\rho_n = 90\,\mu\Omega$cm) films on sapphire substrates. The resonator was formed by inverting the substrate and placing it on top of another sapphire substrate, with a bulk niobium foil below serving as the ground plane. The kinetic inductance fraction of this arrangement is quite low due to the 130 μm substrate thickness. The measurement fits indicate zero-temperature residual surface resistances of 1.3 $\mu\Omega$ (Nb) and 5.9 $\mu\Omega$ (NbTiN), which correspond to $Q_s \approx 1.3\times10^3$ for both films, comparable to or somewhat lower than earlier work.

[97] J. C. Booth and C. L. Holloway, *IEEE Trans. Micr. Theory Tech.* 47 (1999) 769
[98] J. Gao, Ph.D. thesis, Caltech, Pasadena CA (2008); http://thesis.library.caltech.edu/2530.
[99] J. Gao et al., Nucl. *Instrum. Meth.* A 559 (2006) 585
[100] A. J. Dinardo et al., *J. Appl. Phys.* 42 (1971) 186
[101] R. Pöpel, *IEEE Trans. Micr. Theory Tech.* 31 (1983) 600
[102] A. Andreone et al., *J. Appl. Phys.* 73 (1993) 4500

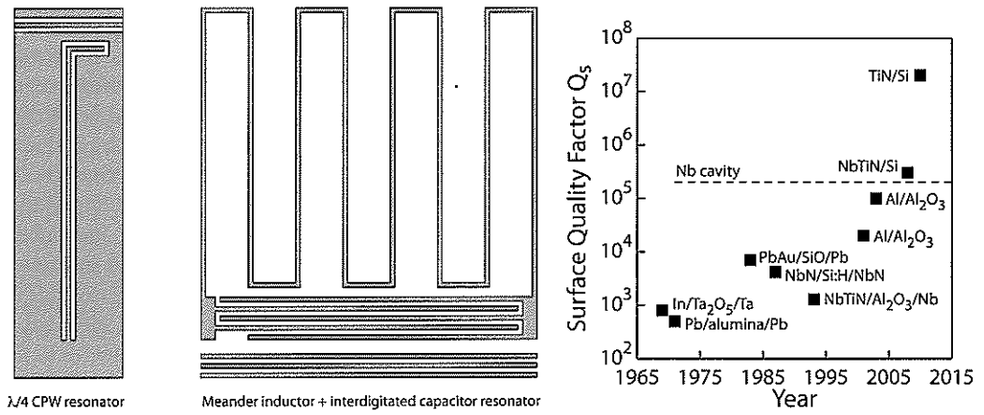

FIGURE 8.22: Far left: A $\lambda/4$ coplanar-waveguide (CPW) shunt-coupled transmission line resonator. The CPW feedline used to excite the resonator is visible at the top. Left center: A lumped-element resonator consisting of a meandered inductor and an interdigitated capacitor. The CPW feedline visible at the bottom has finite-width ground strips and couples to the interdigitated capacitor. Right: This plot shows lower limits to the surface impedance quality factor $Q_s = X_s/R_s = Q_\sigma/\gamma$ derived from measurements of superconducting microresonators. The lower limits are derived by assigning the total measured resonator loss to the superconductor. Points labeled by three materials are microstrip structures. Points labeled by two materials indicate resonators made from a single superconducting film deposited on a crystalline substrate. The dashed line indicates typical results achieved with bulk Nb cavities. The points plotted are limited to the work discussed in Section 8.5.3 and do not represent a comprehensive literature search. Nonetheless, the graph serves to illustrate the general trend.

Recent Work

Starting in 2000, the possibility of using superconducting microresonators as detectors stimulated exploratory measurements at Caltech and JPL. Initially this work was focused on thin-film microstrip resonators using materials such as Nb and Al using evaporated SiO as the dielectric, and resonator quality factors around 5×10^4 were measured (see Figure 8.24). However, these resonators did not follow the Mattis-Bardeen predictions but rather showed complex behavior as a function of temperature and microwave power. This behavior was not understood at the time; the work of Martinis et al. (2005) later showed that two-level systems in the amorphous thin-film dielectric were responsible for such effects.[103] In an effort to simplify the situation, the Caltech/JPL group switched to resonators using coplanar waveguide lines (see Figures 8.21 and 8.22), made from a single superconducting film deposited on a high-quality crystalline substrate such as silicon or sapphire. In some cases, very high quality factors were achieved,[104] around $Q_r = 2\times10^6$, indicating a surface impedance quality factor of at least $Q_s \sim 10^5$. These results have now been reproduced and extended by a number of other groups.[105]

In 2008, Barends et al.[106] published measurements of a CPW resonator made using NbTiN deposited on a silicon substrate. The 300 nm thick NbTiN film had $T_c = 14.8$ K and $\rho_n = 170\,\mu\Omega$cm,

[103] J. M. Martinis et al., *Phys. Rev. Lett.* 95 (2005) 210503
[104] B. A. Mazin et al., *AIP Conf. Proc.* 605 (2002) 309; P. K. Day et al., *Nature* 425 (2003) 817
[105] D. S. Wisbey et al., J. Appl. Phys. 108 (2010) 093918; J. M. Sage et al., ArXiV eprint 1010.6063 (2010).
[106] R. Barends et al., *Appl. Phys. Lett.* 92 (2008) 223502

giving a kinetic inductance fraction of $\alpha_{CPW} = 0.35$. The measured quality factor was $Q_r = 6 \times 10^5$, indicating a lower limit to the surface impedance quality factor of $Q_s = 3 \times 10^5$. This result was surprisingly high, over two orders of magnitude improvement compared to the measurements of Andreone et al. (1993), and comparable to or even somewhat better than the results for niobium cavities and aluminum CPW resonators. Even higher values of Q_s were established in 2010 by Leduc et al.[107] using TiN films patterned into lumped-element resonators[108] of the type shown in figure 8.22. Stoichiometric TiN films deposited on silicon substrates gave $T_c = 4.5\,\mathrm{K}$, $\rho_n = 100\mu\Omega\,\mathrm{cm}$, and a kinetic inductance fraction $\alpha = 0.74$. The measured internal quality factor $Q_i = 3 \times 10^7$ indicates a lower limit of $Q_s = 2 \times 10^7$. TiN resonators with similarly high internal quality factors have now been reproduced in other laboratories.[109]

Radiation Loss

As illustrated in Figure 8.22, the performance of superconducting microresonators has improved dramatically over the past four decades. Resonator quality factors above 10^6 are now routinely achieved using single-layer structures deposited on high-quality, low-loss crystalline substrates. Achieving high quality factors requires minimizing all potential sources of dissipation including radiation loss. Low radiation loss is possible using small, micron-scale feature sizes easily achieved with modern lithography. Indeed, a rough estimate is obtained by considering a $50\,\Omega$, half-wave CPW resonator on a semi-infinite substrate with dielectric constant $\epsilon_r = 10$. If the kinetic inductance fraction is small so that the effect on the phase velocity may be neglected, this structure has a radiation quality factor of[110] $Q_{rad} \approx 5 \times 10^{-3} (\lambda_0/w)^2$. Here λ_0 is the free-space wavelength at the resonance frequency and w is the center strip width. For $Q_{rad} > 10^6$, we require $w/\lambda_0 < 7 \times 10^{-5}$, or $w < 2\mu$m at 10 GHz. Radiation loss may be reduced by using lower frequencies, minimizing the size of the resonator structure through the use of high kinetic inductance materials such as TiN or NbTiN, by adopting a lumped-element resonator design as shown in Figure 8.22, or all of the above.

Dissipation from Two-Level Systems

In practice, the maximum internal quality factor Q_i is often not limited by the superconducting material or radiation but instead by dissipation due to two-level systems (TLS) in amorphous dielectrics. The prevalence of TLS in amorphous materials was proposed four decades ago as a way to explain the anomalous bulk properties (e.g., heat capacity) of these materials at low temperatures.[111] TLS arise due to the random structure of amorphous materials, since occasionally it is possible for an atom or group of atoms to move between two local minima of the potential energy landscape by quantum tunneling over a barrier. The random nature of the amorphous material implies that the potential energy minima and the barrier height are also random, leading to a random, uniform distribution of TLS energy splittings.

Thermal occupation of the upper state causes the TLS loss tangent to vary as $\delta_{TLS}(\omega, T) = \delta_0 \tanh(\hbar\omega/2k_BT)$, where δ_0 is the $T \to 0$ limiting value. Therefore a simple way to reduce TLS loss is to operate at low frequencies, $\omega \ll k_BT/\hbar$, although dissipation due to TLS relaxation[112] sets in below ~ 0.3 MHz $(T/1\,\mathrm{K})^3$. A second method to reduce loss is to use microwave fields that are strong enough to saturate the TLS.[113] Neither of these two methods is applicable if the resonator is

[107] H. G. Leduc et al., *Appl. Phys. Lett.* 97 (2010) 102509
[108] S. Doyle et al., *J. Low Temp. Phys.* 151 (2008) 530
[109] M. R. Vissers et al., *Appl. Phys. Lett.* 97 (2010) 232509
[110] A. Vayonakis and J. Zmuidzinas, unpublished (2002); B. Mazin, Ph.D. thesis, Caltech, Pasadena CA (2003), http://thesis.library.caltech.edu/3910/
[111] P. W. Anderson et al., *Phil. Mag.* 25 (1972) 1; W. A. Phillips, *J. Low Temp. Phys.* 351 (1972) 7
[112] G. Frossati et al., *J. Phys.* C. 10 (1977) L515
[113] M. Von Schickfus and S. Hunklinger, *Phys. Lett.* 64A(1977) 144

intended to operate in the quantum-mechanical regime. A third method to reduce TLS loss is to find materials that have a lower TLS density. Martinis et al.[103] showed that SiN_x ($\delta_0 \sim 2 \times 10^{-4}$) could have considerably lower loss than SiO_2 ($\delta_0 \sim 2 \times 10^{-3}$). More recent work[114] has shown that amorphous silicon and silicon-rich SiN_x films deposited using the inductively-coupled plasma chemical vapor deposition technique can achieve $\delta_0 \sim 2 \times 10^{-5}$. A final method for reducing TLS loss is to avoid use of amorphous dielectric films. Indeed, this was the route that led to high-Q CPW resonators, which are fabricated on crystalline substrates. However, even these resonators do have some TLS loss, arising from a thin (few nm) layer on the surface of the device.[115] This layer could either be surface oxides or an adsorbed layer. The dissipation caused by this surface layer may be reduced by increasing the separation of the electrodes in the capacitive portion of the resonator because this reduces the fraction of the electric field energy that is contained in the lossy TLS layer. Finally, parallel-plate capacitors with crystalline silicon dielectrics have recently been shown to have very low microwave dissipation.[116]

8.5.4 Superconducting Microresonator Detectors

The demonstration of superconducting microresonators with very high quality factors has opened up numerous new possibilities for superconducting detectors. A wide variety of schemes has been proposed and considered; the common denominator is the use of an array of microresonators spaced in frequency to allow multiplexed readout. This approach provides a simple, elegant solution to the long-standing readout problem that has impeded development of large arrays of superconducting detectors. Furthermore, wideband frequency multiplexing has become eminently practical given the advances in high-speed digital signal processing that allow a large number of carrier frequencies to be readily generated and measured by standard room-temperature electronics.[117] The simplest scheme is to use the resonator itself as the detector. The absorption of photons in the superconductor causes Cooper pair breaking and quasiparticle production, and this leads to a perturbation $\delta\sigma = \delta\sigma_1 - j\delta\sigma_2$ of the complex conductivity; to first order, $\delta\sigma$ is proportional to the change in quasiparticle density δn_{qp}. This leads to a perturbation of the complex surface impedance δZ_s, given by Eq. 8.41, which may be sensed by measuring the changes δf_r in the resonator frequency and δQ_r^{-1} in the resonator dissipation. This approach, now commonly known as the microwave kinetic inductance detector or MKID, will be covered in detail below. However, we will first review a number of important precursors that led to the development of MKIDs.

Precursors

As mentioned earlier, superconductors have been used for detection for over seven decades. The first devices were bolometers[118] operated on the resistive transition at $T = T_c$. The possibility of a superconducting detector operating at $T \ll T_c$ was first suggested by Burstein et al. in 1961[119], who proposed the use of a superconducting tunnel junction to measure the quasiparticles produced by the absorption of energy capable of breaking Cooper pairs. The development of tunneling detectors and related ideas is detailed in Section 8.3.

Another interesting suggestion for $T < T_c$ operation was McDonald's proposal to use the temperature-dependent kinetic inductance for bolometer readout.[120] This device can be understood

[114] A. D. O'Connell et al., *Appl. Phys. Lett.* 92 (2008) 112903; H. Paik and K. D. Osborn, *Appl. Phys. Lett.* 96 (2010) 072505
[115] J. Gao et al., *Appl. Phys. Lett.* 92 (2008) 152505
[116] S. Weber et al., arXiv:1102.2917v1 (2011)
[117] B. A. Mazin et al., *Nucl. Instrum. Meth.* A 559 (2006) 799; S. J. C. Yates et al., *Appl. Phys. Lett.* 95 (2009) 042504
[118] P. L. Richards, *J. Appl. Phys.* 76 (1994) 1
[119] E. Burstein et al., *Phys. Rev. Lett.* 6 (1961) 92
[120] D. G. McDonald, *Appl. Phys. Lett.* 50 (1987) 775

by writing

$$\frac{\sigma_2(\omega,T)}{\sigma_n} \approx \frac{\pi\Delta(T)}{\hbar\omega}[1-2f(\Delta(T))] \tag{8.44}$$

which holds for $\hbar\omega << \Delta(T)$ and shows that the temperature dependence of the gap energy $\Delta(T)$ is responsible for the variation of inductance with temperature. McDonald proposed that the changes in kinetic inductance could be read out using a SQUID monitoring a bridge circuit excited by a ~ 100 kHz current. At temperatures far below the transition, $T << T_c$, the temperature variation of the kinetic inductance becomes exponentially small, $\propto e^{-\Delta_0/k_B T}$. However, the kinetic inductance continues to respond in a linear fashion to nonequilibrium changes in the quasiparticle population even as $T \rightarrow 0$. The presence of the distribution function $f(\Delta)$ in Eq. 8.44 is a clear indication of this, although the BCS gap equation shows that Δ also responds linearly to $f(E)$. This point was understood by Bluzer[121], who proposed a nonequilibrium detector that used SQUIDs to measure the nonequilibrium changes in kinetic inductance produced by pair-breaking photons. A key aspect of such a device is that the fundamental noise limit is set by the generation-recombination fluctuations of the quasiparticle population, and the noise produced by thermal quasiparticles vanishes exponentially with decreasing temperature.[122] The dissipative component of the conductivity (σ_1) also responds linearly to nonequilibrium quasiparticles, as is evident from the Mattis-Bardeen integral; the effect is analogous to the current response of a tunnel junction detector, as was pointed out by Gulian and Van Vechten.[123] They suggested that X-rays could be detected by illuminating a superconducting film with microwaves and measuring small changes in the reflected power, and discussed the possibility that this response might be enhanced through a positive feedback mechanism involving microwave amplification of the photoproduced quasiparticles.

Clearly, the detector sensitivity is controlled by the ability to measure very small changes in the conductivity $\delta\sigma$. Furthermore, minimizing the superconducting volume is desirable in order to maximize the perturbation $\delta\sigma$ that occurs in response to a fixed energy deposition δE or a change δP in the radiation power absorbed. Both of these points suggest use of superconducting microresonators, and in fact this idea was described by Michael D. Jack in a 1990 patent assigned to the Santa Barbara Research Center.[124] To quote from the patent: "It has been found that Cooper pair breaking by incident photons results in a change in the kinetic inductance and a consequent shift in the resonance frequency of the superconducting transmission line." The patent goes on to describe a readout technique involving use of Schottky-diode detectors to measure the changes in microwave power transmitted through a resonator resulting from the frequency shift, as well as a multiplexing scheme involving coupling each resonator to the readout diode sequentially by means of superconducting critical-current switches. While the patent is an early recognition of the promise of using superconducting microresonators for detection, the proposed readout scheme is complex and clearly not ideal; the electronics required for simultaneous readout of a frequency-multiplexed MKID array at noise levels approaching fundamental limits was not yet on the horizon in 1990.

Microwave Kinetic Inductance Detectors (MKIDs)

The MKID concept was developed by J. Zmuidzinas and H. G. Leduc in 1999, who were motivated by the previous work of Bluzer[121] and Sergeev and Reizer.[122] The distinguishing features included the use of superconducting microresonators, a homodyne readout method using a wideband, low-noise cryogenic amplifier and room-temperature electronics that could sense either the amplitude or phase shift of the microwave transmission, and multicarrier frequency-domain multi-

[121] N. Bluzer, *J. Appl. Phys.* 78 (1995) 7340

[122] A. V. Sergeev and M. Y. Reizer, Intl. *J. Mod. Phys*. B, 10 (1996) 635

[123] A. M. Gulian and D. Van Vechten, *Appl. Phys. Lett*. 67 (1995) 2560 ; D. Van Vechten et al., *Nucl. Instrum. Meth.* A 370 (1996) 34

[124] M. D. Jack, U.S. Patent 4,962,316, Oct. 9, 1990

plexing. Figure 8.23 depicts the idea as originally conceived. The method of radiation coupling is not shown; the intention was to use an antenna-fed microstrip line to couple submillimeter-wave radiation to the inductor at its center, taking. advantage of the microwave virtual ground at that point.[125] Around this time, frequency-domain multiplexing of superconducting detectors was being discussed in other contexts, e.g., in conjunction with radio-frequency single electron transistor (RF-SET) amplifiers following tunnel-junction detectors,[126] or as a way of multiplexing transition-edge bolometers.[127] In all of these cases, the resonators were elements to be added to the scheme in order to allow multiplexing; in the MKID case, the resonators simultaneously served as detectors, a drastic simplification.

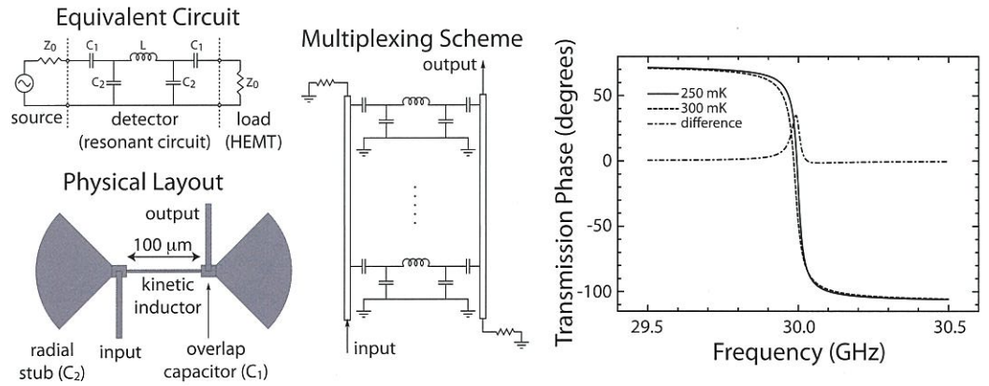

FIGURE 8.23: Description of the MKID concept as proposed by Zmuidzinas and Leduc in 1999. Left: An equivalent circuit diagram and a potential physical realization in microstrip. Center: Frequency-multiplexed readout of an array of MKIDs using two feedlines. Right: Phase response of the proposed circuit, calculated using the Mattis-Bardeen theory.

In early 2000, measurements of Nb/SiO/Nb microstrip resonators were performed in order to verify that the concept was feasible (see Figure 8.24). As mentioned earlier, the microstrip experiments displayed a number of puzzling effects, such as the variation of the resonator quality factor Q with readout power, and half a decade would pass before this behavior was connected to saturation of two-level systems in the amorphous SiO dielectric. Meanwhile, Peter Day suggested switching to CPW resonators (see Figure 8.21) in order to simplify the structure, and by mid-2001[104] this led to the demonstration of resonators with quality factors around $Q_r \sim 10^6$ (see Figure 8.25). Detection experiments using 6 keV X-rays quickly followed, leading by 2003 to the first journal paper describing and demonstrating the concept.[104] Since then, considerable effort has been expended in understanding the frequency noise of these devices, which was shown to be due to TLS-induced capacitance fluctuations.[128] Quasiparticle relaxation is another important issue that has received significant attention.[129]

[125] J. Zmuidzinas et al., *IEEE Trans. Microwave Theory Tech.* 42 (2004) 698

[126] R. J. Schoelkopf et al., *IEEE Trans. Appl. Supercond.* 9 (1999) 2935; T. R. Stevenson et al., *Appl. Phys. Lett.* 80 (2002) 3012

[127] J. Yoon et al., *Appl. Phys. Lett.* 78 (2001) 371

[128] J. Gao et al., *Appl. Phys. Lett.* 90 (2007) 102507; S. Kumar et al., *Appl. Phys. Lett.* 92 (2008) 123503; J. Gao et al., *Appl. Phys. Let.* 92 (2008) 212504

[129] R. Barends et al., *Phys. Rev. Lett.* 100 (2008) 257002; R. Barends et al., *Phys. Rev.* B 79 (2009) 020509

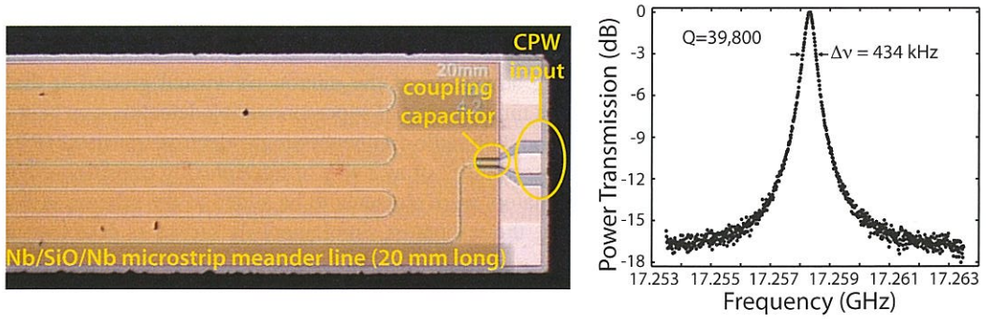

FIGURE 8.24: Left: Photograph of a half-wave Nb/SiO/Nb microstrip resonator measured in early 2000 to demonstrate MKID feasibility. Right: Measurement results, showing $Q_r = 4 \times 10^4$ at 17 GHz. Credit: A. Vayonakis and H. G. Leduc.

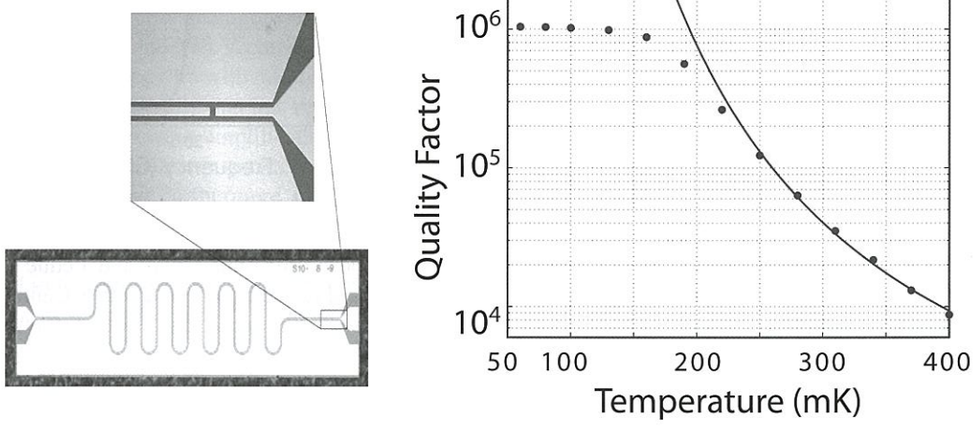

FIGURE 8.25: Left: Photograph of a JPL/Caltech half-wave CPW resonator made using an aluminum film deposited on a sapphire substrate. Right: Measurements obtained in early 2002 of the quality factor vs. temperature, showing $Q_r = 10^6$. The curve shows the Mattis-Bardeen prediction. Credit: P. K. Day,B. A. Mazin, and H. G. Leduc.

MKID Examples

One of the key issues for MKID design is is the method used to couple the photons to be detected into the resonator. Early experiments avoided this issue by flood-illuminating the entire chip with X-rays and measuring the pulse response. Figure 8.26 shows the first attempt to achieve efficient coupling in the millimeter-wave band by using slot-array antennas feeding CPW MKID resonators.[130] In later versions of these devices, the capacitive portion of the CPW resonator has been replaced by an interdigitated capacitor in order to reduce the TLS noise.[131] A multiband millimeter-wave astronomical camera using this array design is now being prepared for use on the Caltech Submillimeter Observatory.[132]

[130] S. Kumar, Ph.D. thesis, Caltech, Pasadena CA (2008), http://thesis.library.caltech.edu/1663/; J. Schlaerth et al., *J. Low Temp. Phys.* 151 (2008) 684

[131] O. Noroozian et al., *AIP Conf. Proc.* 1185 (2009) 148

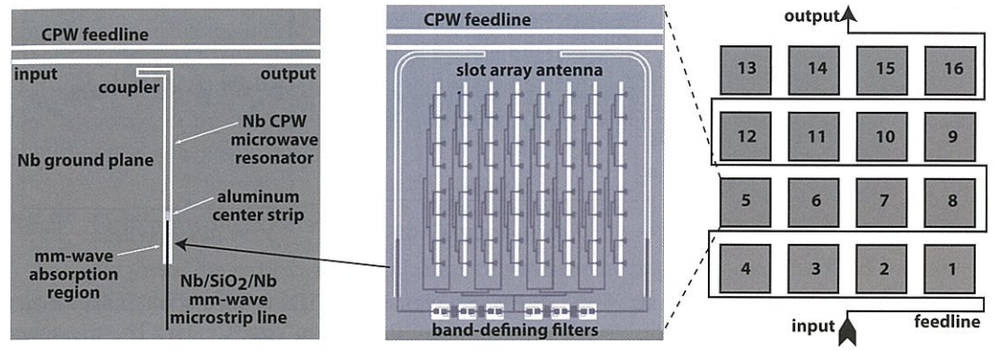

FIGURE 8.26: This figure illustrates the antenna-coupled MKID arrays developed at Caltech/JPL. Left: a $\lambda/4$ CPW resonator is shunt-coupled to a CPW feedline. Millimeter-wave radiation is brought to the resonator using a niobium microstrip line and is absorbed by the aluminum section of the CPW resonator's center strip. Center: A phased-array multislot antenna, two CPW MKIDs, and on-chip band-defining filters are used to make a dual-band pixel. Right: A 4×4 pixel array is multiplexed using a single feedline.

A much simpler and very clever solution to this problem was the lumped-element resonator suggested by Doyle et al.[108] and shown in Figure 8.22, in which the inductor simultaneously serves as the radiation absorber. Efficient radiation absorption requires using either very thin films of ordinary superconductors or highly resistive superconductors such as TiN; a very convenient feature of using TiN films is that T_c may be easily adjusted by changing the stoichiometry.[107] Designing for high absorption efficiency simultaneously guarantees a high kinetic-inductance fraction α; this can be understood through the Mattis-Bardeen relation between the surface inductance and surface resistance, $L_s = \hbar R_s / \pi \Delta_0$. The lumped-element pixel design is being used for the $\lambda = 2$ mm band in the "NIKA" camera built for the Institute for Millimetric Radio Astronomy (IRAM) 30-m telescope.[133] Microwave crosstalk between pixels is a serious problem with this design; however, it is possible to produce large arrays with negligible crosstalk levels by modifying the inductor design using opposite-polarity conductor pairs in close proximity to minimize the microwave dipole moment (see Figure 8.27). In addition, efficient dual-polarization absorption may be obtained using appropriate metallization patterns. A variety of lumped-element, TiN-based MKIDs are now being developed for a wide range of applications including photon detection at millimeter, submillimeter, far-IR, UV/optical, and X-ray wavelengths as well as dark matter detection.

Superconducting Microresonator Bolometers

Given the considerable progress that has been made in the performance and physical understanding of microresonators, as well as the advances in digital frequency-multiplexed readout electronics, McDonald's kinetic-inductance bolometer concept[120] is worth revisiting. Superconducting microresonators have been successfully fabricated on thermally suspended silicon nitride micromesh,[134] so a frequency-multiplexed array of bolometers is straightforward to produce. In a

[132] P. R. Maloney et al., *Proc. SPIE* 7741 (2010)

[133] A. Monfardini et al., arXiv:1102.0870v2 (2011).

[134] H. G. Leduc and P. K. Day 2010, personal communication.

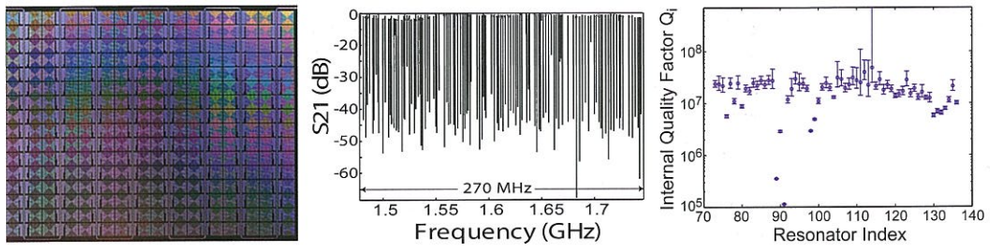

FIGURE 8.27: Left: a 16×16 array of TiN lumped-element MKIDs using a spiral inductor and an interdigitated capacitor. The pixels are approximately 0.6 mm in size. Center: The measured resonances for half the array (128 resonators) are very deep and fall into a 270 MHz band centered at 1.6 GHz. Right: the internal quality factors are uniformly high, $Q_i > 10^7$. Credit: O. Noroozian, P. K. Day, B.-H. Eom, and H. G. Leduc.

standard MKID, quasiparticle recombination provides the bottleneck for power flow, whereas in a bolometer, the bottleneck is set by the geometry of the thermal suspension legs. Therefore, the resonator-bolometer is an interesting option when quasiparticle recombination is too rapid, e.g., at higher temperatures. In addition, the thermally suspended island provides an opportunity to spread the absorbed photon energy uniformly across the inductor, which maximizes responsivity. In contrast, this is not easy to achieve in antenna-coupled MKIDs. In addition, the quasiparticle recombination noise may be greatly reduced. Finally, the noise performance of available transistor amplifiers is considerably better than is needed to reach the fundamental sensitivity limits for bolometers (e.g., photon or phonon noise).

TES Bolometer Multiplexing

Superconducting microresonators may also be used for frequency-multiplexed readout of superconducting transition edge sensor (TES) bolometers. In this scheme, the TES current is sent through a planar coil which couples flux into a single-junction SQUID. Changes in the TES current therefore cause changes in the SQUID inductance, which is sensed by embedding the SQUID into a microresonator.[135]

8.5.5 Parametric Amplifiers

The fact that superconductors exhibit nonlinear behavior at microwave frequencies was already known in 1950 and was discussed theoretically in the context of the BCS theory by Parmenter in 1962.[136] To lowest order, the kinetic inductance varies with current as $L = L_0(1 + I^2/I_*^2)$, where I_* is related to the critical current. That reactive nonlinearities can be used for low-noise amplification has been known for at least a century; the use of the kinetic-inductance nonlinearity for this purpose was suggested and patented by Landauer.[137] Shortly thereafter, amplification was demonstrated using an ultra-thin superconducting film coupled with a waveguide-fed rutile resonator; subsequent work called into question whether the kinetic inductance or intergrain weak links provided the relevant nonlinearity.[138] This is a key issue, because low-noise parametric amplification requires that the nonlinear reactance have low dissipation. The first clear-cut demonstration of parametric

[135] J. A. B. Mates et al., *Appl. Phys. Lett.* 92 (2008) 023514
[136] A. B. Pippard, *Proc. Roy. Soc.* A, 203(1950) 210; R. H. Parmenter, *RCA Review,* 23 (1962) 352
[137] R. Landauer, *Proc. IRE,* 48 (1960) 1328 ; U.S. Patent Number 3,111,628, Nov 1963.
[138] A. S. Clorfeine, *Proc. IEEE* 52, 844 (1964); H. Zimmer, *Appl. Phys. Lett.* 10 (1967) 193

amplification using the kinetic inductance nonlinearity has been given only quite recently,[139] using niobium CPW resonators similar to the one shown in Figure 8.25. An alternative approach is to use a series array of Josephson junctions or SQUIDs to provide the reactive nonlinearity for a resonator.[140] One advantage of this technique is that the resonance frequency may be readily tuned through the application of a magnetic field.

8.5.6 Other Applications

In recent years, the most visible application of superconducting microresonators has been in experiments exploring the prospects for superconducting quantum computing. Superconducting microresonators are a key component for these experiments, and their dissipation must be kept very low in order to prevent loss of quantum coherence, so the use of CPW resonators has had a large impact. The first such experiment to incorporate CPW resonators was performed by the Schoelkopf group at Yale.[141] In this experiment, a Cooper pair box (CPB) acting as a two-level atom was fabricated next to a CPW resonator. In essence, this is a circuit version of a single atom in an optical cavity. The use of a superconducting microresonator allowed the strong-coupling regime to be achieved, in which the vacuum Rabi frequency is considerably larger than the relaxation rates of the CPB and resonator. This experiment received considerable attention, and led to the adoption of superconducting microresonators in a number of other low-temperature experiments. One particularly interesting example is the use of superconducting microresonators to probe the motion of nanomechanical resonators into the quantum regime.[142] These topics are discussed in move detail in Section 8.4.

8.5.7 Summary

Driven by a number of important applications, the study of superconducting microresonators has blossomed over the past decade. A deeper understanding of the physics governing microresonator dissipation and noise has led to considerably improved resonator designs. However, the performance of the best resonators is still not limited by the superconducting material but rather by extrinsic effects such as two-level systems in amorphous dielectrics. Therefore, one can expect resonator performance to continue to improve as methods for avoiding, reducing or eliminating these extrinsic effects are developed.

8.6 Further Reading

Applications of Passive Microwave Filters and Devices in Communication And Related Systems

1. Michael J. Lancaster, *Passive Microwave Device Applications of High Temperature Superconductors*, Cambridge University Press, Cambridge, 1997.

2. M. Nisenoff and H. Weinstock, eds., Microwave Superconductivity, NATO Science Series, Kluwer Dordrecht, The Netherlands, 2001.

[139] E. A. Tholén et al., *Appl. Phys. Lett.* 90 (2007) 253509
[140] M. A. Castellanos-Beltran et al., *Nature Physics* 4 (2008) 929
[141] A. Wallraff et al.,*Nature* 431 (2004) 162
[142] J. D. Teufel et al., *Nature Nanotechnology* 4, 820 (2009); J. B. Hertzberg et al., *Nature Physics* 6 (2010) 213

3. Raafat R. Mansour, Microwave Superconductivity, *IEEE Transactions on Microwave Theory and Techniques*, vol. 50, pp. 750-759, 2002.

4. Randy W. Simon et al., Superconducting microwave filter systems for cellular telephone Base Stations, *Proceedings of IEEE*, vol. 92, pp.1585-1596, 2004.

Microwave Cooling of Superconducting Quantum Systems

1. For a recent review of superconducting qubits:

   (a) J. Clarke and F.K. Wilhelm, Superconducting quantum bits, *Nature* 453 (2008) 1031

   (b) See also in this book Chapter 6 on superconducting qubits.

2. To read more about the cooling presented here, as well as population inversion and related works, in multilevel superconducting systems:

   (a) S. O. Valenzuela, W. D. Oliver, D. M. Berns, K. K. Berggren, L. S. Levitov, T. P. Orlando, Microwave-induced cooling of a superconducting qubit, *Science* 314 (2006) 1589.

   (b) D.M. Berns, M.S. Rudner, S.O. Valenzuela, K. K. Berggren, W. D. Oliver, L. S. Levitov, T. P. Orlando, Amplitude spectroscopy of a solid-state artificial atom, *Nature* 455 (2008) 51.

   (c) D.M. Berns, W.D. Oliver, S.O. Valenzuela, A.V. Shytov, K.K. Berggren, L.S. Levitov, T.P. Orlando, Coherent quasiclassical dynamics of a persistent current qubit, *Phys. Rev. Lett.* 97 (2006) 150502.

   (d) W. D. Oliver, Y. Yu, J. C. Lee, K. K. Berggren, L. S. Levitov, T. P. Orlando, Mach-Zehnder interferometry in a strongly driven superconducting qubit, *Science* 310 (2005) 1653.

3. To read more about cooling a superconducting qubit coupled to a superconducting resonator:

   (a) J.Q. You, Yu-xi Liu, and Franco Nori, Simultaneous cooling of an artificial atom and its neighboring quantum system, *Phys. Rev. Lett.* 100 (2008) 047001.

   (b) M. Grajcar, S.H.W. van der Ploeg, A. Izmalkov, E. Il'ichev, H.-G. Meyer, A. Fedorov, A. Shnirman, and G. Schön, Sisyphus cooling and amplification by a superconducting qubit, *Nature Phys.* 4 (2008) 612.

4. To read more about using these kinds of cooling techniques used to cool other systems:

   (a) A. Naik, O. Buu, M.D. LaHaye, A.A. Clerk, M.P. Blencowe, and K.C. Schwab, Cooling a nanomechanical resonator with quantum back-action, *Nature* 443 (2006) 193.

   (b) A.O. Niskanen, Y. Nakamura, and J.P. Pekola, Information entropic superconducting microcooler, *Phys. Rev. B* 76 (2007) 174523.

   (c) A.V. Timofeev, M. Helle, M. Meschke, M. Mottonen, J.P. Pekola, Electronic refrigeration in the quantum limit, *Phys. Rev. Lett.* 102 (2009) 200801.

   (d) S. Kafanov, A. Kemppinen, Yu. A. Pashkin, M. Meschke, J.S. Tsai, J.P. Pekola, Single-electronic radio-frequency refrigerator, *Phys. Rev. Lett.* 103 (2009) 120801.

   (e) T. Rocheleau, T. Ndukum, C. Macklin, J.B. Hertzberg, A.A. Clerk, and K.C. Schwab, Preparation and detection of a mechanical resonator near the ground state of motion, *Nature* 463 (2010) 72.

Acknowledgements

Microwave Measurements of Fundamental Properties of Superconductors

The work at Lincoln Laboratory cited in this chapter was supported by the Air Force Office of Scientific Research, the Office of Naval Research, the Department of the Air Force, and the Defense Advanced Research Projects Agency.

Superconducting Quantum Electronics Enabling Astronomical Observations

I thank Pieter de Visser, Dan Oates and Tom Phillips for a critical reading of the manuscript. I also acknowledge the collaboration on this subject with Thijs de Graauw over a period of about 25 years.